POVM Validatie uitgangspunten en lange termijn ontwikkeling

POV MACRO STABILITEIT

Auteur: **C. Zwanenburg**
Amine Aboufirass
Hans Teunissen

Versie: 3

Datum: October 2018

POV MACRO STABILITEIT

Summary

The POVM research programme deals with the improvement of dike reinforcement techniques and procedures. In designing dike reinforcements, the behaviour of the soft, often organic, sub soil plays an important role. This behaviour is complex, due to, among others, the sensitivity for creep and anisotropy in stiffness and strength. The sometimes complicated subsoil stress conditions below water retaining structures add to the complexity of predicting the strength behaviour under design conditions. A key aspect for the prediction is the availability of suitable calculation tools. Design of the innovative reinforcement techniques requires the use of finite element software, with appropriate constitutive models. For practical engineering purposes, the SHANSEP MC and SHANSEP NGI-ADP models (PLAXIS, 2016b, Panagoulias & Brinkgreve 2017) have therefore been developed within the POVM framework. These are total stress models, in which the maximum mobilised undrained shear strength is an input parameter that should be assessed by the user.

Within the POV-M programme, a fundamental study has been executed in parallel, in order to improve the understanding of soft, organic, soil behaviour. This fundamental study contains a numerical and experimental part. The document in hand reports on the numerical part, in which a new implementation of the Creep-SCLAY1 model has been build. This model is based on effective stress and accounts for creep and stress-induced anisotropy. The de-structuration part of the original model has been omitted, as de-structuration is considered irrelevant for soft organic soils. Omitting reduces the model complexity and increases its robustness. The new implementation includes also an improved iteration scheme, making the model more robust.

The report in hand describes the model background, gives implementation details, and discusses the results from first application. A thorough full validation of the implementation is not a part of this. A comparison of numerical simulations to the experimental data is required for that purpose. Due to time constraints however, the numerical and experimental parts of the fundamental study were executed in parallel. The required comparison has therefore to be conducted in future studies.

At its current state of development and validation, the implementation is considered suitable for further research purposes. The implementation can be used to analyse laboratory test data and to simulate complex behaviour in boundary value problems. This research usage is expected to yield a better understanding and improved modelling of the behaviour of soft, organic, soil. The implementation provides also a basis for potential further model improvement. After executing more validation and building more experience, the final application in daily engineering practice can follow.

Versie	Datum	Auteur	Paraaf Review	Paraaf	Goedkeuring	Paraaf
3	October 2018	dr.ir. C. Zwanenburg	ir. M.A.T. Visschedijk		ir. L. Voogt	
		dr.ir. J.A.M. Teunissen				
		A. Aboufirass				

State
final

Contents

Notation

CR	=	compression index for 1D loading conditions
C_α	=	creep parameter in $\log(t)$ - ε_v space
D	=	stiffness matrix
E	=	Young's modulus
e, e_0	=	void ratio, initial void ratio
f	=	yield function
G	=	shear modulus
K	=	bulk modulus
K_0^{nc}	=	ratio of horizontal to vertical stresses for normally consolidated conditions
M, M_{tc}, M_{te}	=	angle of critical state line in p', q space, idem for triaxial compression or triaxial extention
m	=	strength gain factor in equation (3.8)
OCR	=	overconsolidation ratio, based on vertical effective stresses, OCR = σ'_{vy}/σ'_v
n	=	number of steps
p'	=	isotropic stress
p'_{eq}, p'_p	=	p' at tip current state surface, CSS respectively normal consolidation surface, NCS, see Figure 2.3
q	=	deviator stress
r	=	extension ratio; $r = M_{te} / M_{tc}$
RR	=	re-compression index for 1D loading conditions
s_u	=	undrained shear strength
S	=	undrained shear strength ratio for normally consolidated conditions
t	=	time
v	=	specific volume, $v = 1+e$
α, α_0	=	orientation of the yield curve, initial orientation of the yield curve
$\alpha_{Ko, nc}$	=	orientation of the yield curve for K_0^{nc} conditions
β	=	ratio of compression indices; $\beta = (\lambda^* - \kappa^*)/\mu^*$
$\varepsilon, \varepsilon^e, \varepsilon^p$	=	strain, elastic strain, plastic strain
ε_{vol}	=	volume strain
γ	=	shear strain, volume weight
$\eta, \eta_{K0,nc}$	=	q/p', q/p' for K_0^{nc} conditions
$\varphi', \varphi'_{tc}, \varphi'_{te}$	=	friction angle, friction angle for triaxial compression, respectively extension conditions
κ	=	recompression index in $\ln(p')$ - ε_{vol} space
κ^*	=	modified recompression index in $\ln(p')$ - ε_{vol} space
λ	=	compression index in $\ln(p')$ - ε_{vol} space, visco-plastic multiplier
λ^*	=	modified compression index in $\ln(p')$ - ε_{vol} space
μ	=	creep index, in $\ln(t)$ - ε_{vol} space
μ^*	=	modified creep index in $\ln(t)$ - ε_{vol} space
ν'	=	Poisson ratio
θ	=	Lode angle
σ	=	stress
σ'_v	=	vertical effective stress
σ'_{vy}	=	vertical yield stress
τ	=	reference time, $\tau = 1$ day
ω, ω_d	=	rotational hardening parameters, see equation (2.4)

1 Introduction

1.1 Background

The research programme POV-Macro stability, POV-M supports the introduction of innovative dike reinforcement techniques. One of the conditions for introduction of new techniques is the availability of calculation tools. Therefore, within the POV-M a taskforce "rekencluster" is initiated to give guidelines how to use available calculation tools and techniques for new innovative reinforcement techniques and develop new calculation tools when needed.

One of the main topics of the POV-M programme is the applicability of hard elements like sheet pile walls in dike reinforcements. In designing this type of dike reinforcements the use of finite element calculation techniques is inevitable. In these calculations the constitutive model plays an important role. For engineering practice the SHANSEP MC and the SHANSEP NGI-ADP models (PLAXIS, 2016b, Panagoulias & Brinkgreve, 2017) are developed within the POV-M research programme. These models are based on a total stress approach in which undrained shear strength and shear strength development are prescribed by the user.

A typical sub-soil profile along the Dutch rivers contains soft organic clays and peats. Material behaviour of organic clays and peats is complex. The strong susceptibility for creep, stress induced anisotropy and shear induced pore pressure makes it difficult to properly estimate the undrained shear strength parameters required for the total stress models. The application to water retaining structures adds an extra complexity due to stress rotation induced by the presence of the dike body, the reduction in effective stresses under design conditions and the interaction between soft soil and the hard elements like sheet pile walls. In order to be able to make proper choices on the undrained shear strength development, required for design calculations, the POVM started a fundamental study on soft soil behaviour. This study is referred to as "fundamenteel spoor". This fundamental study should be seen as a step in the direction of better understanding soft, organic, soil behaviour. The aim of the fundamental study is not to yield already a final result, with proven applicability for engineering practice. Further studies and development will be needed for that purpose.

The fundamental study contains an experimental part and a numerical part. Due to time constraints both parts were run in parallel. In the numerical part, it was therefore not possible to use the results of the experimental part for verification purposes. This needs to be done in a follow-up study.

This report describes the results of the numerical part, in which a new implementation of a constitutive model Creep-SCLAY1 is build. This model is a Cam Clay type model, based on effective stresses, which is able to simulate stress induced anisotropy and creep. Background information on the Creep-SCLAY1 model is given by Wheeler et al, (2003), Karstunen et al (2005), Leoni et al (2008), Grimstad et al (2010), Karstunen et al (2012), Sivasithamparam (2012) and (2015).

At present stage the new implementation is meant for research purposes and not (yet) for practical engineering. The availability of the implementation will allow:
- Studying fundamental soil behaviour by comparing single stress point analysis to laboratory test data with the aim to improve parameter assessment for simpler models.

- Studying complex soil behaviour, for example in soil structure interaction, for boundary value problems. This can be used to validate practical and simpler to use models and working procedures.
- To provide a platform for future extensions when new ideas about modelling soft soil behaviour become available.

In contrast to the original Creep-SCLAY1 implementation the new implementation will not consider de-structuration. De-structuration is not considered relevant for modelling the behaviour of organic soils. Neglecting the de-structuration makes the model easier to implement and more robust to use. Also, the new implementation uses a more robust numerical integration scheme and description of the yield curve in the π-plane.

As explained above the new implementation of the Creep-SCLAY1 model is a step in the study on soft, organic, soil behaviour. At this stage the implementation is meant to be used for research and not (yet) for practical engineering. This report gives a description of implemented mathematical formulations and shows the results of first simulations using the new implementation. These simulations illustrate the features of the model, however the simulations are not a thorough validation of the model. Nor is the report meant as a detailed manual for the use of the model and parameter assessment. This will be addressed in later studies when the results of the above mentioned experimental study are available.

1.2 Aim of this report

The aim of this report is to describe the model background and implementation details, as well as to present first analysis results of model usage. As mentioned already, this report does not describe a full verification. The report is also not intended to give guidance for application in engineering practice.

The application analysis described in this report consists of four steps. The first step makes a comparison to reported simulations by the original implementation of the model. The second step compares the dependency of the simulated undrained shear strength, s_u on the overconsolidation ratio OCR to the SHANSEP formulation, Ladd (1991). The third step tests the robustness of the model for a series of loading conditions and model parameters. The fourth step tests the time dependent behaviour of the model in a boundary value problem.

The reason behind the second step is the prescribed usage of undrained strength according to Ladd in dike stability analysis (OI2014v4 [Min. I & M. (2017)]). The undrained shear strength s_u shows a dependency on the overconsolidation ratio, OCR, which is of importance for dike stability where effective stresses decrease during high external water loads. With only a few constitutive models available to correctly deal with overconsolidated behaviour verification of the implementation for overconsolidated conditions will improve its applicability.

1.3 Report set-up

Chapter 2 of this report discusses the main features of the Creep-SCLAY1 model. These features are discussed in simplified stress space given by the isotropic effective stress p' and deviatoric stress *q*. The exact implemented formulation using the complete stress and strain vector is given in Appendix A. Chapter 3 and 4 discuss applications. Single stress point simulations are discussed first. A comparison to previously reported simulations is followed by a verification of the OCR dependency of the undrained shear strength, s_u and a large series of simulations to test the robustness of the implementation. The individual results of this series is given by Appendix B. The application of the model in a boundary value problem is presented thereafter.

The boundary value problem focusses on the time dependent behaviour of the model. The simulations are compared to the model D-Settlement [Deltares, 2016]. The detailed results of the boundary value problem are given in appendix C. Chapter 5 gives conclusions and recommendations

2 Theoretical background

2.1 Introduction

This chapter gives a brief introduction to the Creep-SCLAY1 model and provides a definition of the main parameters. Details of the exact implementation are given in Appendix A. The next sections first discuss the main features of the model; the modelling of anisotropy, rotational hardening, the modelling of creep and the shape of the yield curve in the π-plane. This chapter finalises with a discussion of the parameter values selected for the verification analysis.

The mathematical background of the model is described in Wheeler et al. (2003), Leoni et al. (2008), Grimstad et al (2010), Sivasithamparam (2012), Sivasithamparam et al (2013), Sivasithamparam et al (2015)

2.2 Stiffness parameters

The Creep-SCLAY1 model can be considered as an advanced version of the Modified Cam Clay model, MCC (a.o. Wood 1990). Equivalent to the MCC model elastic, reversible, deformations and plastic, irreversible deformations are distinguished. The Creep-SCLAY1 model incorporates an isotropic, non-linear elastic behaviour to model the reversible deformations

The Creep-SCLAY1 model simulates anisotropy by moderating the plastic strain development as explained in section 2.3. The type of anisotropy modelled by the Creep-SCLAY1 model can be considered as stress induced anisotropy. Theoretically, an anisotropic elastic model could be implemented. However the combination of anisotropic elasticity and stress induced anisotropy would make the model very complex, see Wheeler et al. (2003).

The Creep-SCLAY1 model uses the modified elastic compression index κ^*, the modified plastic compression index, λ^* and the Poisson ratio, ν, as input for stiffness parameters. The bulk modulus K and shear modulus G are derived from the input parameters as explained in appendix A. The derivation of creep strain is explained in section 2.4.

The modified compression indices κ^* and λ^* are based on the volume strain rather than void ratio, as shown by Figure 2.1 and equation (2.1). Since in engineering practice laboratory test results are often presented as a function of strain rather than void ratio, the use of modified compression indices simplifies parameters assessment. Although, if the initial void ratio, prior to the start of the laboratory test is known, the compression indices are easily calculated from the modified indices. The Deltares Creep-SCLAY1 implementation requires the initial void ratio, e_0 as an input parameter. This allows the calculation results to be plotted as a function of void ratio. However, the void ratio is not used in the implemented constitutive relations.
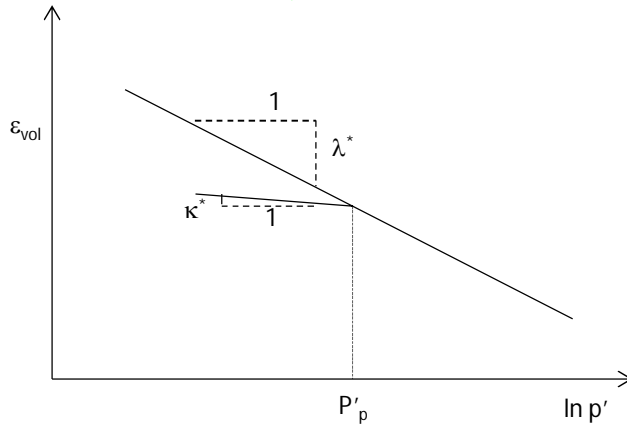
POV MACRO STABILITEIT

Figure 2.1   Definition of modified compression indices κ^*, λ^* and isotropic yield stress p'_p

$$\varepsilon_{vol} - \varepsilon_{vol}^0 = \lambda^* \ln\left(\frac{p'}{p'_0}\right), \quad \text{(normal compression)}$$

$$\varepsilon_{vol} - \varepsilon_{vol}^0 = \kappa^* \ln\left(\frac{p'}{p'_0}\right), \quad \text{(unloading - reloading conditions)} \quad (2.1)$$

$$\lambda^* = \frac{\lambda}{1+e_0}, \quad \kappa^* = \frac{\kappa}{1+e_0}$$

In which,

ε_{vol}, ε_{vol}^0 = volume strain, respectively initial volume strain
e_0 = void ratio
p, p' = isotropic stress, respectively effective isotropic stress

2.3   Anisotropic yield function

In stress space the elastic zone is bounded by a yield envelope, later also referred to as Normal Compression Surface, NCS. The Creep-SCLAY1 model describes plastic anisotropy by allowing rotation of the yield curve as depicted by Figure 2.2. In the isotropic stress space the yield function, *f*, describing the yield envelope in *p' - q* space, is given by (Dafalias, 1987; Wheeler et al, 2003):

$$f = \left(q - \alpha p'\right)^2 - \left(M^2 - \alpha^2\right)\left(p'_p - p'\right)p' = 0 \quad (2.2)$$

In which:

p' = isotropic effective stress
q = deviator stress
M = critical state value of the stress ratio *q/p'*, see Figure 2.2
α = rotation of the yield curve, see Figure 2.2
p'_p = *p'* at the tip of the yield curve, see Figure 2.2

POV MACRO
STABILITEIT
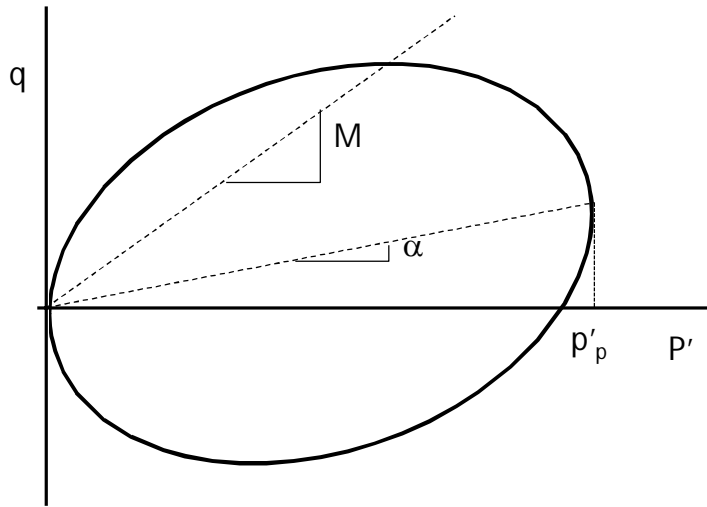

q

M

α

p'_p P'

Figure 2.2   Yield curve, or Normal Compression Surface, NCS, definition of M, α and p'_p

Equivalent to the MCC model, the Creep-SClay1 model assumes associative behaviour. This means that the direction of the plastic principal strain vector is always perpendicular to the yield surface. The yield curve has vertical tangents.(meaning purely volumetric plastic deformation) at the origin and at the point $q/p' = \alpha$ in which $p' = p'_p$. At $q/p' = M$ and $q/p' = -M$ the yield curve has horizontal tangents, meaning purely plastic shear deformation. The inclination α is a measure for the degree of plastic anisotropy. For $\alpha = 0$, the yield curve reduces to the modified cam clay, MCC, yield curve.

The model incorporates two hardening laws. The first hardening law controls the size of the yield curve, following Wheeler et al. (2003):

$$dp_p = \frac{p_p d\varepsilon^p_{vol}}{\lambda^* - \kappa^*}$$

(2.3)

In which $d\varepsilon^p_{vol}$ represents the plastic volume strain increment. This hardening law is equal to the MCC model. Equivalent the MCC model, negative increments of **d**p_p (softening) will occur on the part of the yield surface above the critical state line, due to plastic dilatancy.

The second hardening law controls the rotation of the yield curve, the rotational hardening law. Following Wheeler et al (2003), Dafalias & Taiebat (2013, 2014) the rotational hardening law is given by:

$$d\alpha_d = \omega\left\{\left(\frac{3q}{4p'} - \alpha\right)\langle d\varepsilon^p_{vol}\rangle + \omega_d\left(\frac{q}{3p'} - \alpha\right)d\gamma^p\right\}$$

(2.4)

In which

$\langle \; \rangle$ = McCauley brackets; $\langle d\varepsilon^p_{vol}\rangle = d\varepsilon^p_{vol}$ if $d\varepsilon^p_{vol} > 0$ and $\langle d\varepsilon^p_{vol}\rangle = 0$ if $d\varepsilon^p_{vol} < 0$

$d\gamma^p$ = plastic shear strain increment

$\omega, \; \omega_d$ = rotational hardening parameters

POV
MACRO
STABILITEIT

Following equation (2.4), the yield curve rotation and hence the plastic anisotropy is induced by both, plastic volume strain increments, $d\varepsilon^p_{vol}$ and plastic shear strain increments, $d\gamma^p$. The rotational parameter ω controls the rotation rate. For $\omega = 0$, the yield curve rotation remains constant and plastic anisotropy will not evolve. The rotational hardening parameter ω_d describes the contribution of $d\gamma^p$ relative to the contribution of $d\varepsilon^p_{vol}$ on the rotation hardening. For $\omega_d = 0$, the rotational hardening is only caused by plastic volume strain increments. For $0 < \omega_d < 1$, the plastic volume strain increment has relatively larger impact than the plastic shear strain increment. For $\omega_d > 1$, the plastic shear strain increments have relatively a larger impact.

The components $3q/4p'$ and $q/3p'$ represent the target values for α. These target values are derived from probing tests on Otaniemi clay, Näätänen et al. (1999), Wheeler at al, (2003) and might be soil type dependent. Future research needs to be conducted to confirm the use of these target values for (Dutch) organic soils.

For $\omega_d = 0$, α will reach a value close to $3q/4p'$. A special condition is found for isotropic stress paths. For isotropic stress paths q and $d\gamma^p$ are 0 resulting in the target value $3q / 4p' = 0$. As consequence α will reduce to $\alpha = 0$ for isotropic stress paths. When reaching critical state conditions, plastic shear strain will dominate the deformation behaviour and α will reach $\alpha = q/3p'$. Since, by definition, at critical state condition $q/p' = M$, $\alpha = M/3$ will be reached for critical state conditions.

The Creep-SCLAY1 model uses an associated flow rule, meaning that the plastic strain increments are perpendicular to the yield curve.

2.4 Creep

Following Vermeer et al (1998), Vermeer & Neher (1999), Leonie et al (2008), Sivasithamparam (2012), time dependent viscoplastic behaviour, creep, is modelled by the use of two surfaces. The first surface is the normal consolidation surface, NCS. The NCS is equivalent to the yield contour shown by Figure 2.2. Stress conditions inside the NCS represent the unloading – reloading conditions. The stress conditions on the NCS represent normal consolidated behaviour. The second surface is the current state surface, CSS. The CSS has the same shape and orientation as the NCS and runs through the actual stress condition. For overconsolidated conditions the CSS lays within the NCS. For normal consolidated conditions the CSS lays on top of the NCS.

The isotropic stress at the tip of the NCS is referred to as p'_p, while the isotropic stress at the tip of the CSS is referred to as p'_{eq}, see Figure 2.3.
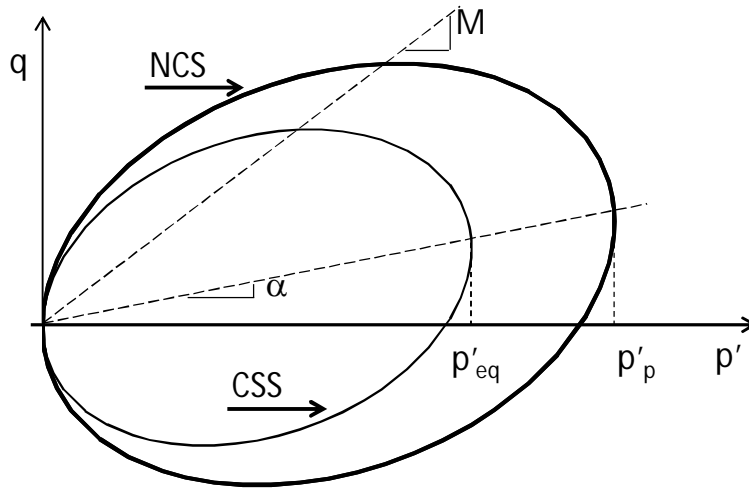
Figure 2.3   Definition sketch of Current Stress Surface, CSS and Normal Compression Surface, NCS

The Creep-SCLAY1 model adopts the isotache concept in modelling creep strain rates, following Leoni et al. (2008):

$$\frac{d\varepsilon_{vol}^c}{dt} = \frac{\mu^*}{\tau}\left(\frac{1}{OCR^*}\right)^{\beta}$$

(2.5)

In which:

$\dfrac{d\varepsilon_{vol}^c}{dt}$ = volume strain rate due to creep

μ^* = modified creep parameter; $\mu^* = C_\alpha / \ln(10)$

τ = reference time, τ = 1 day

β = creep exponent, $\beta = (\lambda^* - \kappa^*)/\mu^*$

OCR^* = ratio p'_p / p'_{eq}

The parameter OCR^* gives the relative difference in size between NCS and CSS. The working of the isotache concept is illustrated when considering a constant load. For a constant load the NCS will develop in time, see equation (2.3) as a result, OCR^* increases in time leading to a reduction in creep strain rate, $d\varepsilon^c_{vol}$ /dt.

In applying equation (2.5) in the Creep-SCLAY1 model, Grimstad (2009), Grimstad et al (2010) and Sivahamparam (2012) is followed:

$$\frac{d\underline{\varepsilon}_{vol}^c}{dt} = \Lambda\frac{\partial p_{eq}}{\partial\underline{\sigma}},$$

$$\Lambda = \frac{\mu^*}{\tau}\left(\frac{p'_{eq}}{p_p}\right)^{\beta}\left(\frac{M_{tc}^2 - \alpha_{K_0^{nc}}^2}{M_{tc}^2 - \eta_{K_0^{nc}}^2}\right)$$

(2.6)

POV MACRO STABILITEIT

In which:

Λ	=	plastic multiplier
M_{tc}	=	ratio q/p' for critical state conditions in triaxial compression
$\eta_{K0,nc}$	=	ratio q/p' for K_0^{nc} stress path, by definition $\eta_{K0,nc} = 3(1-K_0^{nc})/(1+2K_0^{nc})$
$\alpha_{K0,nc}$	=	yield curve rotation reached when following K_0^{nc} stress path

The parameter $\alpha_{K0,nc}$ is found under the assumption that the elastic strains are much smaller than the plastic strains and that the ratio deviatoric and volumetric strain, $d\varepsilon_d / d\varepsilon_v$ equals 2/3, Wheeler et al. (2003):

$$\alpha_{K_0^{nc}} = \frac{\eta_{K_0^{nc}}^2 + 3\eta_{K_0^{nc}} - M^2}{3} \tag{2.7}$$

It should be noted that the ratio $d\varepsilon_d/d\varepsilon_v$ equals 2/3 under one-dimensional confined compression conditions, when the plastic volumetric strain increment equals the plastic normal strain increment. The parameter $\alpha_{K_0^{NC}}$ ensures therefore that the K_0^{NC} ratio will be preserved during one-dimensional (visco)plastic confined compression.

When assuming Jacky's formula, $K_0^{nc} = 1-\sin(\varphi')$, the parameter $\alpha_{K0,nc}$ is directly related to the friction angle φ'. As an illustration for equation (2.7), when considering $\varphi' = 30°$ and $M_{tc} = M_{te} = M$, it follows that $\eta_{K0,n} = 0.75$ and $\alpha_{K0,nc} = 0.46$.

2.5 Modelling strength behaviour in the deviatoric plane

In the new implementation, the shape of the yield curve in the deviatoric plane (π-plane) is described by a novel formulation, equation (2.8), which can be considered as a generalization of the Matsuoka – Nakai surface (Matsuoka & Nakai, 1974).

$$M(\theta) = M_{tc} \frac{\cos\left(\frac{\pi}{3} - \arctan\left(\frac{2r-1}{\sqrt{3}}\right)\right)}{\cos\left(\frac{1}{3}\arccos\left(\cos\left(3\arctan\left(\frac{2r-1}{\sqrt{3}}\right)\right)\sin 3\theta\right)\right)} \tag{2.8}$$

In which θ_α denotes the Lode angle and $r = M_{tc} / M_{te}$, in which M_{tc} and M_{te} represent the ratio q/p' for critical state conditions in triaxial compression respectively triaxial extension. Details of this new formulation are to be published later.

In contrast to the formulation used in the original implementation, see Sivahamparam (2012, equation (2.8) ensures a convex surface and is therefore more robust. Figure 2.4 shows a comparison between equation (2.8) and the Drucker – Prager, Mohr – Coulomb and Matsuoka – Nakai surfaces.
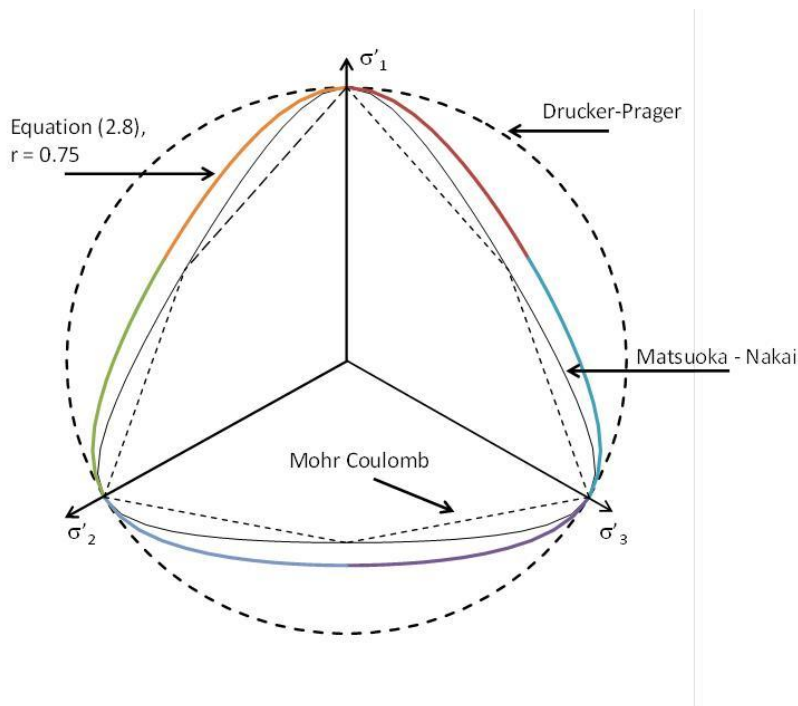
Figure 2.4 Comparison of equation (2.8) to Mohr-Coulomb, Matsuoka-Nakai and Drucker – Pager surfaces in π-plane, for α = 0.

Figure 2.5 shows the π-plane surface for four special values for *r*. The first value is *r* = 1.0, for which equation (2.8) reduces to Drucker – Prager contour. The second value is *r* = (3 − sin(φ'_{tc})) / (3 + sin(φ'_{tc})), for which equation (2.8) coverts to the Matsuoka – Nakai surface. The third value is *r* = 0.5, for which the π-plane surface reduces to a triangular shape with the triaxial compression points at the corners of the triangle. The fourth value is *r* = 0.4 is added for illustration purposes. The value for *r* is bounded by 1.0 ≥ *r* ≥ 0.5. It should be noted that this constraint holds for all π-plane criteria. Figure 2.5 shows that for r < 0.5, the compression strength predicted by equation (2.8) is smaller than M_{tc}.

It should be noted that the software allows for the value *r* = -1. For *r* = -1 the Matsuoka - Nakai surface is adopted using $r = \dfrac{3 - \sin\left(\varphi'_{tc}\right)}{3 + \sin\left(\varphi'_{tc}\right)}$. This option is frequently used in appendix B and C.
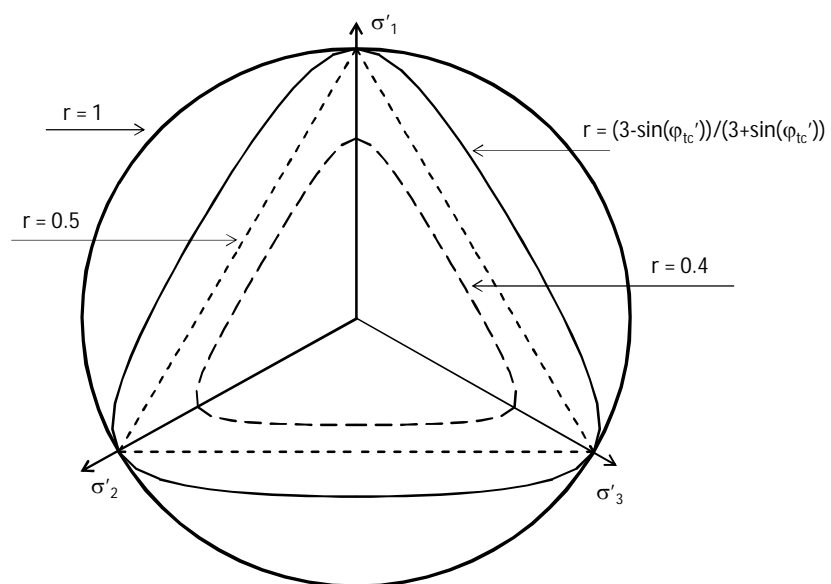
Figure 2.5   Shape π-plane surface for different values for r following equation (2.8), for $\alpha = 0$.

3 First applications

3.1 Parameter assessment

Besides the general parameters unit weight, γ and permeability, k, the implemented Creep-SCLAY1 model requires the following 11 parameters:

κ^{*} = unloading – reloading index in the ε_{vol} – ln(p') space, [-]

λ^{*} = normal compression index in the ε_{vol} – ln(p') space, [-]

μ^{*} = creep parameter, follows from the ε_{vol} – ln(t/τ) response, [-]

τ = reference time, [day], default τ = 1 day.

ν = Poisson ratio, [-]

φ'_{tc} = friction angle in triaxial compression, [-]

r = ratio M_{tc} / M_{te}, with M_{tc} = q/p' for critical state conditions in triaxial compression and M_{te} = q/p' for critical state conditions in triaxial extension, [-]

ω, ω_d = rotational hardening parameters, [-]

α_0 = initial yield curve rotation

OCR = ratio p'$_p$/ p'$_{eq}$, for initial stress conditions [-]

e_0 = initial void ratio, [-]

The initial void ratio, e_0, is only required to allow graphical output in which user-selected parameters can be plotted as a function of void ratio. The void ratio is not used by the model.

This section discusses the parameters applied for the validation calculations discussed in the following sections. The parameter selection is based on laboratory tests conducted on remoulded Oostvaardersplassen Clay, OVP. The OVP clay is a plastic organic clay with the following characteristics:

Water content, w   = 113 %

Plastic limit   = 165 %

Liquid limit   = 56 %

Plasticity index   = 110 %

Organic content   = 9.5 %

Since only the results of K_0- CRS test were available, when conducting the validation analysis, the parameters were selected based on only the K_0- CRS results. It should be noted that at this stage the validation is focussed on the behaviour of the model for realistic soil parameters. In future research, when more laboratory tests are available, simulations of test results will be conducted.

The K_0 –CRS test has the ability to measure the horizontal stress development during the tests (Den Haan & Kamao, 2003) and therefore provides the option to determine κ^{*}, λ^{*} and μ^* directly. The parameters κ^{*} and λ^{*} follow from the slope of the ε_{vol} – ln(p') space, see Figure 3.1. The value for μ^* follows from curve fitting the relaxation phase of the K_0-CRS tests, according to Den Haan & Kamao (2003), see Figure 3.2. The initial void ratio of this tests is e_0 = 3.02.

For the Poisson ratio, the default value, ν = 0.15 is selected. The following stiffness parameters are found:

POV
MACRO
STABILITEIT

$\kappa^* = 0.01149$
$\lambda^* = 0.1134$
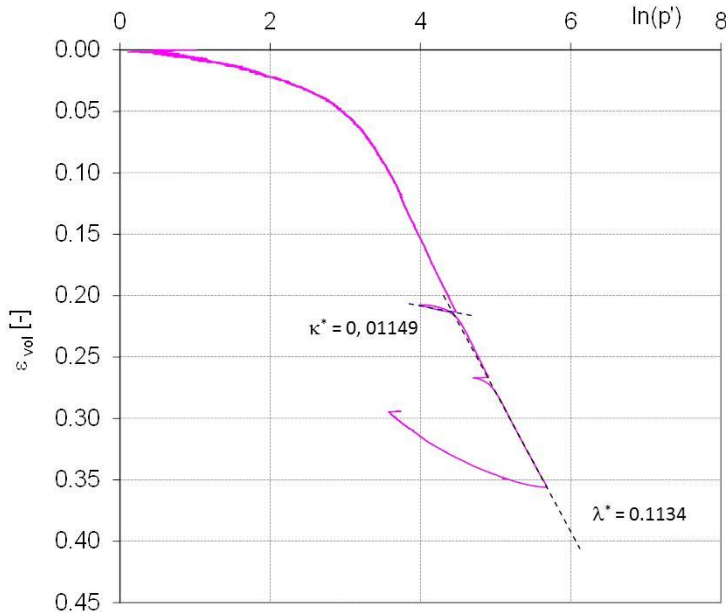$\mu^* = 0.0065$
$\nu = 0.15$

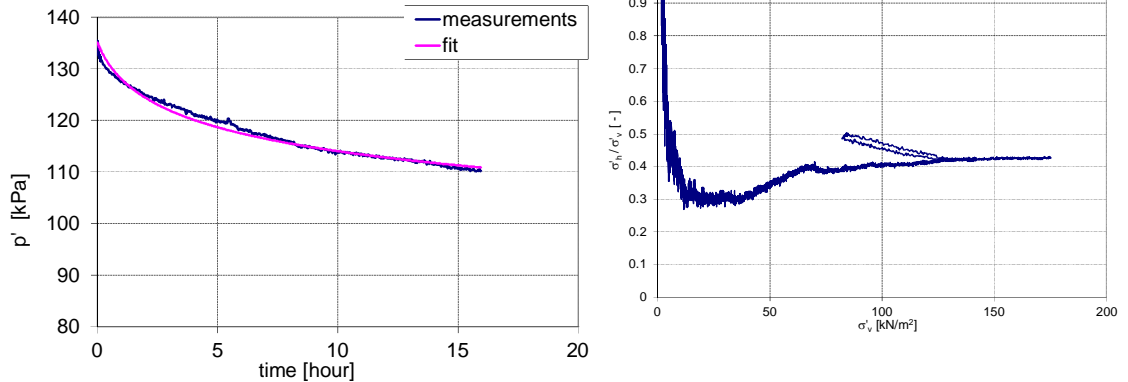Figure 3.1 Derivation of λ^* and κ^* from K_0-CRS test

Figure 3.2 Results of K_0 CRS tests, left hand side, comparison of simulated and measured decay in p' during relaxation, for $\mu^* = 0.0065$; right hand side, the development of σ'_h / σ'_v during the test.

The friction angle φ'_{tc} is estimated from the measured K_0 using the Jacky relation, $K_0^{nc} = 1-\sin(\varphi')$. Figure 3.2 shows that $K_0^{nc} = 0.42$, indicating $\varphi'_{tc} = 35°$.

No information on the friction angle for triaxial extension conditions was available when conducting the validation tests. The value for $r = M_{te} / M_{tc}$ is selected as the one that represents the Matsuoka-Nakai fit on the Mohr-Coulomb yield surface:

$$r = \frac{3-\sin\left(\varphi'_{tc}\right)}{3+\sin\left(\varphi'_{tc}\right)}$$ (3.1)

For $\varphi' = 35°$ follows from equation (3.1) $r = 0.68$.

POV MACRO STABILITEIT

The stiffness parameters κ^*, λ^* and ν are used in different Cam Clay- type models, like Modified Cam Clay, Soft Soil and Soft Soil Creep model. Also, the parameters κ^*, λ^* and μ^* show a strong resemblance to the compression indices, RR, CR and Cα. The stiffness parameters can be considered as rather well-known parameters. Also the friction angle φ' can be considered as a well-known parameter, which can be selected with confidence. The rotational hardening parameters ω and ω_d and the initial yield curve rotation α_0 are typical for the SClay1-models and assessment of these parameters is relatively new. The validation discussed in chapter 3 and 4 is focussed on varying these parameters and studying the influence of the variation on the results.

Equation (2.7) gives already the α value that ensures that the K_0^{NC} stress path will be followed during confined plastic compression, under the condition that the stress point is already on the K_0^{NC} path after reloading to the normally consolidated state. This α value is therefore also a suitable initial value, as indicated by Wheeler et al. (2003)

$$\alpha_0 = \frac{\left(\dfrac{q}{p'}\right)^2_{K_0^{nc}} + 3\left(\dfrac{q}{p'}\right)_{K_0^{nc}} - M_{tc}^2}{3} \tag{3.2}$$

In which $(q/p')_{K0,nc}$ represent the ratio q/p' for K_0 consolidated conditions. By definition this ratio is given by:

$$\left(\frac{q}{p}\right)_{K_0^{nc}} = \frac{3\left(1 - K_0^{nc}\right)}{1 + 2K_0^{nc}} \tag{3.3}$$

$$M_{tc} = \frac{6\sin\left(\varphi'_{tc}\right)}{3 - \sin\left(\varphi'_{tc}\right)} \tag{3.4}$$

Follows that α_0 is a function of φ'_{tc}. For $\varphi'_{tc} = 35°$ is found $\alpha_0 = 0.55$.

Wheeler et al. (2003) also gives an expression for the rotational hardening parameter ω_d:

$$\omega_d = \frac{3}{8} \frac{4M_{tc}^2 - 4\left(\dfrac{q}{p'}\right)^2_{K_0^{nc}} - 3\left(\dfrac{q}{p'}\right)_{K_0^{nc}}}{\left(\dfrac{q}{p'}\right)^2_{K_0^{nc}} - M_{tc}^2 + 2\left(\dfrac{q}{p'}\right)_{K_0^{nc}}} \tag{3.5}$$

With equation (3.3) and (3.4) ω_d is a function of φ'_{tc}. For $\varphi'_{tc} = 35°$ is found $\omega_d = 0.96$.

Leoni et al. (2008) provide an estimation for the rotational hardening parameter ω:

$$\omega = \frac{1}{\lambda^*} \ln\left(\frac{10M^2 - 2\alpha_0\omega_d}{M^2 - 2\alpha_0\omega_d}\right) \tag{3.6}$$

It should be noted that equation (3.6) is an estimation based on, among others, the assumption that anisotropy is practically erased when α is reduced to 10 % of its original value. Applying the values for λ^*, α_0, M and ω_d gives $\omega = 26.3$.

Sivasithamparam et al (2013) concludes that for some parameter combinations might result in negative values, which have no physical meaning. This behaviour is explained by the validity of the assumptions made to derive equation (3.6) Instead for ω is suggested, following Zentar et al (2002):

$$\frac{10}{\lambda^*} \leq \omega \leq \frac{20}{\lambda^*} \tag{3.7}$$

Applying equation (3.7) to the OVP data results in $88 \leq \omega \leq 176$. It should be noted that result of equation (3.6), $\omega = 26.3$, falls beyond this range.

Finally, Den Haan (2014) shows simulations of laboratory tests on peat. The test results indicate negative values for α_0, ω and ω_d. Although a further experimental study is needed to support these findings, it may have consequences for the applicability of equations (3.2) to (3.7) for organic clays.

The applications in the following sections deal with testing some of the main features of the implementation. Therefore the calculations are focussed on testing the rotational hardening, the yield criterion in the π-plane and modelling creep. Parameter variation is applied for α_0, ω, ω_d, OCR and r, while stiffness and strength parameters are kept constant.

Parameter	unit	Value
λ^*	[-]	0.1134
κ^*	[-]	0.01149
μ^*	[-]	0.0065
ν	[-]	0.15
K_0^{nc}	[-]	0.4264
c'	[kPa]	0
φ'	[°]	35
r	[-]	[-1, 0.75, 1]
τ	[day]	1
e_0	[-]	3
α_0	[-]	[0, 0.25, 0.5, 0.75, 1.0]
ω	[-]	[0, 12.5, 25, 50, 100]
ω_d	[-]	[0, 0.5, 1, 2]
OCR	[-]	[1, 1.75, 2]

Table 3.1   Parameter values applied in the validation analysis

Table 3.1 shows the parameters used in the analysis. The derivation of the stiffness and strength parameters is explained in the text above. For the parameters α_0, ω, ω_d, OCR and r the applied range is shown. The actual parameters for the individual calculations are given in chapter 3 and 4.

The applied range in values is established considering that:

- For the extension ratio r the values r = -1, 0.75 and 1.0 are used. For r = -1 the yield surface in the π-plane equals to the Matsuoka – Nakai surface, resulting, for this case

POV MACRO STABILITEIT

in, in $r = 0.68$. For $r = 1$ the Drucker –Prager criterion is found. The value $r = 0.75$ is selected as an intermediate value.

- For the rotational hardening parameter ω, $\omega = 26.3$ is derived from the OVP-clay, following Leonie et al. (2008) and $88 \leq \omega \leq 176$, following Zentar et al (2002). The applied range is selected based on these values: $\omega = 0, 12.5, 25, 50$ and 100. It should be noted that for $\omega = 0$ no rotational hardening occurs.
- For the rotational hardening parameter ω_d is found $\omega_d = 0.98$ for the OVP-clay. Hence, the range of values is selected including one larger and two smaller values; $\omega_d = [0, 0.5, 1.0, 2.0]$. It should be noted that for $\omega_d = 0$, the yield curve still rotates, provided that $\omega > 0$. For $\omega_d = 0$ and $\omega > 0$, the rotational hardening only depends on the volumetric strain development. Also, for $\omega = 0$, the value for ω_d is irrelevant, see equation (2.4).
- For the initial yield curve rotation, α_0, is found $\alpha_0 = 0.5$ and a range of smaller and larger values is selected; $\alpha_0 = [0, 0.25, 0.5, 0.75, 1.0]$. It should be noted that for $\alpha_0 = 0$ and $\omega = 0$, the model reduces to an isotropic model.
- Formally consolidated and lightly overconsolidated behaviour is simulated by applying OCR = 1.0, 1.75 and 2.0.

3.2 Comparison to previous published work

Sivasithamparam et al. (2013) and Sivasithamparam et al. (2015) provide an example of the strain rate dependency of the undrained shear strength as found by the Creep S-Clay1 model in simulating triaxial compression tests. This section discusses the simulation of the same test conditions by the Deltares implementation. The applied parameters, see Table 3.2, correspond to parameters applied by Sivasithamparam et al (2013) and are based on the Bothkennar clay characteristics.

symbol	value	unit
κ^*	6.70E-03	[-]
λ^*	0.1	[-]
μ^*	5.07E-03	[-]
ν	0.2	[-]
φ_{tc}	36.87	[°]
r	1	[-]
ω	50	[-]
ω_d	1	[-]
τ	1	[day]
α_0	0.59	[-]
OCR	1.0	[-]

Table 3.2   Material model values for Bothkennar clay.

The applied initial stress level is $\sigma'_3 = 50$ kN/m^2 and $K_0 = 0.5$. It should be noted that Sivasithamparam et al. (2013) indicates that OCR = 1.5 and $\sigma'_3 = 100$ kN/m^2 have been used. However, for these values the results presented by Sivasithamparam et al. (2013) cannot be reproduced a perfect reproduction, using the original model, is found for OCR = 1.0 and $\sigma'_3 = 50$ kN/m^2, which is used in the further analysis.

A stepwise change in strain rate influences the stress – strain behaviour of undrained soils. Experimental evidence for this behaviour is given by among others Grimstad et al (2010) and Tatsuoka et al (2002). This verification tests if the new implementation reproduces the same behaviour as reported for the original Creep-SCLAY1 implementation.

POV MACRO
STABILITEIT

Figure 3.3 and Figure 3.4 show the stress strain behaviour for monotonous loading rates by the coloured, dotted lines in the left hand graph and thin red lines in the right hand graph. The strain rates shown represent 2%, 0.2 %, 0.02% and 0.002 %. In the simulation of the undrained shearing, the initial shearing rate is 2% per day followed by a reduction to 0.02% per day, an acceleration to 2% per day, a decline to 0.002 % per day and an acceleration to 0.2 % per day.
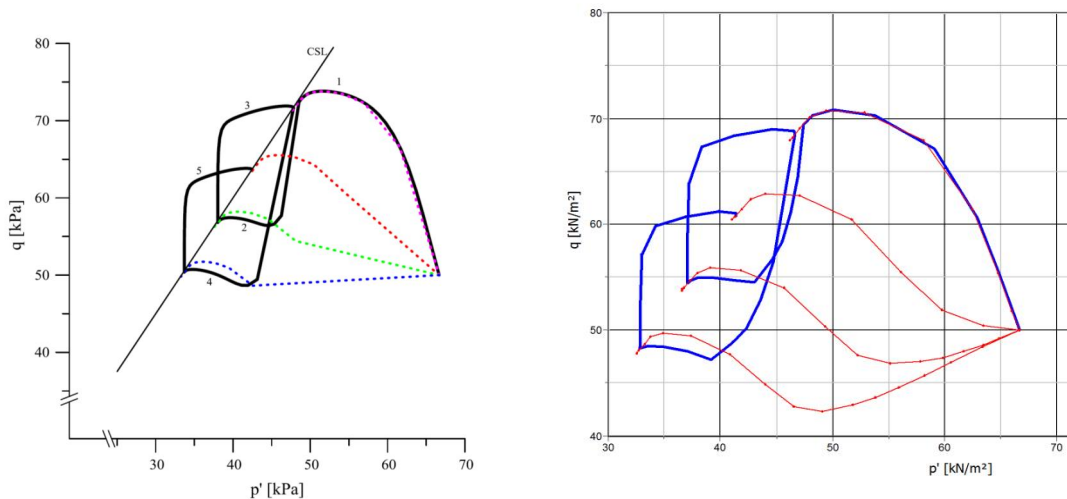

Figure 3.3   Stress paths for varying strain rates found by the Creep S-Clay1 simulations.Left hand side: from: Sivasithamparam et al. (2013), right: hand side: results Deltares implementation.
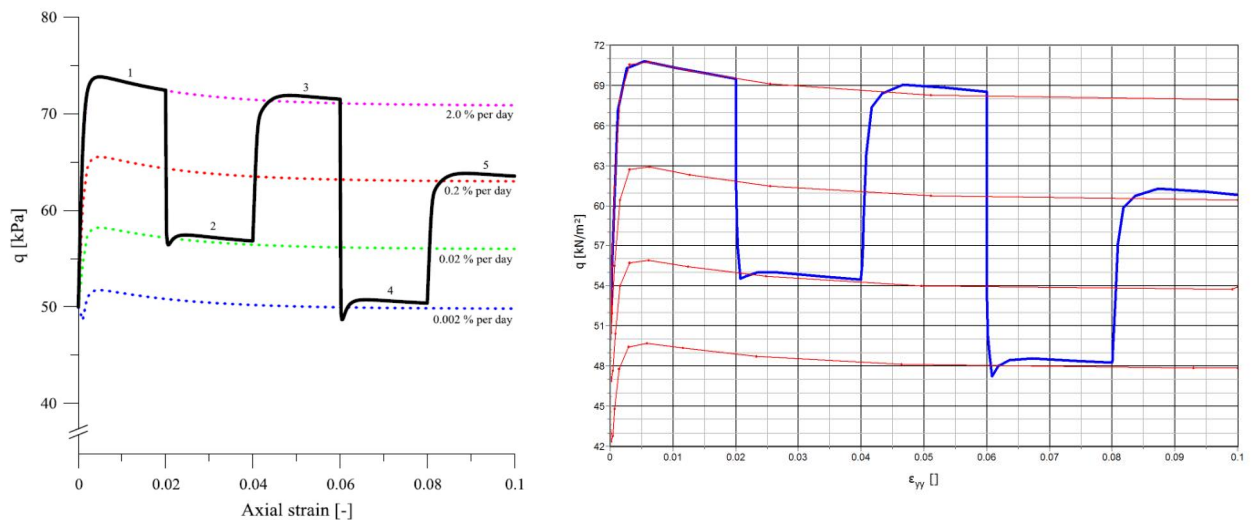
Figure 3.4   Stress – strain for undrained triaxial testing including varying strain rates found by the Creep S-Clay1 left: from: Sivasithamparam et al. (2013), right: results Deltares implementation.

Both models show that after each change in strain rate the stress path and stress – strain curves merge with the paths observed for the monotonous loaded samples. For loading cycles 1, 3 and 5, see left hand graph in Figure 3.4, the stress – strain curve shows a small decline in deviator stress at the end of these cycles. This, small, decline cannot clearly be seen in the stress path development. However at close inspection an equivalent minor decline in deviator stress can also be found in the stress paths at the end of cycles 1, 3 and 5.

POV MACRO STABILITEIT

It should be noted that the exact values for *p'* and *q* differ slightly between the original and new Creep-SCLAY1 implementation. More remarkable are the differences in stress paths for the monotonically loaded conditions. The dotted lines in left hand graph of Figure 3.3 show the monotonic response given by Sivahamparam et al (2013), hereafter referred to as the original model. For the strain rates of 0.2 %/day, 0.02 %/day and 0.002 %/day the original model shows an initial straight part is found followed by a curved development towards the critical state line. Only for the strain rate of 0.002 %/day an initial decay is found. The thin red lines in the right hand side graph of Figure 3.3 show the monotonic response of the new implementation. For the new implementation more curved stress paths are found. For the strain rates 0.02 %/day and 0.002%/day an initial decay is found.

The differences in observed monotonic behaviour are studied in more detail. A monotonic undrained triaxial compression is simulated in de Soil Test module available in the computer programme PLAXIS 2D 2017. The applied strain rate is 0.02 %/day to a maximum strain ε_{max} = 10 %, soil parameters are given in Table 3.2 and initial stress conditions, σ'_1 = 100 kN/m^2, σ'_3 = 50 kN/m^2.
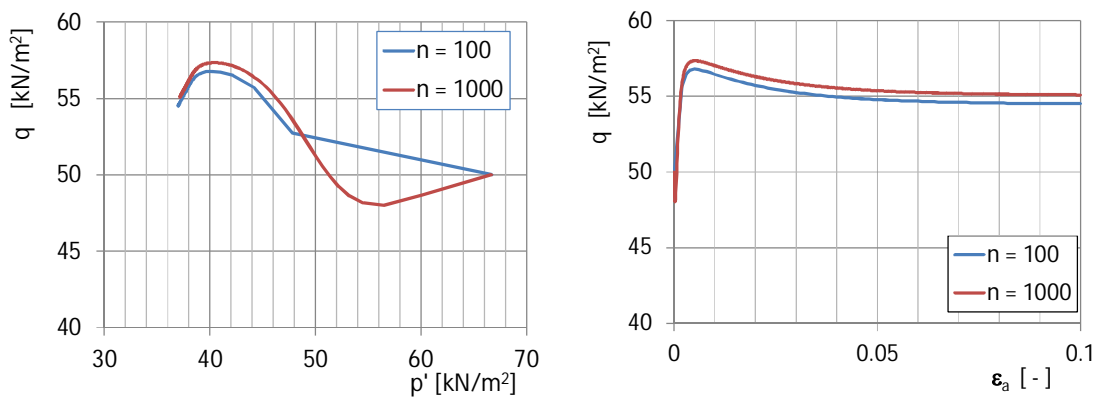
Figure 3.5   Simulations with original model, Sivahamparam (2013) for number of calculation steps, n = 100 and 1000. Left hand side; stress path. right hand side; stress – strain curve

Figure 3.5 shows two simulations with the original model. In the first simulation the number of calculation step is set to 100, which is the default value. In the second analysis the number calculation steps, *n*, is increased to 1000. The results for *n* = 100 corresponds to the results shown in the left hand graph in Figure 3.3. For *n* = 1000 a more curved stress path is found. Also for *n* = 1000 a slightly larger value for *q* is found at the end of the shearing stage.
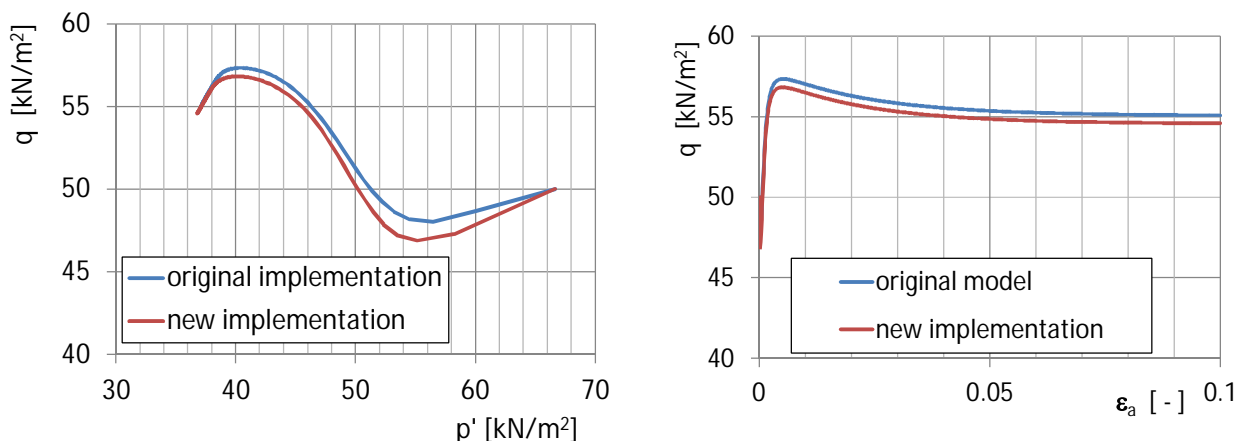
Figure 3.6   Simulations with the original model and new implementation, for n = 1000. Left hand side; stress path. right hand side; stress – strain curve

POV ⟳ MACRO STABILITEIT

Figure 3.6 shows a comparison between the original model and the new implementation. The shape of both predictions is the same, although there is a small difference in exact value for *q*. From Figure 3.5 and Figure 3.6 it is concluded that the differences observed in the simulations for the original model and the new implementation in Figure 3.3 and Figure 3.4 are mainly caused by differences in number of calculation steps or applied tolerated error.
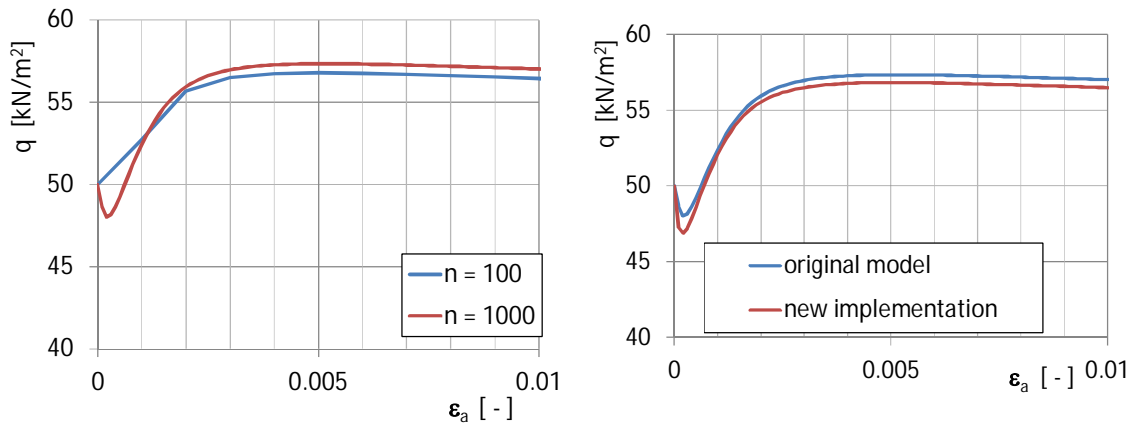

Figure 3.7   Stress strain curves zoomed in on the start of the shearing phase. Left hand graph, comparison between n = 100 and n = 1000 for original model, right hand graph comparison between the original model and new implementation for n = 1000.

Figure 3.7 zooms in on the origin of the stress – strain curve. For both, the original model and the new implementation the initial decline in *q* is clearly found. The initial decline in both *p'* and *q* can be explained by the initial creep rate in relation to the low shearing rate of 0.02 %/day. For increasing OCR and / or decrease in μ^* a reduction in initial creep rate will be found resulting in a smaller or no decline in *q* for a shearing rate of 0.02 %/day.

3.3 Verification of the OCR dependency of undrained shear strength s_u

This section verifies the OCR dependency of the simulated shear strength for undrained conditions by comparing simulation results to equation (3.8), Ladd (1991)

$$s_u = S\left(OCR\right)^m \sigma'_v \tag{3.8}$$

in which:
- s_u = undrained shear strength
- *S* = undrained shear strength ratio for normally consolidated conditions, S = $(s_u/\sigma'_{vy})_{NC}$.
- OCR = Overconsolidation ratio
- *m* = power
- σ'_v = vertical effective stress.

Wroth (1984) shows that based on the critical state soil mechanics the parameter *m* can be expressed as a function of the compression indices. Since the Cam Clay model can be considered as a 3D implementation of the CSSM, the parameter *m* can also be expressed as a function of the Cam Clay stiffness parameters:

$$m = \frac{\lambda^* - \kappa^*}{\lambda^*} \tag{3.9}$$

POV MACRO STABILITEIT

In which:
- λ^* = Cam Clay 3D compression index for normally consolidated conditions.
- κ^* = Cam Clay 3D compression index for unloading and reloading conditions.

Since the Creep S Clay1 model is an advanced Cam clay type model, it is to be expected that the model reproduces equation (3.8) in combination with equation (3.9). In the following this expectation is verified by running several simulations of undrained triaxial tests by the Deltares implementation for different OCR values.

parameter	unit	values
volume weight, γ	[kN/m^3]	13,14
compression index, λ^*	[-]	0.1134
recompression index, κ^*	[-]	0.01149
creep index, μ^*	[-]	0.0065
poison ratio, ν	[-]	0.15
friction angle, φ'	[°]	35
extension ratio, r	[-]	1

Table 3.3   Applied soil parameters

The simulations of an anisotropically consolidated undrained triaxial test are conducted using the *Soil Test* module, PLAXIS 2D 2016. Table 3.3 shows the parameters that were kept constant in all simulations. The applied boundary conditions are given by Table 3.4. Table 3.5 shows the applied values for α, ω and ω_d for the cases 1 to 5. For each case simulations are made for OCR = 1.0, 1.25, 1.5, 2 and 5.

condition	unit	value
initial ratio hor. and vertical stress	[-]	0.68
lateral consolidation stress, $\sigma_{3,c}$	[kN/m^2]	50
maximum applied shear strain, ε_{max}	[%]	25
test duration	[day]	1
number of steps, n	[-]	500

Table 3.4   Boundary conditions for the undrained triaxial test simulations

parameter	case 1	case 2	case 3	case 4	case 5	case 6
α	0	0.5	0	0	0	0.5
ω	0	0	25	25	100	25
ω_d	0	0	0	1	1	1

Table 3.5   Applied values in α, ω, ω_d for the cases 1 to 5.

OCR	s_u/σ'_{vi} [-]					
	case 1	case 2	case 3	case 4	case 5	case 6
1	0.38	0.41	0.40	0.50	0.50	0.40
1.25	0.46	0.50	0.48	0.61	0.61	0.49
1.5	0.55	0.58	0.55	0.72	0.72	0.57
2	0.71	0.76	0.71	0.93	0.93	0.74
5	1.61	1.72	1.61	2.12	2.12	1.69

Table 3.6   Simulation results

POV MACRO STABILITEIT
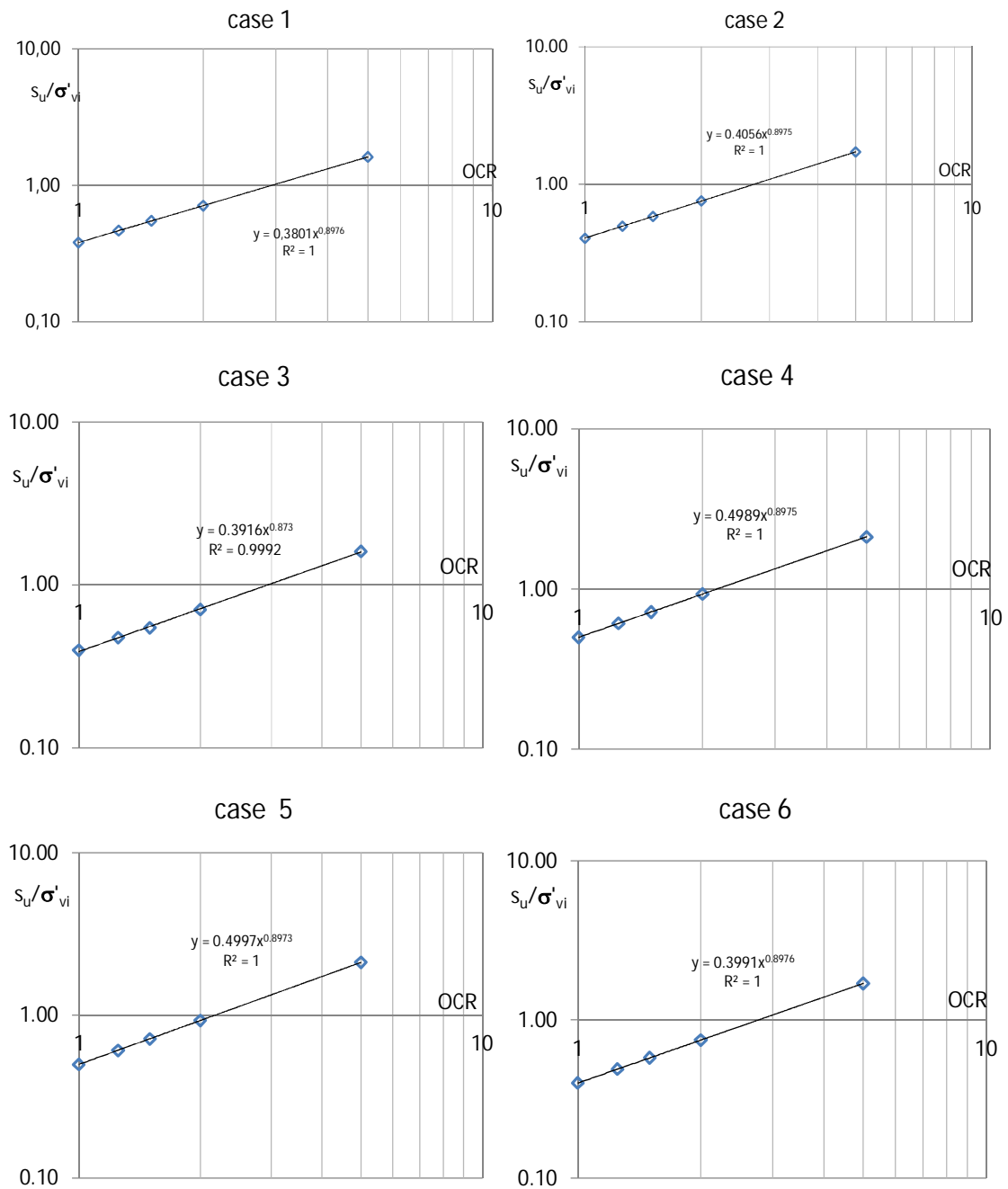
Figure 3.8   Simulation results

case	S [-]	m [-]	R² [-]
1	0.38	0.898	1.00
2	0.41	0.898	1.00
3	0.39	0.873	0.999
4	0.50	0.898	1.00
5	0.40	0.897	1.00
6	0.40	0.898	1.00

Table 3.7 Comparison of simulation results to equation (3.8), R^2 representing least squares sum

POV MACRO STABILITEIT

Table 3.6 and Figure 3.8 show the simulation results, Table 3.7 give a comparison of the results to equation (3.8). The comparison is made by fitting the simulation results for each case, using the excel automated least squares option. The fit is also shown by Figure 3.8. The applied variations in α, ω and ω_d mainly result in a variation of S. The value for parameters m is fairly constant for the different cases. It should be noted that from the applied stiffness parameters follows, $m = (\lambda^* - \kappa^*)/\lambda^* = 0.899$.

The different cases show a good agreement with equation (3.8) and (3.9). Case 3 shows some deviation. To investigate the nature of this deviation, a smaller value for ω is applied in case 5, leading to a closer agreement with equation (3.8). The simulations show that the model reproduces equation (3.8) in combination with equation (3.9) correctly.

It should be noted that Wroth (1984) also provides equations for the evaluation of undrained shear strength ratio for normally consolidated conditions, S. In follow-up studies these equations should be used to validate the prediction of the parameter S by the Creep-SCLAY1 model. Also the influence of the parameters α_0, ω and ω_d on the parameter S will be studied follow-up studies.

3.4 Laboratory test simulations

Appendix B shows a number of laboratory test simulations. The simulations are conducted using the Soil Test module of the computer programme PLAXIS. For comparison reasons some simulations are also conducted as a boundary value problem.

The applied conditions are given in Table 3.9 and contain simulations of triaxial compression test, a biaxial test and a Direct Simple Shear test. Simulation of triaxial compression tests is chosen, as it is one of the conventional tests for geotechnical parameter assessment in engineering practice. Simulation of Direct Simple Shear tests is chosen as this type of test is one of the few geotechnical tests in which a shear stress is actively applied on the sample. Typically for a direct simple shear test a rotation in principal stress direction will occur. This is significantly different from triaxial testing. Biaxial testing is rarely used in engineering practice for parameter assessment. However, the biaxial test is one of the very few geotechnical tests for which the tested sample is not axi-symmetric. The plane strain conditions of the test comply with the boundary conditions usually applied in stability analysis in engineering practice.

The results are given by appendix B. The applied soil parameters are selected in accordance to section 3.1. In the simulations mainly the rotational hardening has been tested by varying the values for α_0, ω, and ω_d. Simulations have been made for normally consolidated conditions OCR = 1.0 and over-consolidated conditions, OCR = 2.0.

Parameter	unit	Value
λ^*	[-]	0.1134
κ^*	[-]	0.01149
μ^*	[-]	0.0065
ν	[-]	0.15
K_0^{nc}	[-]	0.4264
c'	[kPa]	0
φ'	[°]	35
r	[-]	varies
τ	[day]	1
e_0	[-]	3
α_0	[-]	varies
ω	[-]	varies
ω_d	[-]	varies
OCR	[-]	varies

Table 3.8   Parameters applied for single stress point analysis, values for r, α_0, ω, ω_d and OCR varies as shown by Table 3.9

Case	α_0	ω	ω_d	OCR	r
1	[0.0,0.25,0.5,0.75,1.0]	0.0	0.0	1.0	1.0
2	[0.0,0.25,0.5,0.75,1.0]	0.0	0.0	2.0	1.0
3	0.5	25	[0.5,1,2]	1.0	1.0
4	0.5	[12.5,25,50]	0.75	1.0	1.0
5	0.5	25	[0.5,1,2]	2.0	1.0
6	0.5	[12.5,25,50]	0.75	2.0	1.0
7	0.5	25	0.75	1.0	[-1, 0.75, 1]

Table 3.9   Definition of 7 cases applied single stress point analysis

For each case and each test type a drained and an undrained simulation is conducted, leading to 42 simulations. Appendix B gives the simulation results. Appendix B follows the sign convention used in the PLAXIS programme, in which tensile stress and volume strain are considered positive.

The simulation results lead to the following conclusions:
General:

- The implementation is numerically stable for the tested input. It should be noted that the input parameters are based on laboratory tests on a typical organic clay, see section 3.1 and therefore realistic for the intended field of application.
- The simulations of a triaxial compression test by a single point analysis and by a boundary value approach give equal results, see appendix B.2.1. This holds both for drained and undrained analysis. The results of this comparison are as expected and this comparison acts as a check on a different use of the implementation.
- For normally consolidated conditions the initial creep rate is relatively large, depending on the creep parameter μ^*. This makes the size of time step for the first

POV MACRO STABILITEIT

phase important. This holds especially for a nil-step applied after the stress initialization.

Triaxial test simulations
- Simulations are conducted for a vertical effective stress, σ'_v = 100 kN/m^2 and horizontal effective stress σ'_v = 50 kN/m^2, applied K_0 = 0.5, a maximum axial strain, $\varepsilon_{a,max}$ = 10% is applied, which is reached in 1 day.
- Appendix B.2.2 and B.2.3 show the large influence of the initial yield curve rotation, α_0 for both drained and undrained analysis. The influence is found in the development of the shear stress development and the volume strain for drained tests and pore pressure for undrained tests. This is explained by the associative nature of the model, meaning that the plastic strain directions are based on the derivatives of the yield curve. For specific stress conditions on the yield curve, a different orientation causes a difference in calculated plastic strain. Equation (3.2) seems to provide a good estimation for α_0.
- For normally consolidated drained triaxial compression tests, no clear peak strength is found. The deviator stress, q, increases for increasing α_0, see Figure B.5.
- For over consolidated drained triaxial compression tests, a clear peak strength, q_{peak} is found, see Figure B.6. The size of the peak strength strongly depends on α_0. The strength found at maximum axial strain, ε_1 = 0.1, is independent of α_0.
- For undrained testing, the initial yield curve rotation has a strong influence on the pore pressure development, with the curvature of the undrained stress path as a consequence. For normally consolidated undrained conditions the induced excess pore pressure increases for increase α_0 and consequently the curvature of undrained stress paths is stronger for increasing α_0, see Figure B.12. For over consolidated conditions the realized under pressure due to shearing increases for increasing α_0. This is explained by stronger tendency for dilatant behaviour for increasing α_0, as shown by Figure B.13.
- The influence of the rotational hardening parameters ω and ω_d is small to negligible, see Figure B.7, Figure B.8, Figure B.9, Figure B.10, Figure B.14, Figure B.15, Figure B.16 and Figure B.17. It should be noted that the simulations start at anisotropic stress conditions. When loading in triaxial compression critical state conditions are found relatively rapidly, allowing only little yield curve rotation.
- The value for r has no influence on the simulation of the triaxial compression tests, see Figure B.11 and Figure B.18. This complies with theory, as shown in Figure 2.4, the position of the compression points in the deviatoric plane do not change for different values for r.

Biaxial test simulations
- In engineering practice, calculations are often conducted for plain strain conditions, while parameters are derived from axial symmetric tests, like triaxial compression tests. To test the model for plain strain calculation results biaxial test simulations are conducted.
- Simulations are conducted for a vertical effective stress, σ'_v = 100 kN/m^2 and horizontal effective stress σ'_v = 50 kN/m^2, applied K_0 = 0.5, a maximum vertical strain, $\varepsilon_{yy,max}$ = 10% is applied, which is reached in 1 day. The horizontal strain in x and z direction are kept constant.

- The initial yield curve rotation, α_0, has a clear influence on the test simulations, see Figure B.19, Figure B.20, Figure B.26 and Figure B.27. Equivalent to the simulations of the triaxial compression tests this is explained by the associative nature of the model.
- For drained biaxial tests, the influence of α_0 manifest itself by a different σ'_2 development, with a stronger σ'_2 development for lower α_0, see Figure B.19 and Figure B.20.
- For drained overconsolidated behaviour, α_0 has a strong influence on volume strain, with a stronger volume strain development for smaller values for α_0, see Figure B.20.
- For drained over consolidated behaviour the biaxial test simulations show a remarkable deviator stress development. For the undrained analysis and the drained, normally consolidated conditions, the deviator stress, q, increases for increasing α_0., see Figure B.19, Figure B.26 and Figure B.27. In simulations of biaxial drained over consolidated behaviour, at small strain level larger q for larger α_0 is found. At maximum applied vertical strain, $\varepsilon_1 = 0.1$, the reached value for q seems independent for α_0.
- The influence of the rotational hardening parameters ω and ω_d in drained analyses is in the order 10 % on the value for q, σ'_2 and ε_{vol} reached at 10 % axial strain, see Figure B.21 to Figure B.24. For undrained the influence of the rotational hardening parameters ω and ω_d are mainly found in the σ'_2 development with differences in the range of 5 – 10% reached at 10 % axial strain, see Figure B.28 to Figure B.31.

Direct Simple Shear simulations
- Direct Simple Shear tests directly apply a shear strain onto the soil sample. For this reason the graphs of shear stress, σ_{xy} versus vertical stress, σ_{yy} and shear stress, σ_{xy} versus shear strain γ_{xy} are added to the results presented in appendix B.4.
- Simulations are conducted for a vertical effective stress, $\sigma'_v = 100$ kN/m^2 and horizontal effective stress $\sigma'_v = 50$ kN/m^2, applied $K_0 = 0.5$, a maximum shear strain, $\gamma_{xy\ max} = 10\%$ which is reached in 1 day.
- In laboratory testing the development of both horizontal stresses is not known and therefore stress paths in terms of isotropic stress p' and deviator stress q, from laboratory testing cannot given. The simulations presented in appendix B.4 show clear differences in σ_2 and σ_3 developments for the different tested parameter sets. At this stage it is not technically possible to validate the simulation results in terms of p and q, or σ_2 and σ_3 with laboratory test data.
- The initial yield curve rotation α_0 has a strong influence on the simulations results. With a larger strength, σ_{xy} for smaller α_0 values, see Figure B.33, Figure B.34, Figure B.40 and Figure B.41. Equivalent to the simulations of the triaxial compression tests and simulations of biaxial tests this is explained by the associative nature of the model.
- For over consolidated tests the size of the initial rotation of the yield curve, α_0, distinguishes between different behaviour, with compaction for $\alpha_0 = 0$, 0.25 and 0.5 and dilatant behaviour for $\alpha_0 = 0.75$ and 1.0, see Figure B.34 and Figure B.35. It should be noted that for the applied parameter set $\alpha_0 = 0.5$ is closest to natural behaviour, see paragraph 3.1.

POV MACRO STABILITEIT

- Equivalent to the biaxial tests the influence of the rotational hardening parameters ω and ω_d is in the order of 10 to 20% of the calculated stress and strain, see Figure B.35 to Figure B.38. and Figure B.42 to Figure B.45.

3.5 Boundary value problem

3.5.1 General set-up and initial calculations

This chapter describes a first quick check on the applicability of the new implementation to boundary value problems. It is emphasized that a thorough validation of this new implementation to boundary value problems should be conducted in following studies.

A characteristic feature of the Creep-SCLAY1 model is the ability of modelling creep behaviour. The calculations discussed in this chapter are focussed on simulation of creep behaviour of a newly build embankment on soft soil. This section discusses the simulation results when using the parameters ranges as applied in chapter 3. Appendix C describes the set-up and calculation results in detail. A few of the highlights are given in this chapter. Section 3.5.2 compares the calculation results found by the Creep-SCLAY1 model to the results found by Soft Soil Creep model and by the computer programme D-Settlement, Deltares (2016).

Figure 3.9 shows the geometry, mesh, boundary conditions and material entities. The width of the dike crest is 1.5 m, the slope angle 1 (V):2.5 (H). The soft soil layer thickness is 10 m, the ground water table is 0.5 m below ground level.
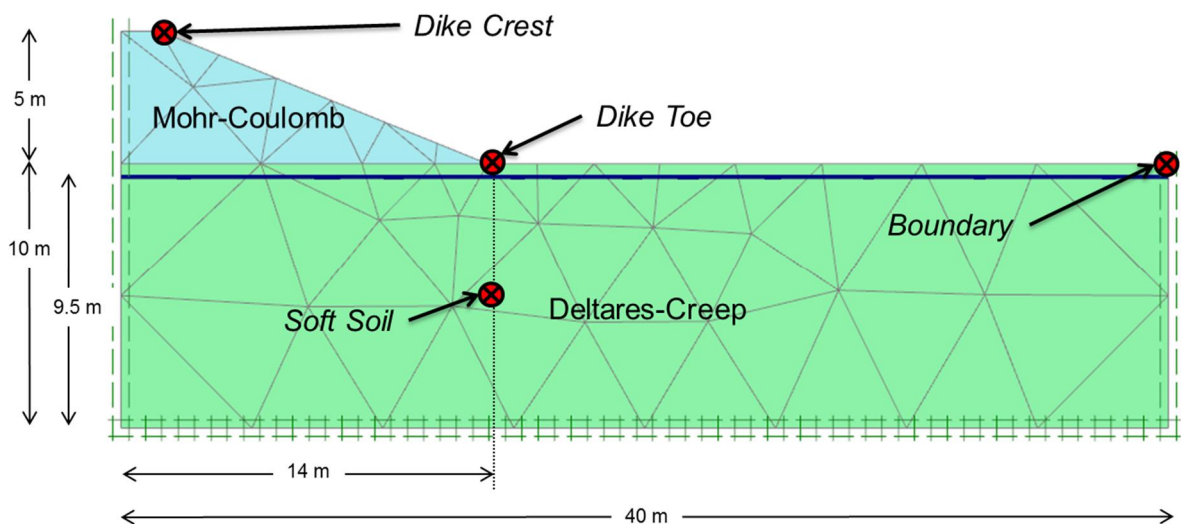
Figure 3.9   Applied geometry for testing boundary value problem

The tested problem consists of a deformation of a dike body on soft soil due to creep. The applied soil parameters are adopted from Table 3.1. For the rotational hardening parameters, ω and ω_d, initial yield curve rotation, α_0, Over Consolidation Ratio, OCR and extension ratio, r, 3 different cases are tested. The 3 cases are explained in Table 3.10. The back ground of the selected values for α_0, ω, ω_d and r is explained in section 3.1. As explained later in this section, for OCR = 1 maximum creep strain rates will be calculated. More realistic settlement behaviour is found for larger values for OCR, which is applied in section 3.5.2.

POV MACRO
     STABILITEIT

Case	α_0	ω	ω_d	OCR	r
1	[0.0, 0.5]	0.0	0.0	1.0	1.0
2	[0.0, 0.5]	25	1.0	1.0	1.0
3	0.5	25	1.0	1.0	[-1.0, 0.8, 0.9, 1.0]

Table 3.10   Tested ranges for α_0, ω, ω_d and r

Preliminary calculations resulted in a numerical error during the creep phase. Sub dividing the simulating creep time in sub steps, as shown below and the use of a coarse mesh is applied to avoid the numerical error. The occurrence of the error should be solved before the new implementation can be used in other studies.

A coarse mesh has been applied to test if other problems with the applicability of the new implementation occur. The coarse mesh contains 56 elements, 15 nodes per element and 505 nodes. This mesh is very coarse and for practical applications finer meshes will be preferred. To test the influence of the mesh coarseness on the calculation results additional calculations with a less coarse mesh are conducted for case 3, with r = -1. The results are discussed at the end of this section.

Since the Creep-SCLAY1 model is an anisotropic model, in which the anisotropy interacts with the actual stress conditions, the initial stress conditions are activated using an isotropic model. Here the linear elastic model is used. After stress initialisation the material model is switched from the linear elastic model to the Creep-SCLAY1 model.

The calculation phases are divided as follows:

- Initial Phase: Initialization of stresses by K0 procedure.
- Phase 1: Material Switch Phase (duration = 1 day).
- Phase 2: Activate Dike Body (duration = 1 day).
- Phase 3: 1st Creep Phase (duration = 10 days).
- Phase 4: 2nd Creep Phase (duration = 100 days).
- Phase 5: 3rd Creep Phase (duration = 1000 days).
- Phase 6: 4th Creep Phase (duration = 9000 days).

The total duration of analysis is approximately 10000 days from the activation of the dike.

Four points are used to show the development of stresses and / or displacements. These points are referred to as *Dike Crest*, *Dike Toe*, *Soft Soil* and *Boundary*. The locations of the points are shown in Figure 3.9.

calculation		Crest[*]	Toe	Boundary
case 1	$\alpha_0 = 0$	3.5	0.70	0.47
	$\alpha_0 = 0.5$	4.0	0.48	0.47
case 2	$\alpha_0 = 0$	2.8	0.61	0.37
	$\alpha_0 = 0.5$	3.2	0.68	0.5
case 3		3.2	0.68	0.5

Table 3.11   Calculated settlement in [m] after 10 000 days for the different cases and D-Settlement, for OCR = 1.0.[*]
[*] = settlement found at the top soft soil layer, compaction of the dike body itself is not included.

The results given in Table 3.11 show a large influence of the initial yield curve rotation, α_0. This is explained by the fact that Creep-SCLAY1 is an associative model and determines the

POV MACRO STABILITEIT

direction of the plastic strain by the derivatives of yield curve. For specific stress conditions on the yield curve, a different orientation of the yield curve leads to different derivatives and hence different plastic strain increments. Calculations show differences in horizontal displacement pattern for the different cases. These horizontal displacements interact with the vertical displacements that contribute to the lowering of the crest level.

In general, applying OCR = 1 in isotach based settlement calculations, will strongly overestimate settlements found for most practical applications. Among others this is explained by Deltares (2016), in which the concept of green field settlement is introduced. The green field settlement is the calculated settlement when no load increment is applied. In this example, green field settlements are found for the location *boundary*, as shown in Figure 3.9. At this location the stress increment due to the activation of the weight of the dike body is negligible, still Table 3.11 predicts, green field, settlement ranging from 0.37 to 0.5 m. This is explained by the difference in α_0 and the resulting creep strain.

To check on the influence of the mesh coarseness on the calculation results a less coarse mesh is build using 429 elements, 3591 nodes, see Figure 3.10.
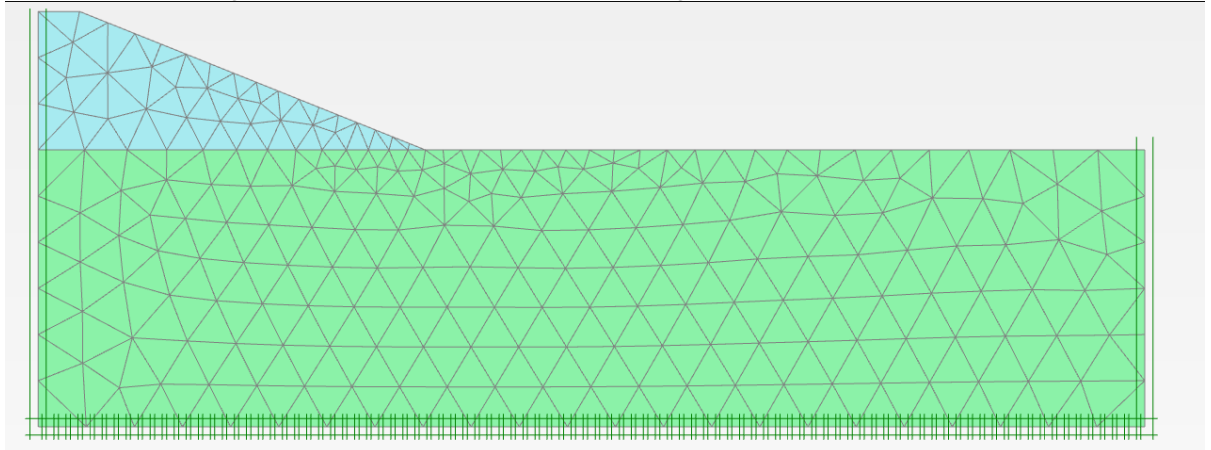
Figure 3.10 Applied mesh after re-finement

The dimensions of the embankment and sub soil are the same as applied for the coarse mesh, see Figure 3.9. The applied soil parameters are taken from Table 3.1 combined to case 3 from Table 3.10 and *r* = -1.
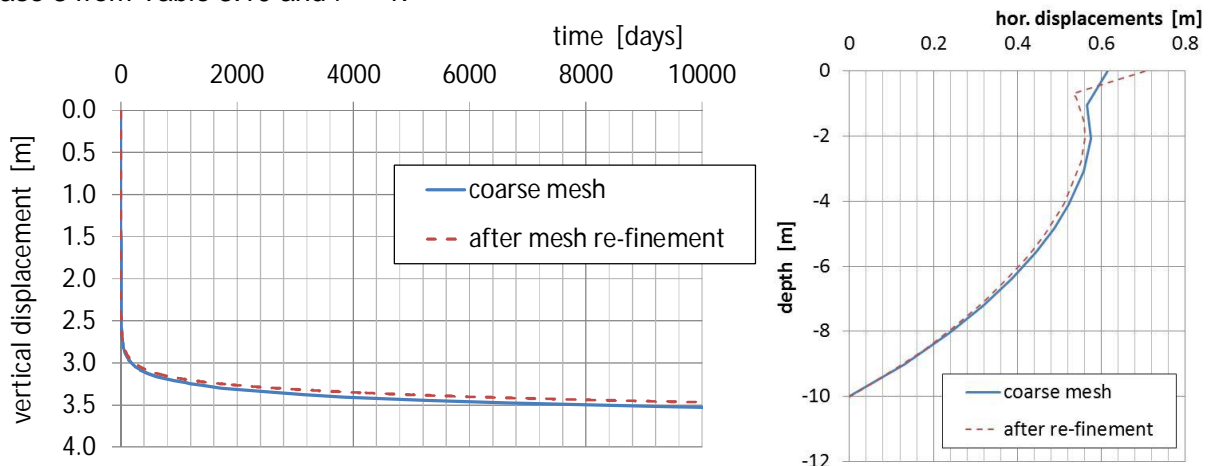
Figure 3.11 Comparison calculated displacements for different mesh coarseness, left hand side, comparison vertical displacements of the crest right hand side, comparison horizontal displacements along a vertical at the toe of the dike.

POV MACRO STABILITEIT

Figure 3.11 shows the calculated displacements for the coarse mesh and after mesh re-finement. The left hand graph gives the vertical displacements at the crest of the embankment. The right hand side shows the horizontal displacements along a vertical at the toe of the embankment. The differences in calculated displacements found for the coarse mesh and after re-finement of the mesh are remarkably small.

Besides mesh coarseness, the influence of the tolerated error is tested. The default value for the tolerated error in PLAXIS is 0.02. An additional calculation is made using the parameter set for case 3 and applying a tolerated error equal to 0.001. Figure 3.12 shows the results. The difference in calculated settlement at the locations boundary and crest for both tolerated errors are negligible.
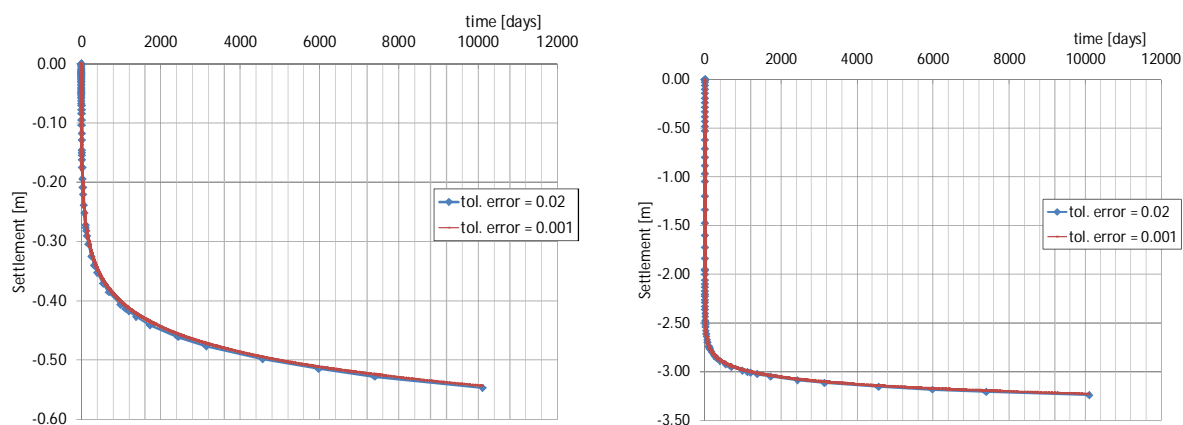
Figure 3.12 Influence of tolerated error on calculated settlements. Left hand side settlements calculated at location boundary, right hand side settlements calculated at location crest

3.5.2 Comparison to other calculation models

The results of the boundary value problem calculation are compared to the calculation results obtained with the Soft Soil Creep model and the computer programme D-Settlement.

The soft Soil Creep model is a constitutive model, available in PLAXIS, that is developed for modelling soft soil behaviour. It is a Cam Clay type model combined with the Mohr-Coulomb failure criterion. Details are given in PLAXIS (2016a). The Soft Soil Creep model uses the same stiffness and strength parameters, as the Creep-SCLAY1 model as shown by Table 3.12. This facilitates direct comparison. It should be noted that the Soft Soil Creep model obtains the ratio of horizontal to vertical stress for normally consolidated condition, K_0^{nc} and the position of the critical state line, M, such that for K_0^{nc} loading conditions, a K_0^{nc} deformation pattern is found. In the Creep-SCLAY1 model the initial yield curve rotation angle has a strong influence on the deformation pattern. For a relevant comparison between the calculation results of the Soft Soil Creep model and Creep-SCLAY1 model the best estimates for rotational parameters, α_0, ω and ω_d are used as discussed in section 3.1. It should be noted that in section 3.3, 3.4 and 3.5.1 a range of values for the rotational parameters have been used to study trends. Here the best estimate is used.

The geometry and applied mesh are discussed in section 3.5.1 and are the same for SSC and Creep-SCLAY1 model calculations. The period for the material switch phase, required in the Creep-SCLAY1 calculation, is kept as short as possible, 0.001 day. It should be noted that a period of 0 days leads to numerical problems. The Soft Soil Creep model does not require a material switch. The period in which the dike body weight is activated, is also kept as short as possible, 0.001 day. It should be noted that the Soft Soil Creep does allow

POV MACRO STABILITEIT

for a phase period of 0 days. However, for comparison reasons 0.001 day duration for activating the dike body is applied Soft Soil Creep calculation as well. In both calculations the tolerated error is set to 0.001.

parameter	unit	SSC-model	Creep-SCLAY1
volume weight, γ	[kN/m³]	13.14	13.14
compression index, λ^*	[-]	0.1134	0.1134
recompression index, κ^*	[-]	0.01149	0.01149
creep index, μ^*	[-]	0.0065	0.0065
poison ratio, ν	[-]	0.15	0.15
friction angle, φ'	[°]	35	35
reference time, τ	[day]	1	1
OCR	[-]	1	1
extension ratio, r	[-]	n.a.	-1
initial yield curve rotation, α_0	[-]	n.a.	0.55
rotational hardening parameter, ω	[-]	n.a.	26
rotational hardening parameter, ω_d	[-]	n.a.	1

Table 3.12 Applied parameters for the Soft Soil Creep, SSC, model and Creep-SCLAY1 model, n.a. = not available

The D-Settlement computer software is based on analytical solutions for 1D settlement theory. The D-Settlement analysis is based on the following choices :

- Calculations are made using D-Settlement version 16.1
- Calculation model is the isotache approach using the NEN-Bjerrum parameters
- In contrast to the FEM simulations the full dike body is modelled. This is required for correctly modelling the stress distribution in D-Settlement.
- The dike body is modelled as a load, and deformations of the dike body are not taken into account
- In accordance with the FEM analysis, drained behaviour is assumed.
- In accordance with the FEM analysis submerging is not considered.
- The required soil parameters are estimated from the FEM input:

$$RR = \kappa^* \ln(10) \cdot \frac{\ln\left(\dfrac{\left(2 \cdot K_0^{NC} + 1\right)}{\left(2 \cdot K_0^{NC} + 1\right) - \left(1 - \dfrac{1}{OCR}\right) \cdot \left(2 \cdot \dfrac{\nu'}{1-\nu'} + 1\right)}\right)}{\ln OCR}$$

$$CR = \lambda^* \ln(10) \tag{3.9}$$

$$C_\alpha = \mu^* \ln(10)$$

For this case equation (3.9) results in $RR = 0.022$, $CR = 0.26$ and $C_\alpha = 0.015$.

In which:

RR	= re-compression index
CR	= compression index
C_α	= creep parameter
K_0^{NC}	= ratio of horizontal to vertical stress for normally consolidated conditions
ν'	= Poisson ratio

POV MACRO STABILITEIT

Figure 3.13 shows the D-Settlement schematisation. Settlements are calculated in 4 vertical profiles. Vertical profile 1 corresponds to the centre of the dike crest. Profile 2 corresponds to the location *crest* in Figure 3.9. Profile 3 corresponds to location *toe* and profile 4 corresponds to location *boundary*.
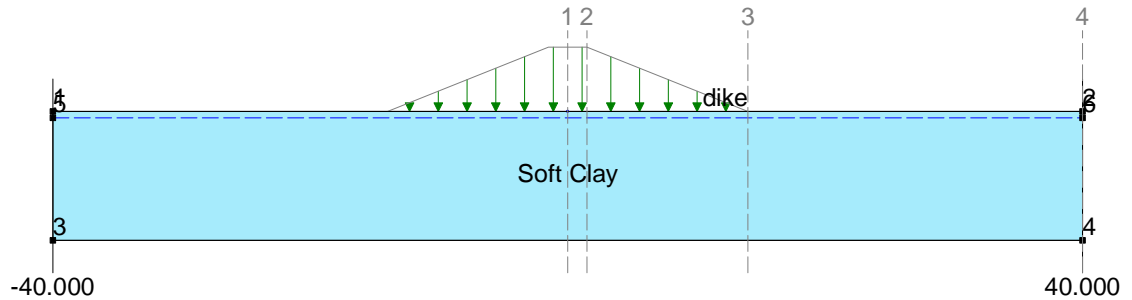
Figure 3.13 D-Settlement schematisation

calculation	Crest[*]	Toe	Boundary
Creep-SCLAY1	3.32	0.74	0.54
Soft Soil Creep	2.97	0.78	0.56
D-Settlement	2.50	0.95	0.60

Table 3.13 Calculated settlement in [m] after 10 000 days for the Creep-SCLAY1, Soft Soil Creep and D-Settlement, for OCR = 1.0. [*] = settlement found at the top soft soil layer, compaction of the dike body itself is not included.

Table 3.13 shows a summary of the calculation results. The vertical displacements found at the right hand boundary of the mesh and at the toe are slightly larger for the D-Settlement calculation in comparison to both finite element calculations. For the vertical displacements found at the crest, the finite element calculations predict larger settlement.

The displacements found at the right hand side boundary, the green field settlements, are easily validated by an analytical solution. Since the stress is expected to stay equal at the right hand side boundary, the creep strain is easily estimated from:

$$\varepsilon_c = C_\alpha \log\left(\frac{10000}{1}\right) = \mu^* \ln\left(\frac{10000}{1}\right) = 0.06$$

For a 10 m clay layer the settlement due to creep is 0.6 m. This value is exactly found by the D-Settlement calculations, but not by the Creep-SCLAY1 and SSC calculations. A quick check with a 1D simulation of a 10 m thick soil layer with the parameters given in Table 3.12 showed that the differences between the D-Settlement results and Creep-SCLAY1 respectively Soft Soil Creep simulations can be explained by the low stresses near the ground level. Application of a pre-load on top of the 1D-model led to a better agreement between the PLAXIS models and theory. This should be further elaborated in future research with a special focus on practical applicability.

POV
MACRO
STABILITEIT
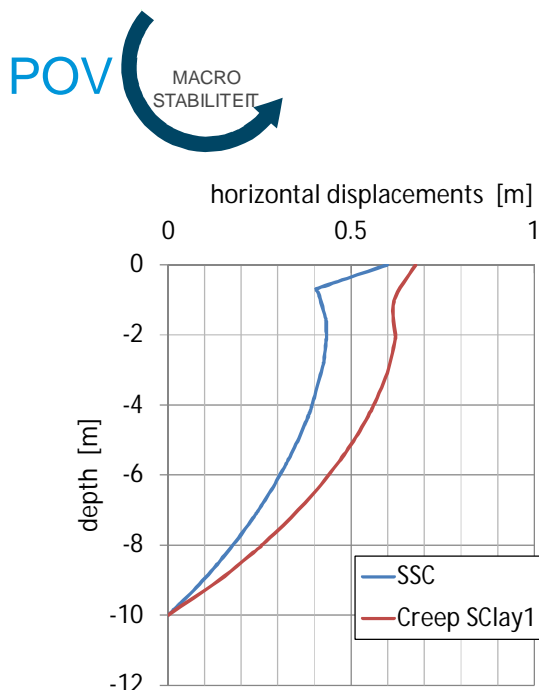
Figure 3.14 Horizontal displacements calculated by the Sot Soil Creep, SSC model and Creep-SCLAY1 model at the toe of the embankment, x = 14.

The differences in vertical displacements at the crest found by the different calculation techniques not only reflect differences in calculated vertical strain, but also a difference in displacement pattern. Application of the Creep-SCLAY1 model yields larger horizontal displacements than application of the SSC model. The Creep-SCLAY1 model predicts also the largest vertical displacements at the crest. D-Settlement accounts only for vertical strain, resulting in the lowest predicted vertical displacements at the crest.

For the Soft Soil Creep calculations a c' / φ' reduction analysis is conducted, resulting in ΣMsf = 1.78. The large ΣMsf value indicates that the calculated horizontal and vertical displacements are not caused by slope instability.

To study the influence of OCR on the green field settlement case 1 is re-calculated for OCR = 1.75. Table 3.14 gives a summary of the calculation results. As to be expected the calculated settlement strongly reduces for increasing OCR. For OCR = 1.75 the green field settlements, as found at location boundary, reduces to a few centimetre for both Creep-SCLAY1 simulations as well as for the D-Settlement simulation. Again the D-Settlement analysis predicts a smaller settlement at the location *crest* then found by the Creep-SCLAY1 model. This is explained by the horizontal displacements.

calculation	Crest[*]	Toe	Boundary
Creep-SCLAY1	2.41	0.35	0.05
Soft Soil Creep	2.16	0.38	0.07
D-Settlement	1.86	0.33	0.04

Table 3.14 Calculated settlement in [m] after 10 000 days for the Creep-SCLAY1 model Soft Soil Creep and D-Settlement, for OCR = 1.75

3.6 Conclusions

Although a complete and thorough validation of the implementation needs to be conducted in future analysis, this chapter discusses some calculation results. Four different tests of the model have been reported. First, a simulation reported in literature using the original implementation is reproduced by the new implementation. This simulation deals with the influence of the applied strain rate on the shear strength development. The results are

discussed in section 3.1. A good match in simulation results with the original and new implementation is found.

Second, the OCR dependency of the undrained shear strength predicted by the model is compared to the relation given by Ladd (1991) and Mayne et al (2009). The implementation reproduces the OCR dependency nicely. In future research more effort will be put on understanding the development in s_u-ratio.

Third, a series of laboratory tests consisting of triaxial compression tests, direct simple shear tests and biaxial tests are simulated for a range of parameter values. These simulations test the numerical stability of the new implementation for the range of parameter values. No numerical stability problems were observed. Although it should be noted that in this series parameter values are derived from CRS tests on organic clay and are believed to be realistic values for soft soil. In this stage the numerical stability has not been tested for awkward or unusual values. The simulation of the laboratory tests is also used to get some understanding of the model. The simulations show a strong influence of the initial yield curve rotation, α_0 on the simulation results, which is explained by associative nature of the model; with the plastic strain vector being normal to the yield curve, the orientation of the yield curve has a strong influence on the plastic strain development. The rotational hardening reflected by the parameters ω and ω_d have an influence on the simulations of biaxial and Direct Simple Shear tests and a minor influence on the simulations of triaxial compression tests.

Fourth, the model is applied to a boundary value problem, simulating the settlement behaviour of an embankment. The tested boundary value problem consisted of a 5m high dike body on a 10 m thick soft soil layer. The boundary value problem was used to test the time dependent behaviour of the model. In conducting these calculations errors were found. Application of short time steps in the creep analysis was used as a work-around. The occurrence of error messages should be solved in the further development of the model.

The predicted settlement, after a creep period of 10 000 days, is compared to the results of the analytical model D-Settlement and PLAXIS simulations using the Soft Soil Creep model. In comparison to the D-Settlement calculations, the Creep-SCLAY1 and Soft Soil Creep predict more settlements at the centre of the embankment. This realistic behaviour is explained by horizontal displacements, which are not accounted for in the D-Settlement calculations. Equivalently, the difference in vertical displacement found at the crest found by the Creep-SCLAY1 and Soft Soil Creep model can be explained by the difference in horizontal displacements. Creep-SCLAY1 model predicts larger horizontal displacements than the Soft Soil Creep model and consequently more vertical displacement.

At the right hand side boundary of the boundary value problem, the calculated displacements are completely dominated by creep strain. Both, the Creep-SCLAY1 and Soft Soil Creep model predict slightly smaller vertical displacements than found by D-Settlement. Inspection of the calculation results shows that the low stresses near the ground level explain the observed differences. How to deal with these differences in practical applications should be dealt with in future research.

4 Summary and recommendations

4.1 Summary

The POV-M research programme aims to improve the applicability of innovative dike reinforcement techniques. One of the key aspects is the availability of calculation tools. Design of the innovative reinforcement techniques require the use of FEM leading to the development of constitutive models within the POVM framework. For practical engineering purposes the SHANSEP MC and SHANSEP NGI-ADP models (PLAXIS, 2016b, Panagoulias & Brinkgreve 2017) have been developed.

Both SHANSEP models are total stress models in which the maximum mobilised undrained shear strength is an input parameter and should be assessed by the user. Typical Dutch sub soil stratification contains organic clays and peat. The behaviour of organic materials is complex and the assessment of the undrained shear strength is not always straightforward. Therefore, the POVM felt the need for a more fundamental study on soft, organic, soil behaviour, referred to as "fundamenteel spoor". This fundamental study can be seen as a step in better understanding soft soil behaviour and follow up studies are required to implement the outcome in daily engineering practice. A practical tool for studying soft organic soil behaviour would be an effective stress based constitutive model that accounts for creep and anisotropy. Such a model could be used to analyse laboratory test data, simulate complex behaviour in boundary value problems and provide a platform that can be used to extend the model to further improve simulating soft soil behaviour.

The fundamental study contains a numerical and experimental part. This report describes the numerical part which consists of building a new implementation of the Creep-SCLAY1 model, which is an effective stress model that accounts for creep and anisotropy. It is emphasised that the implementation is meant to be used for research and this report describes the details of the implementation and discusses the first simulation results using the model. A thorough and complete validation of the implementation was not part of the study should be conducted in follow up studies. Nor does the report provide a detailed manual for application of the model or parameter assessment.

This report describes the implementation of the model and some analysis results. In contrast to the original implementation of the model de-structuration is not included. The new implementation is intended to be used to describe the behaviour of soft organic soils for which de-structuration is considered not to be relevant. Omitting the de-structuration reduces the complexity of the model and increases its robustness.

Compared to the original implementation of the Creep-SCLAY1 model, the new implementation includes a new integration scheme resulting in an improved robustness of the model.

4.2 Recommendations

Building the new implementation is a first step. With the availability of the implementation a thorough and consistent validation needs to be done in following research.

This follow-up research should be focussed on:

- Testing the implementation on numerical stability and practical problems.

POV MACRO STABILITEIT

- Understanding the model by validating results against analytical solutions when available, other models and measurement data.
- Practical applicability in terms of parameter assessment, calculation time, robustness etc.

Validation will be a stepwise procedure in which validation of this particular implementation and the general Creep SCLAY1 model will be issues that cannot be separated from each other. Preferably the validation will start with relative simple calculations like single element tests and 1D calculations, of which this report already discusses a first start. These simple calculations will be followed by more complex calculations, for example simulations of field trials. More in detail, the following steps are recommended:

- Single element and 1D simulations for testing the simulation of creep behaviour. This is an extension of the simulations discussed in paragraph 3.5.2. In testing the simulation of creep behaviour the influence of OCR, the simulation of creep strain after loading – unloading should be considered and validated against analytical solutions and Soft Soil Creep simulations.
- The prediction of the undrained shear strength ratio, *S*, should be validated against the solution presented by Wroth (1984), as discussed in section 3.3. The results should be compared to results of simulations using the Modified Cam Clay model, Soft Soil Creep.
- In comparing the results of the different simulations between the different models, the predicted development of the intermediate stress should be considered. For plain strain calculations, the intermediate stress plays an important role and seems to be different for the different material models.
- Simulation of laboratory data. This report shows some simulations of laboratory tests, however, a comparison to real measurement data has not been made yet. Such an analysis should indicate how well the Creep-SCLAY1 model predicts soft soil behaviour. For this purpose the laboratory data to be simulated should contain organic clay and peats, which are typical for the Dutch subsoil. In the validation of the model by laboratory test data, the current formulation of the rotational hardening law should be evaluated and potentially improved when required.
- Simulation of field trials and test embankments. Data of different field trials and test embankments are available. For Dutch conditions cases like the *Leendert de Boers polder*, *IJkdijk*, *Dijken op Veen* and *Bergambacht* provide field data. Also from international prospective cases like the Murro test embankment and others are available for simulations. It should be noted that the original Creep-SCLAY1 was tested for the Murro test embankment. Besides differences in calculation results, aspects like robustness and calculation time should be considered.
- To comply with the POVM frame work, cases including sheet pile walls should be considered.
- With respect to the latter and similar to the SSC model, the model should be extended to become applicable for both time steps and load steps,. Also similar to the SSC model, the initialization of the OCR should be possible from the input of a spatially distributed POP field.
- The results of the simulations mentioned above should lead to summarized best practices, providing information on parameters assessment and other application issues.

References

Borst R., Heeres O.M. (2002) A unified approach to the implicit integration of standard, non-standard and viscous plasticity models *Int. J. Numerical and analytical methods in geomechanics* **26**:1059-1070 (DOI: 10.1002/ng.234)

Dafalias, Y.F. (1987) Anisotropic critical state clay plasticity model *In: proceedings of the 2nd International Conference on Constitutive Laws for engineerig materials* Tucson, Arizona, Elsevier N.Y. vol1 p 513-521

Dafalias Y.F. Taiebat M. (2013) Anatomy of rotational hardening in clay plasticity *Géotechnique* 63, no 16 p. 1406-1418

Dafalias Y.F. Taiebat M. (2014) Rotational hardening with and without anisotropic fabric at critical state *Géotechnique* 64 no 6p 507-511

Deltares (2016) D-Settlement user manual, version 16.1

Den Haan E.J., Kamao S. (2003) Obtaining isotache parameters from a CRS K0 oedometer *Soils and Foundations* vol 43. no 4 p 203-214

Fung Y.C. (1965) Foundation of solid mechanics, *Prentice Hall*

Grimstad G., Degago S., Nordal S., Karstunen M. (2010) Modelling creep and rate effects in structured anisotropic soft clays *Acta Geotechnica,* vol. 5, pp. 69-81, 2010

Karstunen M., Krenn H., Wheeler S.J., Koskinen M., Zentar R. (2005) Effect of anisotropy and destructuration on the behavior of Murro test embankment *international journal of geomechanics* **5** no 2 p 87

Karstunen M., Rezania M., Sivasithamparam N., Z.-Y Yin (2012) Comparison of anistropic rate-dependent models for modelling consolidation of soft clays *international journal of Geomechanics* doi:10.1061/(ASCE)GM.1943-5622.0000267

Ladd C.C. (1991) stability evaluation during staged construction, 22nd Karl Terzaghi lecture *Journal of Geotechnical engineering* Vol 117 no 4 p 540

Leoni M, Karstunen M, Vermeer P, (2008) Anisotropic Creep Model for Soft Soils *Geotechnique,* vol. 58, no. 3, pp. 216-226, 2008.

Matsuoka H., Nakai T. (1974) Stress-deformation and strength characteristics of soil under three different principal stresses *Proceedings of JSCE* 232:59-70

Mayne P.W., Coop M.R., Springman S. Huang A-B, Zornberg J.(2009) State-of-the-art Paper (SOA-1): Geomaterial Behavior and Testing *Proc. 17th Int. conf. Soil Mechanics & Geotechnical Engineering* Vol. 4 Milpress/IOS Press Rotterdam p 2777-2872

Min. I & M. (2017). *Handreiking ontwerpen met overstromingskansen, Veiligheidsfactoren en belastingen bij nieuwe overstromingskansnormen, versie OI2014v4.* Ministerie van Infrastructuur en Milieu

Muir Wood D. (1990) Soil Behaviour and Critical State Soil Mechanics, Cambridge University Press, ISBN 0-521-33782-8

Panagoulias S., Brinkgreve R.B.J. (2017) SHANSEP NGI-ADP, model description and verification examples *POVM report.*

Plaxis (2016) Soft Soil Creep model – undrained triaxial creep behaviour of Haney clay [Online]. Available: https://www.plaxis.com/support/verifications/soft-soil-creep-model-undrained-triaxial-creep-behaviour-of-haney-clay/. [Accessed 6 November 2017].

Plaxis (2016a) Material Models Manual

Plaxis (2017) "Triaxial test with Hardening Soil model," 07 November 2012. [Online]. Available: https://www.plaxis.com/support/verifications/triaxial-test-with-hardening-soil-model/. [Accessed 6 November 2017].

Plaxis (2016b) The SHANSEP MC model, *Panagoulias, Palmieri, Brinkgreve (eds)*

Sivasithamparam N., (2012) Modelling Creep Behaviour of Soft Soils, *report PLAXIS b.v. & University of Strathclyde*

Sivasithamparam N., Karstunen M., Brinkgreve R., Bonnier P. (2013) Comparison of two anisotropic creep models at element level. in: *International Conference on Installation Effects in Geotechnical Engineering*, Rotterdam, NL., 2013

Sivasithamparam N., Karstunen M., Brinkgreve R., Bonnier P., (2015) Modelling creep behaviour of anisotropic soft soils, Computers and Geotechnics, Volume 69, September 2015, Pages 46-57

Wheeler S.J., Näätänen A., Karstunen M., Lojander M. (2003) An anisotropic elastoplastic model for soft clays *Can. Geotech. J.,* vol. 40, p. 403, 2003
Wood D.M. (1990) Soil behaviour and critical state soil mechanics, Cambridge University Press ISBN 0-521-33782-8

Wroth C.P. (1984) The interpretation of in soil tests *Géotechnique* **34** no 4. p 449-489

POV ⌒ MACRO STABILITEIT

A   Implementation details

A.1   Introduction
Chapter 2 gives a brief introduction to the Creep-SCLAY1 model in which the main features of the model are explained in simplified *p' – q* stress space. The implementation is based on the complete stress and strain tensor, which makes the mathematical formulation of the model more complex than explained in chapter 2. This appendix gives the actual formulation that is used to build the code. The simplified description in chapter 2 is meant as an illustration of the theory and explanation of the basic concepts of the model.

This appendix describes the mechanics as well as the numerical integration as implemented in the user defined soil model. The implementation of the model is partly novel. The material model is stated in geo-mechanical terms. This implies positive values for compression in stress and strain. Note that PLAXIS and Abaqus follow the mechanical description, with a reversed sign definition. This implies that a conversion is needed between the FEM program and the user defined model.

For the explanation of the different symbols used in the mathematical descriptions below, it is referred to the notation list at the start of this report and chapter 2. For background information on the Creep-SCLAY1 model it is referred to Wheeler et al (2003), Karstunen et al (2005), Leoni et al (2008), Grimstad et al (2010), Sivasithamparam et al (2013), Sivasithamparam (2015) and chapter 2.

A.2   Strain decomposition
The strain rate is composed out of an elastic and a visco-plastic part.

$$\dot{\underline{\varepsilon}} = \dot{\underline{\varepsilon}}^e + \dot{\underline{\varepsilon}}^c \tag{A.1}$$

The stress increment follows from the elastic part minus the visco-plastic correction.

$$\dot{\underline{\sigma}} = \underline{\underline{D}}\,\dot{\underline{\varepsilon}} - \underline{\underline{D}}\dot{\underline{\varepsilon}}^c \tag{A.2}$$

A.3   Elasticity
The elastic bulk modulus K depends on the isotropic effective stress, *p'*, the specific volume, *v* and the swelling index κ:

$$K' = \frac{vp'}{\kappa}$$

Together with a constant Poisson's ratio v' this gives for the Youngs modulus: $E = 3(1 - 2v')K'$, and for the shear modulus: $G' = \dfrac{E}{2(1+v')}$. The definition of the specific volume is: *v* = 1 + *e*, where *e* is the void ratio. The specific volume *v* is only an internal parameter. Therefore, the parameter κ^* is introduced: $\kappa^* = \dfrac{\kappa}{v}$. Note that all parameters with star relate to parameters without specific volume in the same way.

These parameters determine the isotropic elastic stiffness matrix D and compliance matrix and $\dot{\underline{\varepsilon}}^e = \underline{\underline{D}}^{-1}\dot{\underline{\sigma}}$. Further on, it is assumed that the stiffness is constant in a time increment.

POV (MACRO STABILITEIT

A.4 Visco-plasticity

A.4.1 Anisotropic yielding
Section 2.3 and 2.4 describe the use of Normal Consolidation Surface, NCS and Current State Surface, CSS which repeated in Figure A.1.

.
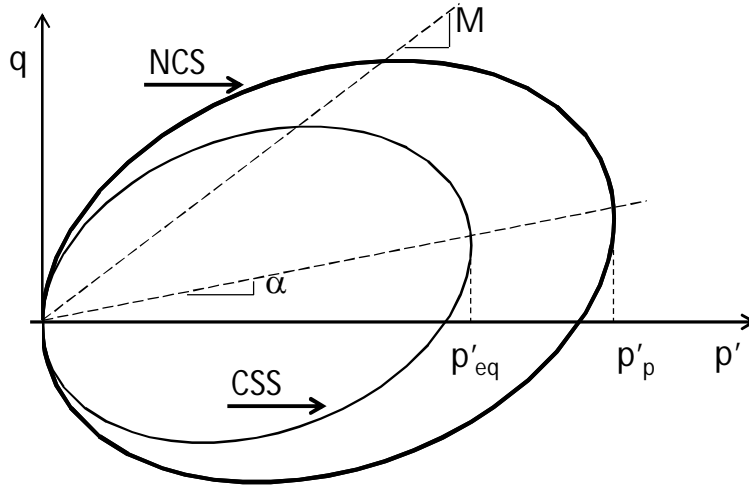
Figure A.1 Current state surface and normal consolidation surface of Creep-S-Clay1 in triaxial stress space

Vermeer et al (1998), Vermeer & Neher (1999), Leonie et al (2008), Sivasithamparam (2012) describes the handling of the CSS and NCS, which is basically followed here. The yield function reads:

$$f = p_{eq} - p'_p = 0 \tag{A.3}$$

With the following definition of the equivalent stress, p_{eq}:

$$p_{eq} = \frac{3}{2} \frac{\left(\underline{\sigma}_d - p'\underline{\alpha}_d\right)^T \left(\underline{\sigma}_d - p'\underline{\alpha}_d\right)}{\left(M^2\left(\underline{\sigma}_d, \underline{\alpha}_d\right) - \frac{3}{2}\underline{\alpha}_d{}^T \underline{\alpha}_d\right)p'} + p' \tag{A.4}$$

At yield, a normally consolidated stress state applies.

In handling the plastic strain the associated flow rule is assumed.

In general the position of the critical state line depends on the stress characteristics, $M\left(\underline{\sigma}_d, \underline{\alpha}_d\right)$ see section 2.5, which means that the critical state slope M depends on the intermediate stress. The critical state line for triaxial compression is determined by the angle:

$$M_{tc} = \frac{6\sin\phi_{tc}}{3 - \sin\phi_{tc}} \tag{A.5}$$

In which φ'_{tc} represents the friction angle for triaxial compression. The inverse reads:

POV MACRO STABILITEIT

$$\sin\phi_{tc} = \frac{3M_{tc}}{6+M_{tc}}$$ It is noted that this is only valid with the definition of the second

stress invariant $J_2 = \frac{3}{2}\underline{\sigma}_d^{\,T}\underline{\sigma}_d = q^2$, conform Muir Wood [1990].

For the Lode angle applies: $\sin 3\theta = -\frac{27}{2}\frac{J_3}{J_2^{\frac{3}{2}}}$ with $\theta = -30^0$ for compression and $\theta = 30^0$ for

extension. The definition of the deviatoric stress tensor σ_d used follows Wheeler ea. (2003).

$$\underline{\sigma}_d = \begin{pmatrix} \sigma_{xx} - p' \\ \sigma_{yy} - p' \\ \sigma_{zz} - p' \\ \sqrt{2}\sigma_{xy} \\ \sqrt{2}\sigma_{yz} \\ \sqrt{2}\sigma_{zx} \end{pmatrix}, \qquad p' = \frac{1}{3}\left(\sigma_{xx} + \sigma_{yy} + \sigma_{zz}\right), \qquad q^2 = \frac{3}{2}\underline{\sigma}_d^{\,T}\underline{\sigma}_d \qquad \text{(A.6)}$$

The definition of deviatoric strain tensor ε_d is:

$$\underline{\varepsilon}_d = \begin{pmatrix} \frac{1}{3}\left(2\varepsilon_{xx} - \varepsilon_{yy} - \varepsilon_{zz}\right) \\ \frac{1}{3}\left(-\varepsilon_{xx} + 2\varepsilon_{yy} - \varepsilon_{zz}\right) \\ \frac{1}{3}\left(-\varepsilon_{xx} - \varepsilon_{yy} + 2\varepsilon_{zz}\right) \\ \sqrt{2}\varepsilon_{xy} \\ \sqrt{2}\varepsilon_{yz} \\ \sqrt{2}\varepsilon_{zx} \end{pmatrix} = \begin{pmatrix} \frac{1}{3}\left(2\varepsilon_{xx} - \varepsilon_{yy} - \varepsilon_{zz}\right) \\ \frac{1}{3}\left(-\varepsilon_{xx} + 2\varepsilon_{yy} - \varepsilon_{zz}\right) \\ \frac{1}{3}\left(-\varepsilon_{xx} - \varepsilon_{yy} + 2\varepsilon_{zz}\right) \\ \frac{\gamma_{xy}}{\sqrt{2}} \\ \frac{\gamma_{yz}}{\sqrt{2}} \\ \frac{\gamma_{zx}}{\sqrt{2}} \end{pmatrix} \qquad \varepsilon_{vol} = \varepsilon_{xx} + \varepsilon_{yy} + \varepsilon_{zz} \rightarrow \varepsilon_d^{\,2} = \frac{2}{3}\underline{\varepsilon}_d^{\,T}\underline{\varepsilon}_d \quad \text{(A.7)}$$

Equivalent to $\underline{\varepsilon}_d$ the deviatoric fabric tensor $\underline{\alpha}_d$ is defined. The deviatoric fabric tensor describes the plastic anisotropy, which is manifested by the yield curve rotation, α.

POV MACRO
STABILITEIT

$$\underline{\alpha}_d = \begin{pmatrix} \frac{1}{3}\left(2\alpha_{xx} - \alpha_{yy} - \alpha_{zz}\right) \\ \frac{1}{3}\left(-\alpha_{xx} + 2\alpha_{yy} - \alpha_{zz}\right) \\ \frac{1}{3}\left(-\alpha_{xx} - \alpha_{yy} + 2\alpha_{zz}\right) \\ \sqrt{2}\alpha_{xy} \\ \sqrt{2}\alpha_{yz} \\ \sqrt{2}\alpha_{zx} \end{pmatrix} = \begin{pmatrix} \alpha_{xx} - 1 \\ \alpha_{yy} - 1 \\ \alpha_{zz} - 1 \\ \sqrt{2}\alpha_{xy} \\ \sqrt{2}\alpha_{yz} \\ \sqrt{2}\alpha_{zx} \end{pmatrix}, \quad \frac{1}{3}\left(\alpha_{xx} + \alpha_{yy} + \alpha_{zz}\right) = 1, \quad \alpha^2 = \frac{3}{2}\underline{\alpha}_d{}^T\underline{\alpha}_d \quad \text{(A.8)}$$

The fabric tensor follows the stresses definition. The choice made by Wheeler ea. (2003) for these expressions of tensors seems to be driven by having a simple inner product of the tensors.

A.4.2 Creep Law
The creep strain is defined by, see also section 2.4:

$$\dot{\underline{\varepsilon}}^c = \dot{\Lambda}\frac{\partial p_{eq}}{\partial \underline{\sigma}} \quad \text{(A.9)}$$

The creep intensity is formulated following Grimstad et al (2010):

$$\dot{\Lambda} = \frac{\mu^*}{\tau}\left(\frac{p'_{eq}}{p_p}\right)^\beta\left(\frac{M_{tc}^2 - \alpha_{K_0^{nc}}^2}{M_{tc}^2 - \eta_{K_0^{nc}}^2}\right) \quad \text{(A.10)}$$

In which:

$$\beta = \frac{\lambda^* - \kappa^*}{\mu^*} \quad \text{(A.11)}$$

The last term $\dfrac{M_{tc}^2 - \alpha_{K_0^{nc}}^2}{M_{tc}^2 - \eta_{K_0^{nc}}^2}$ is created during the initiation of material model based on the actual

stress conditions and remains constant.

Note that

$$\frac{\partial \dot{\Lambda}}{\partial \underline{\sigma}} = \dot{\Lambda}\frac{\beta}{p_{eq}}\frac{\partial p_{eq}}{\partial \underline{\sigma}} \quad \text{(A.12)}$$

This term is needed in the numerical handling of the model.

A.4.3 Hardening laws
The model implies two hardening rules, see Wheeler et al (2003) which is followed here. The first hardening rule describes the development of the pre-consolidation as function of the plastic volumetric strain as in the Cam Clay model:

POV MACRO
STABILITEIT

$$\frac{dp_p}{p_p} = \frac{d\varepsilon_{vol}^{p}}{\lambda^* - \kappa^*} \tag{A.13}$$

The second rule describes the changes of orientation of the ellipse orientation, see section 2.3:

$$d\underline{\alpha}_d = \omega\left\{\left(\frac{3\underline{\sigma}_d}{4p'} - \underline{\alpha}_d\right)\left\langle d\varepsilon_{vol}^{p}\right\rangle + \omega_d\left(\frac{\underline{\sigma}_d}{3p'} - \underline{\alpha}_d\right)d\gamma^{p}\right\} \tag{A.14}$$

Note that $\langle\ \rangle$ denote the McCauley brackets with $\langle d\varepsilon^p{}_{vol}\rangle = d\varepsilon^p{}_{vol}$ if $d\varepsilon^p{}_{vol} > 0$ and $\langle d\varepsilon^p{}_{vol}\rangle = 0$ if $d\varepsilon^p{}_{vol} < 0$

A.4.4   Lode angle dependency of M
For the Lode angle dependent critical state parameter the following expression is proposed:

$$M(\theta) = M_{tc}\frac{\cos\left(\frac{\pi}{3} - \arctan\left(\frac{2r-1}{\sqrt{3}}\right)\right)}{\cos\left(\frac{1}{3}\arccos\left(\cos\left(3\arctan\left(\frac{2r-1}{\sqrt{3}}\right)\right)\sin 3\theta_\alpha\right)\right)} \tag{A.15}$$

With extension ratio $r = \dfrac{M_{te}}{M_{tc}}$. This is a novel expression, details are to be published later.

Note that for Matsuoka-Nakai applies: $r = \dfrac{3 - \sin\phi_{tc}}{3 + \sin\phi_{tc}}$.

This function ensures a convex yield function in the deviator-plane.

It is noted that all is focussed on the α-line $\underline{\sigma}_d - \underline{\alpha}_d p$ and thus the angle θ_α is determined with respect to this "stress". This implies that *M* may change during loading.

A.5   Numerical scheme

A.5.1   Introduction
A user-defined model has a number of different tasks to do. It depends on the programme definition of the user defined material model whether these tasks are performed in a single routine or are organised differently. In PLAXIS these tasks are defined by IDTask in the subroutine User_Mod. The following tasks are defined:
    1 : Initialize state variables
    2 : calculate stresses,
    3 : calculate material stiffness matrix
    4 : return number of state variables
    5: inquire matrix properties; return switch for non-symmetric D-matrix; stress/time dependent matrix
    6 : calculate elastic material stiffness matrix

The quality and reliability of the model is determined by the numerical scheme that is used for the stress update, IDTask = 2 and the stiffness matrix update, IDTask = 3.

POV **MACRO STABILITEIT**

A.5.2 Strain rate

The residual reads:

$$\underline{r}_\varepsilon = \Delta\underline{\varepsilon} - \left(\Delta\underline{\varepsilon}^e - \Delta\underline{\varepsilon}^c\right) = \Delta\underline{\varepsilon} - \Delta\underline{\varepsilon}^e - \Delta\Lambda\frac{\partial p'_{eq}}{\partial\underline{\sigma}} \tag{A.16}$$

The residual should be zero so:

$$\Delta\underline{\varepsilon} - \Delta\underline{\varepsilon}^e - \Delta\Lambda\frac{\partial p'_{eq}}{\partial\underline{\sigma}} = 0 \tag{A.17}$$

With definition (A.4), variation of this expression for the residual knowing that $p_{eq}\left(\underline{\sigma}_d,\underline{\alpha}_d\right)$ or $p_{eq}\left(\underline{\sigma},\underline{\alpha}\right)$, gives:

$$\Delta\underline{\varepsilon} - \left(\Delta\underline{\varepsilon}^e + \delta\underline{\varepsilon}^e\right) - \left(\Delta\Lambda + \delta\Lambda\right)\left(\frac{\partial p'_{eq}}{\partial\underline{\sigma}} + \frac{\partial p'_{eq}}{\partial\underline{\sigma}\partial\underline{\alpha}}\delta\underline{\alpha} + \frac{\partial^2 p'_{eq}}{\partial\underline{\underline{\sigma}}^2}\delta\underline{\sigma}\right) = 0 \tag{A.18}$$

This gives with $\delta\underline{\sigma} = \underline{\underline{D}}\delta\underline{\varepsilon}^e$ or $\underline{\underline{D}}^{-1}\delta\underline{\sigma} = \delta\underline{\varepsilon}^e$:

$$\left(\underline{\underline{D}}^{-1} + \Delta\Lambda\frac{\partial^2 p'_{eq}}{\partial\underline{\underline{\sigma}}^2}\right)\delta\underline{\sigma} + \Delta\Lambda\frac{\partial p'_{eq}}{\partial\underline{\sigma}\partial\underline{\alpha}}\delta\underline{\alpha} + \frac{\partial p'_{eq}}{\partial\underline{\sigma}}\delta\Lambda = \Delta\underline{\varepsilon} - \Delta\underline{\varepsilon}^e - \Delta\Lambda\frac{\partial p'_{eq}}{\partial\underline{\sigma}} \tag{A.19}$$

Here the higher order terms are neglected. The terms $\dfrac{\partial p'_{eq}}{\partial\underline{\sigma}}, \dfrac{\partial^2 p'_{eq}}{\partial\underline{\underline{\sigma}}^2}$ and $\dfrac{\partial p'_{eq}}{\partial\underline{\sigma}\partial\underline{\alpha}}$ are determined numerically just as the term $\dfrac{\partial p_{eq}}{\partial\underline{\alpha}}$ as required further on in the implementation of the model.

It is noted that the following relation holds

$$\delta\underline{\alpha}_d = \omega\left(\left(\frac{3\underline{\sigma}_d}{4p'} - \underline{\alpha}_d\right)\left\langle\delta\varepsilon^p_{vol}\right\rangle + \omega_d\left(\frac{\underline{\sigma}_d}{3p'} - \underline{\alpha}_d\right)\delta\varepsilon^p_d\right) \tag{A.20}$$

$$\delta\underline{\alpha}_d = \omega\left(\left(\frac{3\underline{\sigma}_d}{4p'} - \underline{\alpha}_d\right)\left\langle\delta\varepsilon^p_{vol}\right\rangle + \omega_d\left(\frac{\underline{\sigma}_d}{3p'} - \underline{\alpha}_d\right)\delta\varepsilon^p_d\right) \tag{A.21}$$

And the terms $\delta\varepsilon^p_{vol}$ and $\delta\varepsilon^p_d$ follow directly from $\dfrac{\partial p_{eq}}{\partial\underline{\sigma}}$. This gives:

$$\delta\varepsilon^p_{vol} = \left\langle\frac{\partial p_{eq}}{\partial\sigma_{xx}} + \frac{\partial p_{eq}}{\partial\sigma_{yy}} + \frac{\partial p_{eq}}{\partial\sigma_{zz}}\right\rangle\delta\Lambda \tag{A.22}$$

$$\delta\varepsilon^p_d = \sqrt{\frac{2}{3}\left(\frac{\partial p_{eq}}{\partial\underline{\sigma}}_d\right)^T\left(\frac{\partial p_{eq}}{\partial\underline{\sigma}}_d\right)}\delta\Lambda \tag{A.23}$$

POV MACRO STABILITEIT

With the introduction of the following tensor:

$$\underline{h}_d = \omega \left(\left(\frac{3\underline{\sigma}_d}{4p'} - \underline{\alpha}_d \right) \left\langle \frac{\partial p_{eq}}{\partial \sigma_{xx}} + \frac{\partial p_{eq}}{\partial \sigma_{yy}} + \frac{\partial p_{eq}}{\partial \sigma_{zz}} \right\rangle + \omega_d \left(\frac{\underline{\sigma}_d}{3p'} - \underline{\alpha}_d \right) \sqrt{\frac{2}{3} \left(\frac{\partial p_{eq}}{\partial \underline{\sigma}}_d \right)^T \left(\frac{\partial p_{eq}}{\partial \underline{\sigma}}_d \right)} \right) \quad \text{(A.24)}$$

And then follows:

$$\delta \underline{\alpha}_d = \underline{h}_d \, \delta\lambda \quad \text{(A.25)}$$

Note that $\dfrac{\partial \alpha}{\partial \underline{\alpha}_d}$ transforms the change of the fabric tensor. This transformation is given by:

$$\frac{\partial \underline{\alpha}}{\partial \underline{\alpha}_d} = \begin{pmatrix} 1 & 0 & 0 & 0 & 0 & 0 \\ 0 & 1 & 0 & 0 & 0 & 0 \\ 0 & 0 & 1 & 0 & 0 & 0 \\ 0 & 0 & 0 & \frac{1}{\sqrt{2}} & 0 & 0 \\ 0 & 0 & 0 & 0 & \frac{1}{\sqrt{2}} & 0 \\ 0 & 0 & 0 & 0 & 0 & \frac{1}{\sqrt{2}} \end{pmatrix} \quad \text{(A.26)}$$

So $\delta\underline{\alpha}$ is related to $\delta\underline{\alpha}_d$ with the following expression:

$$\delta\underline{\alpha} = \frac{\partial \underline{\alpha}}{\partial \underline{\alpha}_d} \delta\underline{\alpha}_d = \frac{\partial \underline{\alpha}}{\partial \underline{\alpha}_d} \underline{h}_d \, \delta\Lambda = \underline{h}\delta\Lambda \quad \text{(A.27)}$$

Then results for the residuals:

$$\left(\underline{\underline{D}}^{-1} + \Delta\Lambda \frac{\partial^2 p'_{eq}}{\partial \underline{\underline{\sigma}}^2} \right) \delta\underline{\sigma} + \left(\frac{\partial p'_{eq}}{\partial \underline{\sigma}} + \Delta\Lambda \frac{\partial p'_{eq}}{\partial \underline{\sigma}\partial \underline{\alpha}} \underline{h} \right) \delta\lambda = \Delta\underline{\varepsilon} - \Delta\underline{\varepsilon}^e - \Delta\Lambda \frac{\partial p'_{eq}}{\partial \underline{\sigma}} \quad \text{(A.28)}$$

The norm of the residual should be below a pre-defined threshold. The variables in the system are $\delta\underline{\sigma}$ and $\delta\Lambda$.

A.5.3 Plastic intensity
The residual for the plastic intensity reads:

$$r_\Lambda = \Delta\Lambda - \dot{\Lambda}\Delta t \quad \text{(A.29)}$$

The residual should be zero:

$$\Delta\Lambda - \dot{\Lambda}\Delta t = 0 \quad \text{(A.30)}$$

With the definition of the visco-plastic strain rate as given:

POV MACRO
STABILITEIT

$$\dot{\Lambda} = \frac{\mu^*}{\tau} \left(\frac{p'_{eq}}{p_p} \right)^{\beta} \left(\frac{M^2 - \alpha^2_{K_0^{nc}}}{M^2 - \eta^2_{K_0^{nc}}} \right) \qquad (A.31)$$

The following derivatives can be found for $\dot{\Lambda}(\underline{\sigma}, \underline{\alpha}, p_p)$:

$$\frac{\partial \dot{\Lambda}}{\partial p_{eq}} = \dot{\Lambda} \frac{\beta}{p_{eq}}, \quad \frac{\partial \dot{\Lambda}}{\partial \underline{\sigma}} = \dot{\Lambda} \frac{\beta}{p_{eq}} \frac{\partial p_{eq}}{\partial \underline{\sigma}}, \quad \frac{\partial \dot{\Lambda}}{\partial \underline{\alpha}} = \dot{\Lambda} \frac{\beta}{p_{eq}} \frac{\partial p_{eq}}{\partial \underline{\alpha}}, \quad \frac{\partial \dot{\Lambda}}{\partial p_p} = -\dot{\Lambda} \frac{\beta}{p_p} \qquad (A.32)$$

Variation of the expression for plastic intensity with $\dot{\Lambda}(\underline{\sigma}, \underline{\alpha}, p_p)$ gives:

$$\Delta \Lambda + \delta \Lambda - \Delta t \left(\dot{\Lambda} + \frac{\partial \dot{\Lambda}}{\partial \underline{\sigma}}^T \delta \underline{\sigma} + \frac{\partial \dot{\Lambda}}{\partial \underline{\alpha}}^T \delta \underline{\alpha} + \frac{\partial \dot{\Lambda}}{\partial p_p} \delta p_p \right) = 0 \qquad (A.33)$$

The residual, r_Λ becomes:

$$\Delta t \frac{\partial \dot{\Lambda}}{\partial \underline{\sigma}}^T \delta \sigma + \Delta t \frac{\partial \dot{\Lambda}}{\partial \underline{\alpha}}^T \delta \underline{\alpha} + \Delta t \frac{\partial \dot{\Lambda}}{\partial p_p} \delta p_p - \delta \Lambda = \Delta \Lambda - \Delta t \Lambda \qquad (A.34)$$

with $\dfrac{\delta p_p}{p_p} = \dfrac{\delta \varepsilon^p_{vol}}{\lambda^* - \kappa^*}$ follows:

$$\Delta t \frac{\partial \dot{\Lambda}}{\partial p_{eq}} \frac{\partial p_{eq}}{\partial \underline{\sigma}}^T \delta \underline{\sigma} + \Delta t \left\{ \frac{\partial \dot{\Lambda}}{\partial p_{eq}} \frac{\partial p_{eq}}{\partial \underline{\alpha}}^T \delta \underline{\alpha} + \frac{\partial \dot{\Lambda}}{\partial p_p} \left(\frac{p_p \delta \varepsilon^p_{vol}}{\lambda^* - \kappa^*} \right) \right\} - \delta \Lambda = \Delta \Lambda - \Delta t \dot{\Lambda} \qquad (A.35)$$

transformation gives:

$$\Delta t \dot{\Lambda} \frac{\beta}{p_{eq}} \frac{\partial p_{eq}}{\partial \underline{\sigma}}^T \delta \underline{\sigma} + \Delta t \dot{\Lambda} \left\{ \frac{\beta}{p_{eq}} \frac{\partial p_{eq}}{\partial \underline{\alpha}}^T \delta \underline{\alpha} - \frac{\beta}{\lambda^* - \kappa^*} \delta \varepsilon^p_{vol} \right\} - \delta \Lambda = \Delta \Lambda - \Delta t \dot{\Lambda} \qquad (A.36)$$

which is identical to:

$$\Delta t \dot{\Lambda} \frac{\beta}{p_{eq}} \frac{\partial p_{eq}}{\partial \underline{\sigma}}^T \delta \underline{\sigma} + \Delta t \dot{\Lambda} \left\{ \frac{\beta}{p_{eq}} \frac{\partial p_{eq}}{\partial \underline{\alpha}}^T \delta \underline{\alpha} - \frac{1}{\mu^*} \delta \varepsilon^p_{vol} \right\} - \delta \Lambda = \Delta \Lambda - \Delta t \dot{\Lambda} \qquad (A.37)$$

This results in:

$$\Delta t \dot{\Lambda} \frac{\beta}{p_{eq}} \frac{\partial p_{eq}}{\partial \underline{\sigma}}^T \delta \underline{\sigma} + \left(\Delta t \dot{\Lambda} \left\{ \frac{\beta}{p_{eq}} \frac{\partial p_{eq}}{\partial \underline{\alpha}}^T \underline{h} - \frac{1}{\mu^*} \left\langle \frac{\partial p_{eq}}{\partial \sigma_{xx}} + \frac{\partial p_{eq}}{\partial \sigma_{yy}} + \frac{\partial p_{eq}}{\partial \sigma_{zz}} \right\rangle \right\} - 1 \right) \delta \Lambda = \Delta \Lambda - \Delta t \dot{\Lambda}$$

$$(A.38)$$

This completes the expression of the residual for the plastic intensity.

A.5.4   Integration scheme

The applied integration scheme presented hereafter is based on a sub stepping algorithm that is partly explicit and partly implicit. The reason not to follow a fully implicit scheme can be

found in the dependency of $\underline{\alpha}$ and the non-linearity of the creep-law. The theoretically larger step size possible for implicit calculations is therefore limited in practice. A consistent tangent stiffness matrix is being used in the integration scheme, but with not all constitutive relations included. This has the advantage of leading to fewer expressions to be solved during the integration.

The combined set for the residuals of the strains and plastic intensity reads:

$$\left(\underline{\underline{D}}^{-1} + \Delta\Lambda \frac{\partial^2 p'_{eq}}{\partial \underline{\underline{\sigma}}^2} \right) \delta\underline{\sigma} + \left(\frac{\partial p'_{eq}}{\partial \underline{\sigma}} + \Delta\Lambda \frac{\partial p'_{eq}}{\partial \underline{\sigma} \partial \underline{\alpha}} \underline{h} \right) \delta\Lambda = \Delta\underline{\varepsilon} - \Delta\underline{\varepsilon}^e - \Delta\Lambda \frac{\partial p'_{eq}}{\partial \underline{\sigma}} \tag{A.39}$$

$$\Delta t \dot{\Lambda} \frac{\beta}{p_{eq}} \frac{\partial p_{eq}}{\partial \underline{\sigma}}^T \delta\underline{\sigma} + \left(\Delta t \dot{\Lambda} \left\{ \frac{\beta}{p_{eq}} \frac{\partial p_{eq}}{\partial \underline{\alpha}}^T \underline{h} - \frac{1}{\mu^*} \left\langle \frac{\partial p_{eq}}{\partial \sigma_{xx}} + \frac{\partial p_{eq}}{\partial \sigma_{yy}} + \frac{\partial p_{eq}}{\partial \sigma_{zz}} \right\rangle \right\} - 1 \right) \delta\Lambda = \Delta\Lambda - \Delta t \dot{\Lambda}$$

$$\tag{A.40}$$

This set is not symmetric due to change of the visco-plastic strain tensor due to the change in fabric orientation.

The resulting tangent matrix reads:

$$\begin{pmatrix} \underline{\underline{D}}^{-1} + \Delta\Lambda \frac{\partial^2 p'_{eq}}{\partial \underline{\underline{\sigma}}^2} & \frac{\partial p'_{eq}}{\partial \underline{\sigma}} + \Delta\Lambda \frac{\partial p'_{eq}}{\partial \underline{\sigma} \partial \underline{\alpha}} \underline{h} \\ \Delta t \dot{\Lambda} \frac{\beta}{p_{eq}} \frac{\partial p_{eq}}{\partial \underline{\sigma}}^T & \Delta t \dot{\Lambda} \left\{ \frac{\beta}{p_{eq}} \frac{\partial p_{eq}}{\partial \underline{\alpha}}^T \underline{h} - \frac{1}{\mu^*} \left\langle \frac{\partial p_{eq}}{\partial \sigma_{xx}} + \frac{\partial p_{eq}}{\partial \sigma_{yy}} + \frac{\partial p_{eq}}{\partial \sigma_{zz}} \right\rangle \right\} - 1 \end{pmatrix} \begin{pmatrix} \delta\underline{\sigma} \\ \delta\Lambda \end{pmatrix} =$$

$$\begin{pmatrix} \Delta\underline{\varepsilon} - \Delta\underline{\varepsilon}^e - \Delta\Lambda \frac{\partial p'_{eq}}{\partial \underline{\sigma}} \\ \Delta\Lambda - \Delta t \dot{\Lambda} \end{pmatrix} \tag{A.41}$$

Because the plastic intensity is strongly non-linear a first estimator can be used based on this last expression. Then it is assumed that $\Delta\Lambda = 0$ and $\delta\underline{\sigma} = \Delta\underline{\sigma}_{trial}$.

$$\delta\Lambda = \frac{\Delta t \dot{\Lambda} \left(1 + \frac{\beta}{p_{eq}} \left(\frac{\partial p_{eq}}{\partial \underline{\sigma}} \right)^T \Delta\underline{\sigma}_{trial} \right)}{1 - \Delta t \dot{\Lambda} \left\{ \frac{\beta}{p_{eq}} \frac{\partial p_{eq}}{\partial \underline{\alpha}}^T \underline{h} - \frac{1}{\mu^*} \left\langle \frac{\partial p_{eq}}{\partial \sigma_{xx}} + \frac{\partial p_{eq}}{\partial \sigma_{yy}} + \frac{\partial p_{eq}}{\partial \sigma_{zz}} \right\rangle \right\}} \tag{A.42}$$

Note that $\dot{\Lambda}$ is given in eq.(9). The expression given above is used to update $\underline{\sigma}_{trail}$, p_m and $\underline{\alpha}$. With these updated parameters $\delta\Lambda$ is calculated again. Also the expression given above gives state for which the Newton-Raphson scheme is applied.

The scheme iterates until the norm of the right-hand side of equation (A.42) is very small.

POV MACRO STABILITEIT

In the approach followed, convergence is not assured. Therefore two additional modifications have been made.

1   First modification divides the increment in substeps. This done based on creating a small increment for the stress integration to assure convergence.

2   The second modification is an overall handling that when no convergence is being found for the given strain increment and time increment that then both are reduced/subdivided in smaller parts until convergence is found. This is done such that the whole strain increment and time increment is handled.

The second modification assures robustness of the scheme but at the same time it blurs the aptness quality of the underlying integration of the constitutive relationships.

The algorithm here is similar to Sivasithamparam ea. (2015). It is based on the scheme of de Borst and Heeres (2002). Sivasithamparam ea. (2015) used it however in a rather arbitrary and inconsistent way. The scheme should apply to 1) the stress updates, 2) the internal variables ($\begin{pmatrix} p_p & \underline{\alpha}_d \end{pmatrix}$, 3) the visco-plastic strain intensity and 4) the elastic secant stiffness.

This implies 6 + 7 + 1 + 2 = 16 equations should be solved in each integration point for every time step. This results in a large number and the computational requirements make the material model then difficult to handle. Therefore assumptions are made to reduce the set equations. First, it is assumed that the elastic stiffness is constant during an increment. The differences due to the change of the isotropic stress are ignored. Second, the changes of internal variables are not handled explicitly for all variables as the scheme de Borst and Heeres (2002) suggests, but partly implicitly. This has the advantage of reducing the number of equations and results in a scheme of only 7 equations, where stress updates have been interchanged with strain updates. It must be noted that de Borst and Heeres (2002) state that as consequence of partly implicit integration of variables the convergence rate of the solution decreases.

The scheme of Sivasithamparam ea. (2015) becomes elaborated:

$$
\begin{pmatrix}
\underline{\underline{D}}^{-1} + \Delta\Lambda \dfrac{\partial^2 p'_{eq}}{\partial \underline{\underline{\sigma}}^2} & \dfrac{\partial p'_{eq}}{\partial \underline{\sigma}} \\[3ex]
\Delta t \dot{\Lambda} \dfrac{\beta}{p_{eq}} \dfrac{\partial p_{eq}}{\partial \underline{\sigma}}^T & \Delta t \dot{\Lambda} \left\{ \dfrac{\beta}{p_{eq}} \dfrac{\partial p_{eq}}{\partial \underline{\alpha}}^T \underline{h} - \dfrac{\beta}{p_{eq}} \dfrac{\partial p_{eq}}{\partial \underline{\sigma}}^T \underline{\underline{D}} \dfrac{\partial p_{eq}}{\partial \underline{\sigma}} \right\} - 1
\end{pmatrix}
\begin{pmatrix} \delta\underline{\sigma} \\[3ex] \delta\Lambda \end{pmatrix}
=
\begin{pmatrix} \Delta\underline{\varepsilon} - \Delta\underline{\varepsilon}^e - \Delta\Lambda \dfrac{\partial p'_{eq}}{\partial \underline{\sigma}} \\[3ex] \Delta\Lambda - \Delta t \dot{\Lambda} \end{pmatrix}
$$

(A.43)

The main difference of the current scheme with Sivasithamparam et al. (2015) is that an additional term in the strain rate residual is now taken account for and the plastic intensity expression is not expressed in the paper but the code gives an unclear expression for the hardening modulus.

The new scheme implies a much better convergence performance because all terms are included and a second order convergence rate may be expected. The original scheme requires more computation time but does not necessarily lead to erroneous results.

The implementation of the model by Sivasithamparam et al (2015) has a serious flaw. This flaw originates from not taking into account the deviatoric strength correctly. For the original implementation it is assumed that M is constant during an integration step and by

POV MACRO STABILITEIT

determining M at the beginning of each step it is assumed that the strength is handled correctly. This is not the case and cannot be case for a model that has dependency on the intermediate stress and fabric. The followed approach cannot be distinguished from a Drucker-Prager approach where M differs due to change of material properties. If the stress dependency of M is not included correctly in the algorithm then the outcome of the model will be untrustworthy for non-triaxial loading conditions. This requires that the stress derivatives of M must enter the formulation. This leads to complex expressions for analytical expressions for the derivatives of p_{eq} to the different stress and fabric components. In the approach followed here this is circumvented by determining the derivatives numerically, using a small perturbation. This may reduce the accuracy but at least it captures all relevant dependencies consistently.

Summary of Integration procedure

Initializing for sub-stepping	Plastic indicator set to zero The strain and time increment is divided in a number of steps. $$nsub = \max\left(1, |d\varepsilon| * 10000\right)$$ $\delta \underline{\varepsilon}_{sub} = \dfrac{1}{n}\delta\underline{\varepsilon}$ and $\delta t_{sub} = \dfrac{1}{n}\Delta t$. The stiffness matrix $\underline{\underline{D}}$ and compliance matrix $\underline{\underline{D}}^{-1}$ are determined before sub-stepping and kept constant.
First an elastic trial sub-step is made.	Stress $\underline{\sigma}^{trial}$ updated with elastic stress sub-increment. $$\underline{\sigma}^{trial} = \underline{\sigma}^{trial} + \delta\underline{\sigma}_{sub}$$ The previous hardening parameters are retrieved Determination of θ_α based on $\underline{\sigma}_d - \underline{\alpha}_d p$, then the new M is calculated. $$M(\theta_\alpha) = M_{tc}\frac{\cos\left(\dfrac{\pi}{3} - \arctan\left(\dfrac{2r-1}{\sqrt{3}}\right)\right)}{\cos\left(\dfrac{1}{3}\arccos\left(\cos\left(3\arctan\left(\dfrac{2r-1}{\sqrt{3}}\right)\right)\sin 3\theta_\alpha\right)\right)}$$ The new p_{eq} is determined $p_{eq} = \dfrac{3}{2}\dfrac{(\underline{\sigma}_d - p'\underline{\alpha}_d)^T(\underline{\sigma}_d - p'\underline{\alpha}_d)}{\left(M^2 - \dfrac{3}{2}\underline{\alpha}_d^T\underline{\alpha}_d\right)p'} + p'$ and Yield function f $f = \dfrac{3}{2}\dfrac{(\underline{\sigma}_d - p'\underline{\alpha}_d)^T(\underline{\sigma}_d - p'\underline{\alpha}_d)}{\left(M^2 - \dfrac{3}{2}\underline{\alpha}_d^T\underline{\alpha}_d\right)p'} + (p' - p'_p)$
Only for $p_{eq} > 2$ is plasticity considered! This implies that there is a threshold value for which plasticity is considered.	Plasticity indicator is increased with 1. Determination $\dfrac{\partial p_{eq}}{\partial \underline{\sigma}}$ numerically based on $p_{eq} = \dfrac{3}{2}\dfrac{(\underline{\sigma}_d - p'\underline{\alpha}_d)^T(\underline{\sigma}_d - p'\underline{\alpha}_d)}{\left(M^2 - \dfrac{3}{2}\underline{\alpha}_d^T\underline{\alpha}_d\right)p'} + p'$, $\dot{\Lambda} = \dfrac{\mu^*}{\tau}\left(\dfrac{p_{eq}}{p_p}\right)^\beta\left(\dfrac{M^2 - \alpha_{K_0^{nc}}^2}{M^2 - \eta_{K_0^{nc}}^2}\right)$

POV MACRO STABILITEIT

	Note that $\left(\dfrac{M^2 - \alpha_{K_0^{nc}}^2}{M^2 - \eta_{K_0^{nc}}^2}\right)$ is determined the initialisation of the hardening parameters, outside the integration routine.
If first guess new stress and $\underline{\alpha}$ is not within given tolerance	Based on the elastic assumptions a first estimate of the plastic intensity is made: $$\delta\Lambda = \frac{\Delta t\dot\Lambda\left(1 + \dfrac{\beta}{p_{eq}}\left(\dfrac{\partial p_{eq}}{\partial\underline\sigma}\right)^T \Delta\underline\sigma_{trial}\right)}{1 - \Delta t\dot\Lambda\left\{\dfrac{\beta}{p_{eq}}\dfrac{\partial p_{eq}}{\partial\underline\alpha}^T \underline{h} - \dfrac{1}{\mu^*}\left\langle\dfrac{\partial p_{eq}}{\partial\sigma_{xx}} + \dfrac{\partial p_{eq}}{\partial\sigma_{yy}} + \dfrac{\partial p_{eq}}{\partial\sigma_{zz}}\right\rangle\right\}}$$ $$d\underline\varepsilon^p = \delta\Lambda\frac{\partial p_{eq}}{\partial\underline\sigma}$$ From $d\underline\varepsilon^p$ the volumetric and deviatoric components are calculated. Then the update of $\underline\sigma^{trial}$ and $\underline\alpha$ and p_p. $$\underline\sigma^{trial} = \underline\sigma^{trial} - \underline{\underline D}d\underline\varepsilon^p$$ $$d\underline\alpha_d = \omega\left\{\left(\frac{3\underline\sigma_d}{4p'} - \underline\alpha_d\right)\langle d\varepsilon_{vol}^p\rangle + \omega_d\left(\frac{\underline\sigma_d}{3p'} - \underline\alpha_d\right)d\gamma^p\right\}$$ $$\underline\alpha = \underline\alpha + d\underline\alpha_d$$ $$dp_p = \frac{p_p d\varepsilon_{vol}^p}{\lambda^* - \kappa^*}$$ $$p_p = p_p + dp_p$$ The hardening parameters are updated and stored. With these updated parameters $\delta\Lambda$ is calculated again Then the difference between the new stress and $\Delta\Lambda$ is checked. These are collected residues of the combined set of equations $\underline{r}$ for both strain and $\Delta\Lambda$.
Then Newton-Raphson iteration procedure starts.	All the terms of the matrix of the combined set of equations of stress and $\Delta\lambda$ are determined and together with the residues the right-hand member is build. $$\begin{pmatrix}\underline{\underline D}^{-1} + \Delta\Lambda\dfrac{\partial^2 p'_{eq}}{\partial\underline{\underline\sigma}^2} & \dfrac{\partial p'_{eq}}{\partial\underline\sigma} + \Delta\Lambda\dfrac{\partial p'_{eq}}{\partial\underline\sigma\partial\underline\alpha_d}\underline{h}_d \\[2ex] \Delta t\dot\Lambda\dfrac{\beta}{p_{eq}}\dfrac{\partial p_{eq}}{\partial\underline\sigma}^T & \Delta t\dot\Lambda\left\{\dfrac{\beta}{p_{eq}}\dfrac{\partial p_{eq}}{\partial\underline\alpha}^T \underline h - \dfrac{1}{\mu^*}\left\langle\dfrac{\partial p_{eq}}{\partial\sigma_{xx}} + \dfrac{\partial p_{eq}}{\partial\sigma_{yy}} + \dfrac{\partial p_{eq}}{\partial\sigma_{zz}}\right\rangle\right\} - 1\end{pmatrix}$$ And: $$\begin{pmatrix}\Delta\underline\varepsilon - \Delta\underline\varepsilon^e - \Delta\Lambda\dfrac{\partial p'_{eq}}{\partial\underline\sigma} \\[2ex] \Delta\Lambda - \Delta t\dot\Lambda\end{pmatrix}$$ Then the set equation is solved to give $\delta\underline\sigma$ and $\delta\Lambda$.

POV **MACRO STABILITEIT**

	The stress $\underline{\sigma}^{trial} = \underline{\sigma}_{sub}^{0} + \delta\underline{\sigma}$ and $\Delta\Lambda$ are updated and subsequently $\underline{\alpha}$ and the p_p by: $$dp_p = \frac{p_p d\varepsilon_{vol}^{p}}{\lambda^* - \kappa^*}$$ $$d\underline{\alpha}_d = \omega\left\{\left(\frac{3\underline{\sigma}_d}{4p'} - \underline{\alpha}_d\right)\langle d\varepsilon_{vol}^{p}\rangle + \omega_d\left(\frac{\underline{\sigma}_d}{3p'} - \underline{\alpha}_d\right)d\gamma^{p}\right\}$$ The updated hardening parameters are stored. The collected residuals of the combined set of equations $\underline{r}$ on both stress and $\Delta\lambda$ are checked to be beyond a threshold. $$\dot{\Lambda} = \frac{\mu^*}{\tau}\left(\frac{p_{eq}}{p_p}\right)^{\beta}\left(\frac{M^2 - \alpha_{K_0^{nc}}^2}{M^2 - \eta_{K_0^{nc}}^2}\right)$$ $$d\Delta\Lambda = \dot{\Lambda}\Delta t_{sub}$$
If the problem has converged	Update of the stress that will be returned to the calculation program Set the plastic indicator to 3 if plasticity

POV MACRO STABILITEIT

A.5.5 Flow chart

This section gives a short overview of the code. The scheme communicating with FEM-code is governed by several routines. These routines are called subsequently. The scheme is focussed on the update of the stress and constitutive parameters. The integration scheme is in subroutine Deltares-creep. All other functionality required for the calculation process in PLAXIS (initiation lengths, initiation parameters, elastic and tangential stiffness) are in Usrmod-sclay1 and usrmod.

Usrmod
User defined material model in Plaxis
initiation, stress updates, (tangent) stiffness

Matrix model
Usrmod-Sclay1
User defined Sclay1 model

Substep
Implies full time and strain increment stepsize
If error back then reduce stepsize; assure that full time increment is reached

Deltares-Creep
Updates stresses and hardening parameters
If not succesfull then report error back

The usrmod routine is the interface to Plaxis. In the routine usrmod-sclay1 the mechanical definitions of stress and strain are converted to geo-mechanical definitions. The usrmod-sclay1 calls the routine substep. The routine substep only handles the size of the increments by which the constitutive model is called. Substep is only activated when it is not possible to achieve a convergent integration of the constitutive relations. Then the step size of time and strain increments is reduced until convergence is reached. Next, the starting point is updated. Simultaneously the routine accounts how much of the externally required step size has been realised. The remaining part is then integrated. This routine creates robustness to the integration of the constitutive relationships at the expense of computational effort. The routine is only required to assure convergence of the constitutive integration.

The basic routine that integrates the Creep-SCLAY1 constitutive model is called Deltares-creep. All the other routines are for the communication with the FEM model outside of the constitutive model. The following text gives a short summary of this routine.

Deltares_creep

Initiation elastic stiffness matrix $\underline{\underline{D}}$, $\underline{\sigma}_{sub} = \underline{\sigma}^0$

POV — MACRO STABILITEIT

Determination of substepsize for n substeps: $\delta\underline{\varepsilon}_{sub} = \frac{1}{n}\delta\underline{\varepsilon}$ and $\delta t_{sub} = \frac{1}{n}\Delta t$

Do ii=1:n

    Assume plastic strain is zero

    Build the elastic trial stress $\underline{\sigma}^{trial} = \underline{\sigma}_{sub} + \underline{\underline{D}}\,\delta\underline{\varepsilon}_{sub}$

    Download state parameters

    Determine with trail stress and hardening parameters, the equivalent pressure p_{eq}

    If p_{eq} >2 then

        Plastic stress correction

$$d\underline{\varepsilon}^{elastic} = d\underline{\varepsilon}_{sub}$$

        Determine all derivatives of the yield function or likewise p_{eq} to the stress and

$\underline{\alpha}$

        Determine $\dot{\lambda}$ and $\delta\lambda^0$ and subsequently $d\underline{\varepsilon}^{plastic} = \delta\lambda^0 \frac{\partial f}{\partial\underline{\sigma}}$

$$\underline{\sigma}^{trial} = \underline{\sigma}^{trial} - \underline{\underline{D}}d\underline{\varepsilon}^{plastic}$$

$$d\underline{\varepsilon}^{elastic} = d\underline{\varepsilon}^{elastic} - d\underline{\varepsilon}^{plastic}$$

        Determine the updated values for $\underline{\alpha}$ and p_p given $d\underline{\varepsilon}^p$

        Determine $\dot{\lambda}$ and $\delta\lambda^t$ for the updated parameters

        If $\left\| d\underline{\varepsilon}_{sub} - d\underline{\varepsilon}^{elastic} - \delta\lambda^0 \frac{\partial f}{\partial\underline{\sigma}} \right\| > tolerance$ and $\left\| \delta\lambda^0 - \delta\lambda^t \right\| > tolerance$ then

            Do i=1:maxit

            Matrix is build up to determine $\delta\underline{\sigma}$ and $\delta\lambda$ given

$$\Delta\underline{\varepsilon} - \Delta\underline{\varepsilon}^e - \Delta\lambda\frac{\partial p'_{eq}}{\partial\underline{\sigma}} \text{ and } \Delta\lambda - \Delta t\dot{\lambda}$$

            Update $\delta\lambda^0 = \delta\lambda^0 + \delta\lambda$ and $\underline{\sigma}^{trial} = \underline{\sigma}^{trial} + \delta\underline{\sigma}$

            Determine the updated values for $\underline{\alpha}$ and p_p given $d\underline{\varepsilon}^p$

            If error smaller then tolerance go to 2

            End do

            If no converge return

2   continue

            End if

    End if

    $\underline{\sigma}_{sub} = \underline{\sigma}^{trail}$

End do

$\underline{\sigma} = \underline{\sigma}^{trail}$

Return

B   Results simulation laboratory tests

B.1   Introduction

This appendix shows the results of a series of laboratory test simulations. The simulated conditions contain triaxial compression tests, biaxial tests and Direct Simple Shear tests. The analysis starts with a comparison between boundary value simulation of a triaxial compression test and an equivalent single stress point analysis, for drained and undrained conditions. After concluding that the single stress point analysis corresponds closely to the boundary value, a series of simulations including triaxial compression tests, biaxial tests and Direct Simple Shear tests, drained and undrained are conducted. The simulations mainly focus on the influence of rotational hardening and OCR on the simulated behaviour. This section first introduces the tested conditions followed by the results grouped per laboratory test type in the following sections.

Table B.1 lists the applied soil parameters. The background of the parameter selection is given in section 3.1.

Parameter	unit	Value
λ^*	[-]	0.1134
κ^*	[-]	0.01149
μ^*	[-]	0.0065
ν	[-]	0.15
K_0^{nc}	[-]	0.4264
c'	[kPa]	0
φ'	[°]	35
r	[-]	varies
τ	[day]	1
e_0	[-]	3
α_0	[-]	varies
ω	[-]	varies
ω_d	[-]	varies
OCR	[-]	varies

Table B.1   Material parameters applied in the model validation

Table B.2 shows the 6 variations in material parameters that were applied, the background of the selected variations is given in section 3.1. The intention was that each case would vary one of the parameters while holding the others fixed. This would enable verification that the constitutive model developed in the soil test environment could perform equally well in the FE environment. It also provided the opportunity to become more familiar with calculation parameters that directly affect the behaviour of the model.

POV MACRO STABILITEIT

Case	α_0	ω	ω_d	OCR	r
1	[0.0,0.25,0.5,0.75,1.0]	0.0	0.0	1.0	1.0
2	[0.0,0.25,0.5,0.75,1.0]	0.0	0.0	2.0	1.0
3	0.5	25	[0.5,1,2]	1.0	1.0
4	0.5	[12.5,25,50]	0.75	1.0	1.0
5	0.5	25	[0.5,1,2]	2.0	1.0
6	0.5	[12.5,25,50]	0.75	2.0	1.0
7	0.5	25	0.75	1.0	[-1, 0.75, 1]

Table B.2   Material parameter validation

B.2   Triaxial tests

B.2.1   Comparison single stress point simulation versus boundary value problem
Table B.3 shows the boundary conditions applied within the PLAXIS Soil Test tool. The first column lists the stress component. The second column lists the initial value of each component. The third column lists the type of incremental loading used. Finally, the fourth column shows the value of increment. For the triaxial test, a non-homogeneous stress state was intentionally initialized whereby the horizontal stresses represented half of the vertical stresses in magnitude. This corresponds to roughly a K_0 value of 0.5.

stress component	Initial [kN/m^2]	Incr.	value
σ_{xx}	-50	$\delta\sigma_{xx}$	0 [kN/m^2]
σ_{yy}	-100	$\delta\varepsilon_{yy}$	-10 [%/day]
σ_{zz}	-50	$\delta\sigma_{zz}$	0 [kN/m^2]
τ_{xy}	0	$\delta\gamma_{xy}$	0 [%/day]

Table B.3   Triaxial testing parameters

The FEM model uses the set-up described PLAXIS (2017) for simulation of a drained triaxial test. The domain consists of a 1 m x 1 m square representing one-quarter of the true geometry. Axes of symmetry lie on the left and bottom boundaries. The following fixities apply:
- Left boundary: Normally Fixed.
- Bottom boundary: Normally fixed.
- Right boundary: Free.
- Top boundary: Free.

The model uses two 15-noded elements each containing 9 stress points for discretization. Figure B.1 shows the problem mesh and dimensions, including the selected stress point for results.
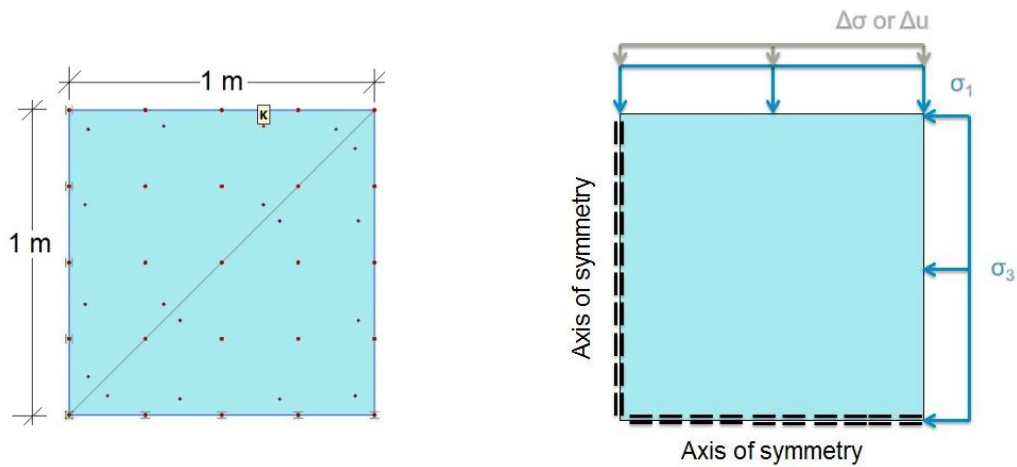
Figure B.1   Left: triaxial test mesh, Right: boundary conditions triaxial tests

The calculation phases consist of the following:
- Initial Phase.
- Phase 1: Initialize Stresses.
- Phase 2: Switch Material.
- Phase 3: Apply displacement.

The initial phase has no effect since the material unit weights are set to zero. Phase 1 utilizes a linear elastic material for time independent stress initialization. Phase 2 switches to the material of interest. Phase 3 applies an incremental displacement.

Phases 2 and 3 utilize the *Plastic* calculation type within PLAXIS and are time dependent. Phase 2 was included to provide more control of the creep prior to incremental displacement. However it was established that the closer phase 2 physical time approached zero, the closer the results of the subsequent phase gets to the Soil Test results.

Figure B.2 shows the effect of time step size for phase 2 on Phase 3 results. The top three subfigures show evolution of principal stresses over incrementally increasing Phase 2 total times. The bottom left and right subfigures show that as the material switch time decreases, the total force and pore water pressure with respect to principal strain approach PLAXIS Soil Test behaviour. The bottom middle subfigure shows that as material switch time decreases, the principal strain with respect to time (creep) approaches PLAXIS Soil Test behaviour.

For this reason the total time for the material switch phase was minimized such that the results approach PLAXIS Soil Test as closely as possible.

POV MACRO STABILITEIT
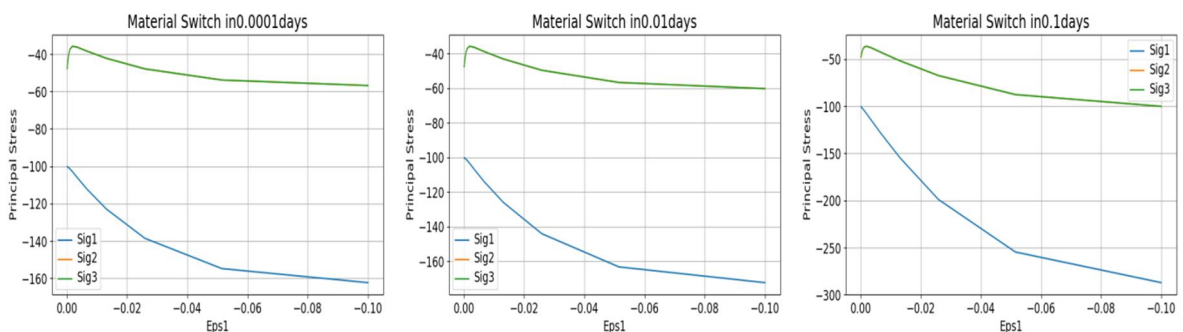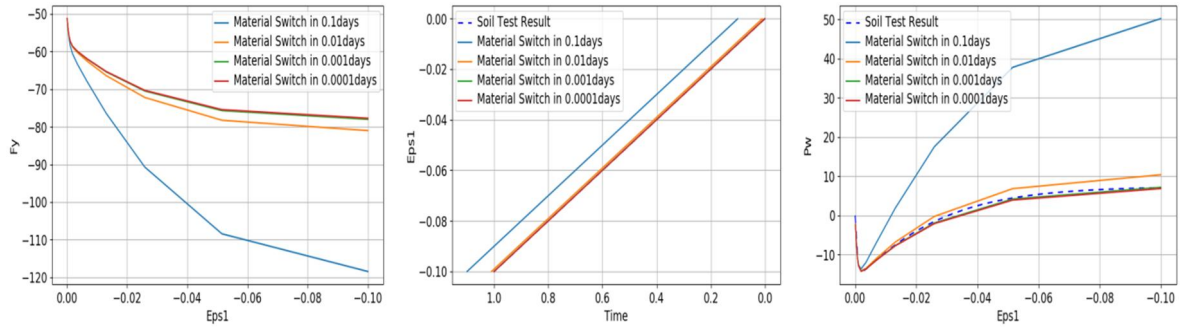
Figure B.2   Effect of Phase 2 (Material Switch) on Phase 3 results

Figure B.3 shows the results for the drained triaxial case and Figure B.4 shows the results for the undrained case. There is very good correspondence between the single stress point simulations and the boundary value problem, for both the drained and undrained case. Based on the results it is decided to simulate the drained and undrained triaxial compression tests with only the single stress point simulations.

POV
MACRO
STABILITEIT
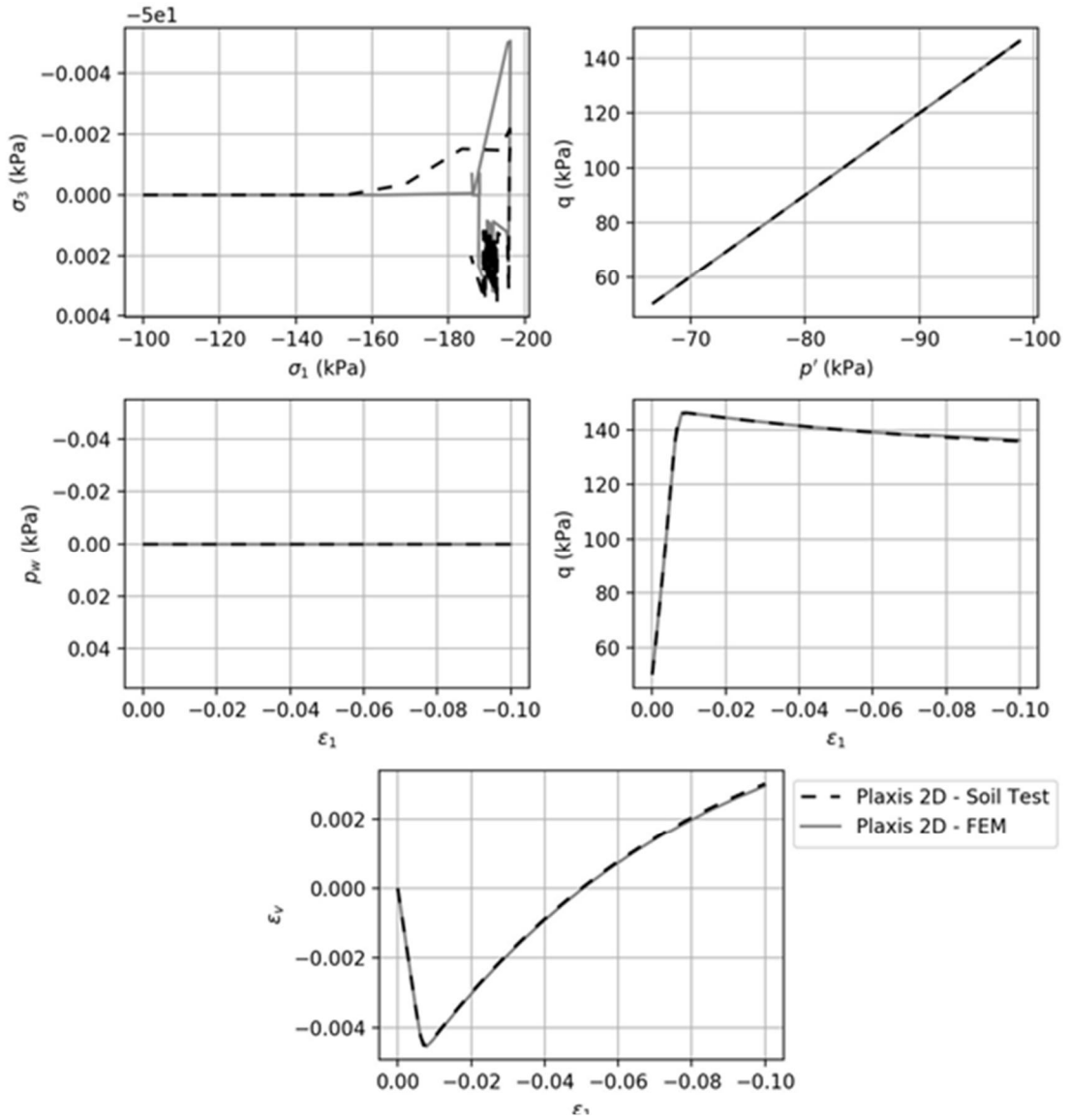
Figure B.3   Comparison of single point and boundary value problem simulations of drained triaxial compression tests; OCR = 2, $\alpha = 0.5$, $\omega = 25$, $\omega_d = 1$, other parameters according to Table B.1

POV MACRO STABILITEIT
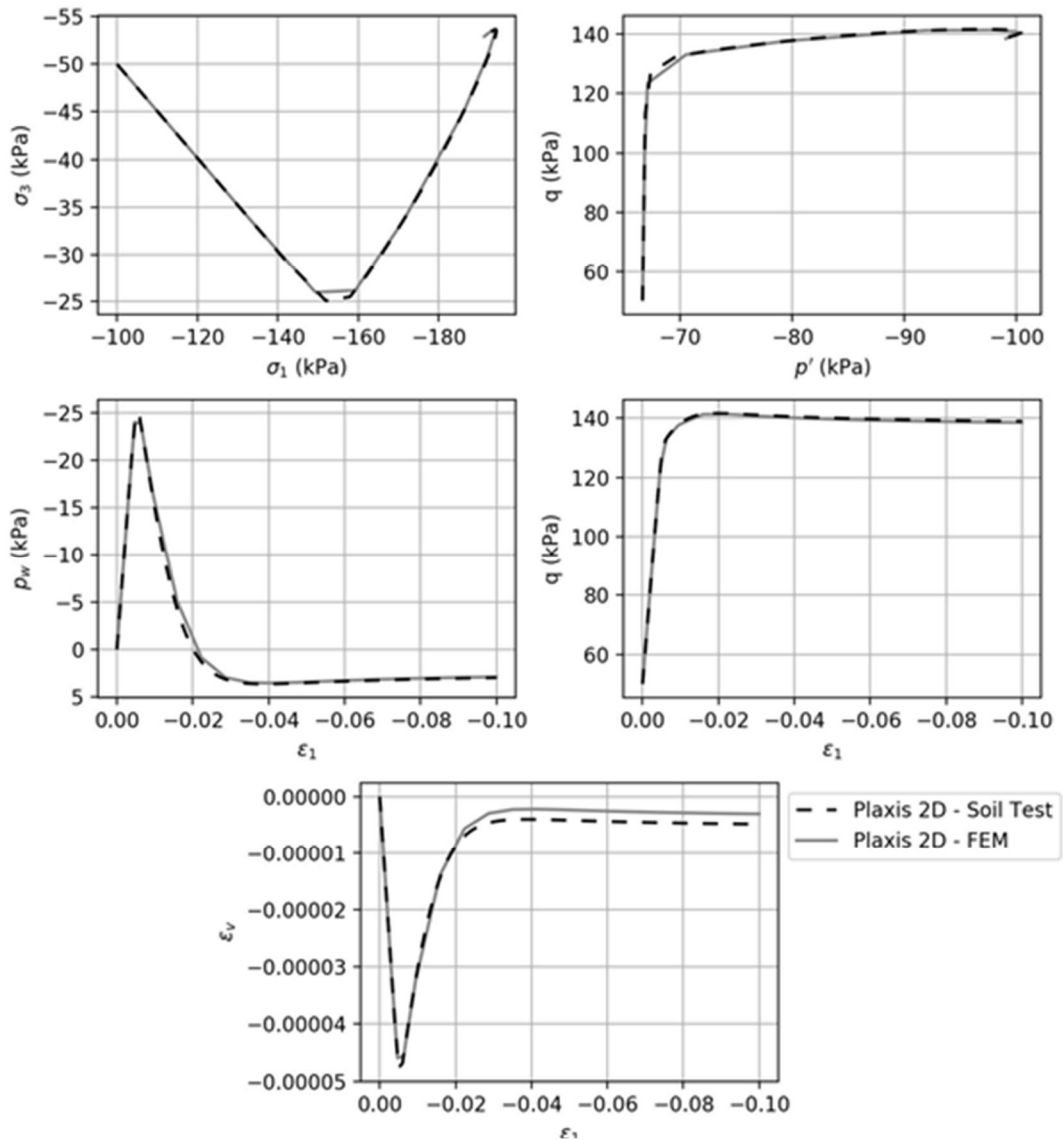
Figure B.4 Comparison of single point and boundary value problem simulations of undrained triaxial compression tests; OCR = 2, α = 0.5, ω = 25, ω_d = 1, other parameters according to Table B.1

B.2.2 Simulation of drained triaxial compression tests

Figure B.5 to Figure B.11 show variations 1 through 7, see Table B.2, for the drained triaxial compression tests. For each variation 5 subfigures are presented, showing stress and strain development. The results are discussed in section 3.4.
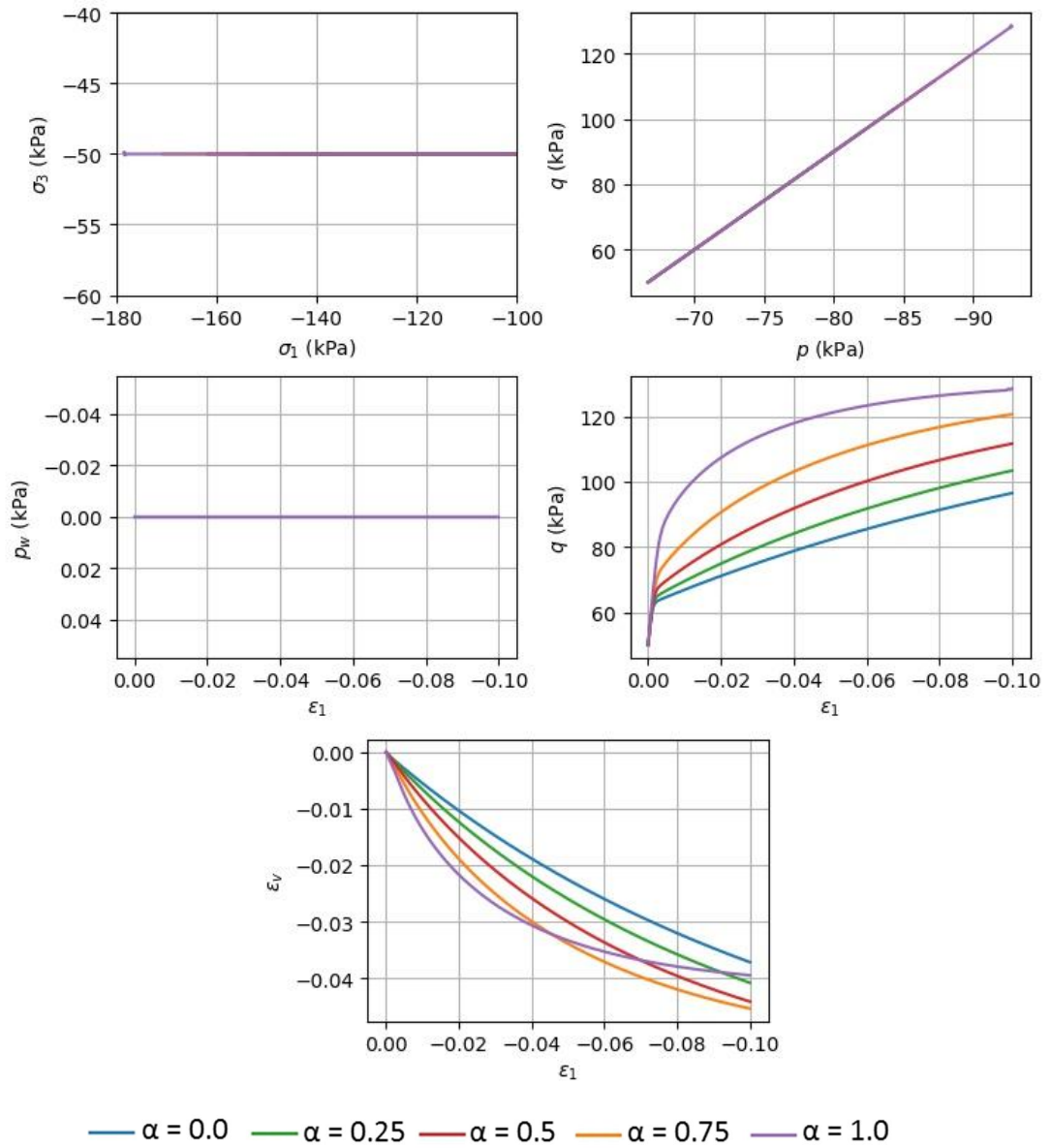
Figure B.5   *Triaxial Test (Drained): Variation 1: $\alpha_0 = [0, 0.25, 0.5, 0.75, 1.0]$, $\omega = 0.0$, $\omega_d = 0.0$, OCR = 1*
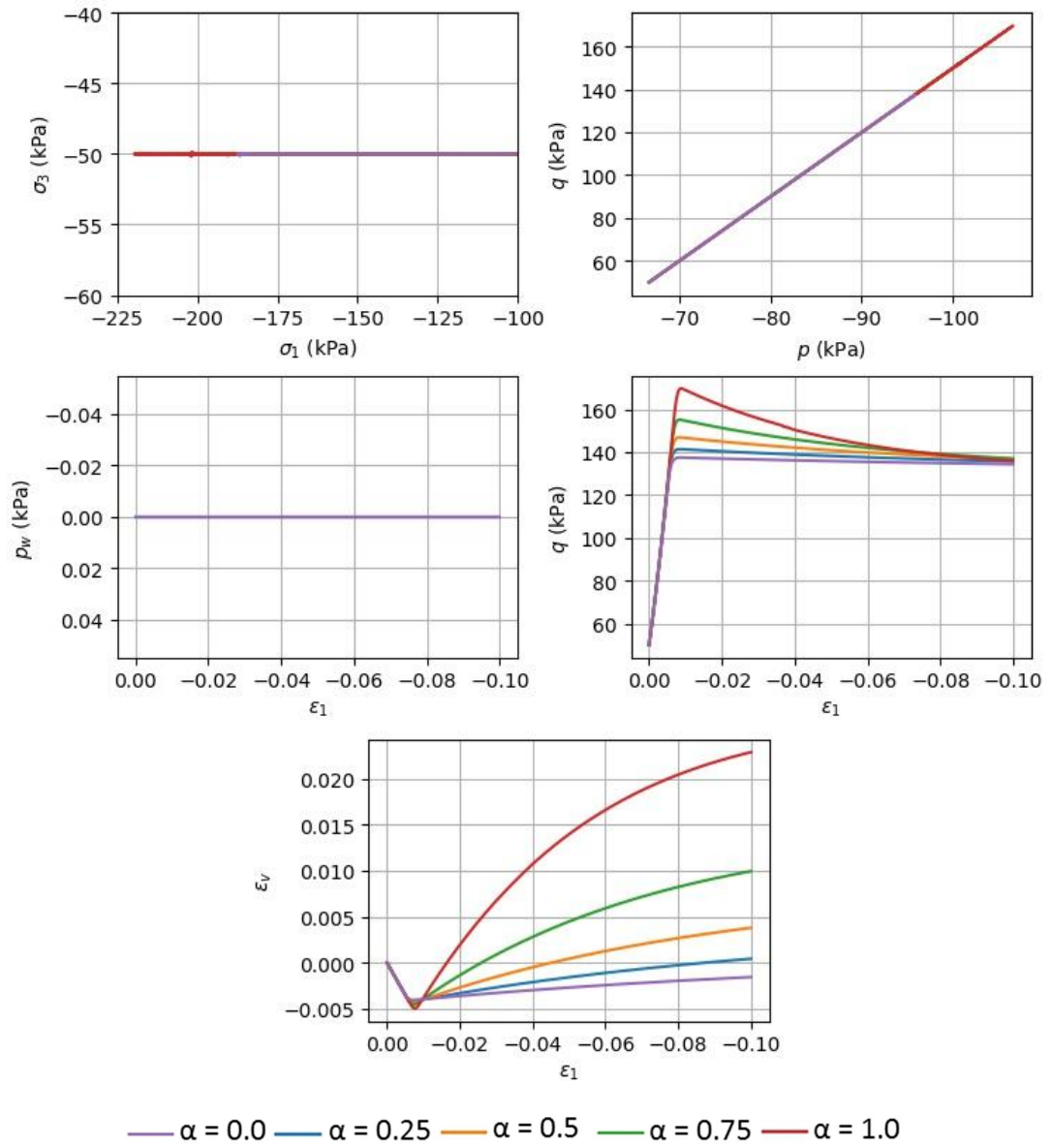
Figure B.6 Triaxial Test (Drained): Variation 2: $\alpha_0 = [0, 0.25, 0.5, 0.75, 1.0]$, $\omega = 0.0$, $\omega_d = 0.0$, OCR = 2
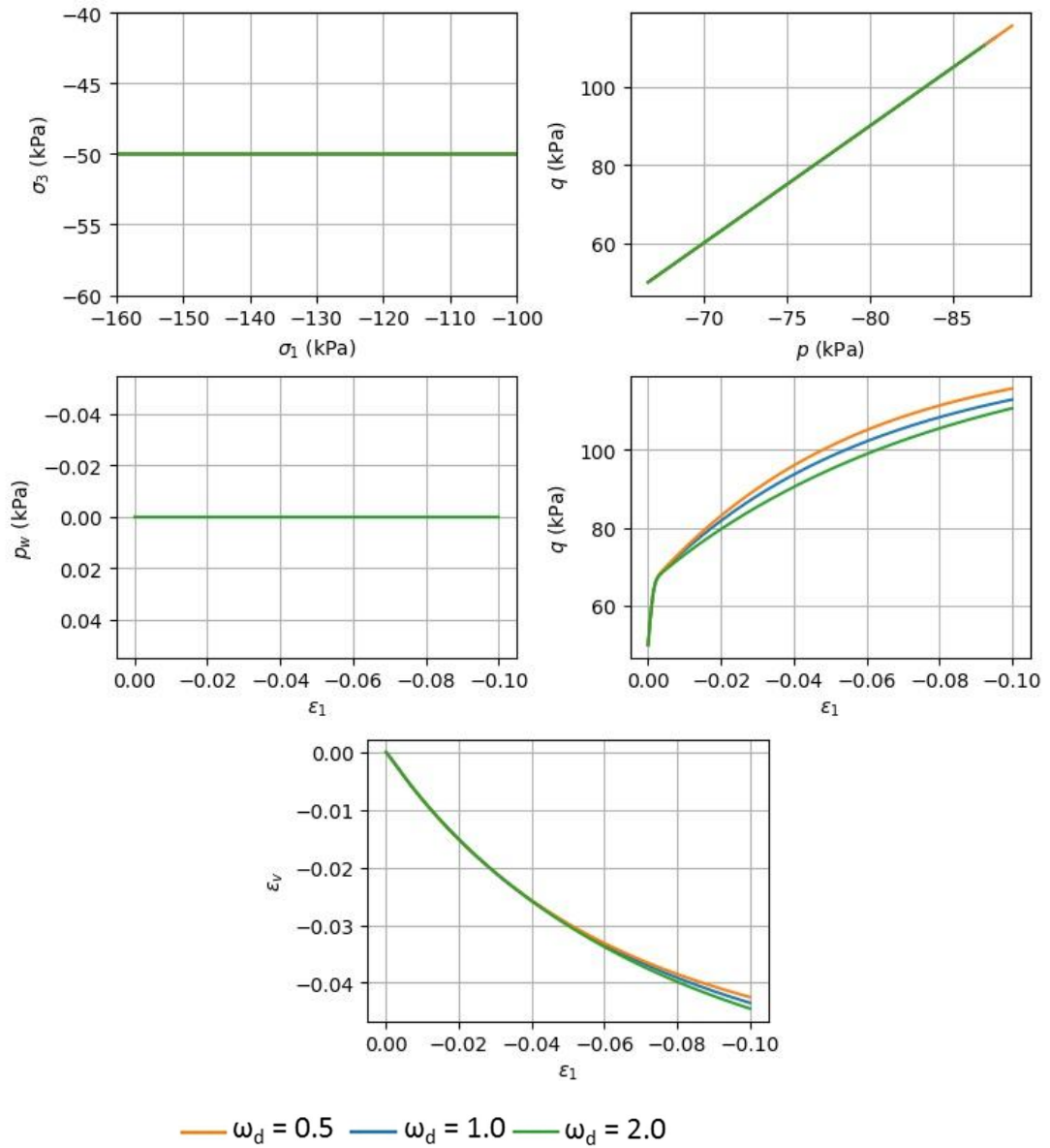
*Figure B.7 Triaxial Test (Drained): Variation 3: $\alpha_0 = 0.5$, $\omega = 25$, $\omega_d = [0.5, 1, 2]$, OCR = 1.0*
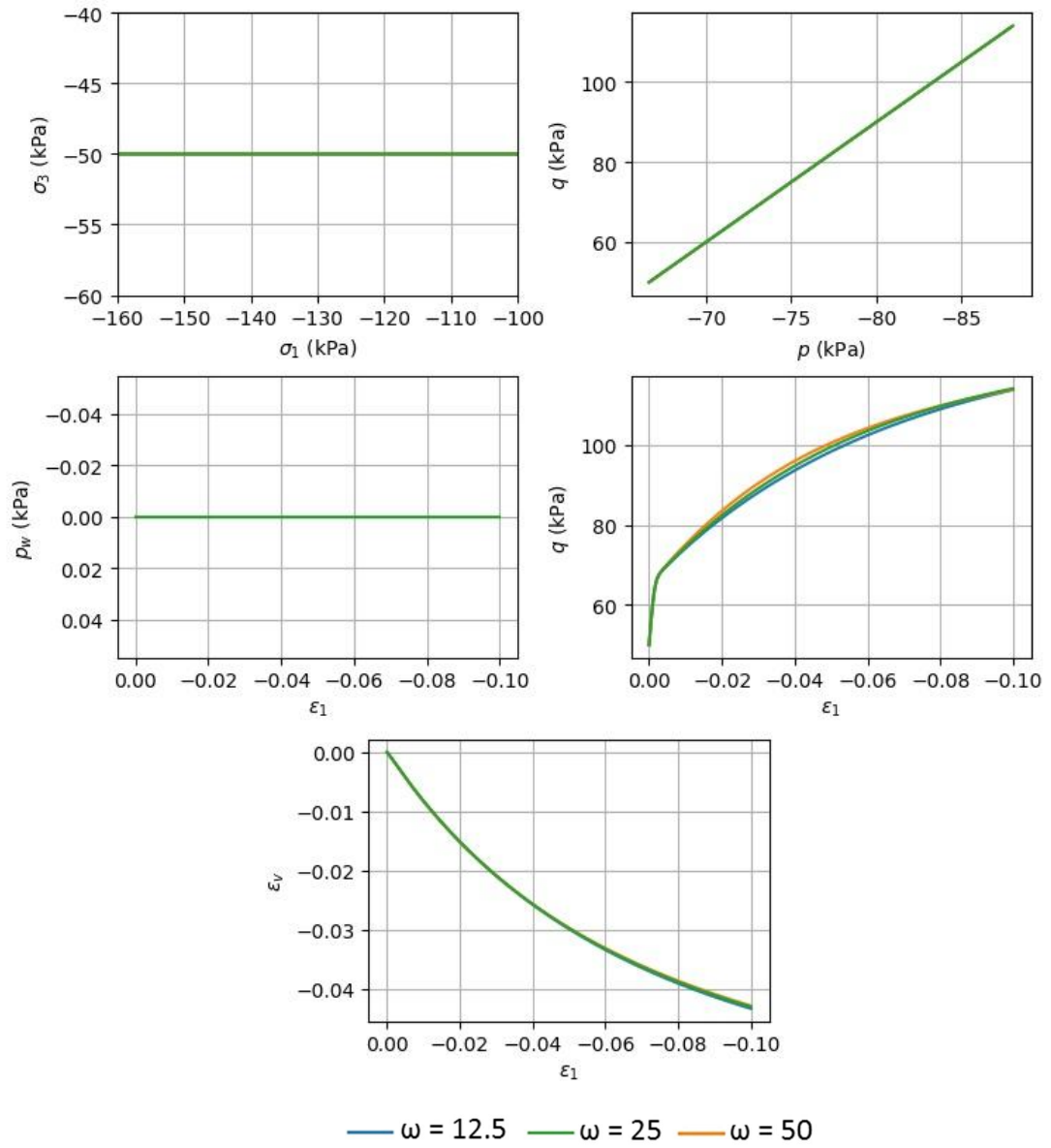
Figure B.8 Triaxial Test (Drained): Variation 4: $\alpha_0 = 0.5$, $\omega = [12.5, 25, 50]$, $\omega_d = 0.75$, OCR = 1.0
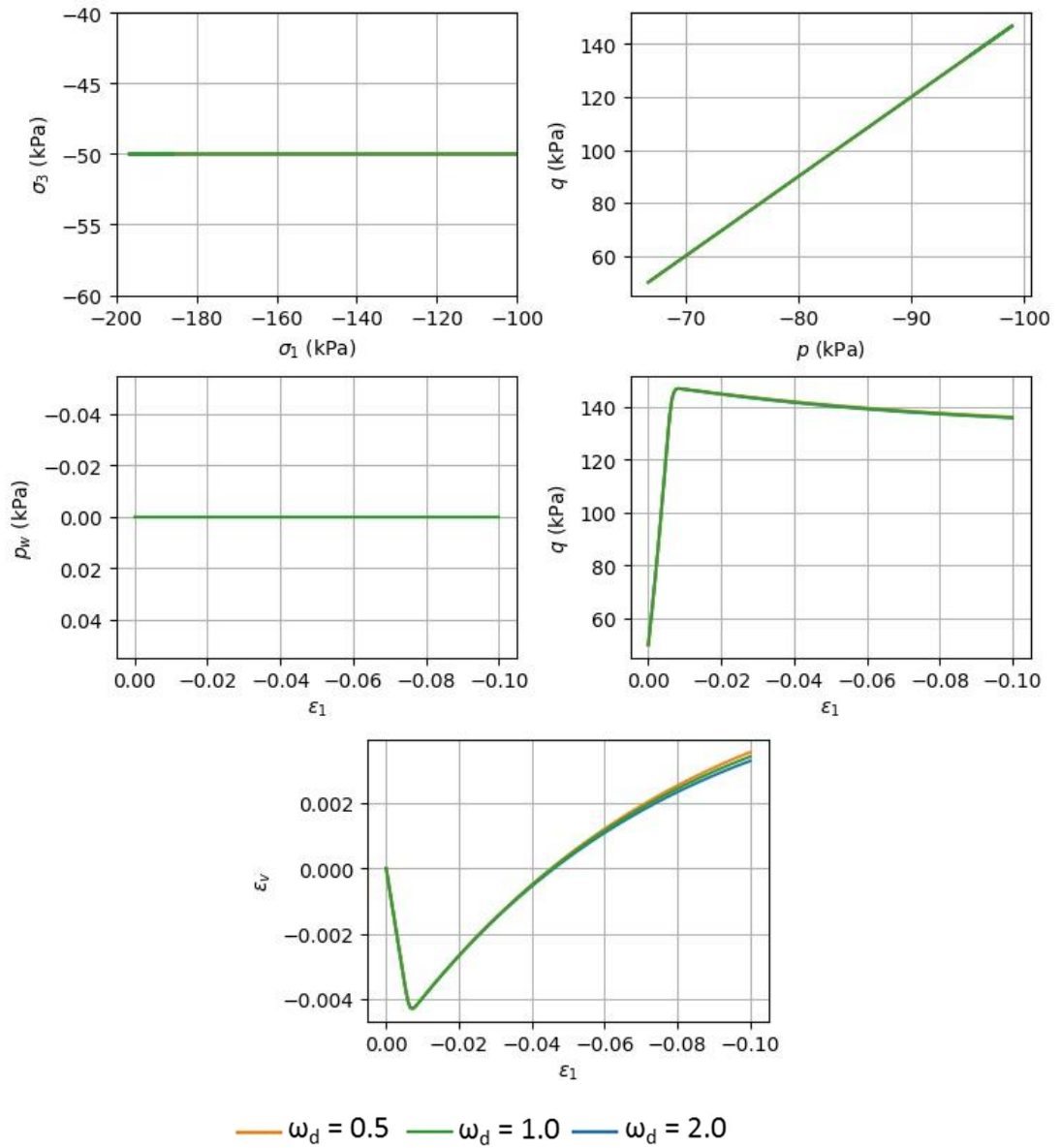
*Figure B.9 Triaxial Test (Drained): Variation 5: $\alpha_0 = 0.5$, $\omega = 25$, $\omega_d = [0.5, 1, 2]$, OCR = 2.0*
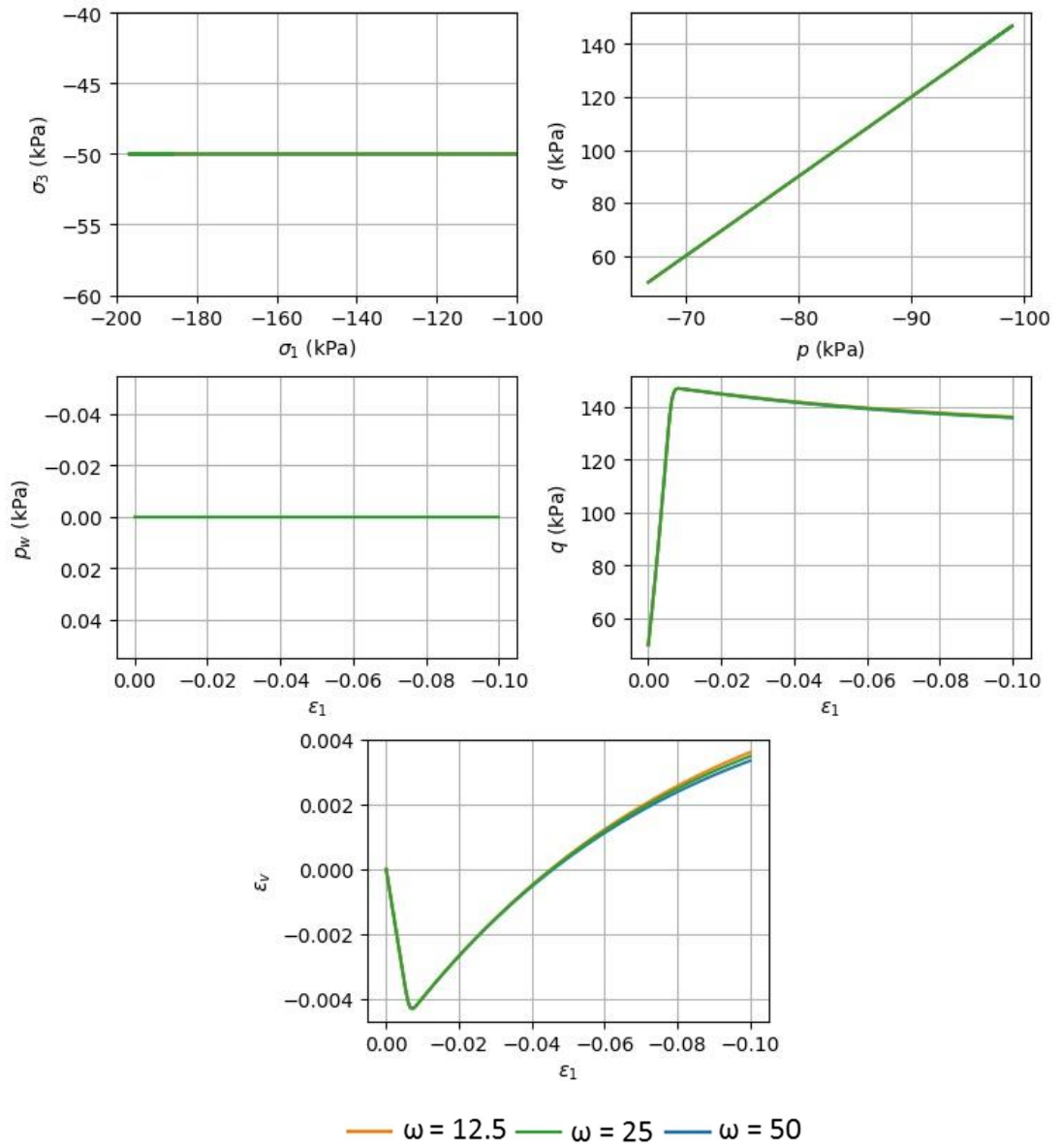
Figure B.10   Triaxial Test (Drained): Variation 6: $\alpha_0 = 0.5$, $\omega = [12.5,25,30]$, $\omega_d = 0.75$, OCR = 2.0
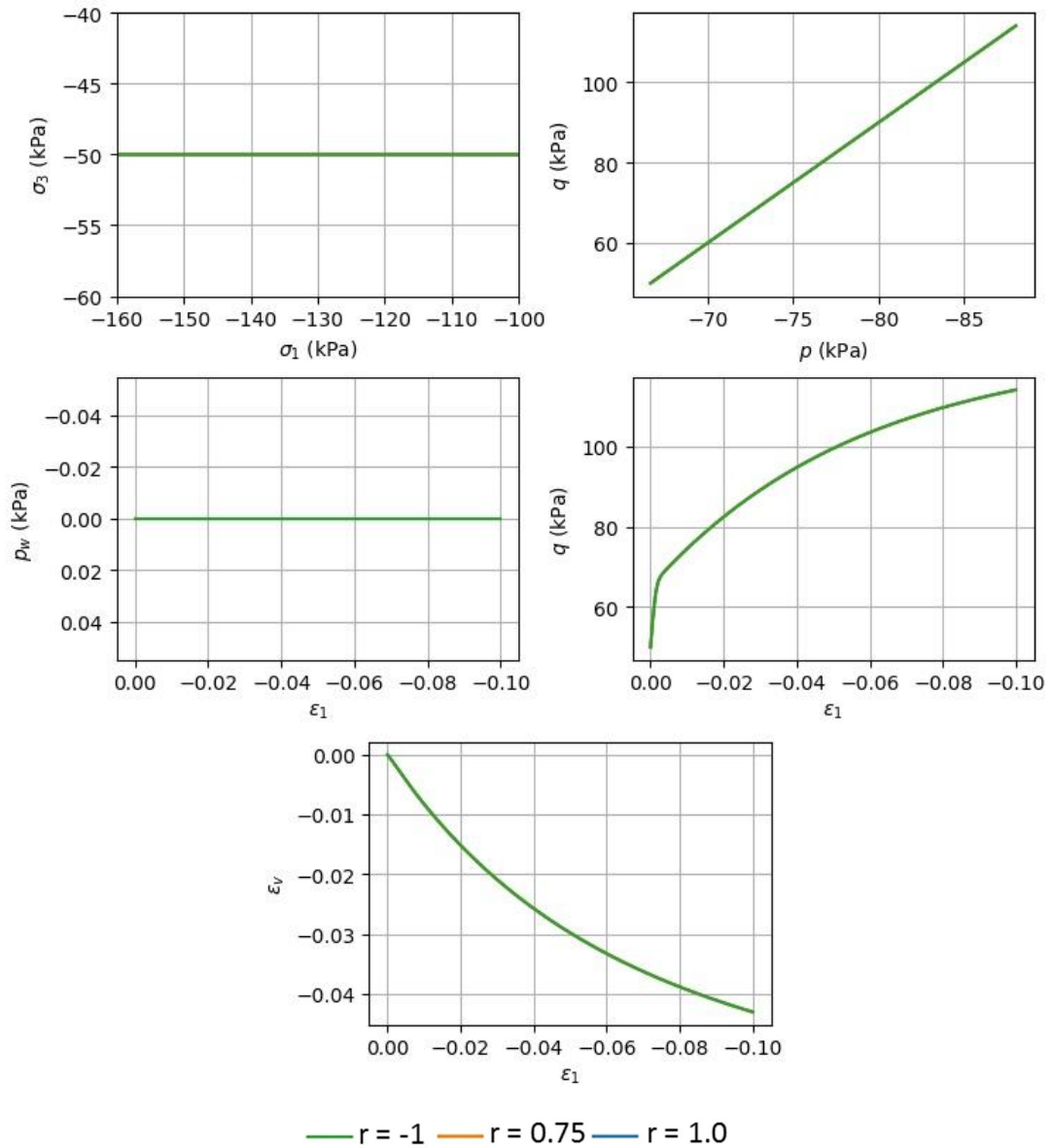
Figure B.11 Triaxial Test (Drained): Variation 7: $\alpha_0 = 0.5$, $\omega = 25$, $\omega_d = 0.75$, OCR = 1.0, r = [-1, 0.75, 1.0]

B.2.3 Undrained tests

Figure B.12 to Figure B.18 show variations 1 through 7, see Table B.2, for undrained triaxial compression tests. For each variation 5 subfigures are presented, regarding stress and strain development. The results are discussed in section 3.4.
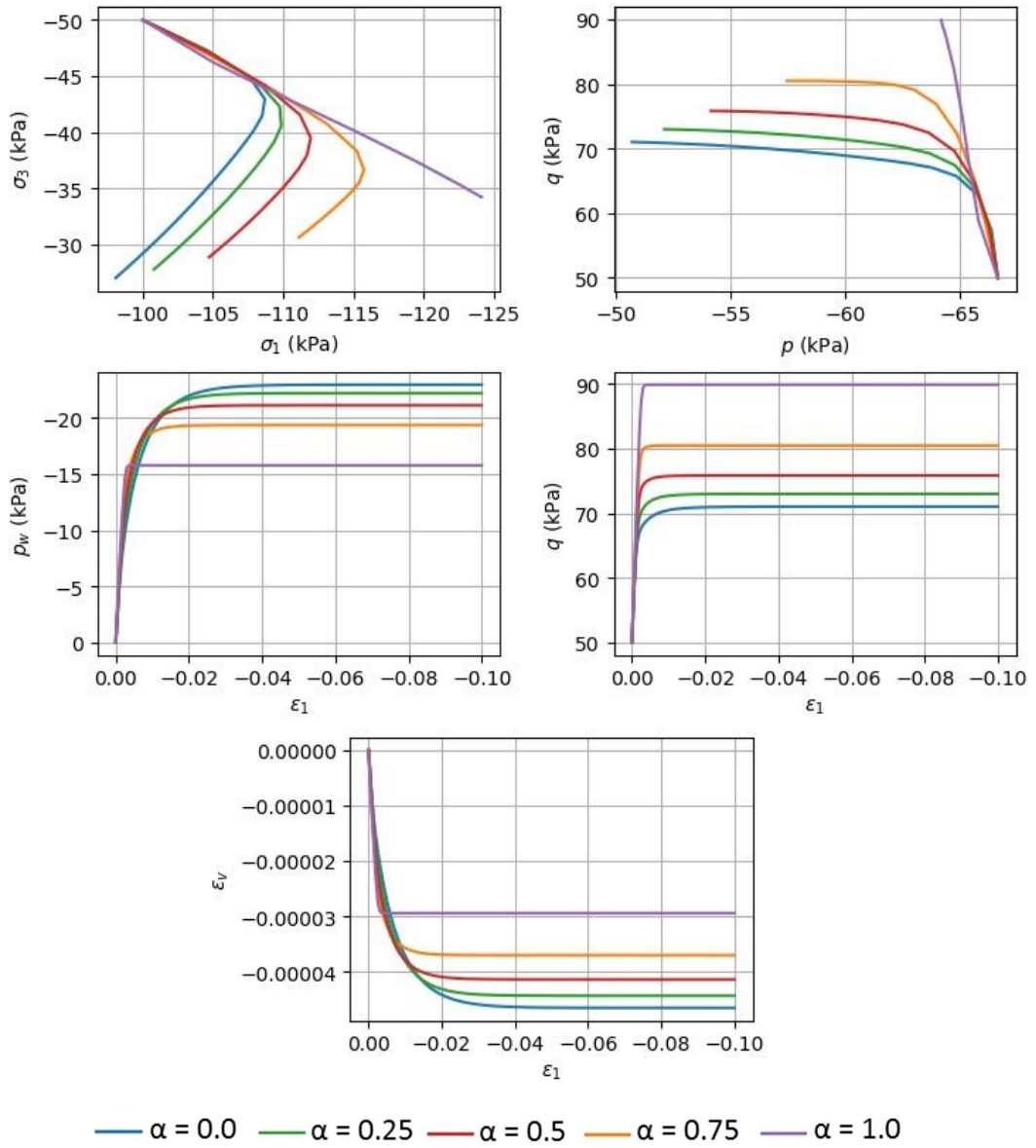
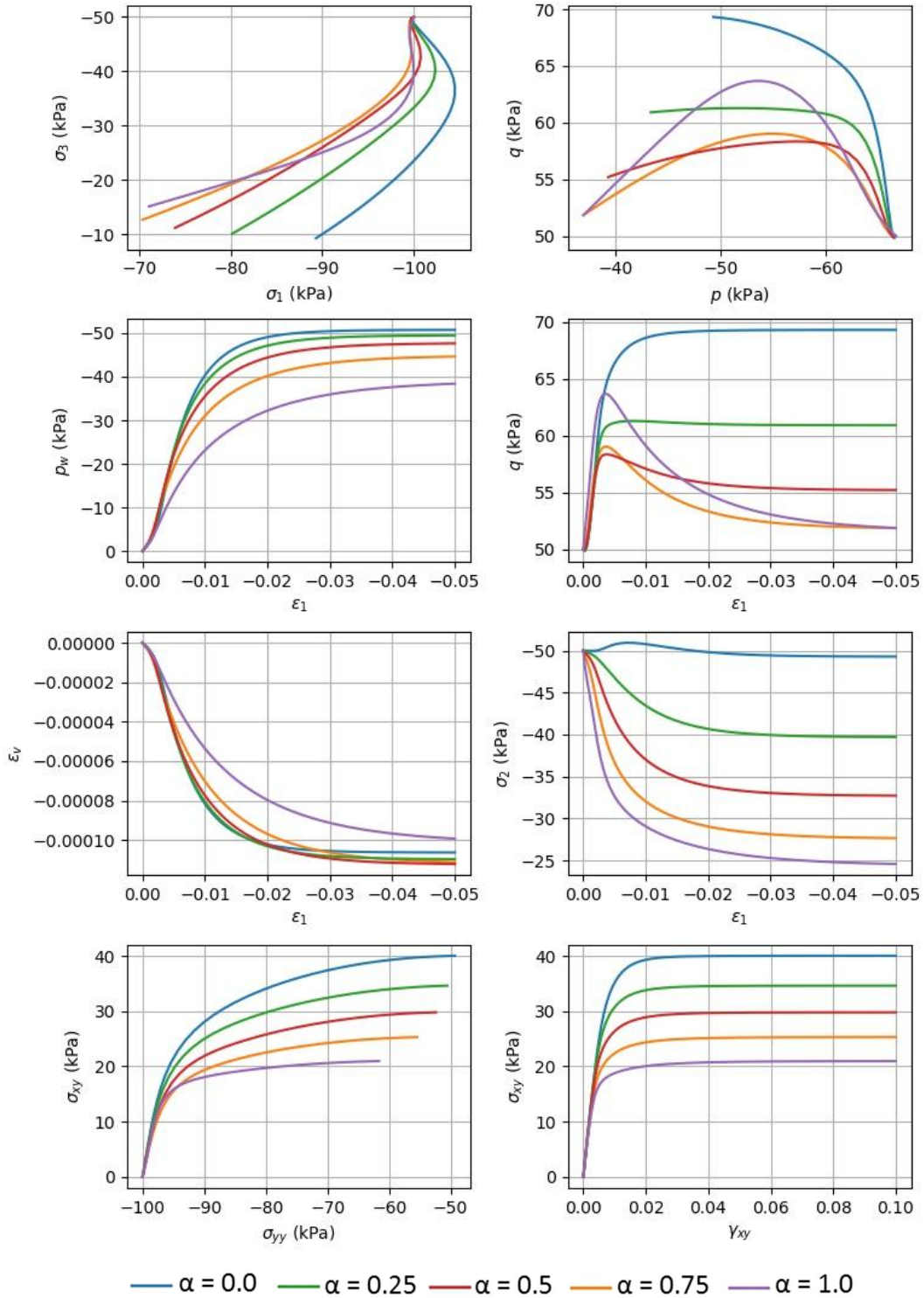*Figure B.12 Triaxial Test (Undrained): Variation 1: $\alpha_0 = [0, 0.25, 0.5, 0.75, 1.0]$, $\omega = 0.0$, $\omega_d = 0.0$, OCR = 1*
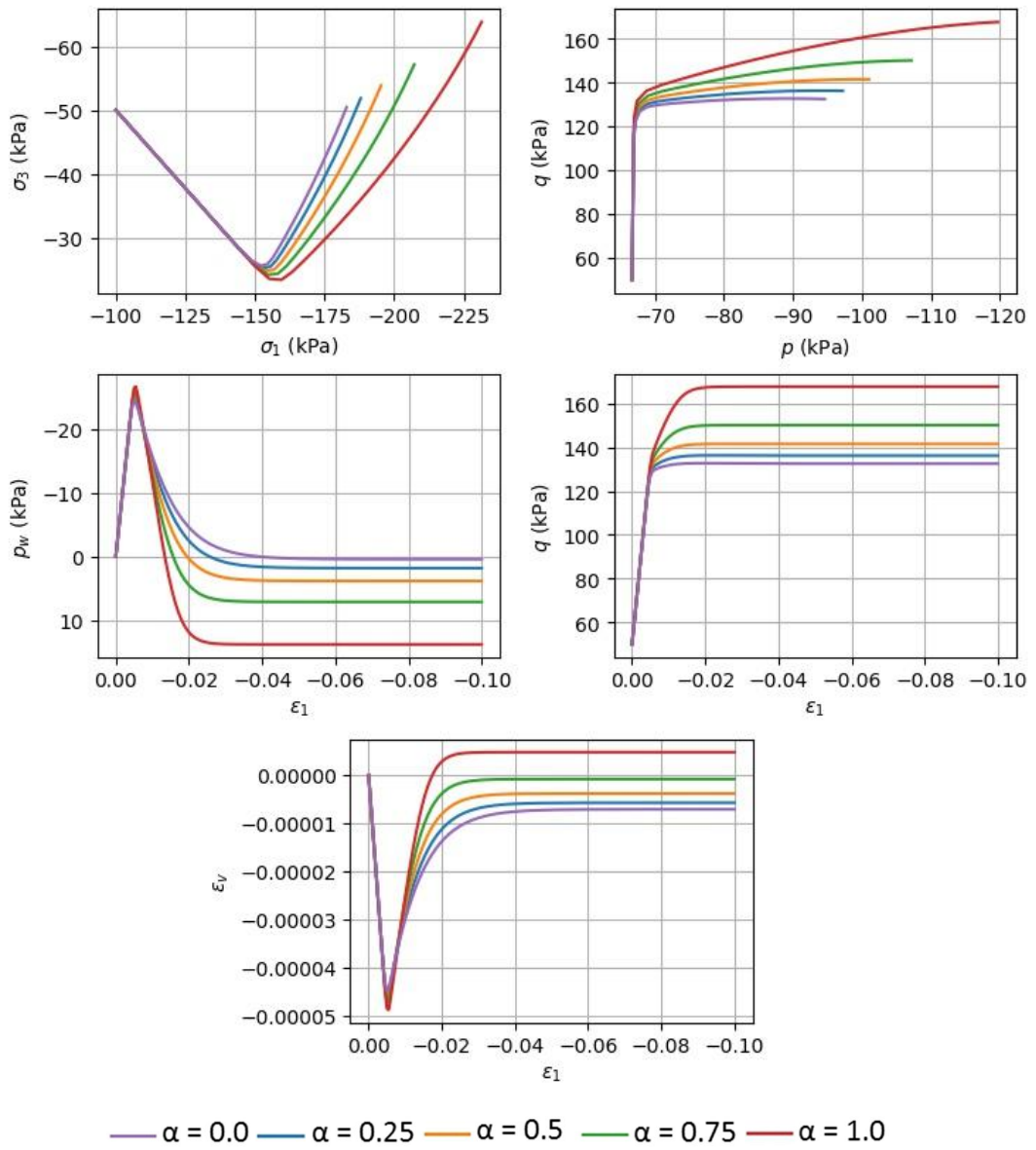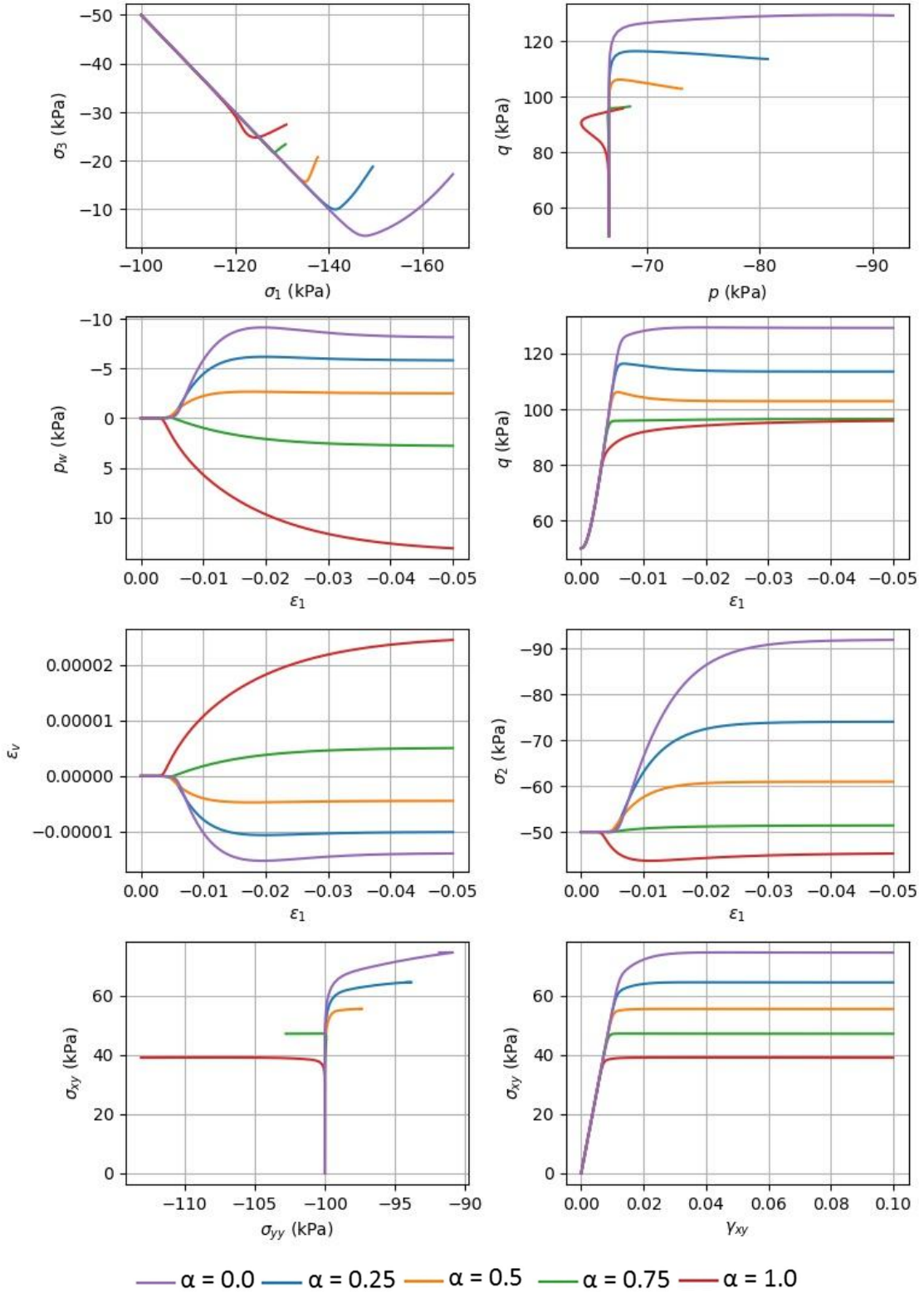
Figure B.13 Triaxial Test (Undrained): Variation 2: $\alpha_0 = [0, 0.25, 0.5, 0.75, 1.0]$, $\omega = 0.0$, $\omega_d = 0.0$, OCR = 2
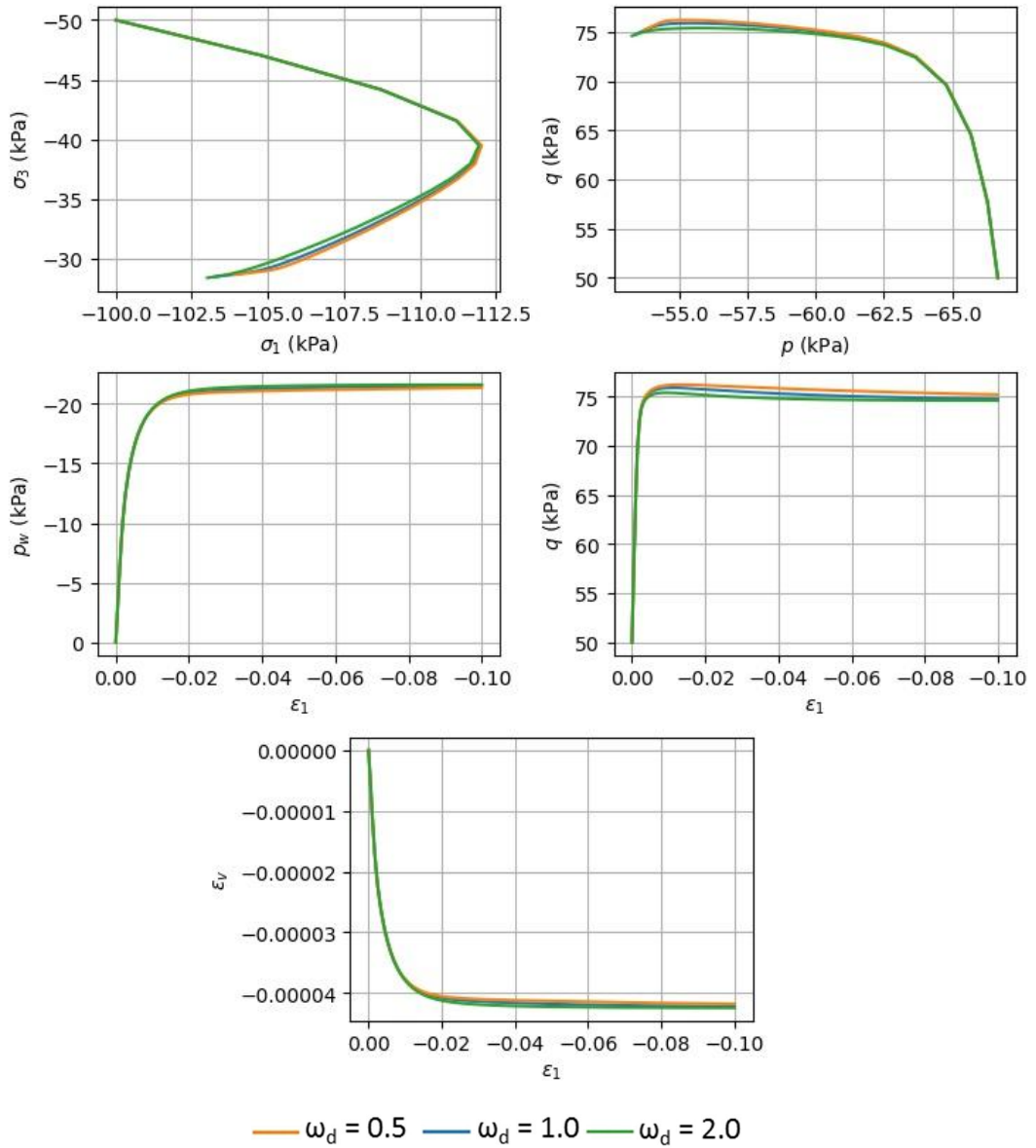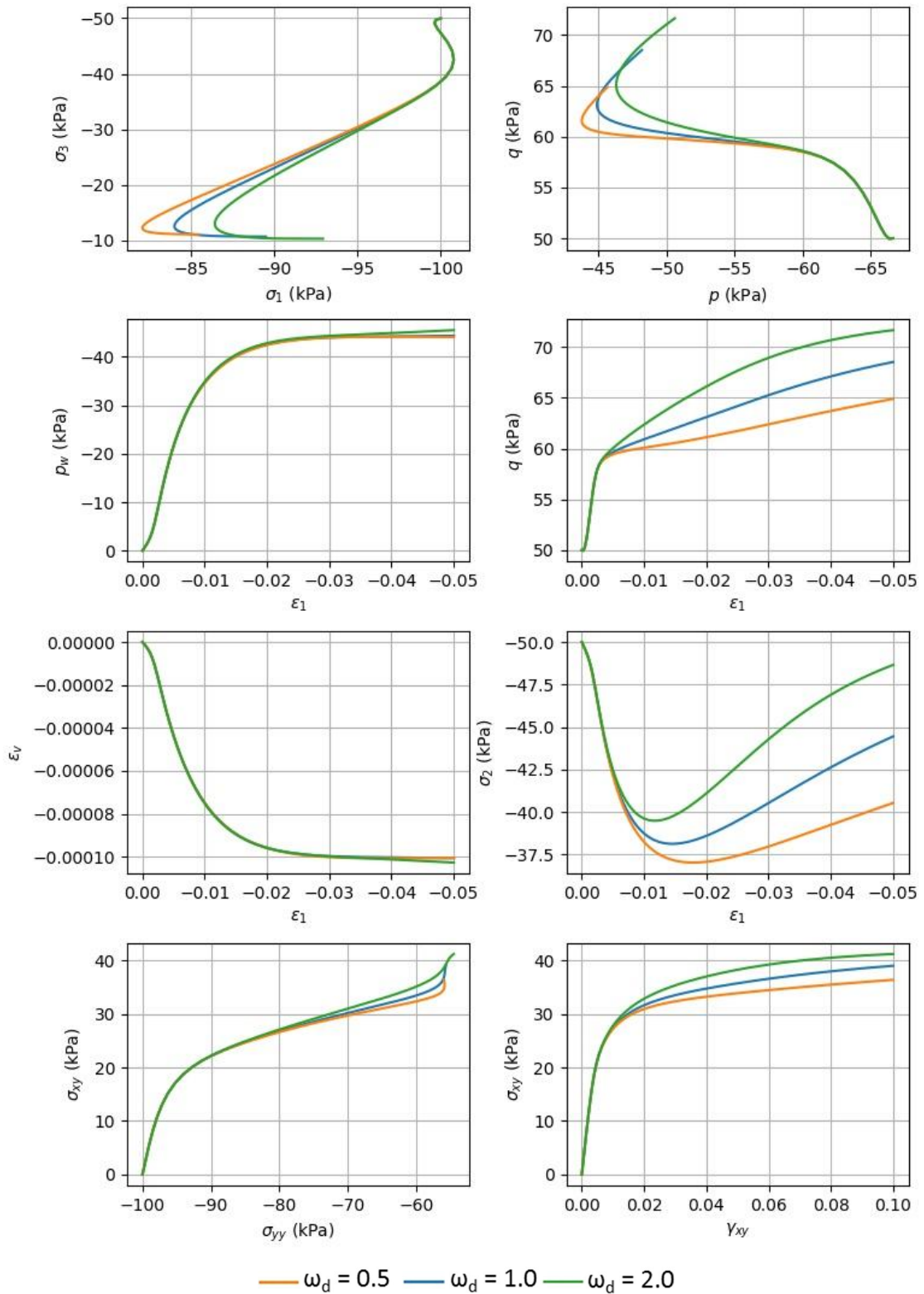
Figure B.14 Triaxial Test(Undrained): Variation 3: α_0 = 0.5, ω = 25, ω_d = [0.5, 1, 2], OCR = 1.0
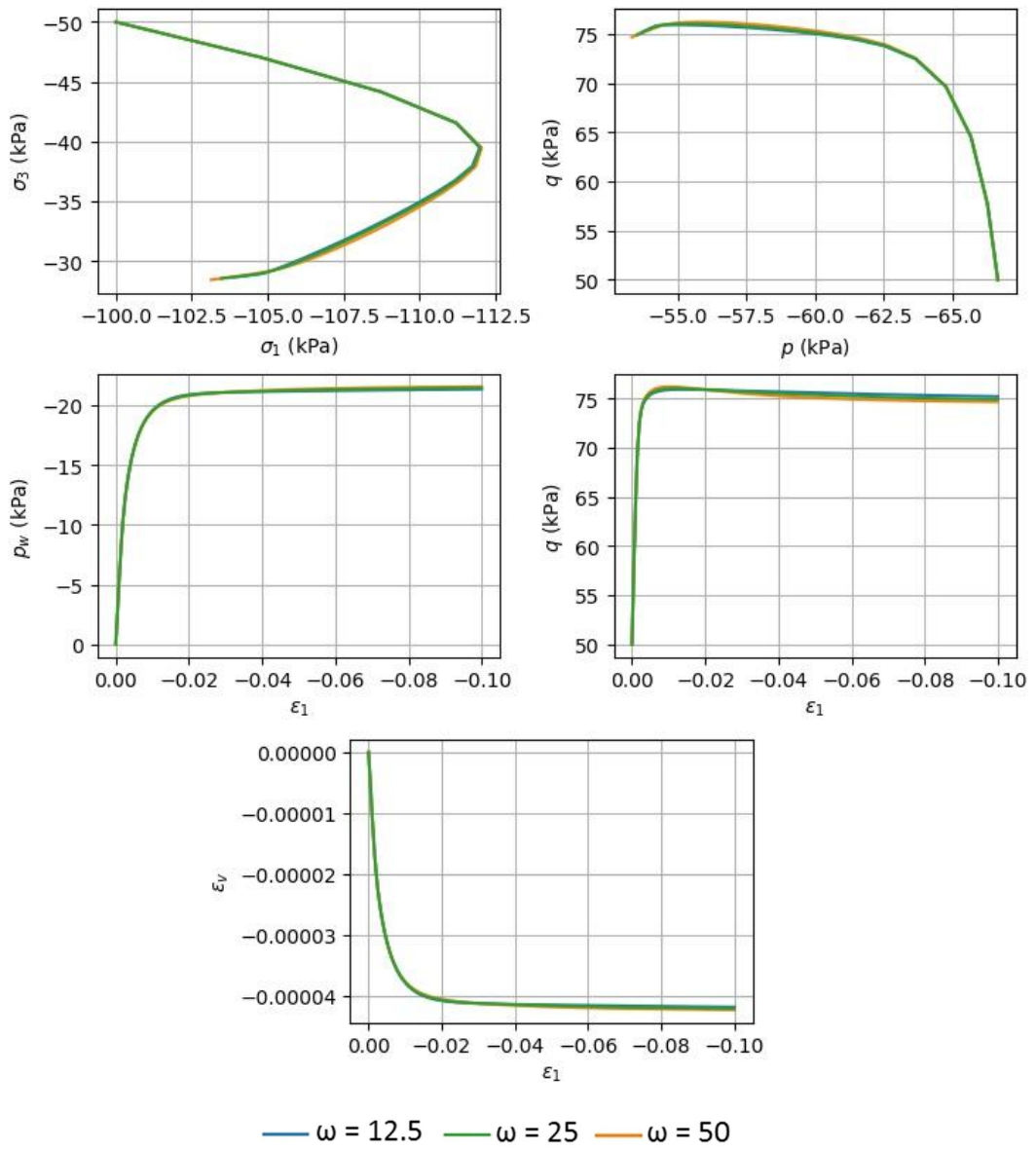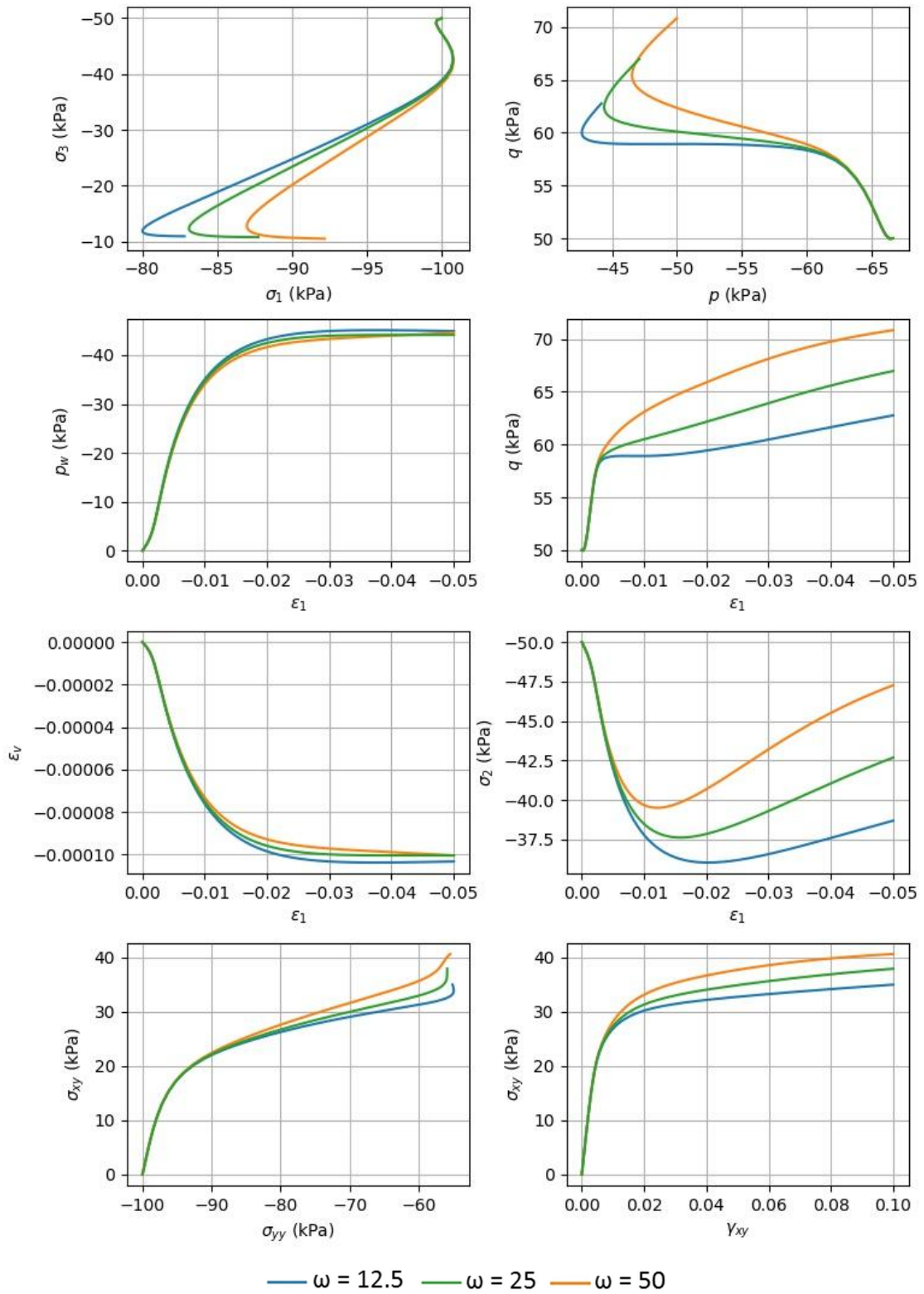
Figure B.15 Triaxial Test(Undrained): Variation 4: $\alpha_0 = 0.5$, $\omega = [12.5, 25, 50]$, $\omega_d = 0.75$, OCR = 1.0

POV MACRO STABILITEIT
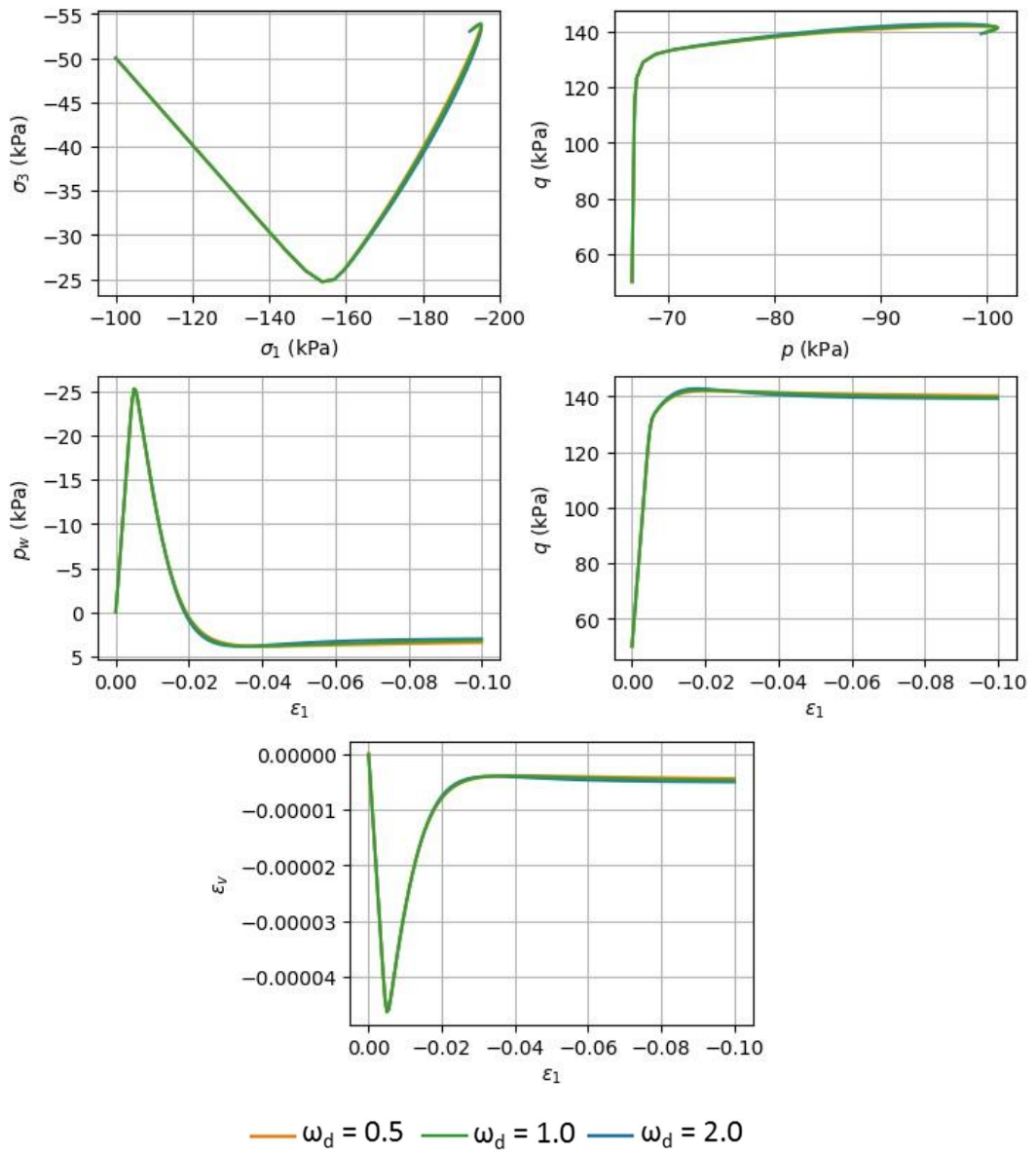
Figure B.16 Triaxial Test (Undrained): Variation 5: $\alpha_0 = 0.5$, $\omega = 25$, $\omega_d = [0.5, 1, 2]$, OCR = 2.0
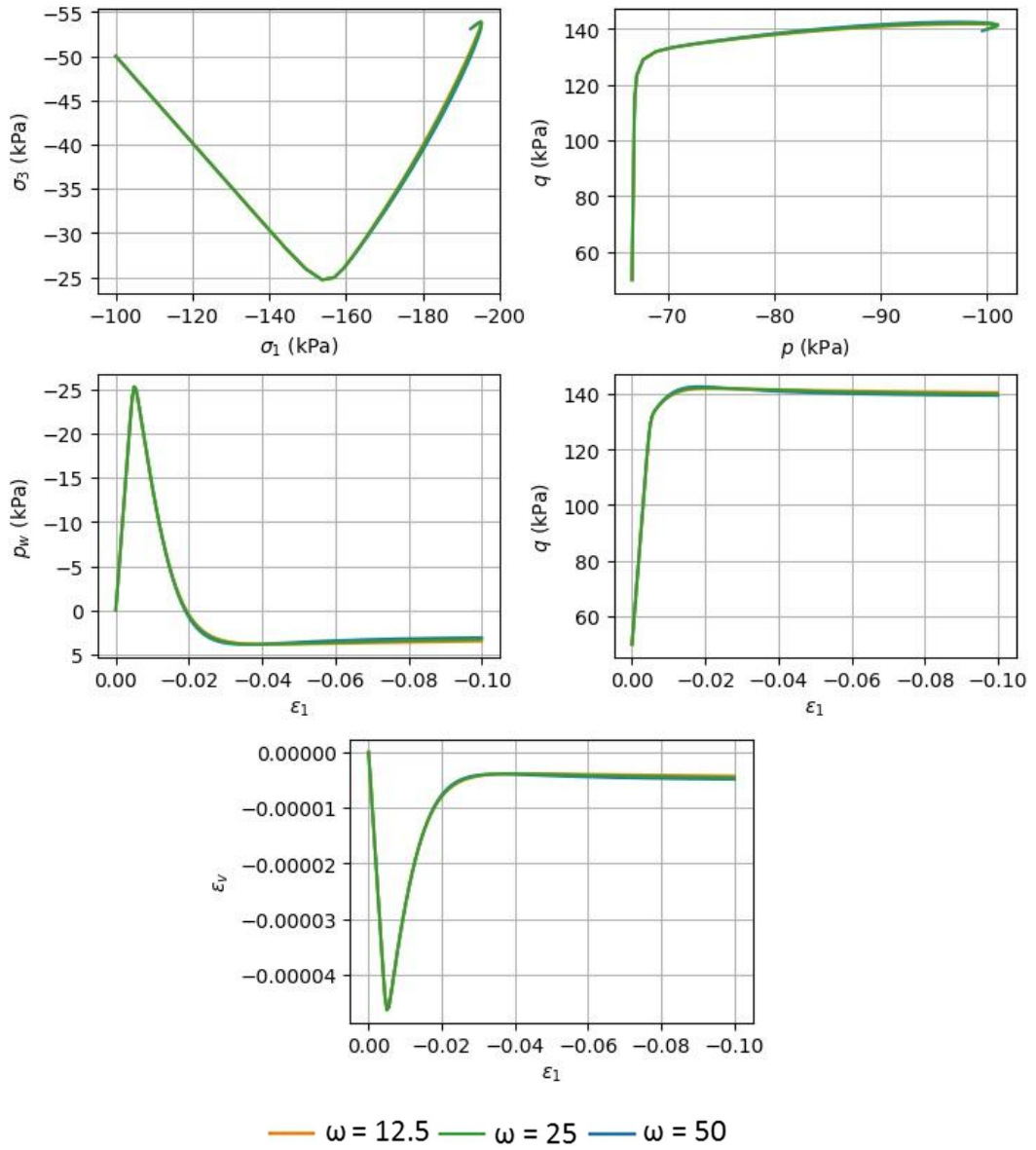
Figure B.17 Triaxial Test (Undrained): Variation 6: $\alpha_0 = 0.5$, $\omega = [12.5, 25, 30]$, $\omega_d = 0.75$, OCR = 2.0
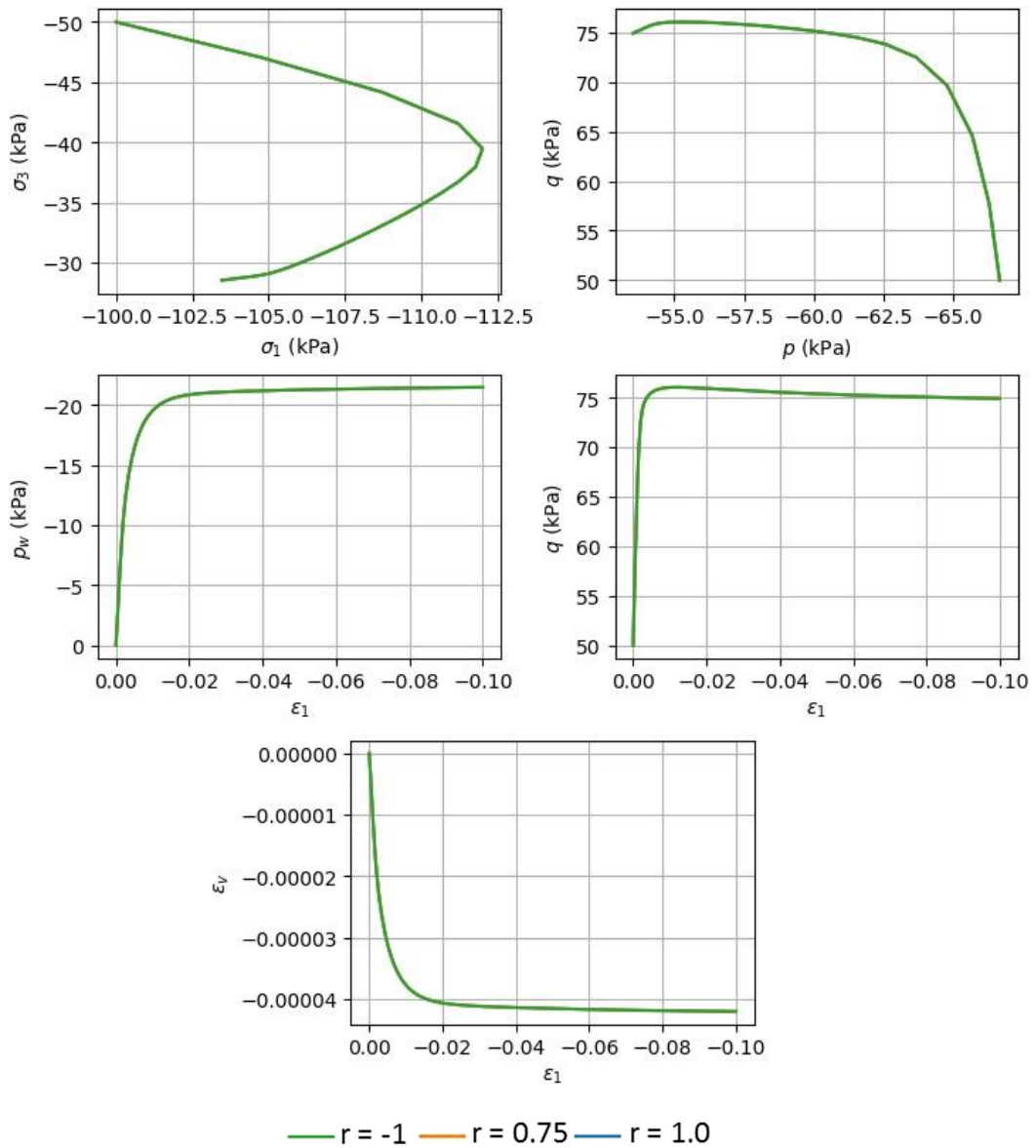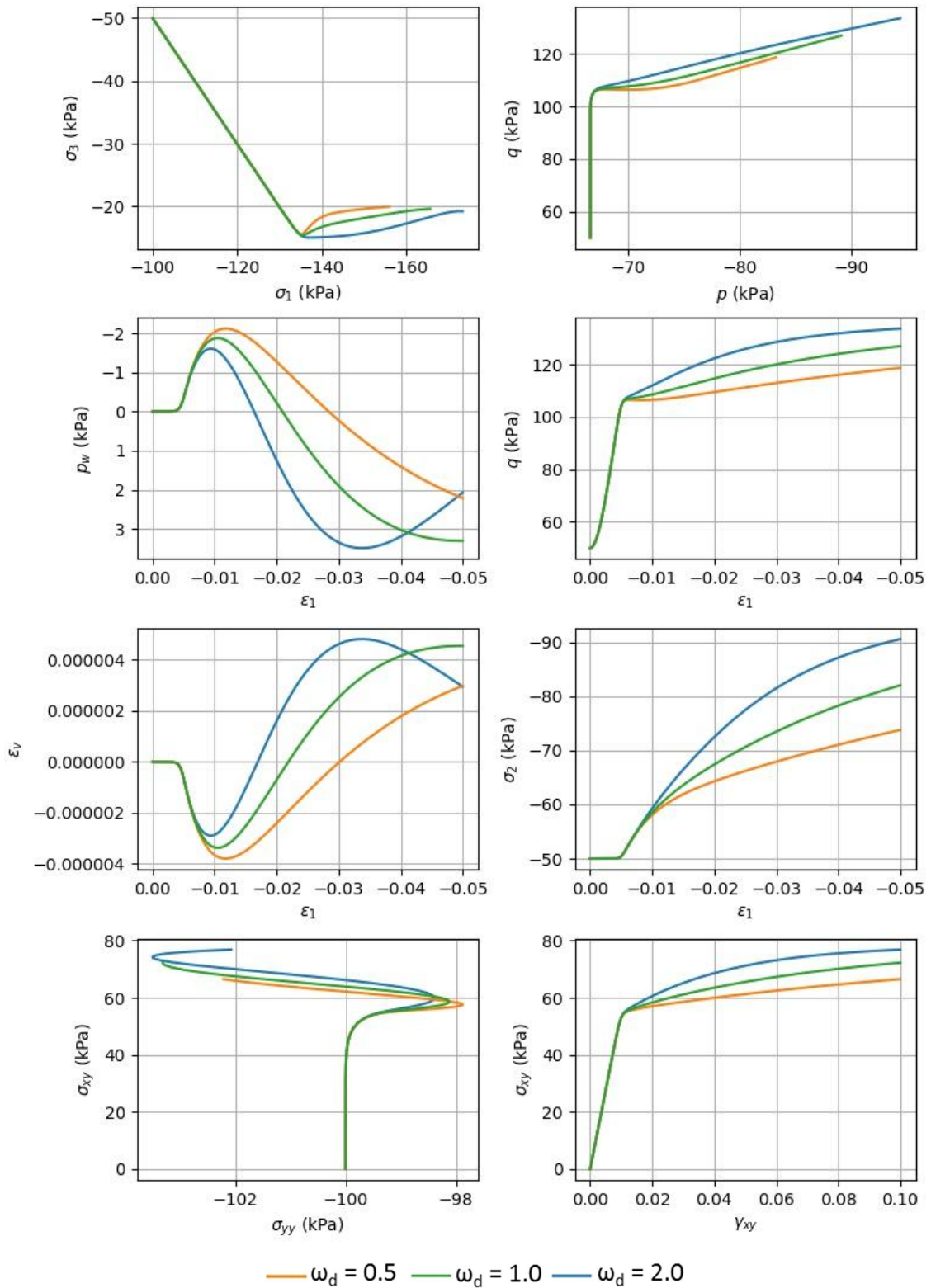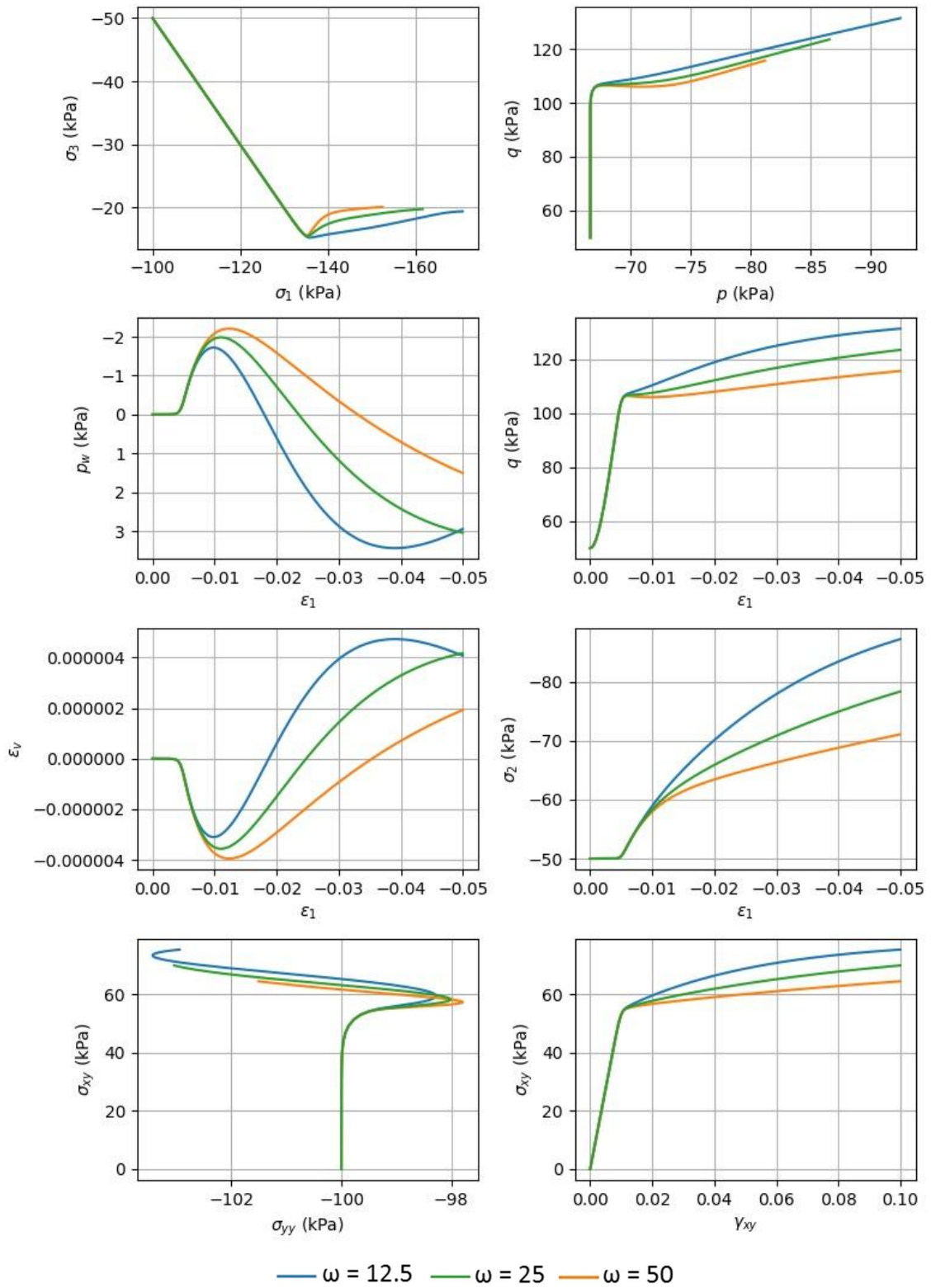
Figure B.18 Triaxial Test (Undrained): Variation 7: $\alpha_0 = 0.5$, $\omega = 25$, $\omega_d = 0.75$, OCR = 1.0, r = [-1, 0.75, 1]

B.3   Biaxial tests

B.3.1   Boundary conditions biaxial testing

This section discusses the simulation of biaxial tests. The initial conditions and boundary conditions are given by Table B.4. Simulations have been made for drained and undrained conditions, regarding the 7 cases explained by Table B.2. Section A.3.2. shows the simulation for the drained tests, section A.3.3 shows the simulations for the undrained case.

POV MACRO STABILITEIT

stress component	Initial [kN/m^2]	Incr.	value
σ_{xx}	-50	$\delta\sigma_{xx}$	0 [kN/m^2]
σ_{yy}	-100	$\delta\varepsilon_{yy}$	-10 [%/day]
σ_{zz}	-50	$\delta\varepsilon_{zz}$	0 [%/day]
τ_{xy}	0	$\delta\gamma_{xy}$	0 [%/day]

Table B.4   Boundary conditions simulation triaxial tests

B.3.2   Drained biaxial tests

Figure B.19 to Figure B.25 show variations 1 through 7, see Table B.2, for drained biaxial tests. For each variation 6 subfigures are presented, regarding stress and strain development. The results are discussed in section 3.4.
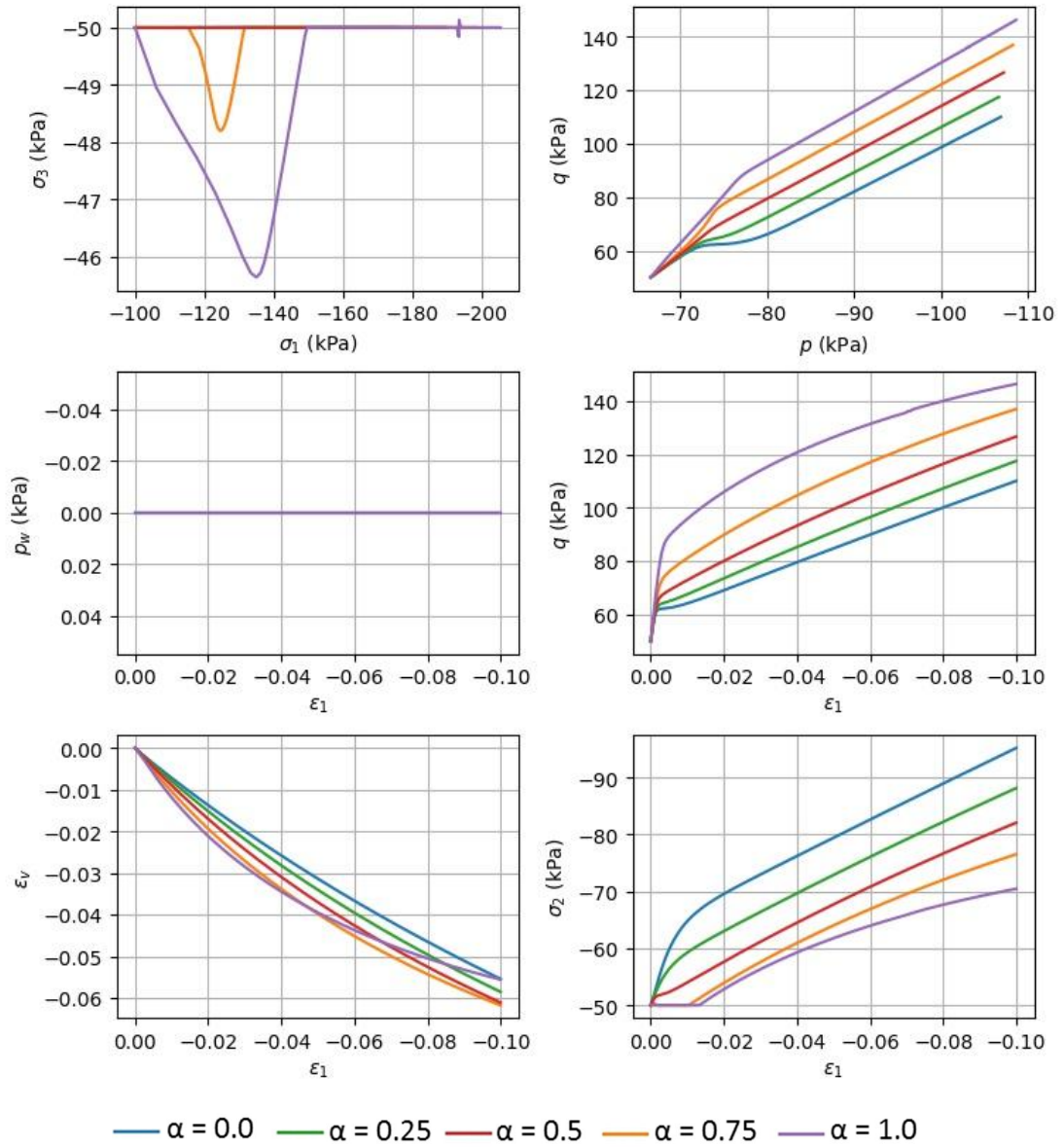
Figure B.19 Biaxial Test (Drained): Variation 1: $\alpha_0 = [0, 0.25, 0.5, 0.75, 1.0]$, $\omega = 0.0$, $\omega_D = 0.0$, OCR = 1

POV MACRO STABILITEIT
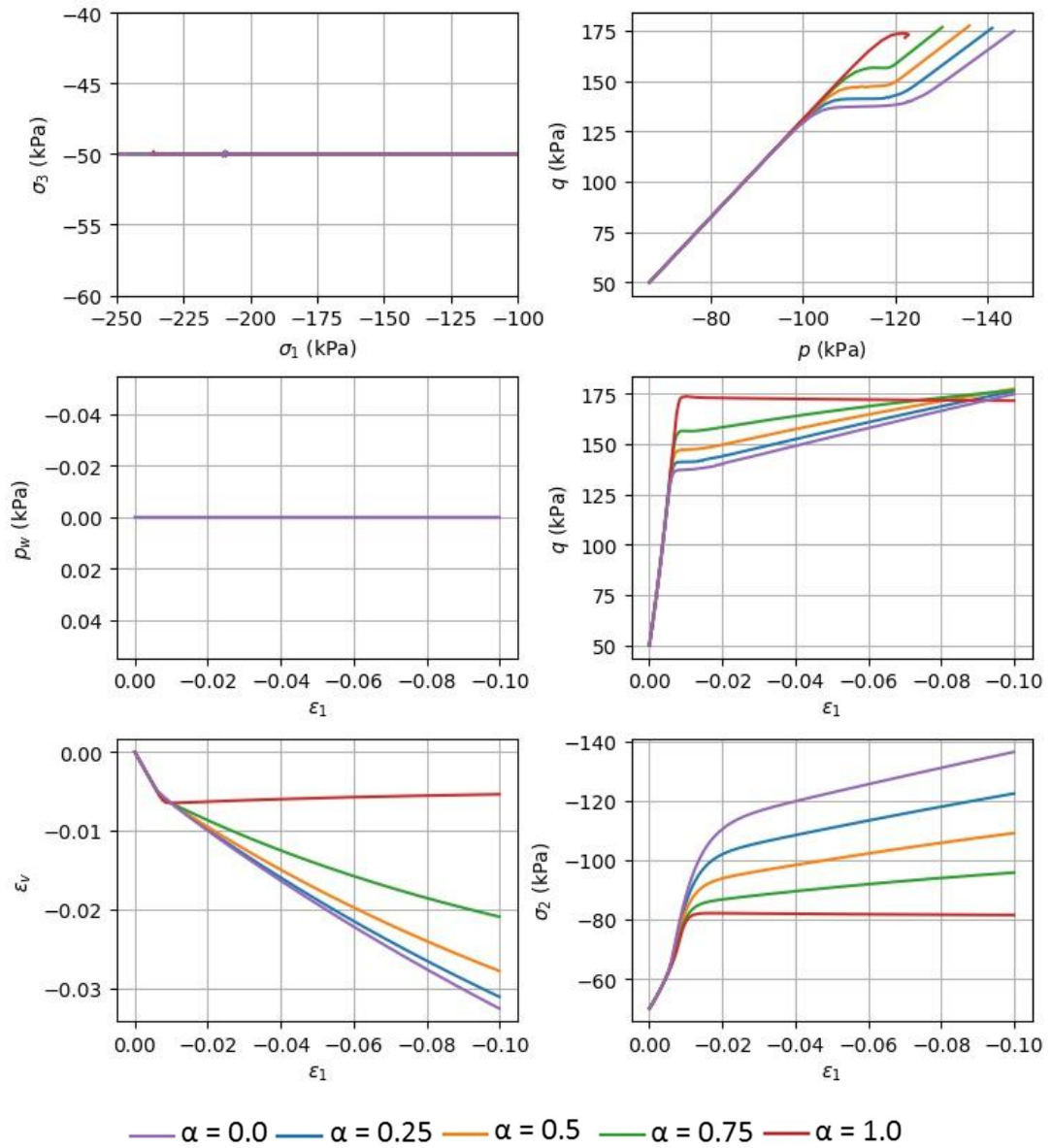
Figure B.20 Biaxial Test (Drained): Variation 2: $\alpha_0 = [0, 0.25, 0.5, 0.75, 1.0]$, $\omega = 0.0$, $\omega_d = 0.0$, OCR = 2
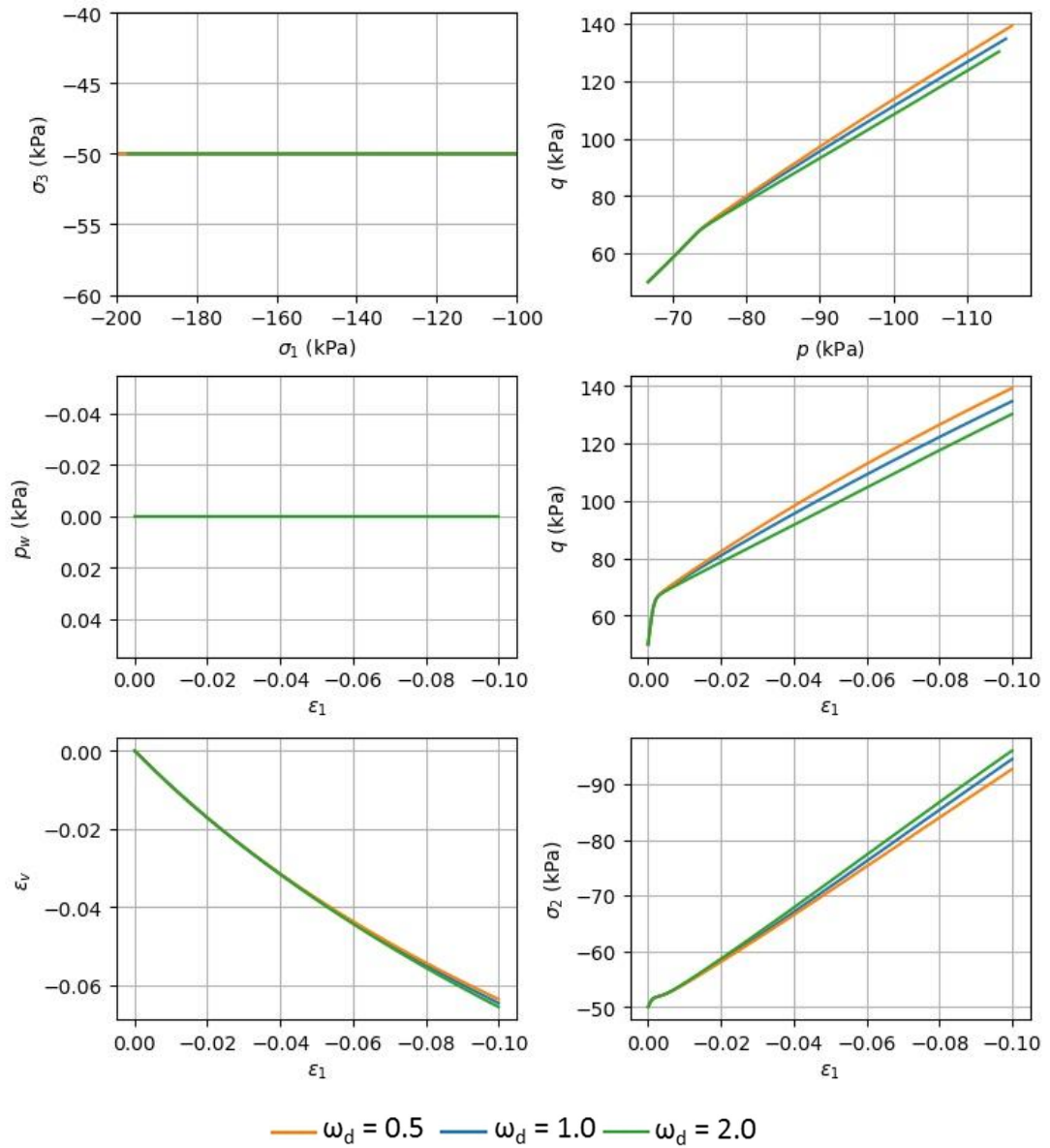
Figure B.21 Biaxial Test (Drained): Variation 3: $\alpha_0 = 0.5$, $\omega = 25$, $\omega_d = [0.5, 1, 2]$, OCR = 1.0
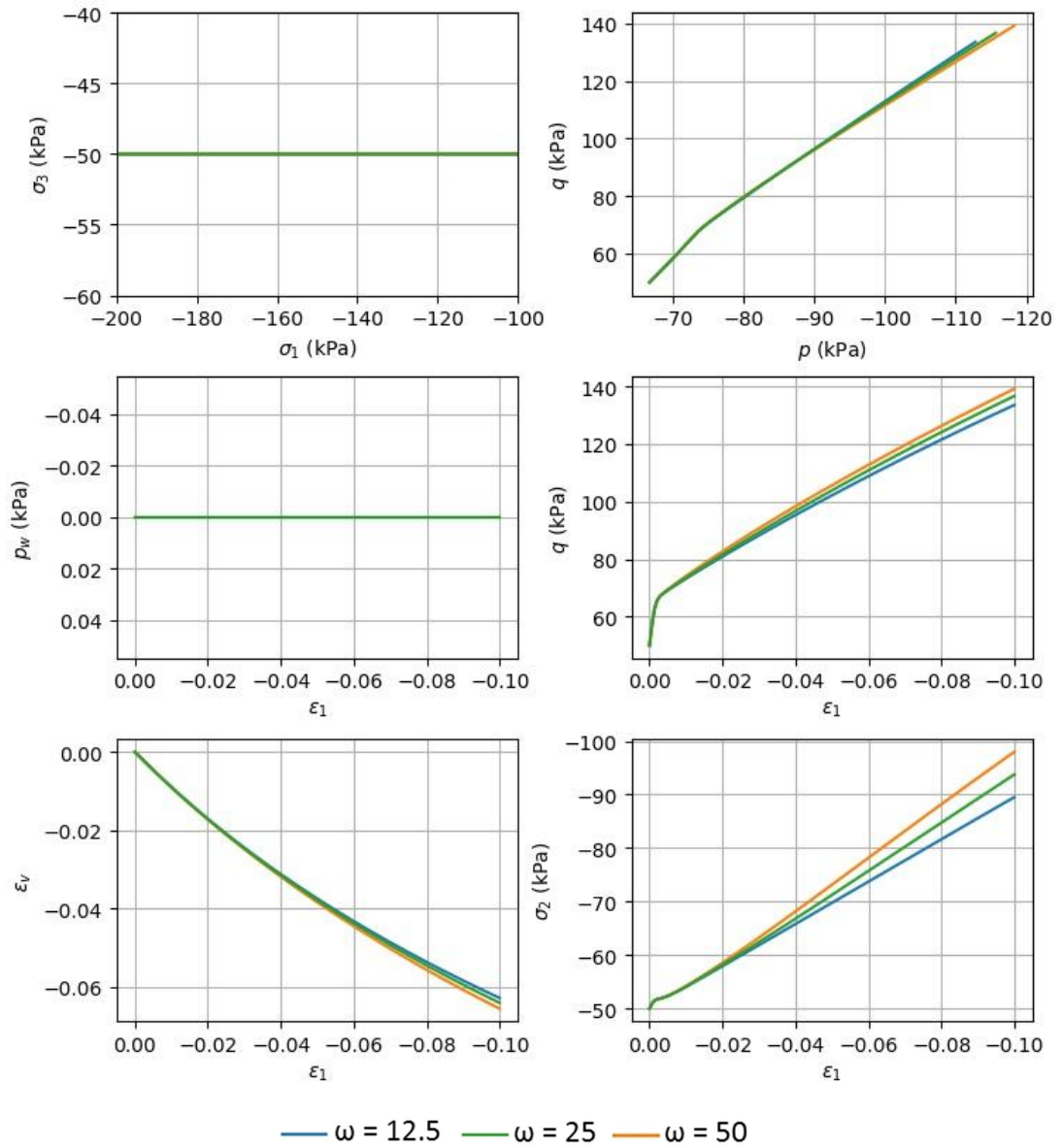
Figure B.22 Biaxial Test (Drained): Variation 4: $\alpha_0 = 0.5$, $\omega = [12.5, 25, 50]$, $\omega_d = 0.75$, OCR = 1.0
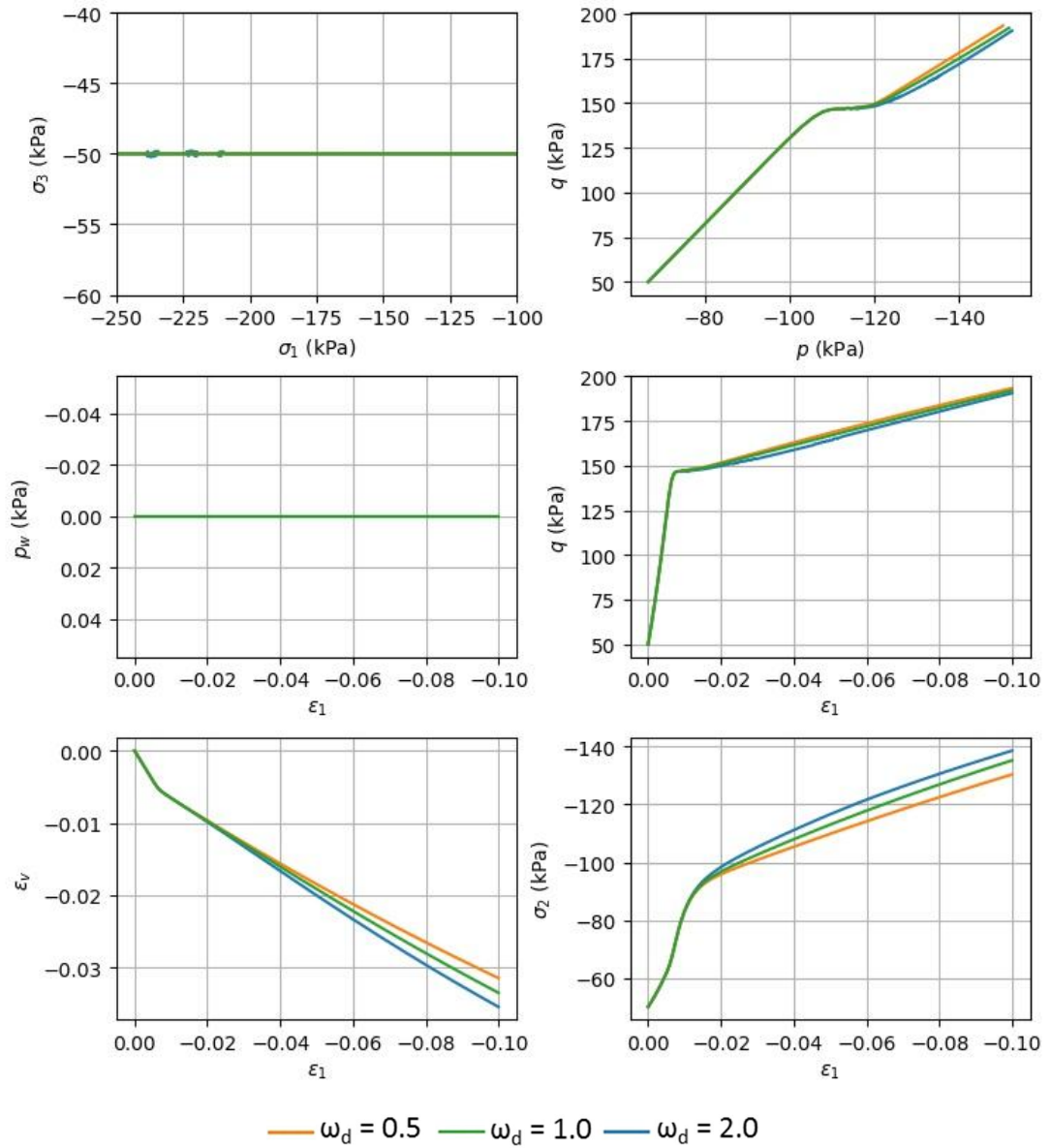
Figure B.23 Biaxial Test (Drained): Variation 5: $\alpha_0 = 0.5$, $\omega = 25$, $\omega_d = [0.5, 1, 2]$, OCR = 2.0
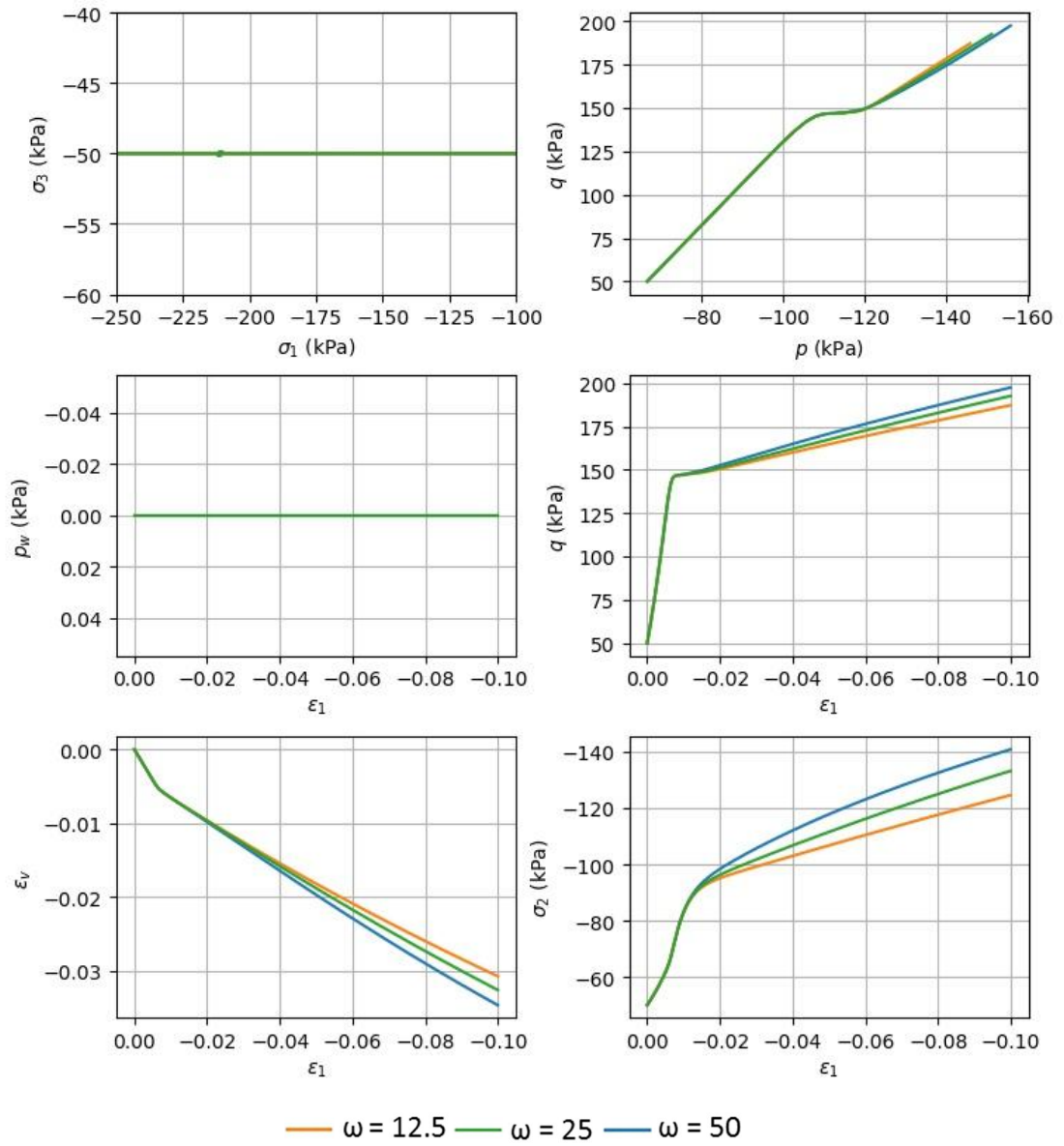
Figure B.24 Biaxial Test (Drained): Variation 6: $\alpha_0 = 0.5$, $\omega = [12.5, 25, 30]$, $\omega_d = 0.75$, OCR = 2.0
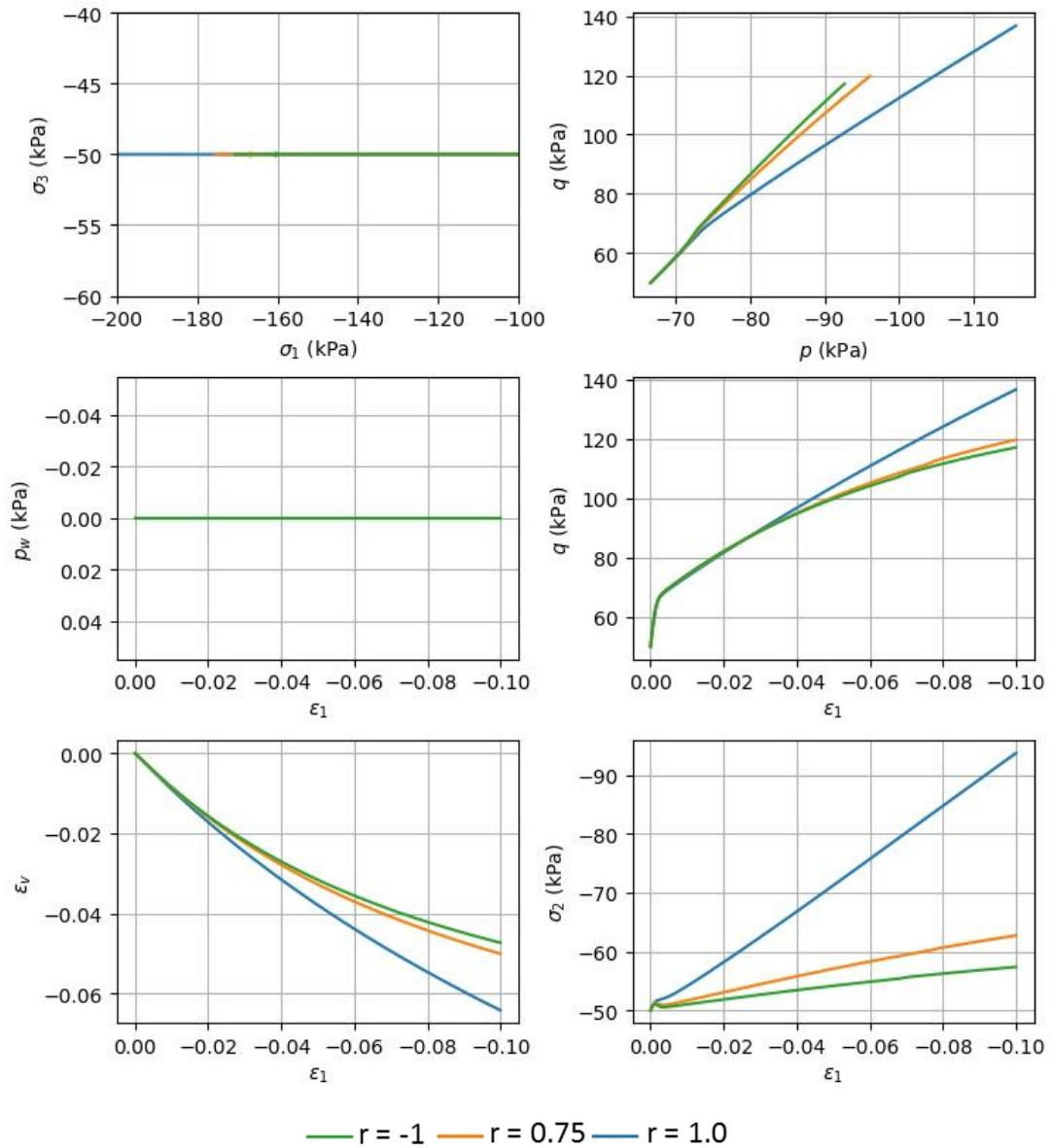
Figure B.25   Biaxial Test (Drained): Variation 7: $\alpha_0 = 0.5$, $\omega = 25$, $\omega_d = 0.75$, OCR = 1.0, r = [-1, 0.75, 1]

B.3.3   Undrained biaxial tests

Figure B.26 to Figure B.32 show variations 1 through 7, see Table B.2, for undrained biaxial tests. For each variation 6 subfigures are presented, regarding stress and strain development. The results are discussed in section 3.4.
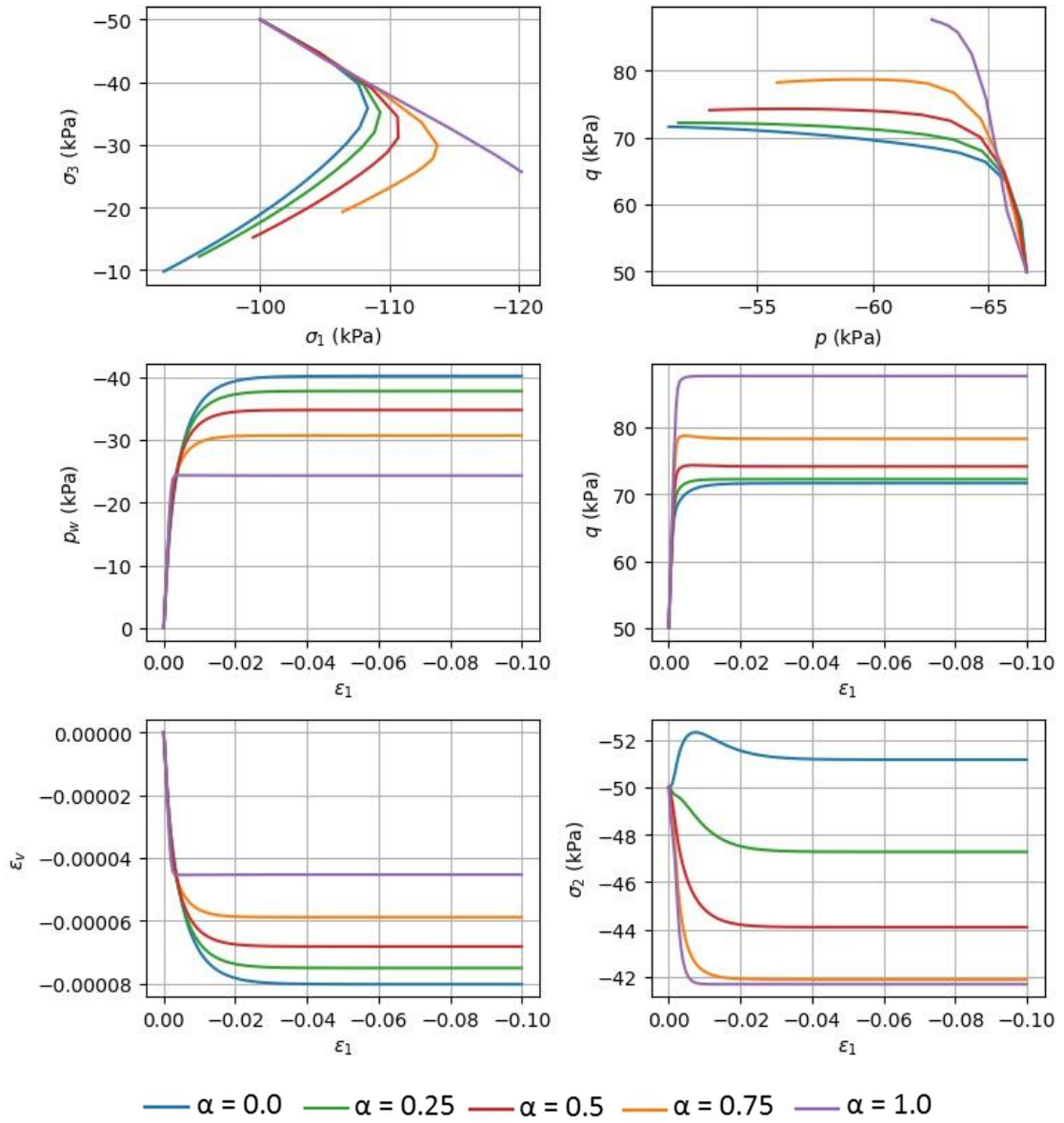
Figure B.26 Biaxial Test (Undrained): Variation 1: $\alpha_0 = [0, 0.25, 0.5, 0.75, 1.0]$, $\omega = 0.0$, $\omega_d = 0.0$, OCR = 1

POV MACRO STABILITEIT
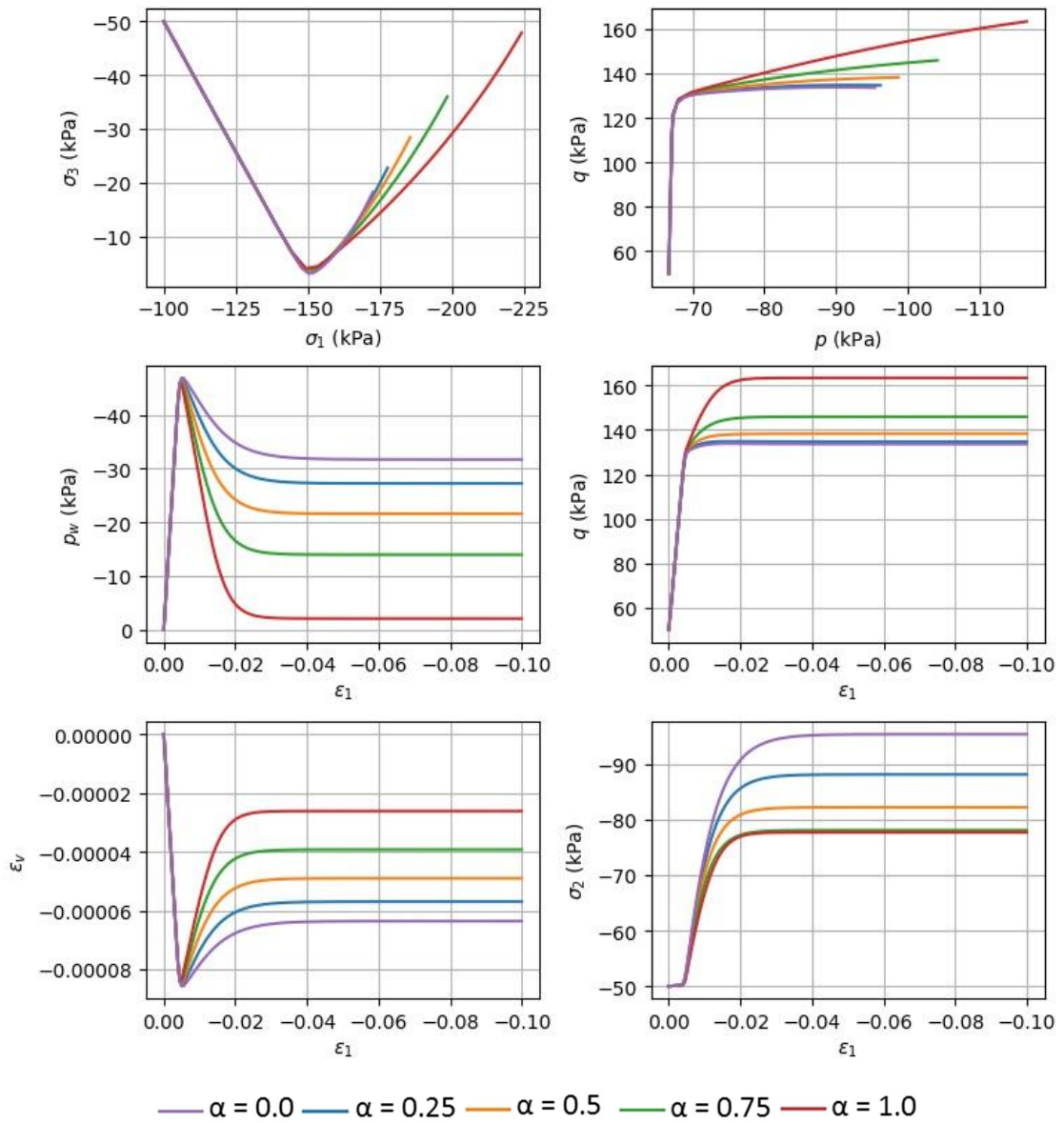
Figure B.27 Biaxial Test (Undrained): Variation 2 : $\alpha_0 = [0, 0.25, 0.5, 0.75, 1.0]$, $\omega = 0.0$, $\omega_d = 0.0$, OCR = 2

POV MACRO STABILITEIT
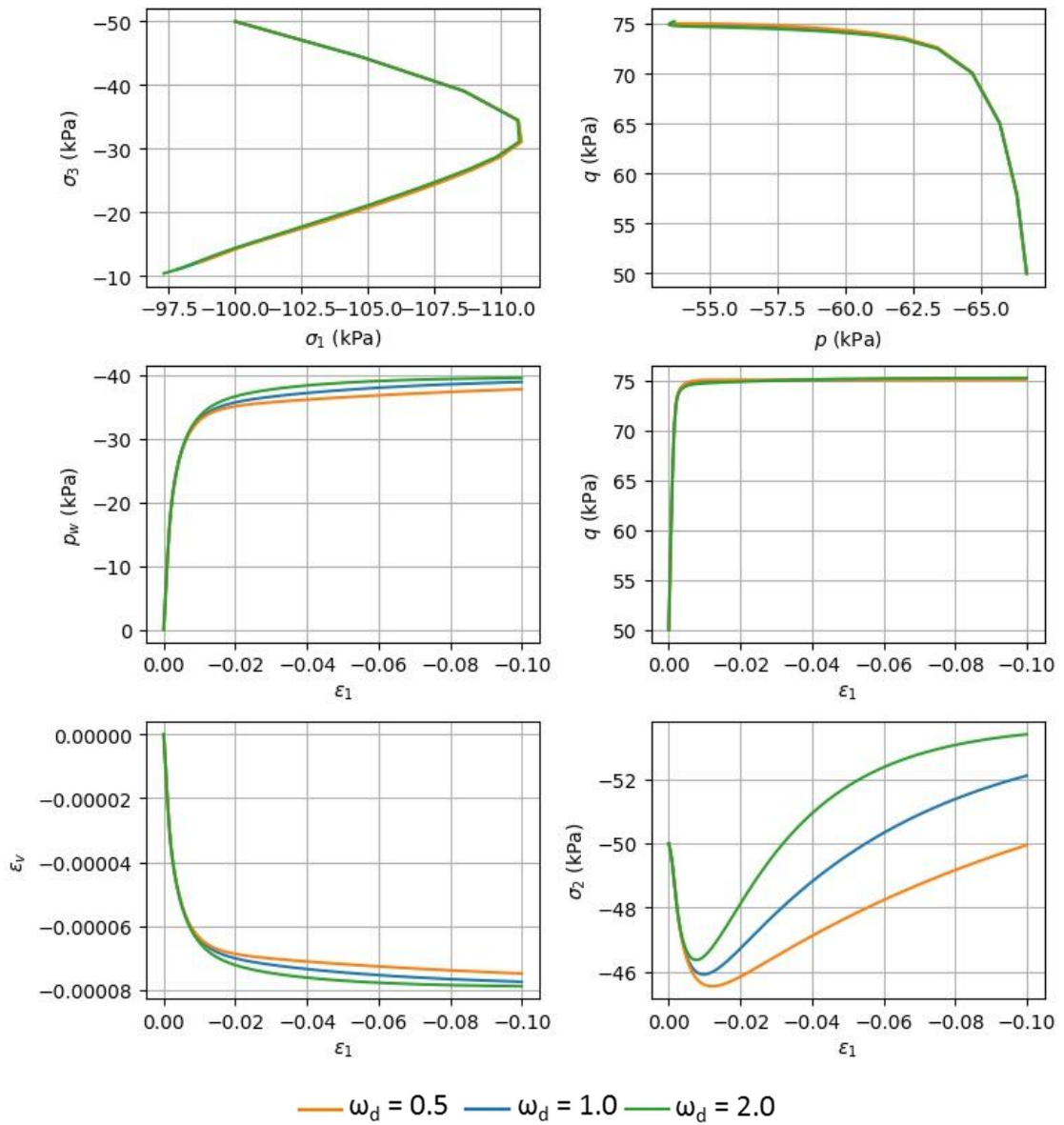
Figure B.28 Biaxial Test (Undrained): Variation 3: $\alpha_0 = 0.5$, $\omega = 25$, $\omega_d = [0.5, 1, 2]$, OCR = 1.0

POV MACRO STABILITEIT
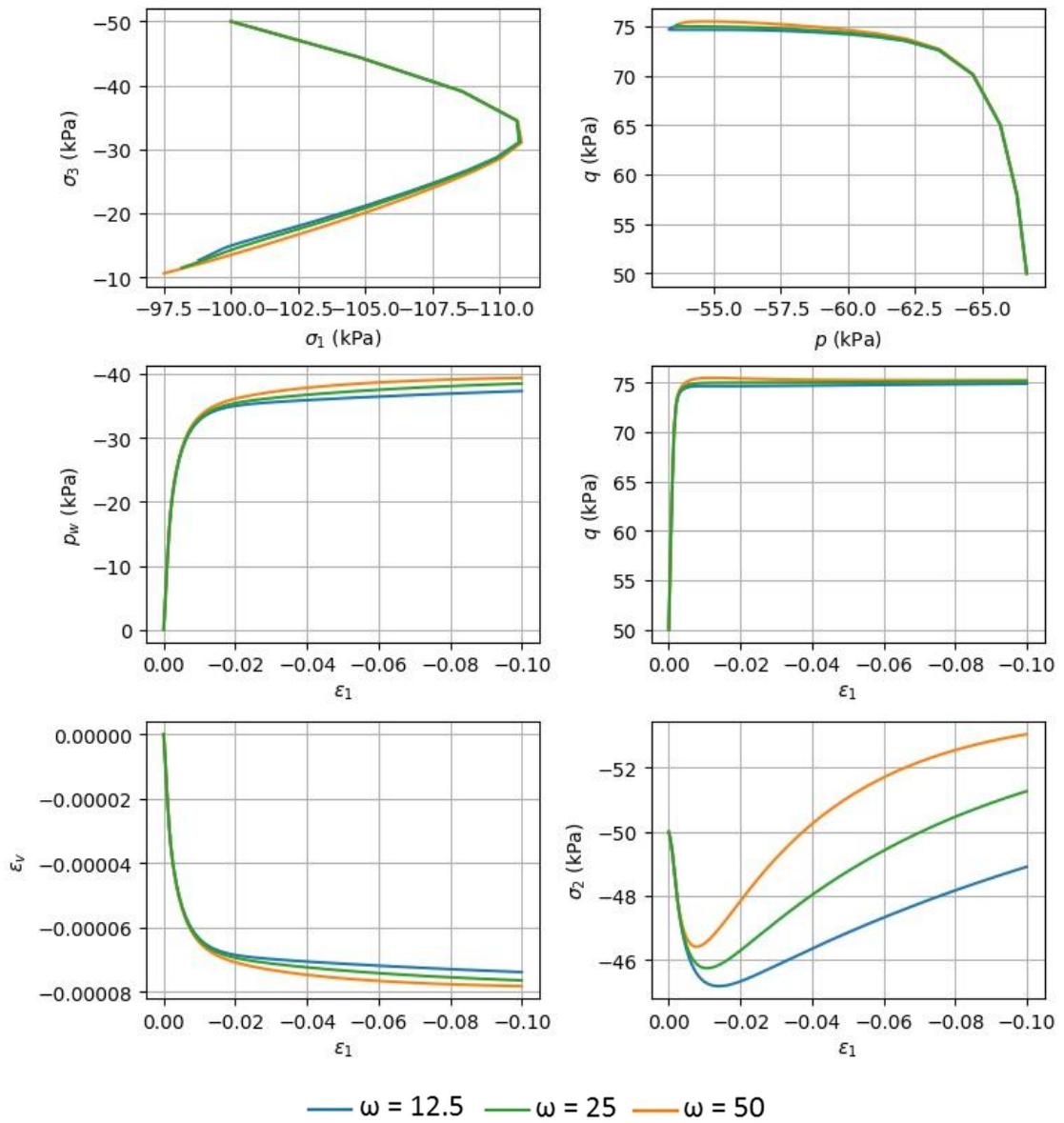
Figure B.29   Biaxial Test (Undrained): Variation 4: $\alpha_0 = 0.5$, $\omega = [12.5, 25, 50]$, $\omega_d = 0.75$, OCR = 1.0
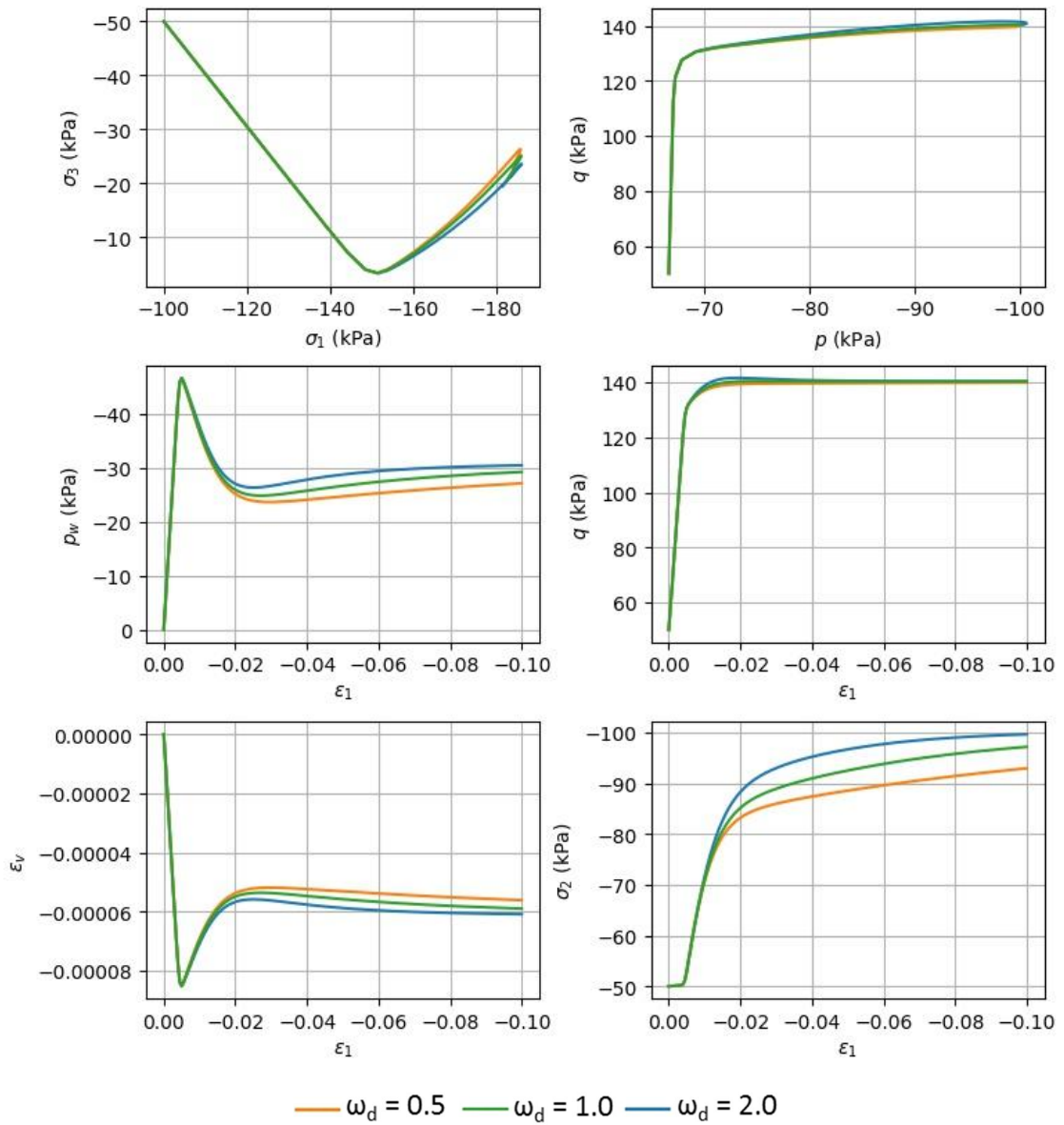
Figure B.30 Biaxial Test (Undrained): Variation 5: $\alpha_0 = 0.5$, $\omega = 25$, $\omega_d = [0.5, 1, 2]$, OCR = 2.0: Variation 5:

POV MACRO STABILITEIT
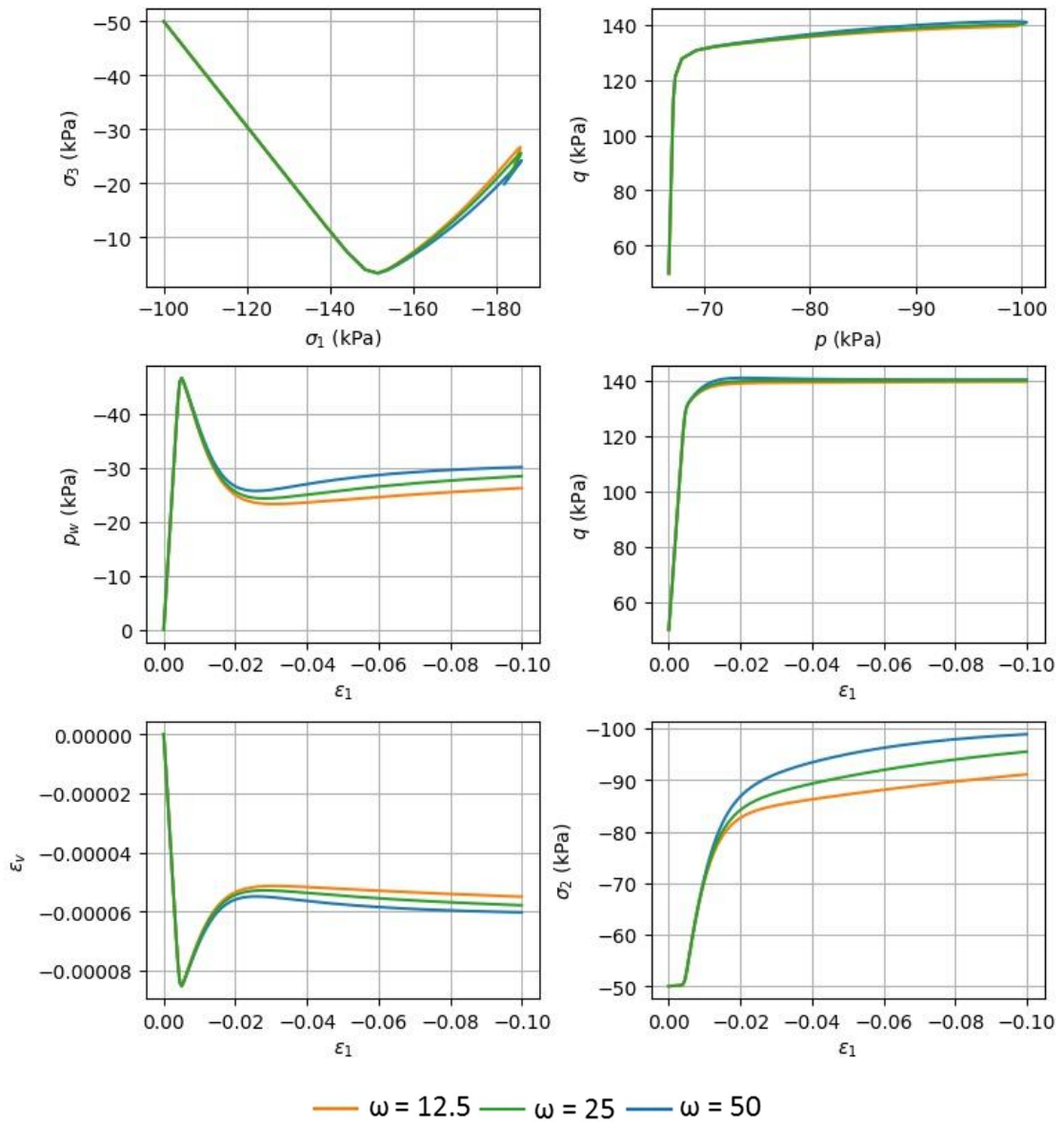
Figure B.31 Biaxial Test (Undrained): Variation 6: $\alpha_0 = 0.5$, $\omega = [12.5, 25, 30]$, $\omega_d = 0.75$, OCR = 2.0
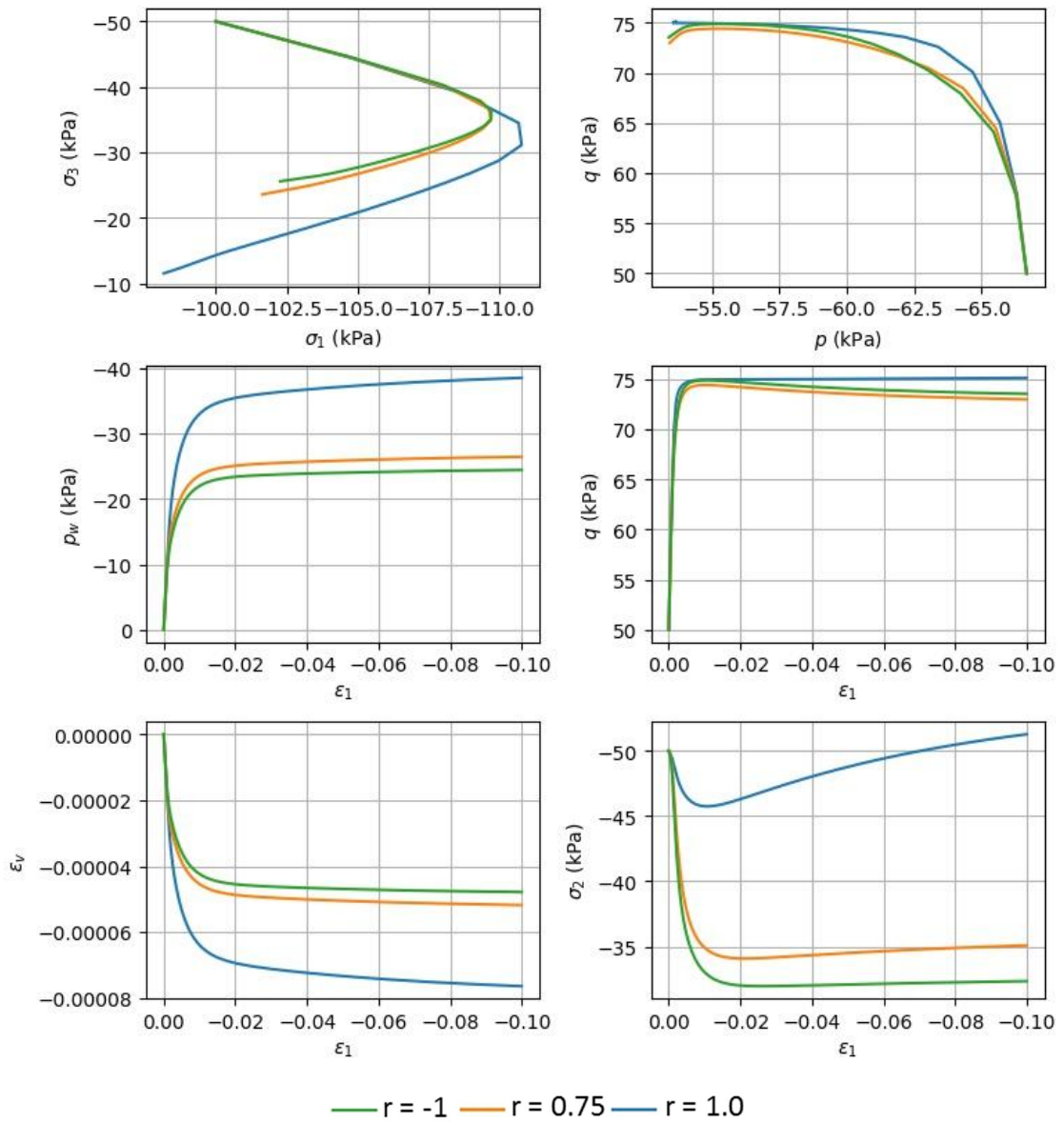
Figure B.32 Biaxial Test (Undrained): Variation 7: $\alpha_0 = 0.5$, $\omega = 25$, $\omega_d = 0.75$, OCR = 1.0, r = [-1, 0.75, 1]

POV MACRO STABILITEIT

B.4 Direct Simple Shear tests

B.4.1 Boundary conditions

This section discusses the simulation of Direct Simple Shear tests. The initial conditions and boundary conditions are given by Table B.5. Simulations have been made for drained and undrained conditions. In accordance to the experimental set up of the test, for drained tests the vertical load is kept constant during shearing, while for undrained tests the vertical strain is kept constant. Simulations have been made for the 7 cases explained by Table B.2. Section A.4.2. shows the simulation for the drained tests, section A.4.3 shows the simulations for the undrained case.

stress component	Initial [kN/m^2]	Incr.	value
σ_{xx}	-50	$\delta\varepsilon_{xx}$	0 [%/day]
σ_{yy}	-100	$\delta\varepsilon_{yy}{}^a$ $\delta\sigma_{yy}{}^b$	0 [%/day] 0 [kPa]
σ_{zz}	-50	$\delta\varepsilon_{zz}$	0 [%/day]
τ_{xy}	0	$\delta\gamma_{xy}$	10 [%/day]

Table B.5   Boundary conditions for simulating Direct Simple Shear testing. ^{a} = for undrained conditions, ^{b} for drained conditions

POV MACRO STABILITEIT

B.4.2 Simulation of drained DSS testing

Figure B.26 to Figure B.32 show variations 1 through 7, see Table B.2, for drained Direct Simple Shear tests. For each variation 8 subfigures are presented, regarding stress and strain development. The results are discussed in section 3.4.
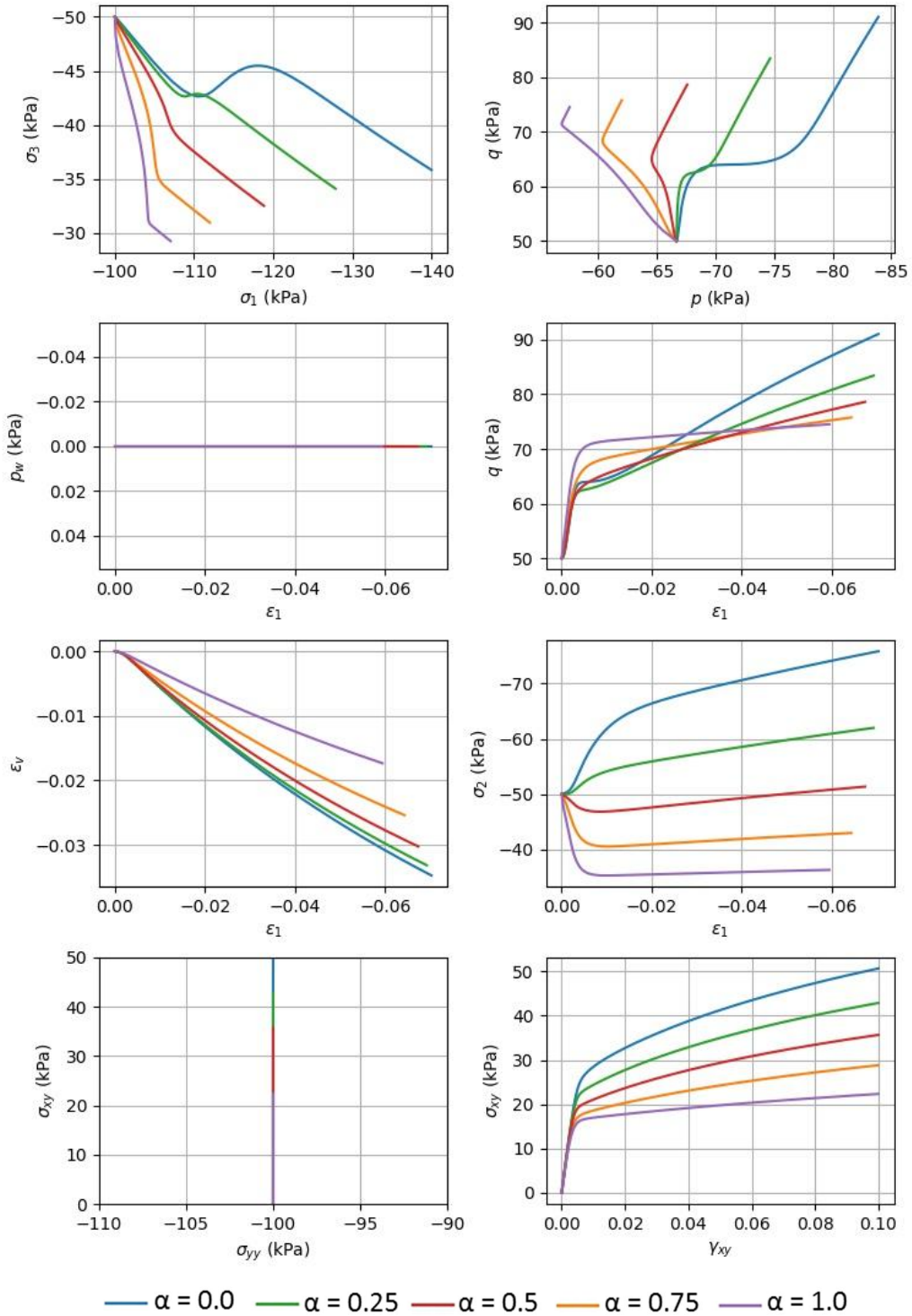
Figure B.33 Direct Shear Test (Drained): Variation 1: α_0 = [0, 0.25, 0.5, 0.75, 1.0], ω = 0.0, ω_d = 0.0, OCR = 1

POV MACRO STABILITEIT
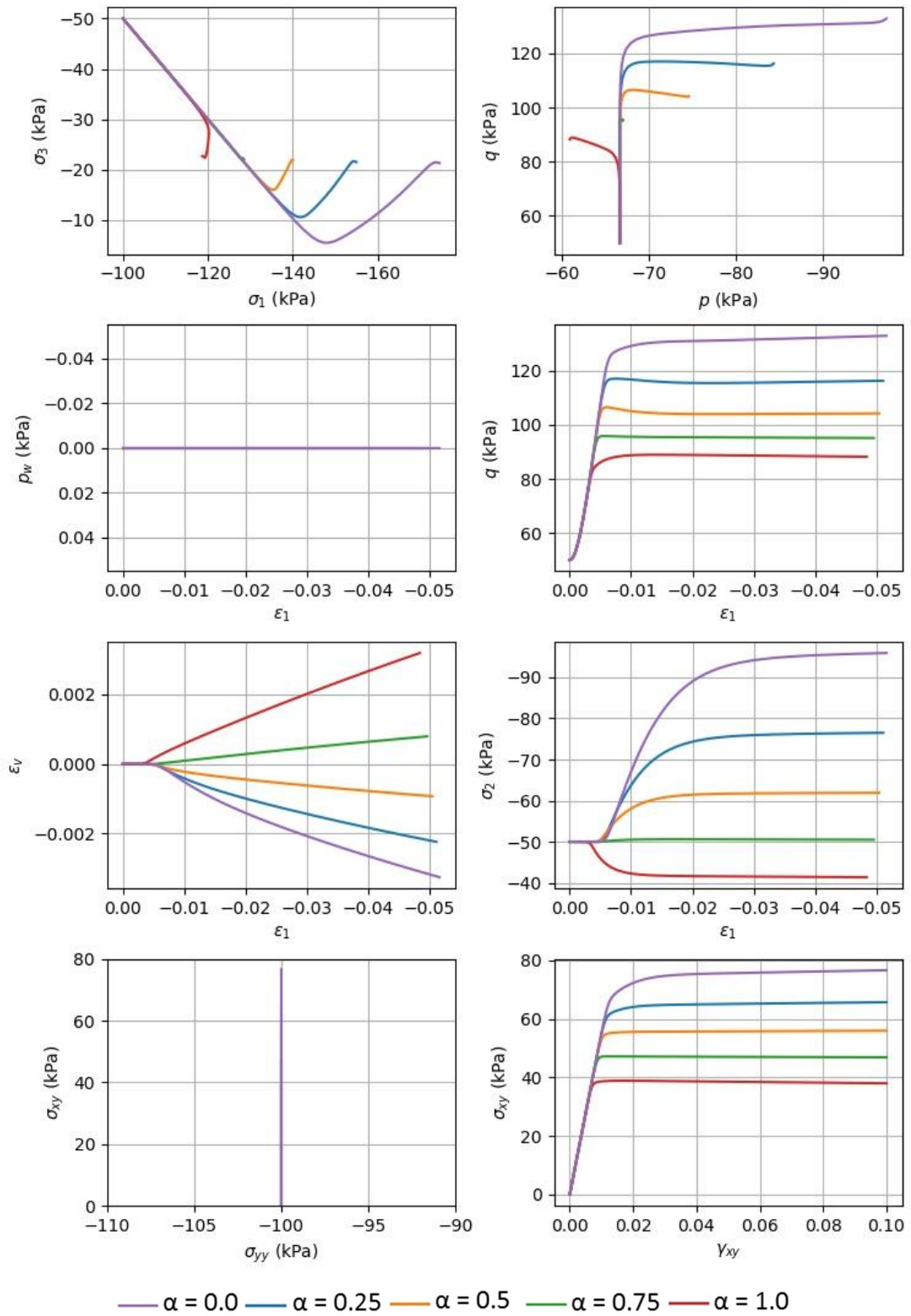
Figure B.34 Direct Shear Test (Drained): Variation 2: $\alpha_0 = [0, 0.25, 0.5, 0.75, 1.0]$, $\omega = 0.0$, $\omega_d = 0.0$, OCR = 2

POV   MACRO
STABILITEIT
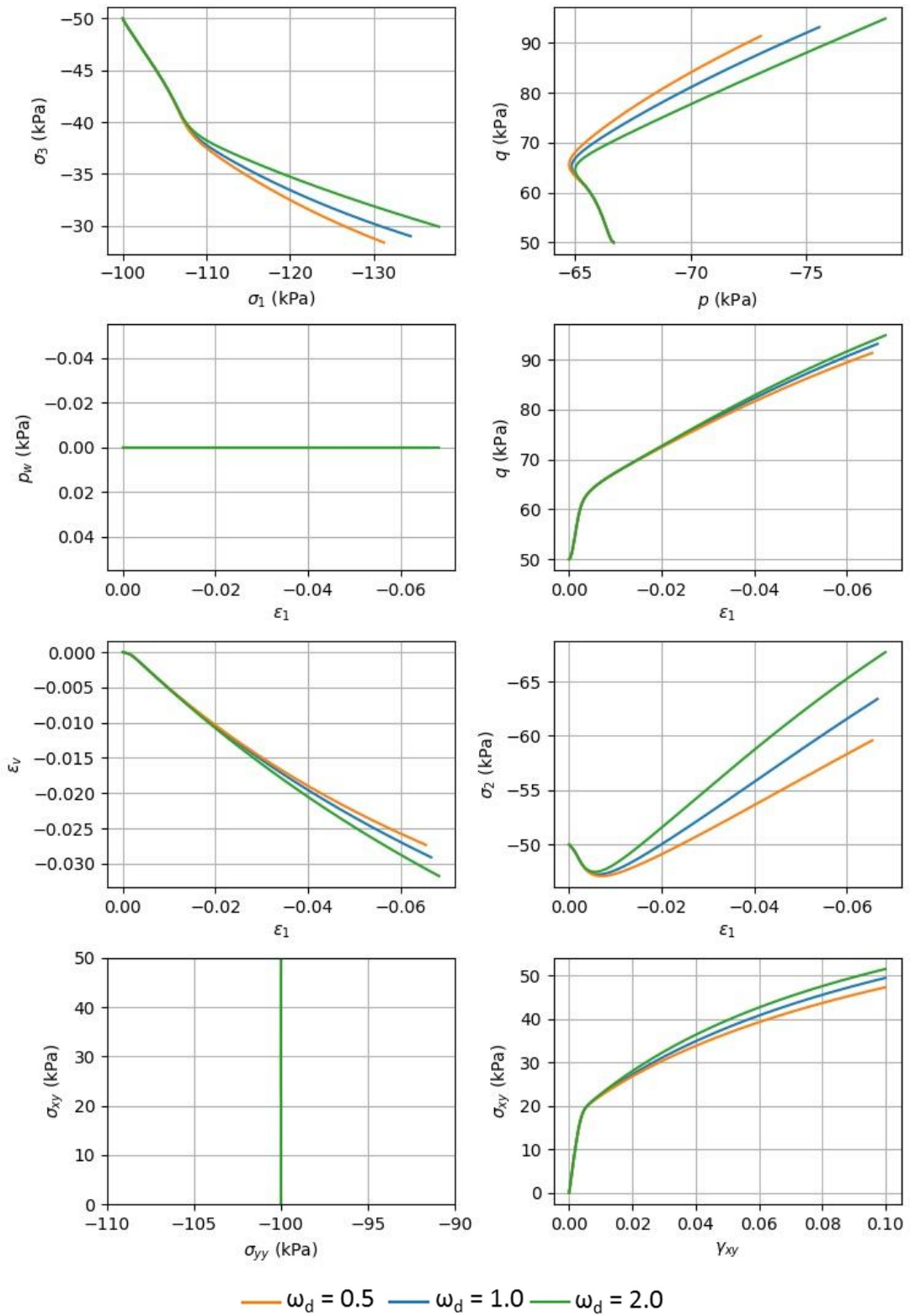
Figure B.35 Direct Shear Test (Drained): Variation 3: α_0 = 0.5, ω = 25, ω_d = [0.5, 1, 2], OCR = 1.0
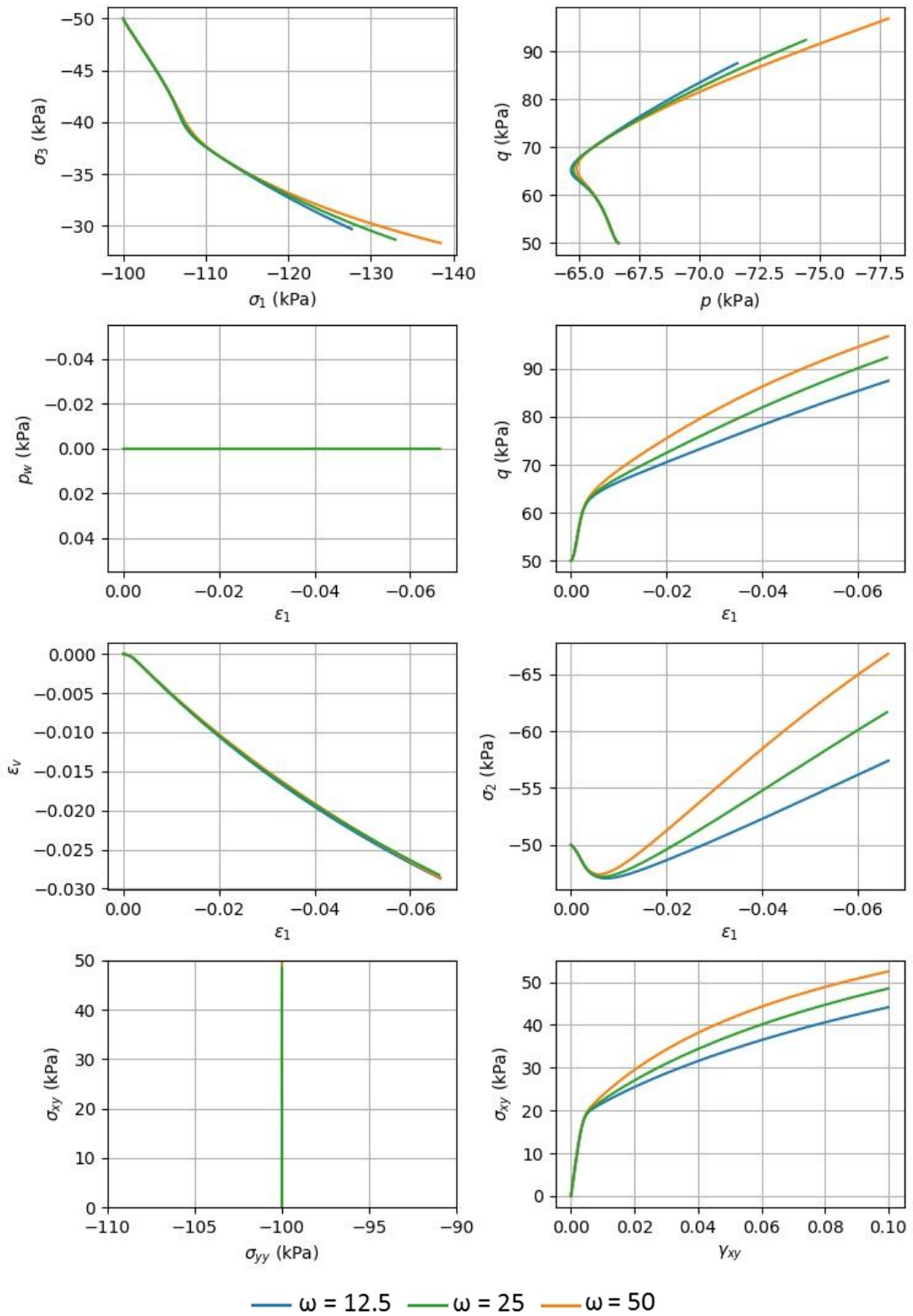
Figure B.36 Direct Shear Test (Drained): Variation 4: $\alpha_0 = 0.5$, $\omega = [12.5, 25, 50]$, $\omega_d = 0.75$, OCR = 1.0
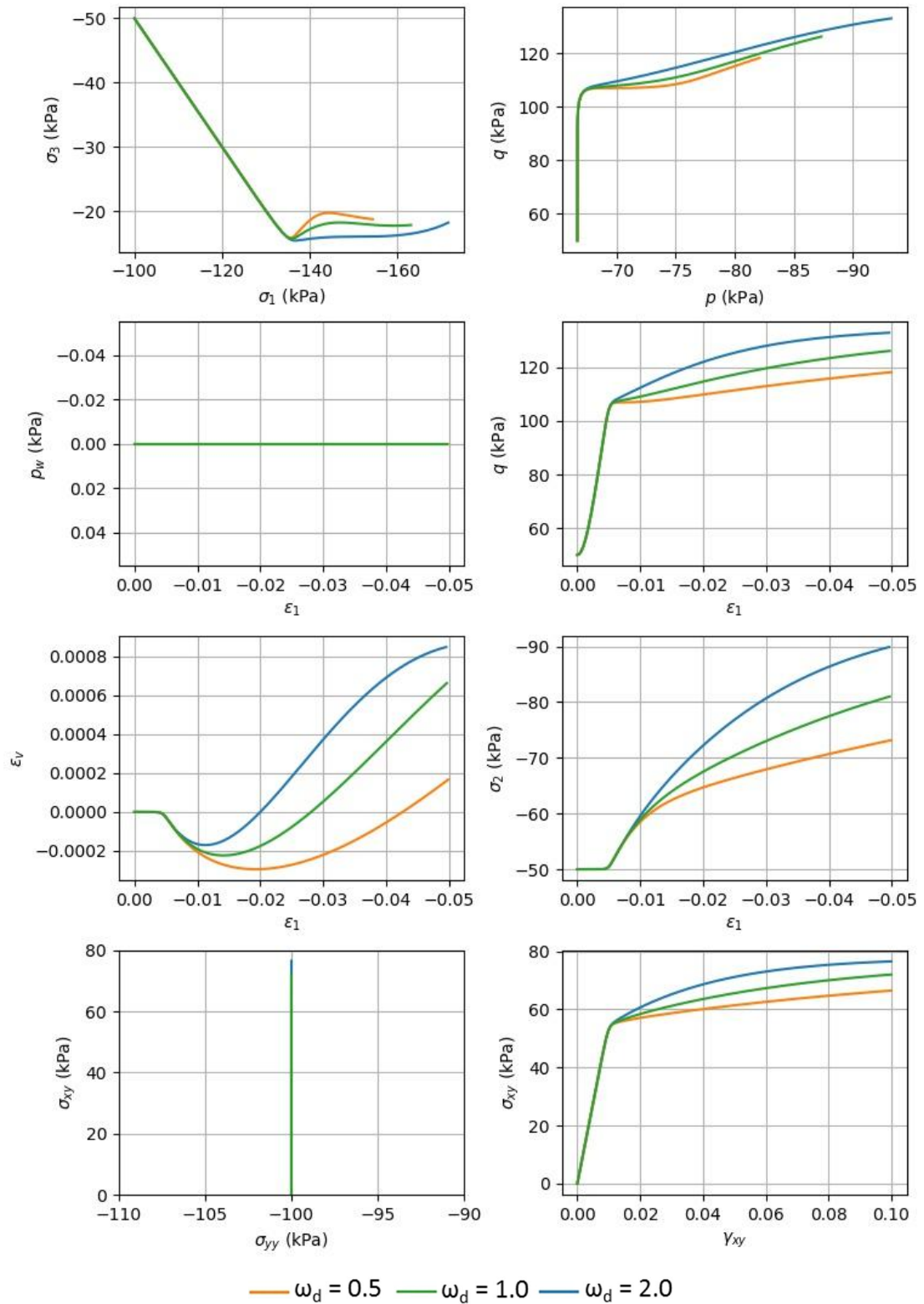
Figure B.37 Direct Shear Test (Drained): Variation 5: $\alpha_0 = 0.5$, $\omega = 25$, $\omega_d = [0.5, 1, 2]$, OCR = 2.0

POV (MACRO STABILITEIT
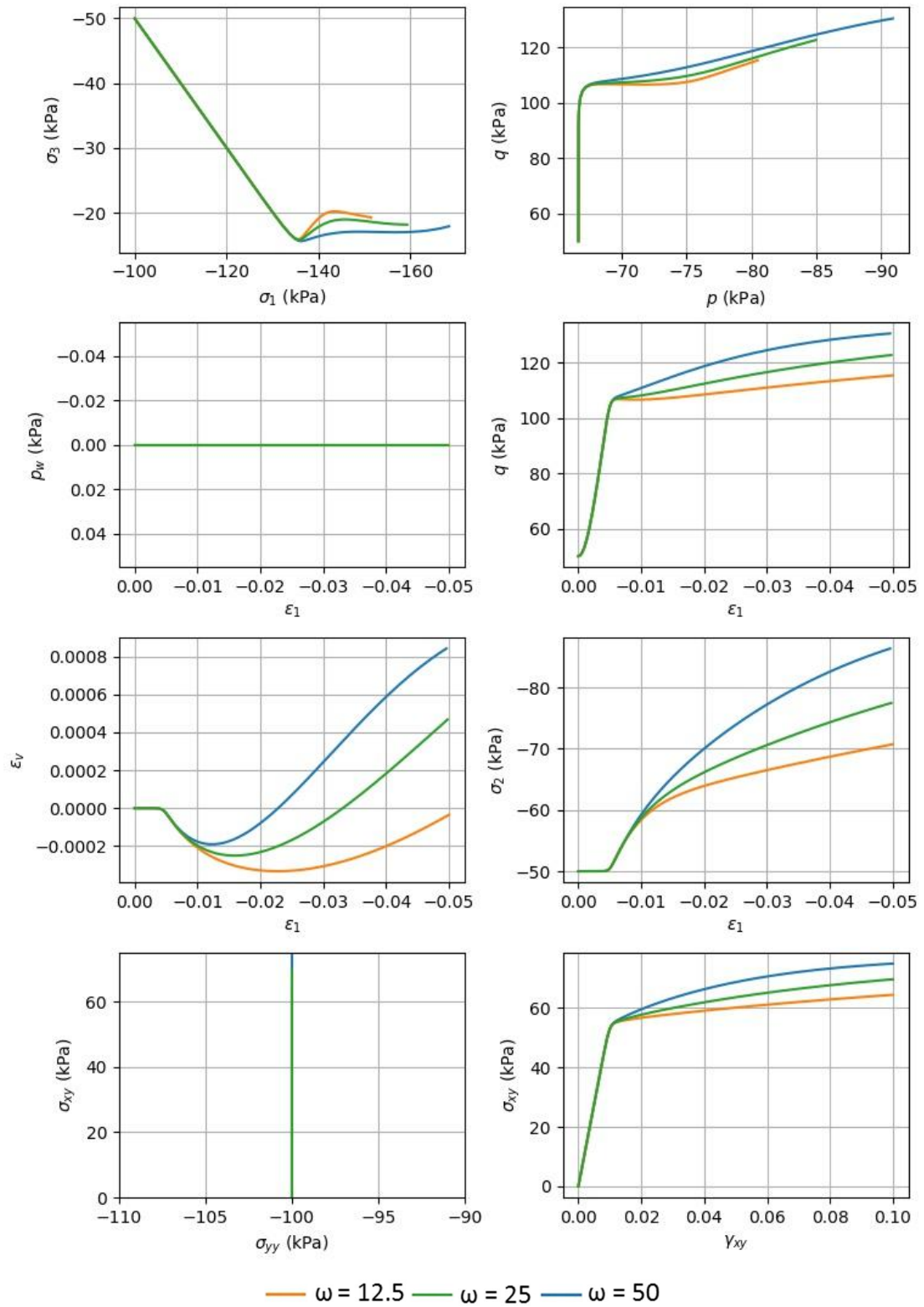
Figure B.38 Direct Shear Test (Drained): Variation 6: $\alpha_0 = 0.5$, $\omega = [12.5, 25, 30]$, $\omega_d = 0.75$, OCR = 2.0
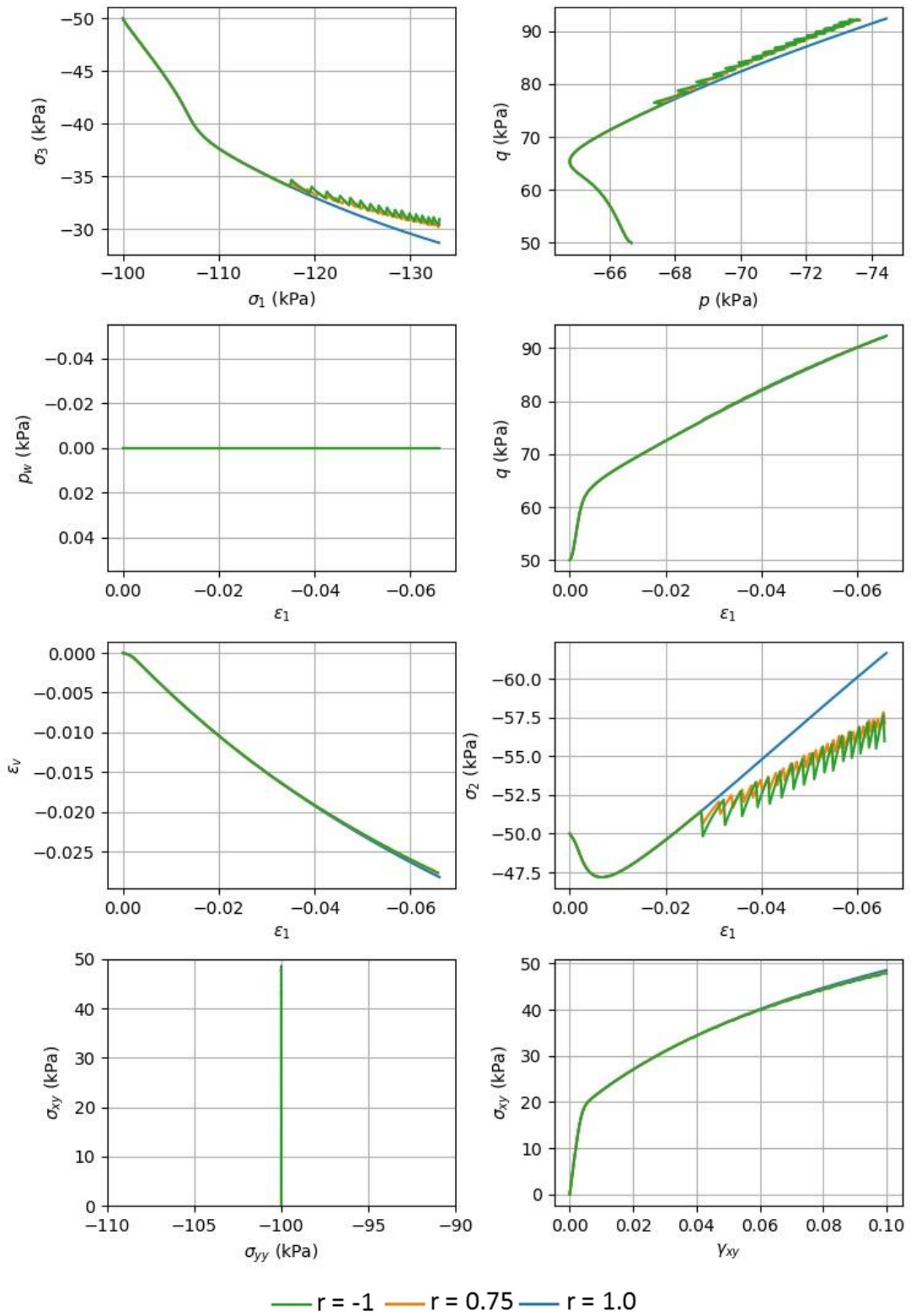
Figure B.39 Direct Shear Test (Drained): Variation 7: $\alpha_0 = 0.5$, $\omega = 25$, $\omega_d = 0.75$, OCR = 1.0, r = [-1, 0.75 1]

POV MACRO STABILITEIT

B.4.3 Simulation of undrained DSS testing

Figure B.26 to Figure B.32 show variations 1 through 7, see Table B.2, for undrained Direct Simple Shear tests. For each variation 8 subfigures are presented, regarding stress and strain development. The results are discussed in section 3.4.

Figure B.40 Direct Shear Test (Undrained): Variation 1: $\alpha_0 = [0, 0.25, 0.5, 0.75, 1.0]$, $\omega = 0.0$, $\omega_d = 0.0$, OCR = 1

POV MACRO STABILITEIT

Figure B.41 Direct Shear Test (Undrained): Variation 2: $\alpha_0 = [0, 0.25, 0.5, 0.75, 1.0]$, $\omega = 0.0$, $\omega_d = 0.0$, OCR = 2

Figure B.42 Direct Shear Test (Undrained): Variation 3: $\alpha_0 = 0.5$, $\omega = 25$, $\omega_d = [0.5, 1, 2]$, OCR = 1.0

Figure B.43 Direct Shear Test (Undrained): Variation 4: $\alpha_0 = 0.5$, $\omega = [12.5, 25, 50]$, $\omega_d = 0.75$, OCR = 1.0

Figure B.44 *Direct Shear Test (Undrained): Variation 5: $\alpha_0 = 0.5$, $\omega = 25$, $\omega_d = [0.5, 1, 2]$, OCR = 2.0:*

POV MACRO STABILITEIT

Figure B.45 Direct Shear Test (Undrained): Variation 6: $\alpha_0 = 0.5$, $\omega = [12.5, 25, 30]$, $\omega_d = 0.75$, OCR = 2.0
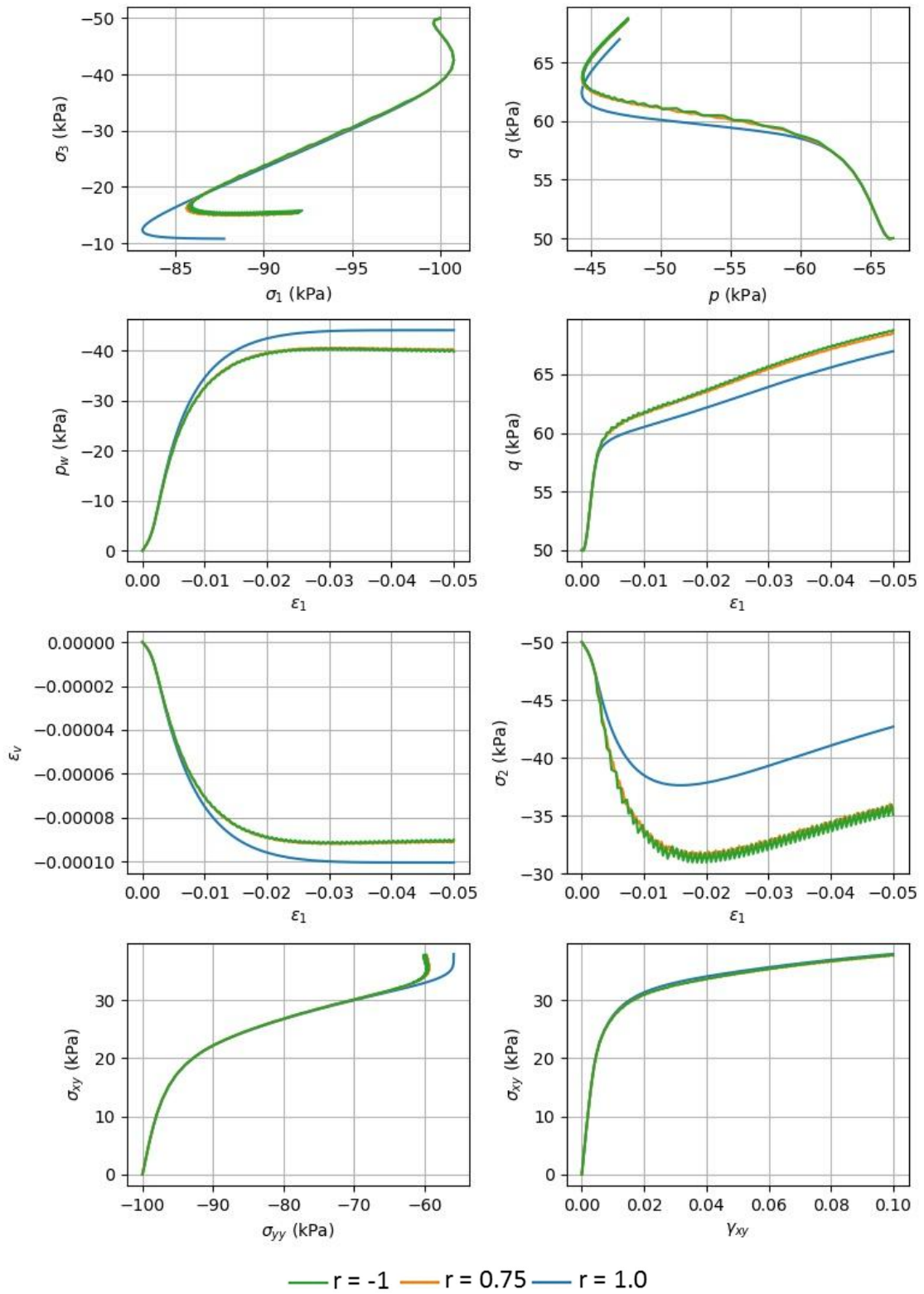
Figure B.46 Direct Shear Test (Undrained): Variation 7: $\alpha_0 = 0.5$, $\omega = 25$,, $\omega_d = 0.75$, OCR = 1.0, r = [-1, 0.75, 1]

C Results boundary value problem

C.1 General Information

In addition to the element tests, a dike on soft soil layer model was investigated. Figure C.1 shows the geometry, mesh, boundary conditions and material entities.
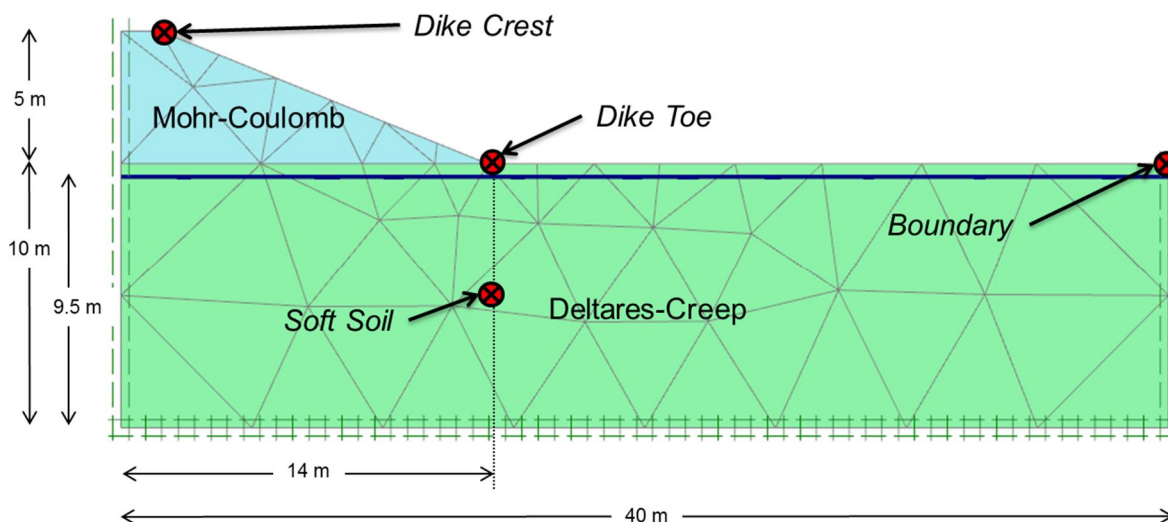
Figure C.1 Applied geometry

A coarse mesh was utilized in order to minimize the number of elements. The integration method is rather costly in terms of computing time and thus a smaller number of elements greatly reduces the time required. Furthermore it was necessary to divide the analysis time following an exponential trend in terms of duration of analysis. For the implemented integration scheme this is necessary due to how Plaxis communicates with the User-defined soil model dll.

The phases are divided as follows.

- Initial Phase: Initialization of stresses by K0 procedure
- Phase 1: Material Switch Phase (duration = 1 day)
- Phase 2: Activate Dike Body (duration = 1 day)
- Phase 3: 1st Creep Phase (duration = 10 days)
- Phase 4: 2nd Creep Phase (duration = 100 days)
- Phase 5: 3rd Creep Phase (duration = 1000 days)
- Phase 6: 4th Creep Phase (duration = 9000 days)

The total duration of analysis is approximately 10000 days from the activation of the dike. Model contains 56 elements and 505 nodes.

C.2 Material Parameters

The same material parameters as those used for Oostvaardersplassen (OVP) clay were used for the dike problem, however the values were varied slightly differently. Table C.1 shows the material parameters for the soft soil layer, Table C.2 shows the material parameters for the dike. Table C.3 shows the cases that were run and compared using all the different results.

POV
MACRO
STABILITEIT

Parameter	Value
γ (kN/m^3)	13.14
λ^*	0.1134
κ^*	0.01149
μ^*	0.0065
ν	0.15
K_0^{nc}	0.4264
c (kPa)	0
ϕ (deg.)	35
r	*varies
τ (day)	1
e_0	3
α_0	*varies
ω	*varies
ω_d	*varies
OCR	1

Table C.1 Material parameters for soft soil layer

γ (kN/m^3)	17
E' (kPa)	2000
ν'	0.33
c' (kPa)	3
ϕ' (deg)	27
ψ (deg	0

Table C.2 Material parameters for dike (Mohr-Coulomb)

Case	α_0	ω	ω_d	OCR	r
1	[0.0,0.5]	0.0	0.0	1.0	1.0
2	[0.0,0.5]	25	1.0	1.0	1.0
3	0.5	25	1.0	1.0	[-1.00,0.8,0.9,1]
4	[0.0,0.5]	0.0	0.0	1.75	1.0

Table C.3 Cases for Dike

C.3 Results

The results are divided into four categories:
- Time dependent results.
- Position dependent results.
- Contour Result.

The time dependent results contain data where time is the parameter. The data are taken at four different points within the problem geometry. These points include the dike crest, dike toe, right boundary and middle of soft soil layer. The points are also shown in Figure C.2.
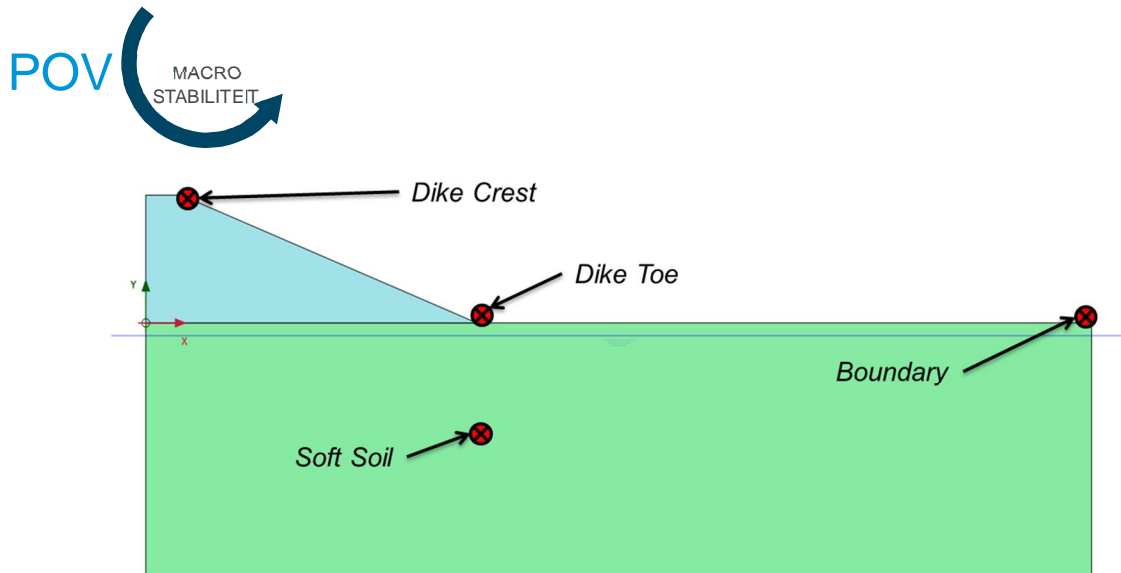
Figure C.2   Location of points from which data is extracted

The position dependent results contain data where time is 'frozen' at a specified moment. This moment was chosen to be the end of the analysis (10000 days). Position dependent results plot vertical stresses for horizontal and vertical sections of the dike. These correspond to sections A-A and B-B in Figure C.3.
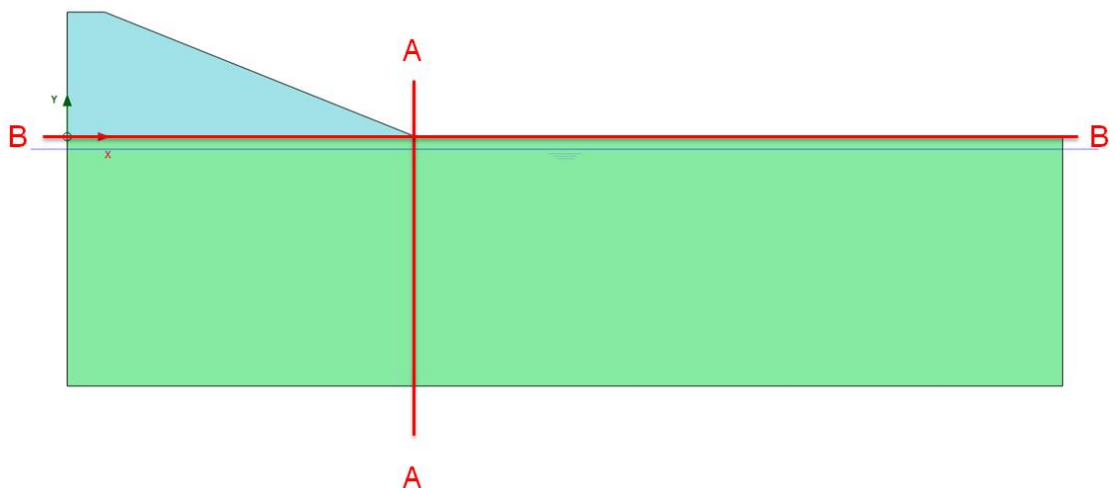
Figure C.3 Sections for position-dependent results

Contour results and deformed mesh results also show data for a specific time, and this time was again chosen to equal to 10000 days. Contour results show a variety of material parameters including principal and Cartesian stresses and vertical displacements.

POV MACRO STABILITEIT

C.3.1   Time Dependent Results

C.3.1.1   Case 1
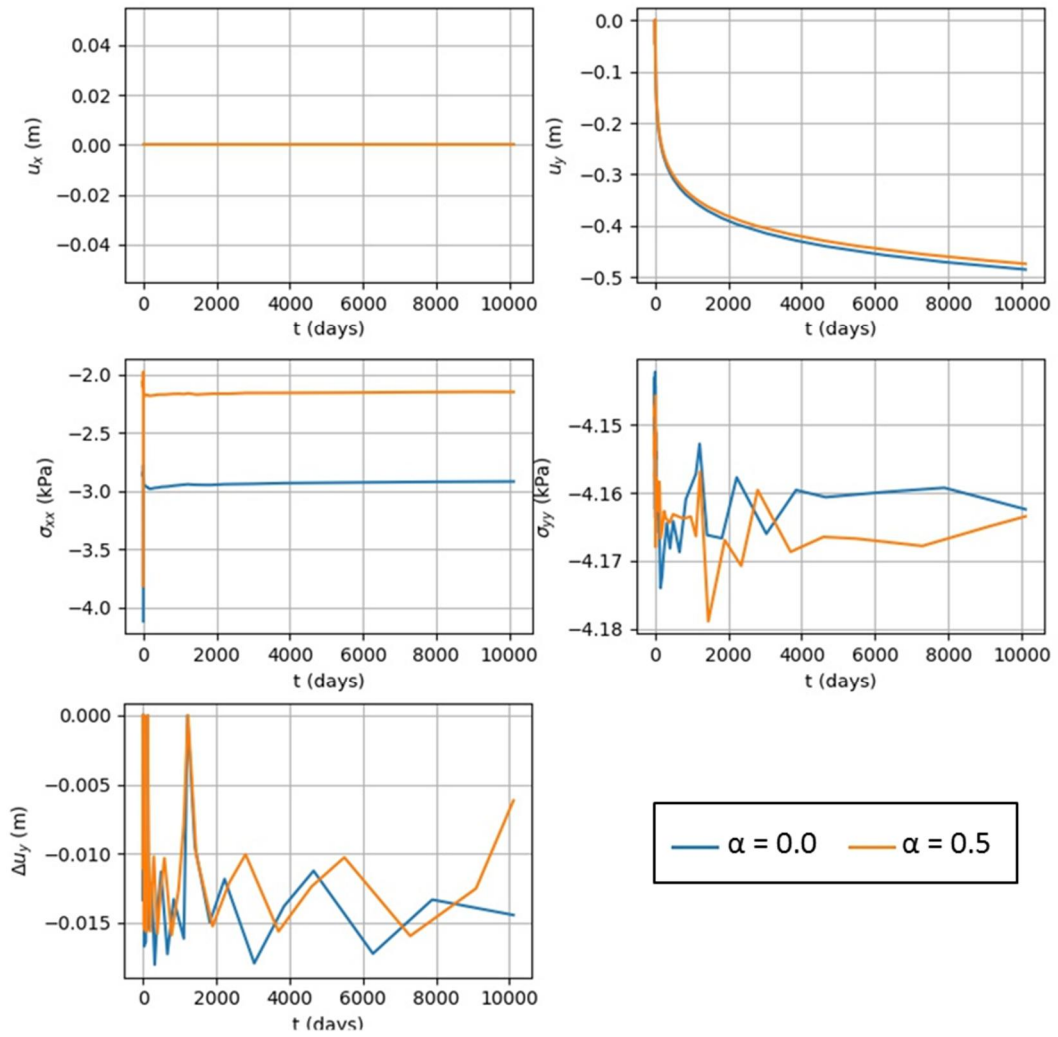
Figure C.4   Case 1: Boundary: alpha_0 = [0,0.5], omega = 0, omega_d = 0, OCR = 1, r = 1

POV MACRO
STABILITEIT
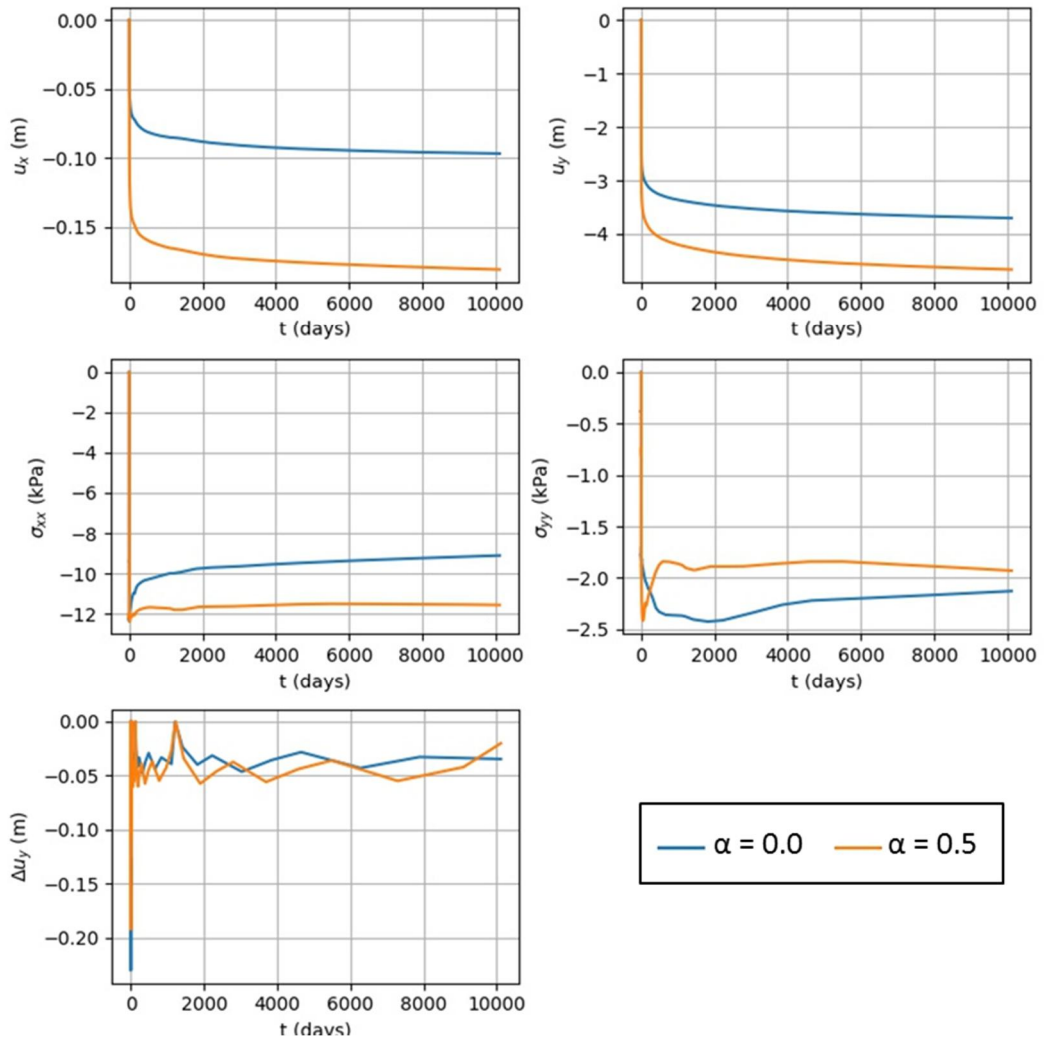
Figure C.5 Case 1: Crest: alpha_0 = [0,0.5], omega = 0, omega_d = 0, OCR = 1, r = 1
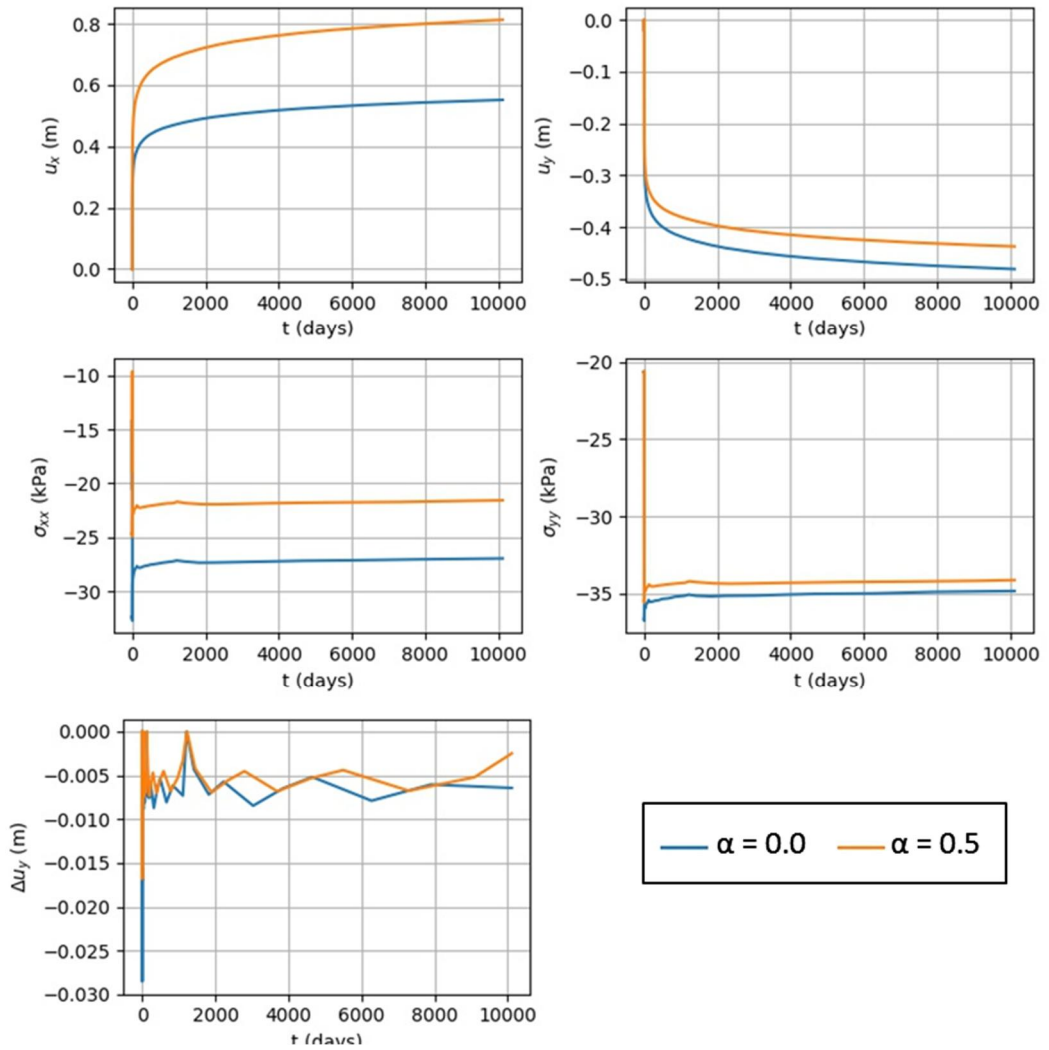
Figure C.6 Case 1: Soft Soil: alpha_0 = [0,0.5], omega = 0, omega_d = 0, OCR = 1, r = 1

Figure C.7 Case 1: Toe: alpha_0 = [0, 0.5], omega = 0, omega_d = 0, OCR = 1, r = 1

POV MACRO STABILITEIT
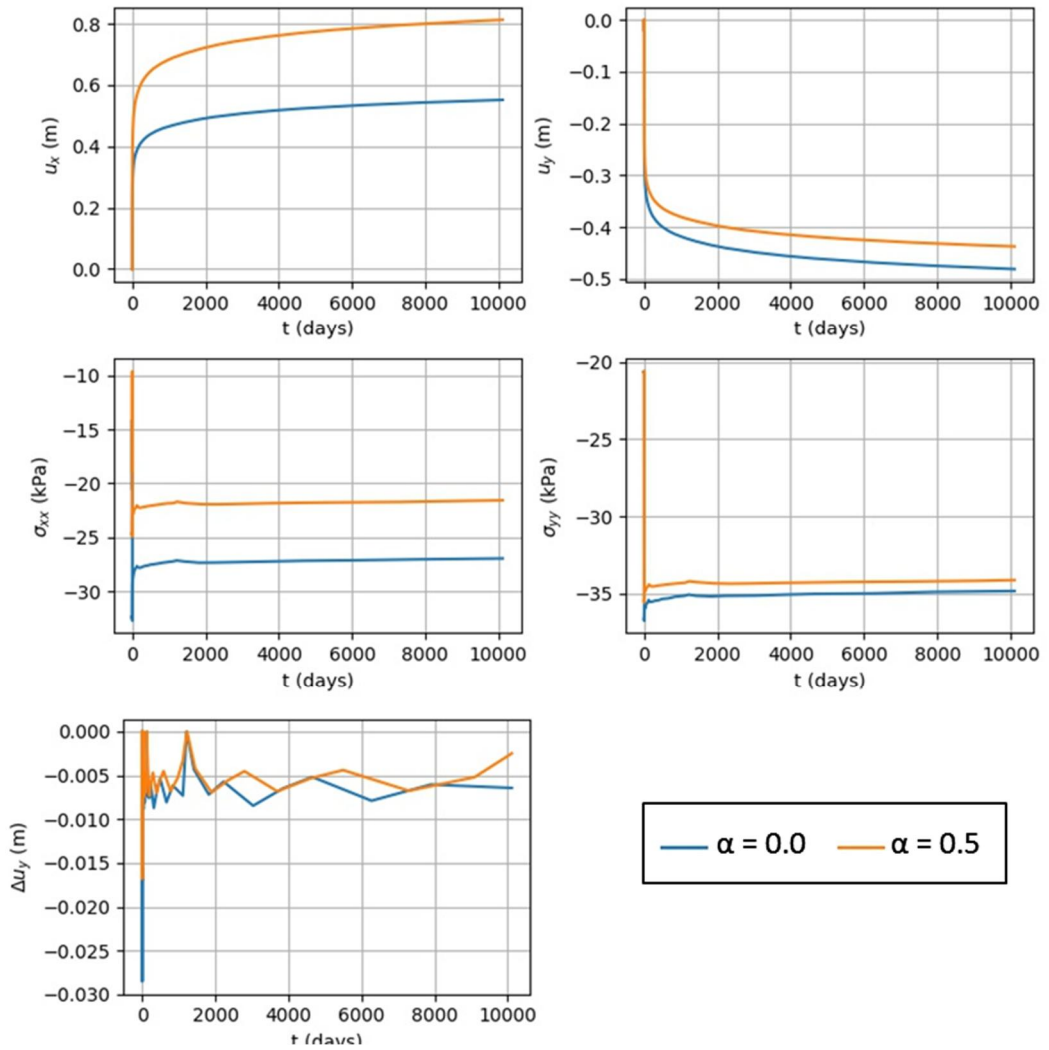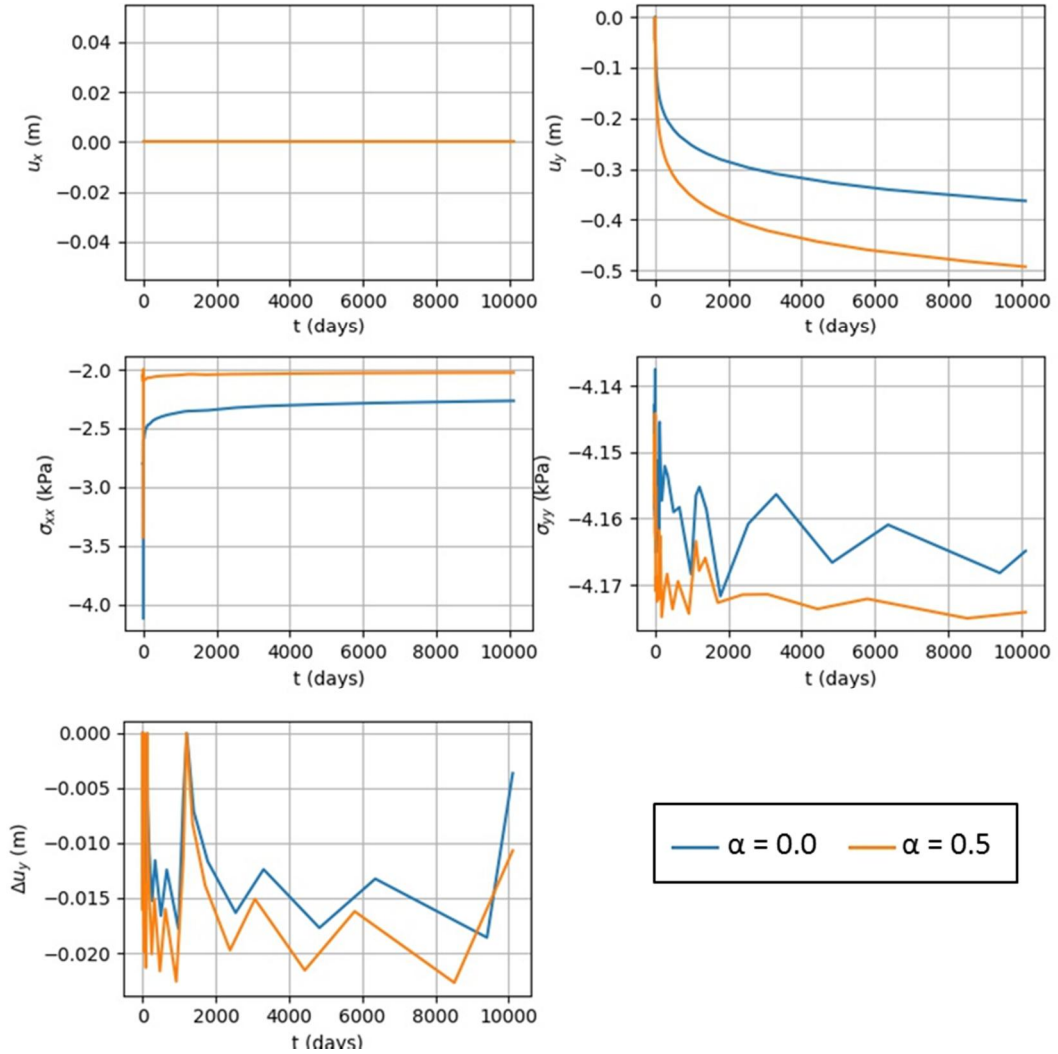
C.3.1.2   Case 2

Figure C.8   Case 2: Boundary: alpha0 = [0,0.5], omega = 25, omega_d = 1, OCR = 1, r = 1
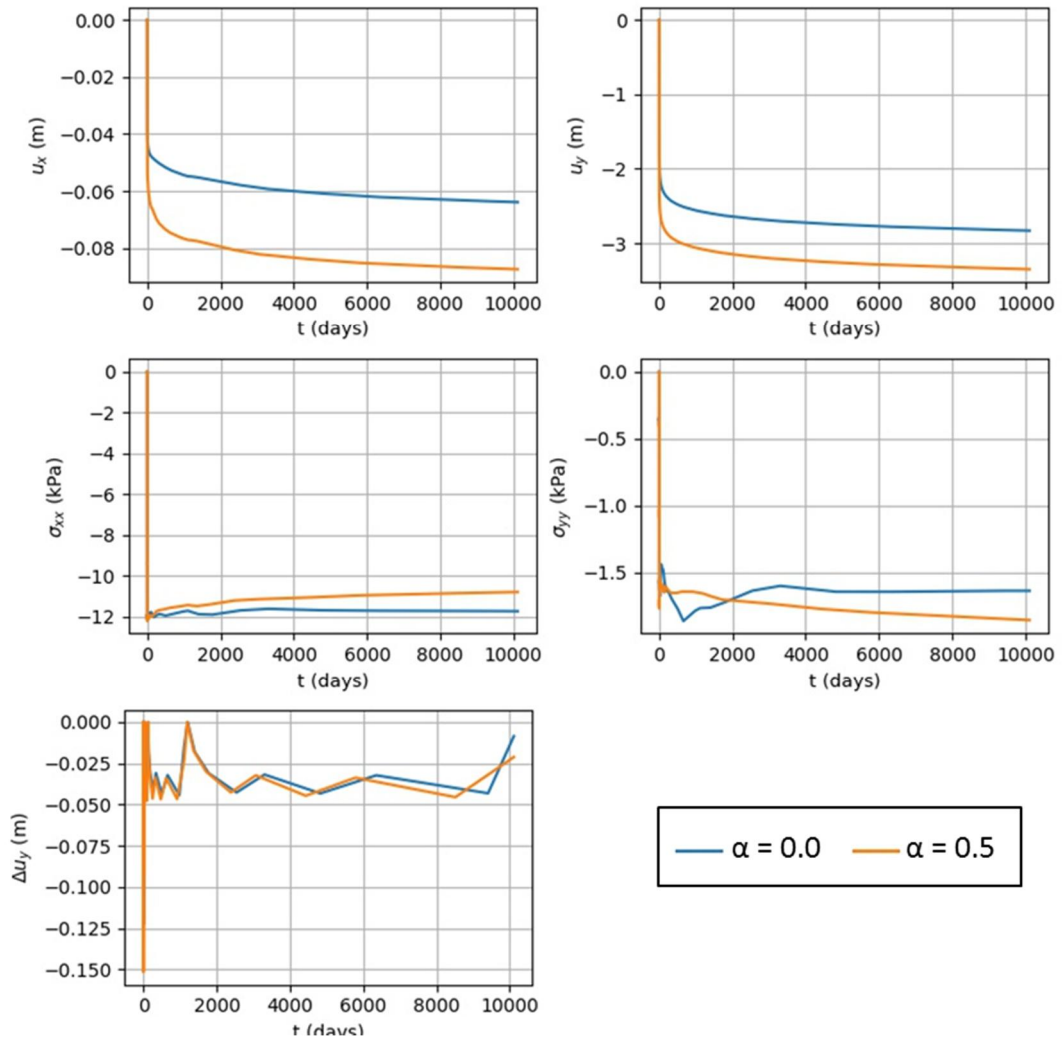
Figure C.9   Case 2: Crest: alpha0 = [0.0,0.5], omega = 25, omega_d = 1, OCR = 1, r = 1
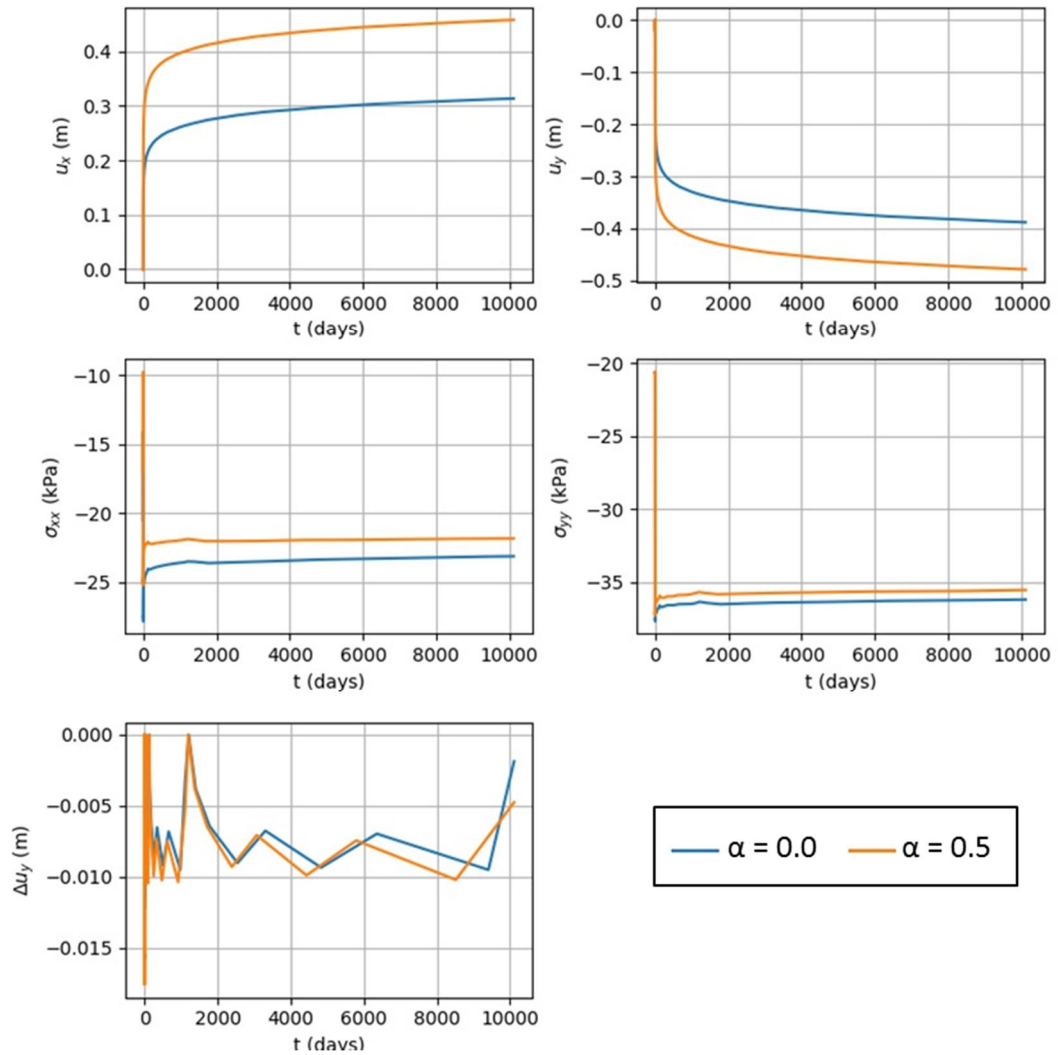
Figure C.10 Case 2: Soft Soil: alpha0 = [0,0.5], omega = 25, omega_d = 1, OCR = 1, r = 1

Figure C.11 Case 2: Toe: alpha0 = [0,0.5], omega = 25, omega_d = 1, OCR = 1, r = 1

POV
MACRO
STABILITEIT
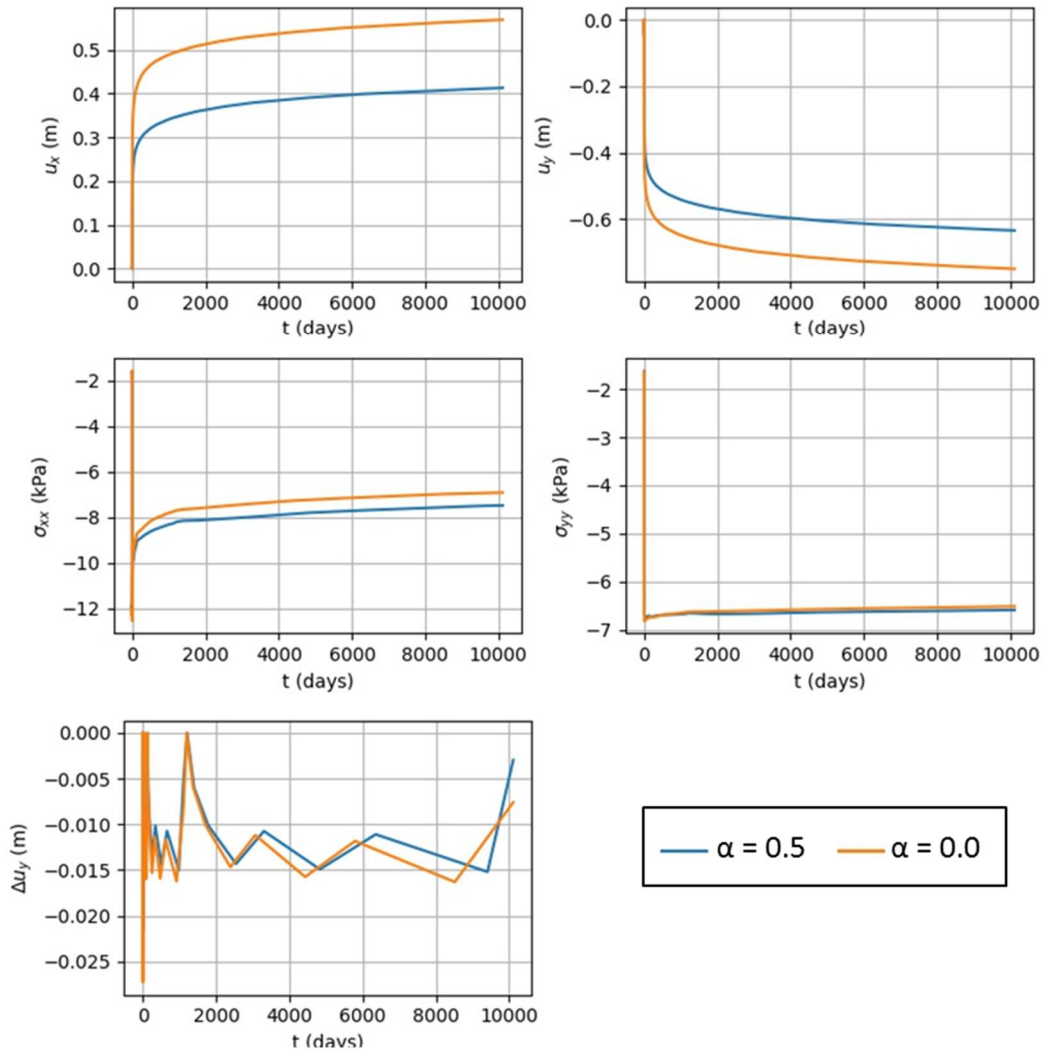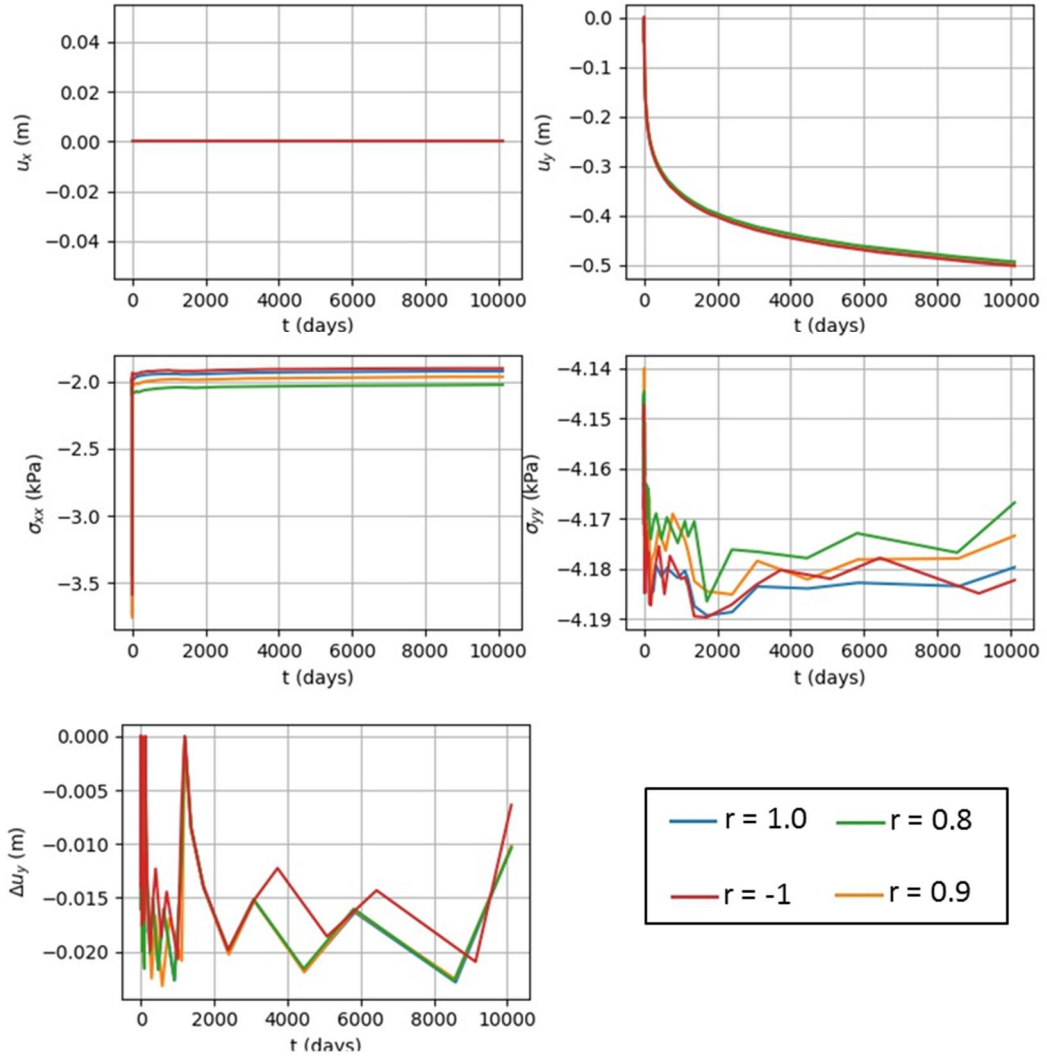
C.3.1.3   Case 3

Figure C.12 Case 3: Boundary: alpha0 = 0., omega = 25, omega_d = 1, OCR = 1, r = [-1, 0.8, 0.9, 1.0]

POV MACRO STABILITEIT
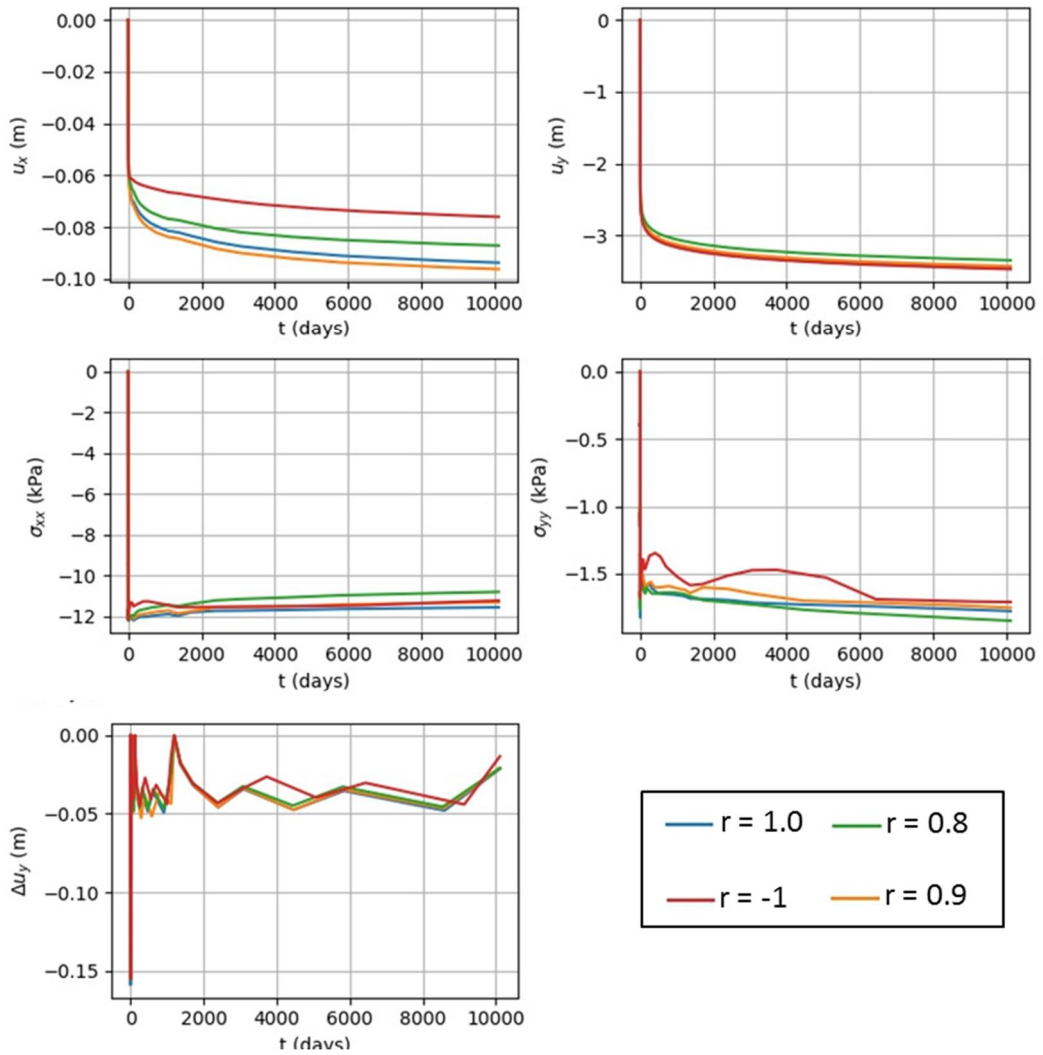
Figure C.13 Case 3: Crest: alpha0 = 0.5, omega = 25, omega_d = 1, OCR = 1, r = [-1, 1.0, 0.8, 0.9]
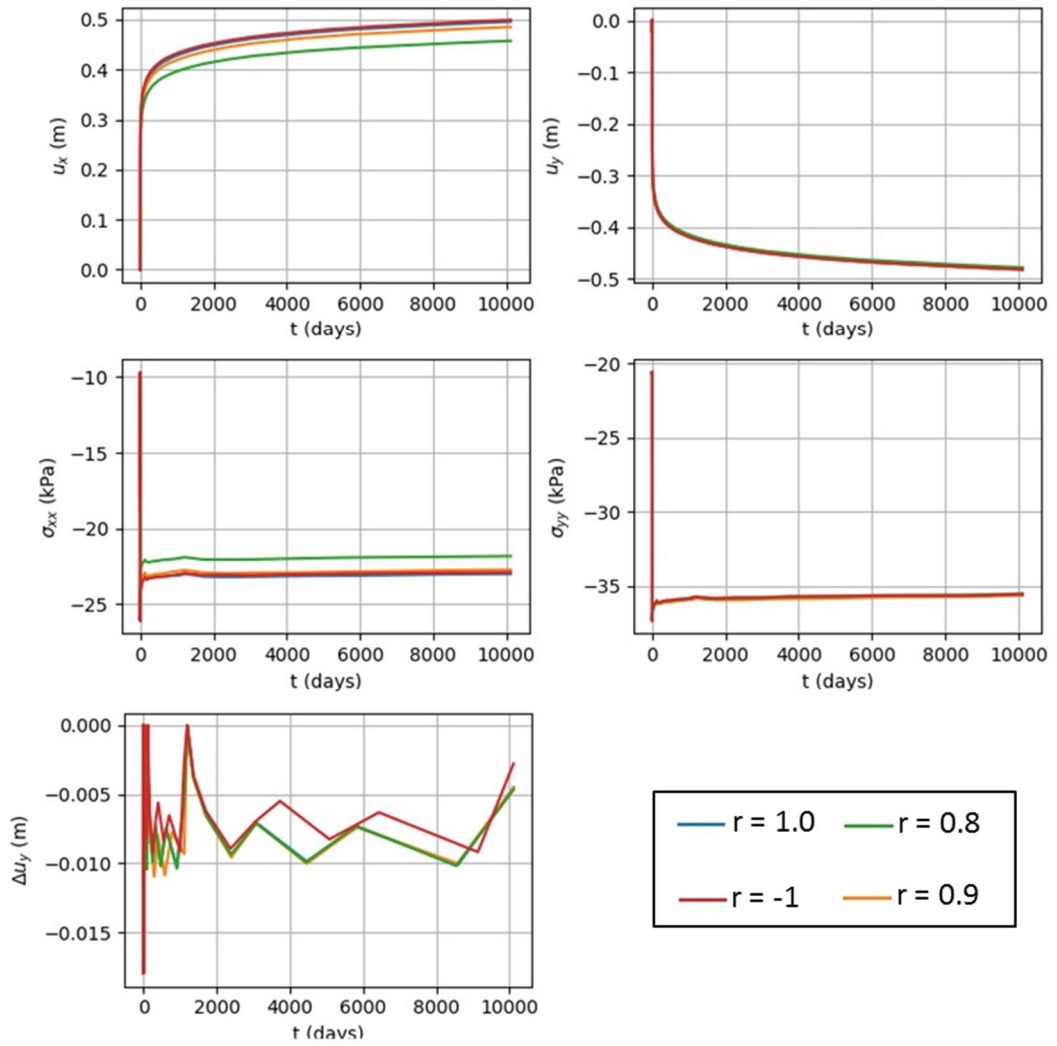
Figure C.14 Case 3: Soft Soil: alpha0 = 0.5, omega = 25, omega_d = 1, OCR = 1, r = [-1, 1.0, 0.8, 0.9]

Figure C.15 Case 3: Toe: alpha0 =0.5, omega = 25, omega_d = 1, OCR = 1, r = [-1, 0.8, 0.9, 1.0]

POV MACRO STABILITEIT
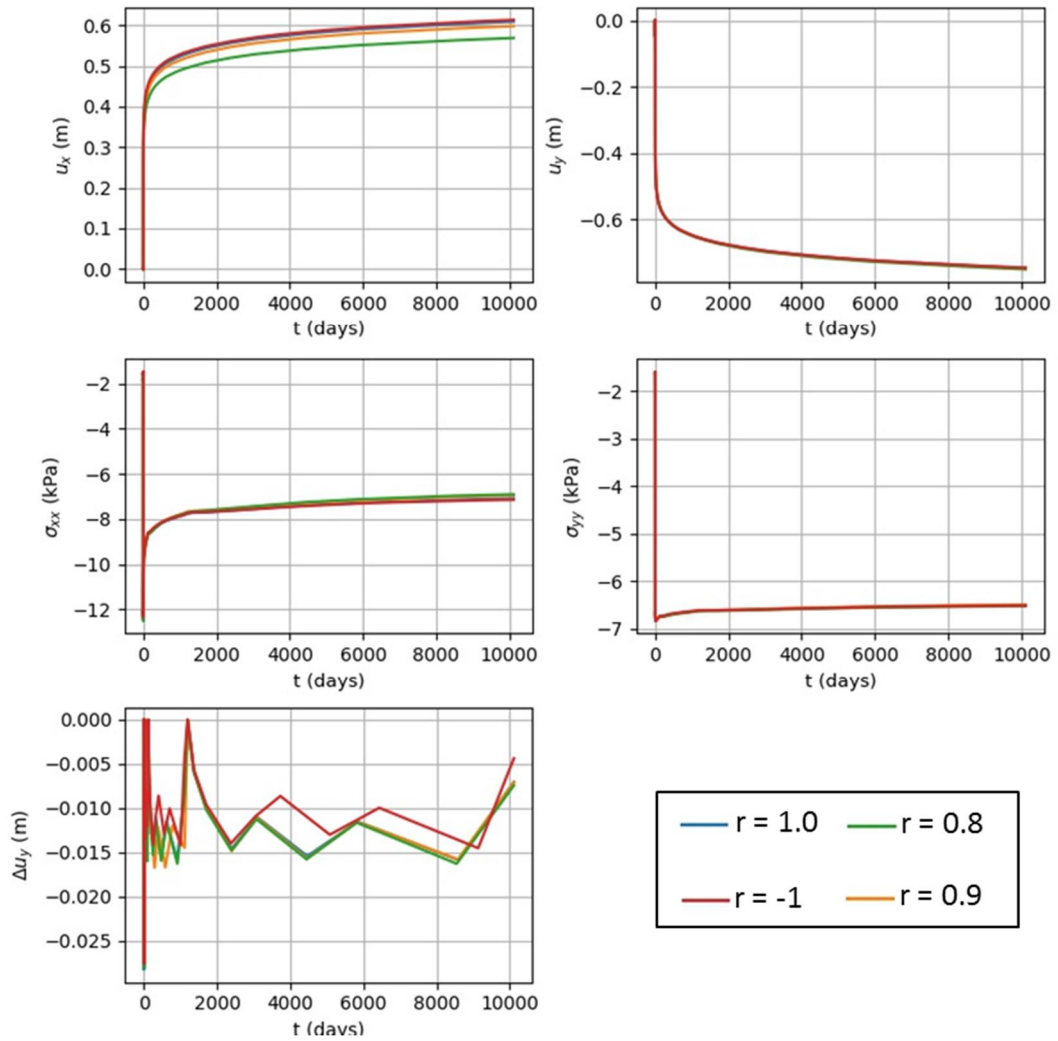
C.3.1.4 Case 3
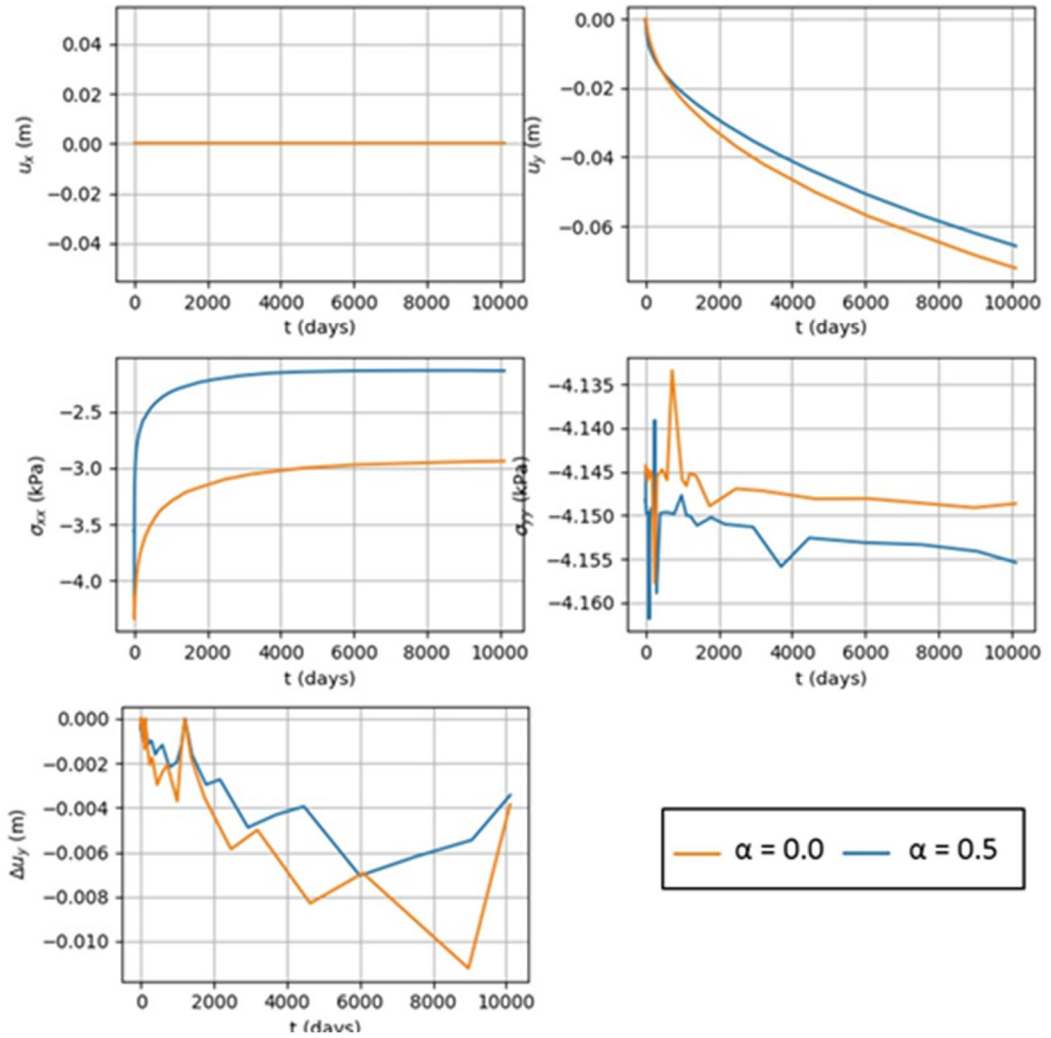
Figure C.16 Boundary: alpha = [0,0.5], omega = 0.0, omega_d = 0.0, OCR = 1.75, r = 1.0

Figure C.17   Crest: alpha = [0,0.5], omega = 0.0, omega_d = 0.0, OCR = 1.75, r = 1.

POV MACRO STABILITEIT
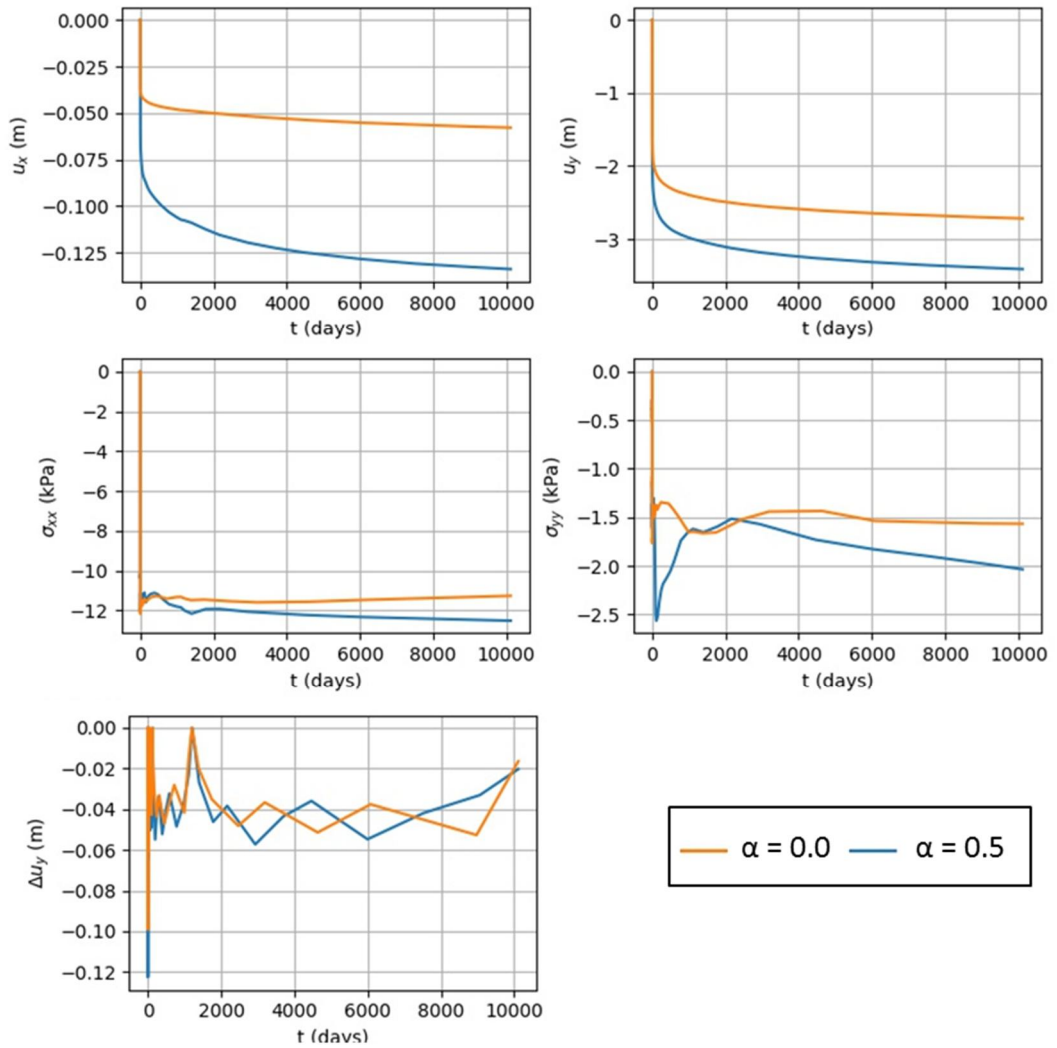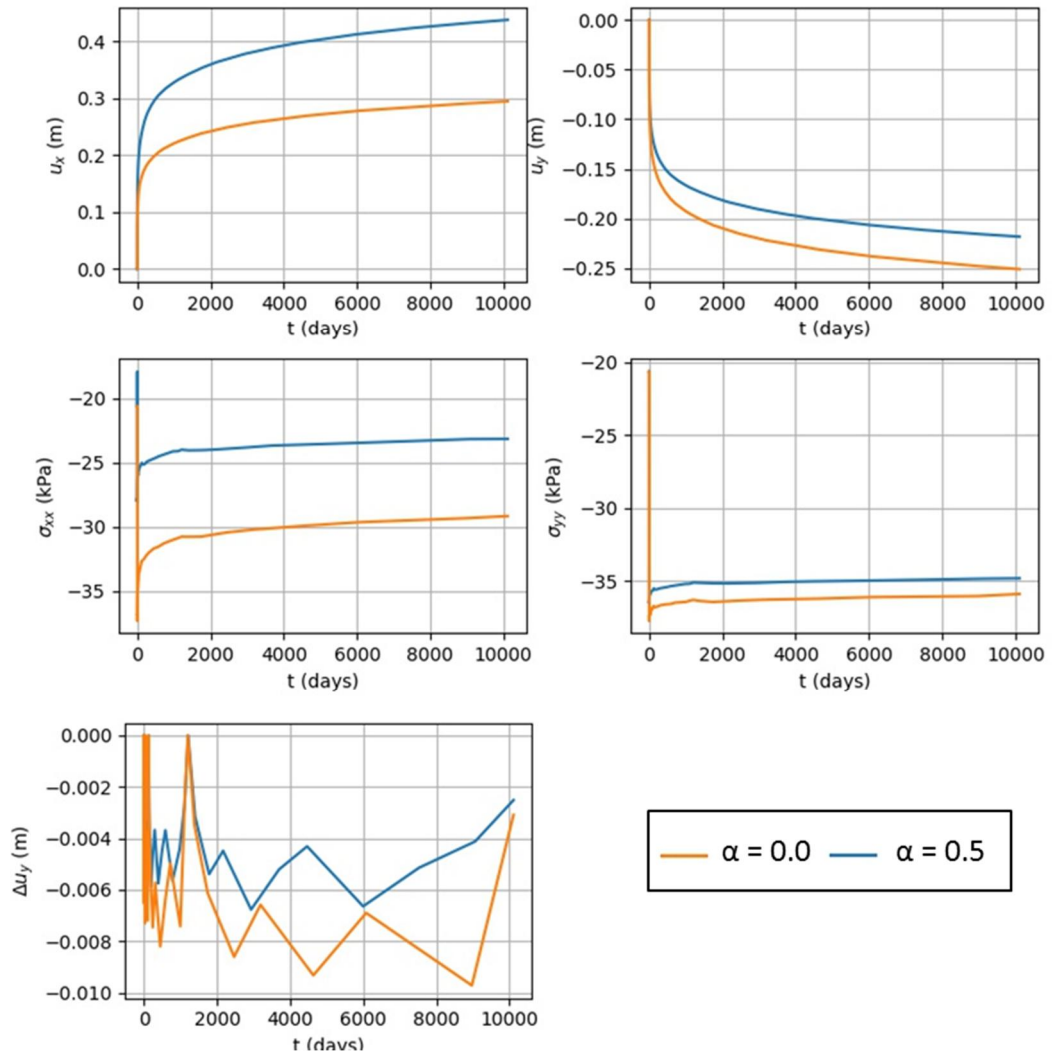
Figure C.18 Soft Soil: alpha = [0,0.5], omega = 0.0, omega_d = 0.0, OCR = 1.75, r = 1.0

Figure C.19 Toe: alpha = [0,0.5], omega = 0.0, omega_d = 0.0, OCR = 1.75, r = 1.0
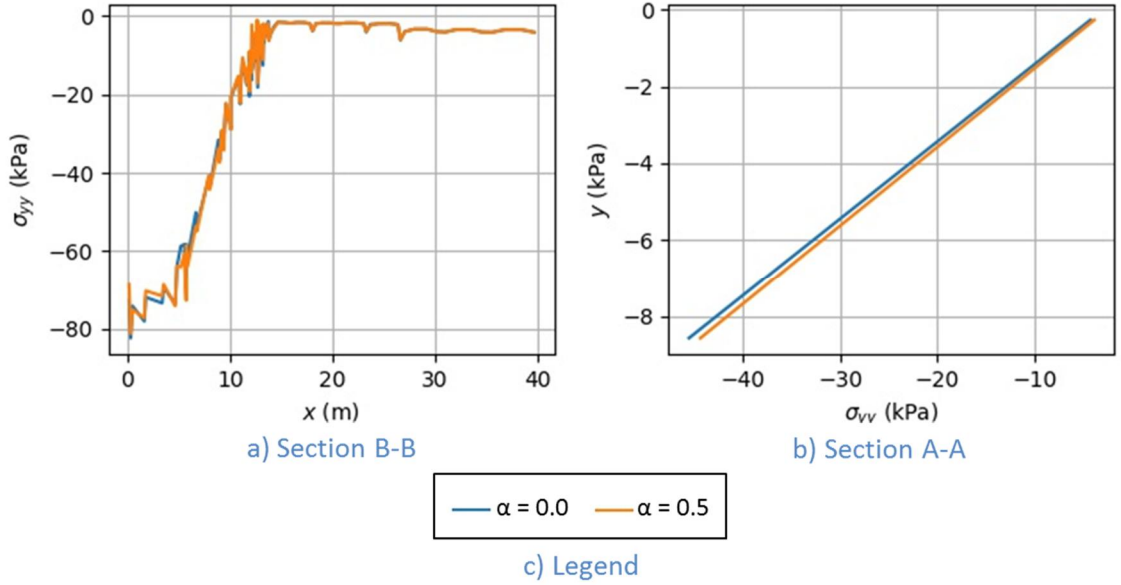
POV MACRO STABILITEIT

C.3.1.5   Position Dependent Results

a) Section B-B

b) Section A-A

| α = 0.0 | α = 0.5 |

c) Legend

Figure 4.1: Case 1: alpha_0 = [0,0.5], omega = 0, omegad_d = 0, OCR = 1, r = 1.

a) Section B-B

b) Section A-A

| α = 0.0 | α = 0.5 |

c) Legend

Figure C.20 Case 2: alpha_0 = [0,0.5], omega = 25, omega_d = 1, OCR = 1, r = 1

a) Section B-B   b) Section A-A

c) Legend

Figure C.21 Case 3: alpha_0 = 0.5, omega = 25, omega_d = 1, OCR = 1, r = [-1, 0.8, 0.9, 1]

a) Section B-B   b) Section A-A

c) Legend
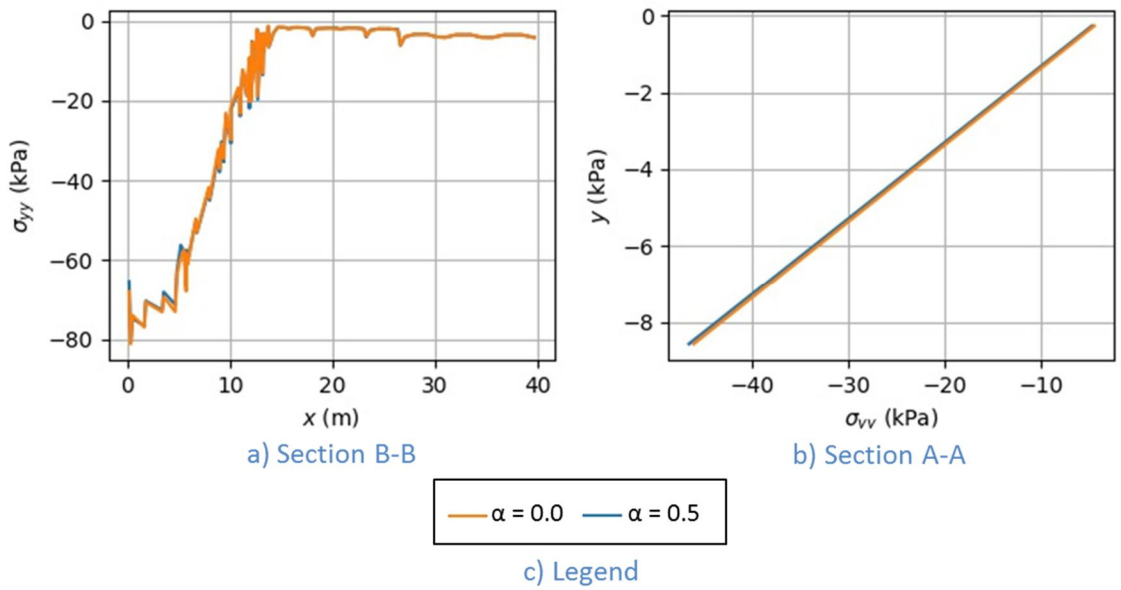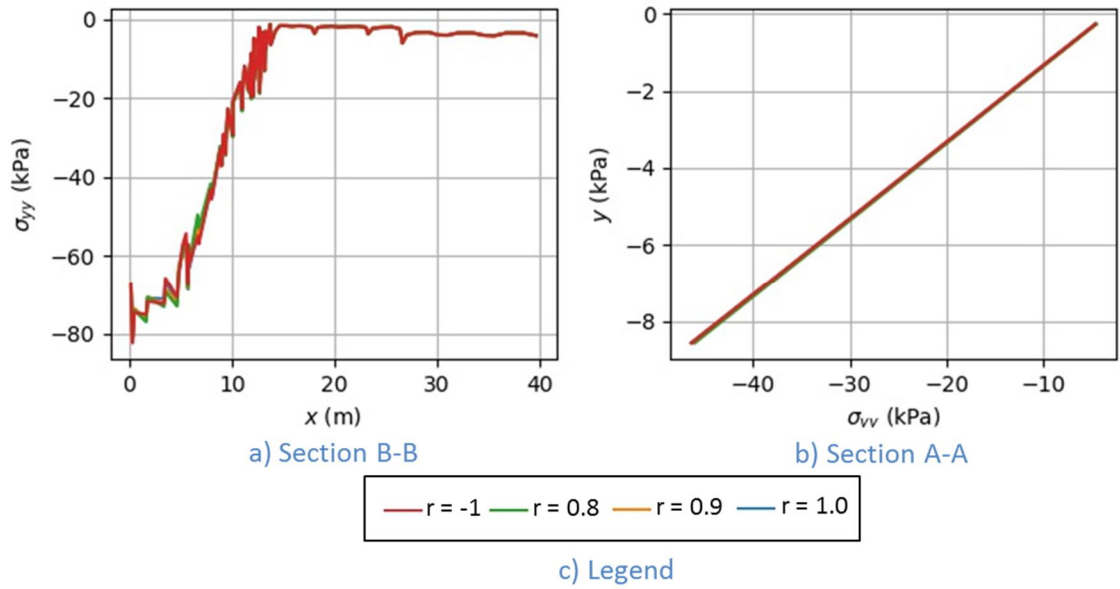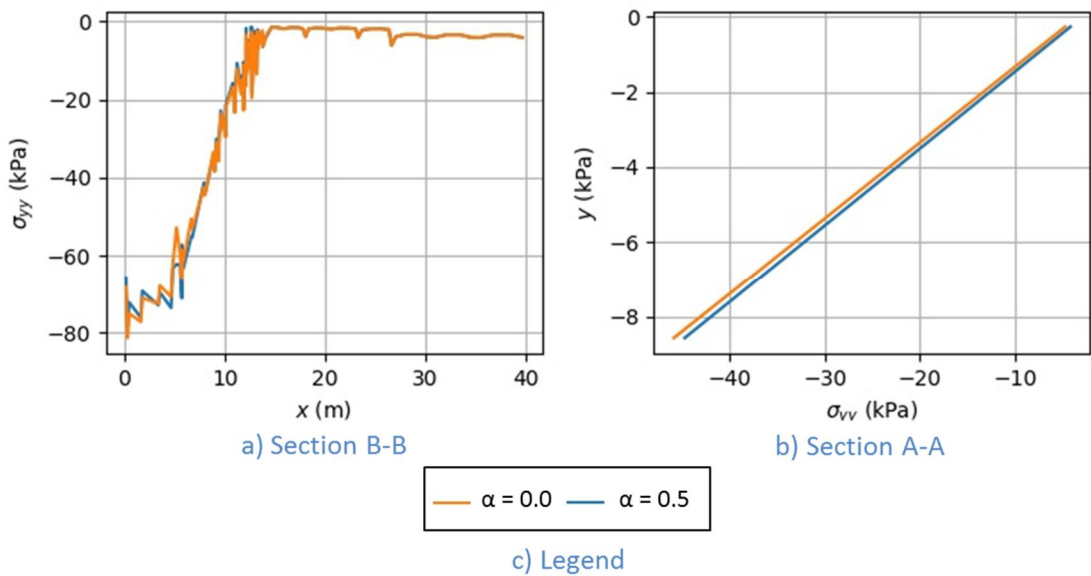
Figure C.22 Case 4: alpha0 = [0,0.5], omega = 0.0, omega_d = 0.0 , OCR = 1.75, r = 1.0

C.3.2   Contour Results

C.3.2.1   Case 1
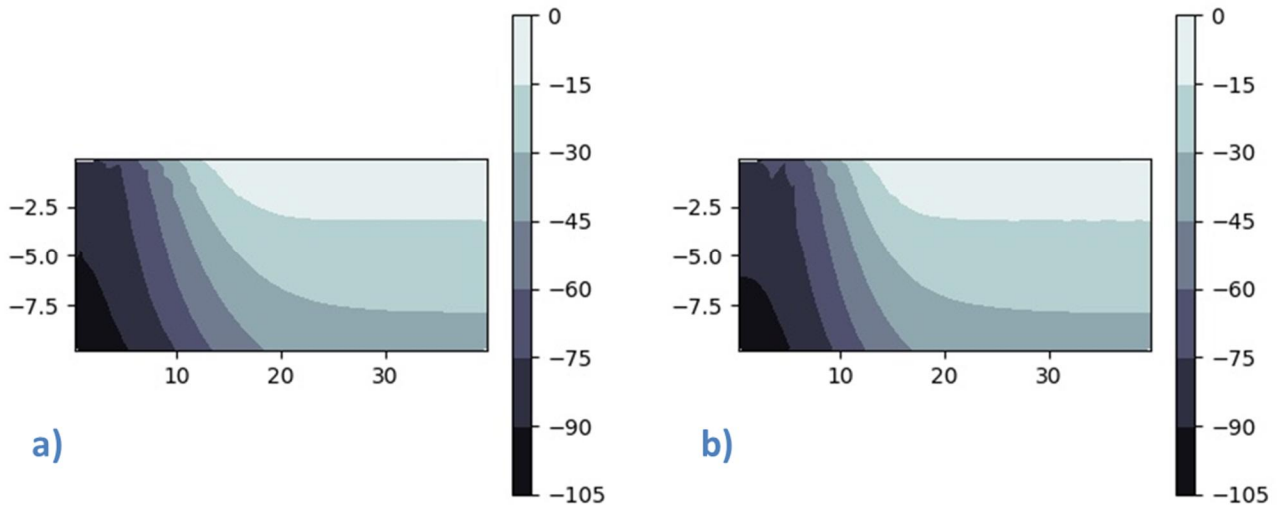
Figure C.23 First principal stress (kPa): Case 1: a) alpha_0 = 0, b) alpha_0 = 0.5
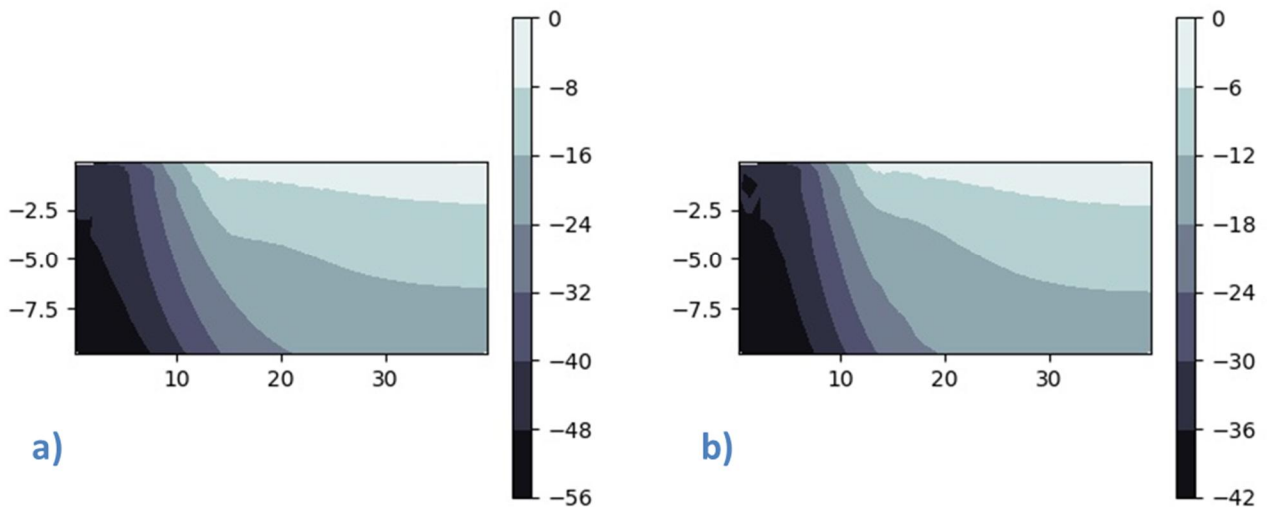
Figure C.24 Second principal stress (kPa): Case 1: a) alpha_0 = 0, b) alpha_0 = 0.5
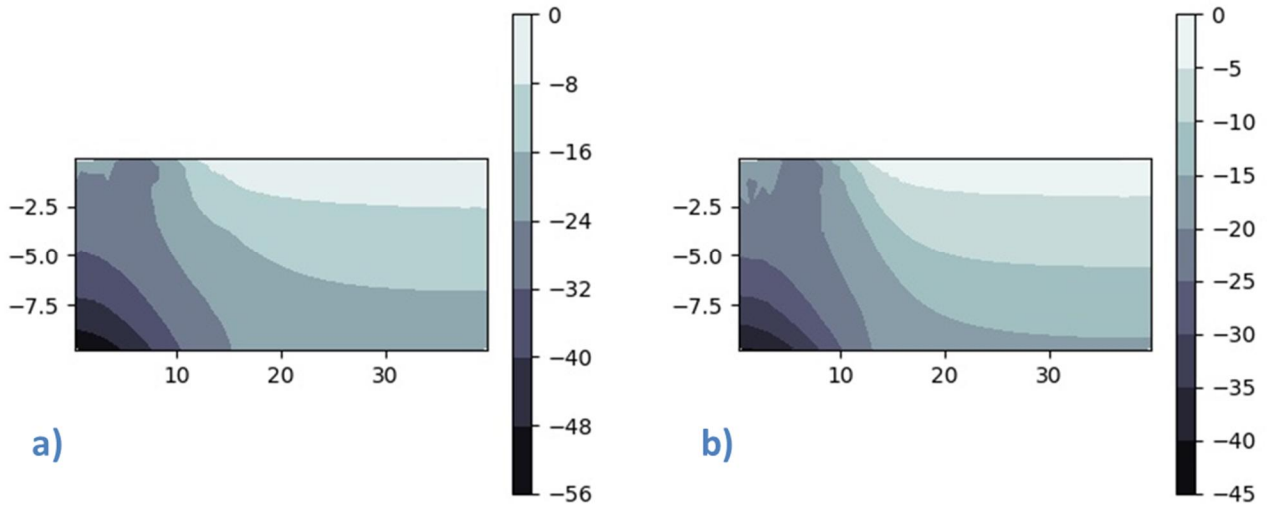
Figure C.25 *Third principal stress (kPa): Case 1: a) alpha_0 = 0, b) alpha_0 = 0.5*
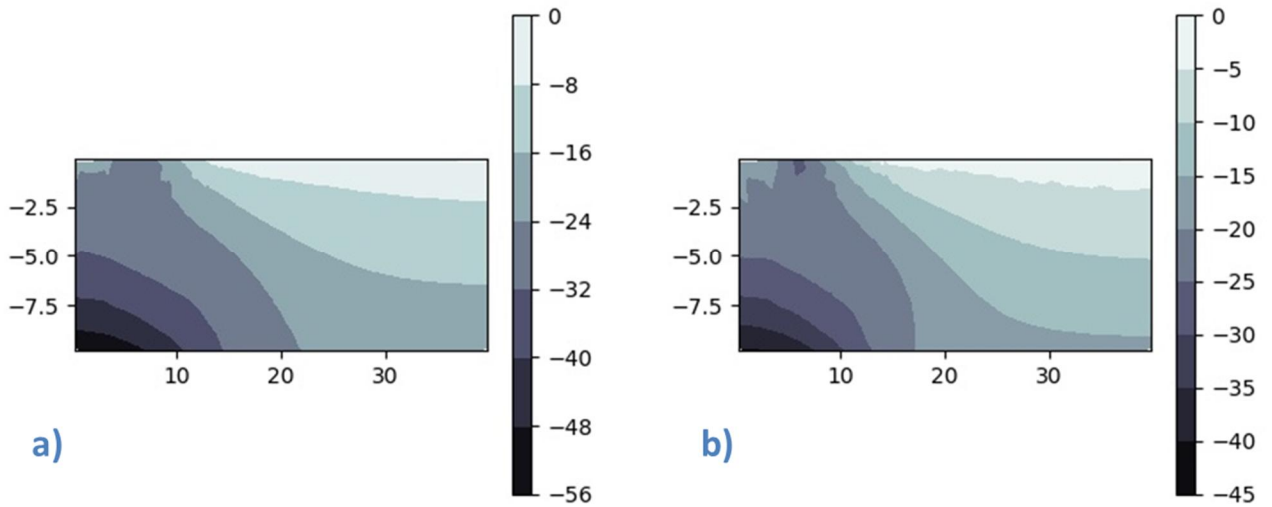
Figure C.26 *Horizontal Effective Stress (kPa): Case 1: a) alpha_0 = 0, b) alpha_0 = 0.5*
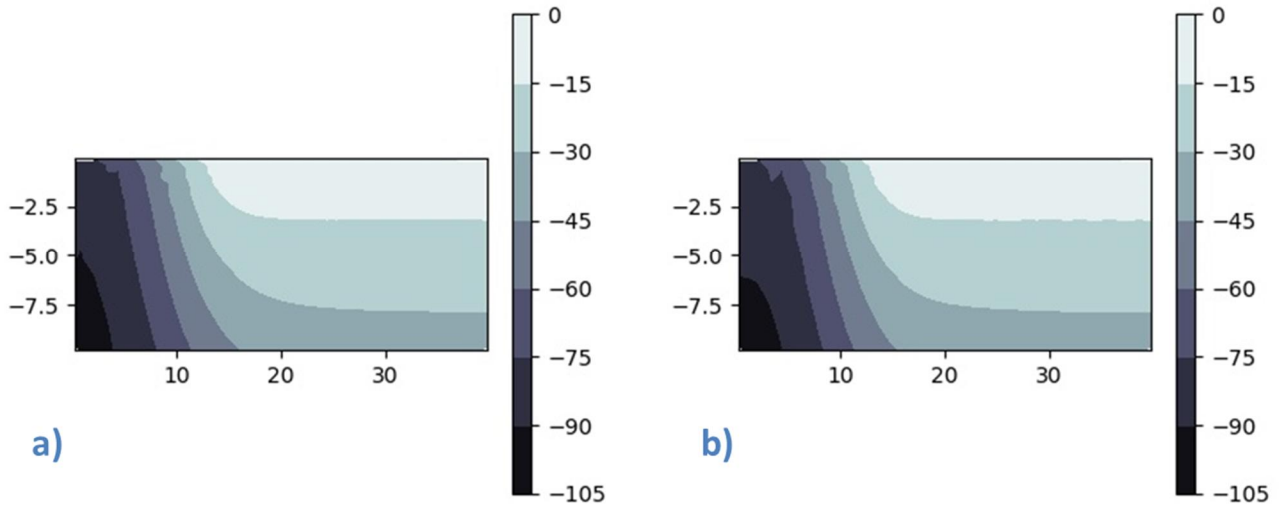
Figure C.27 Vertical Effective Stress (kPa): Case 1: a) alpha_0 = 0, b) alpha_0 = 0.5
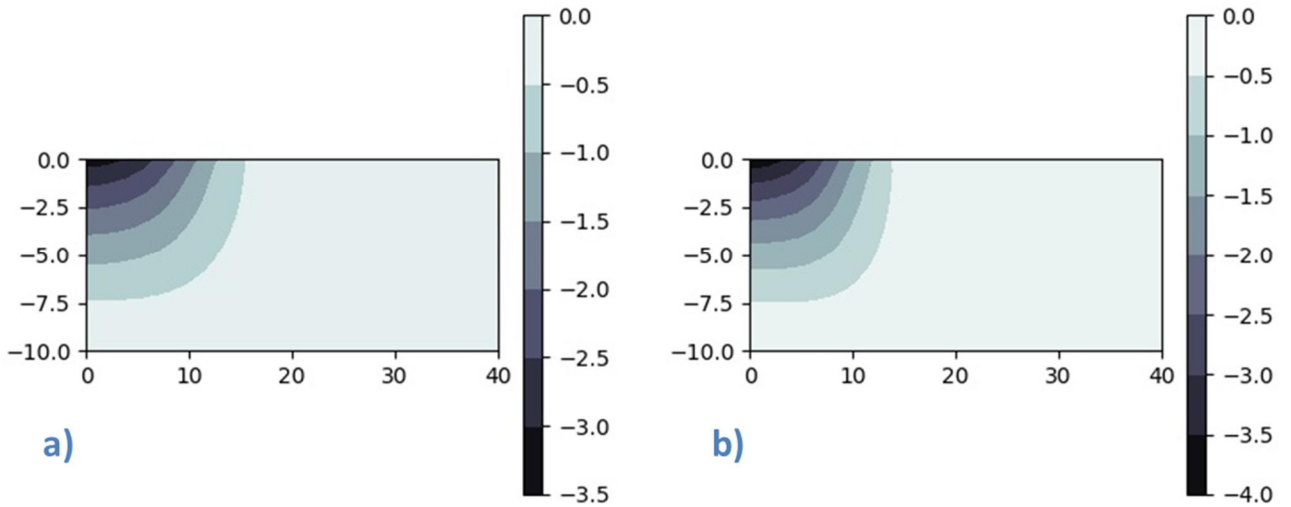
*Figure C.28 Vertical Displacement (m): Case 1: a) alpha_0 = 0, b) alpha_0 = 0.5*

C.3.2.2   Case 2
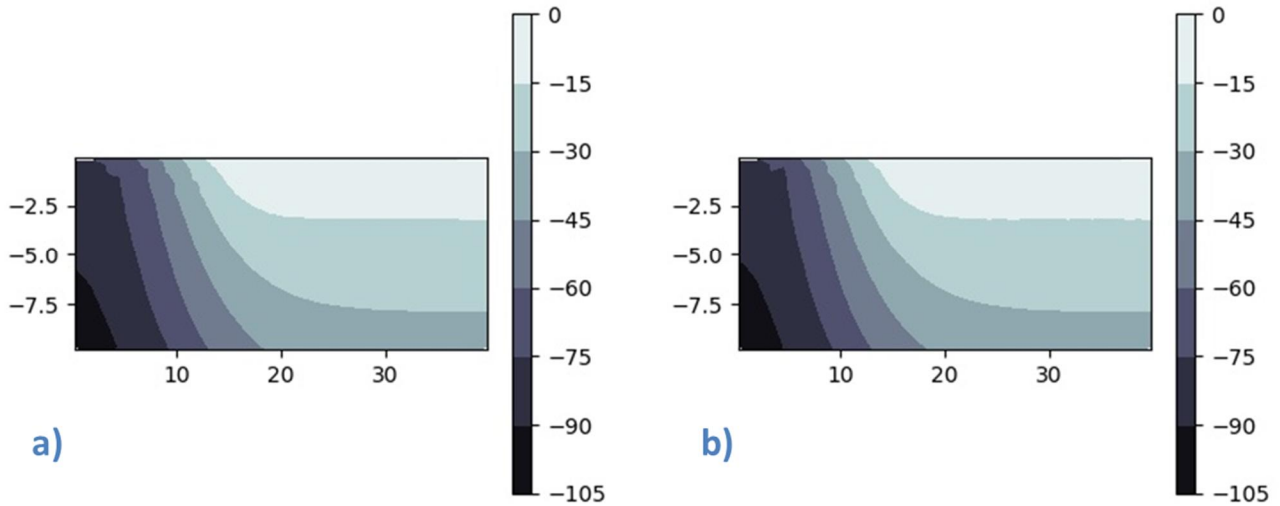
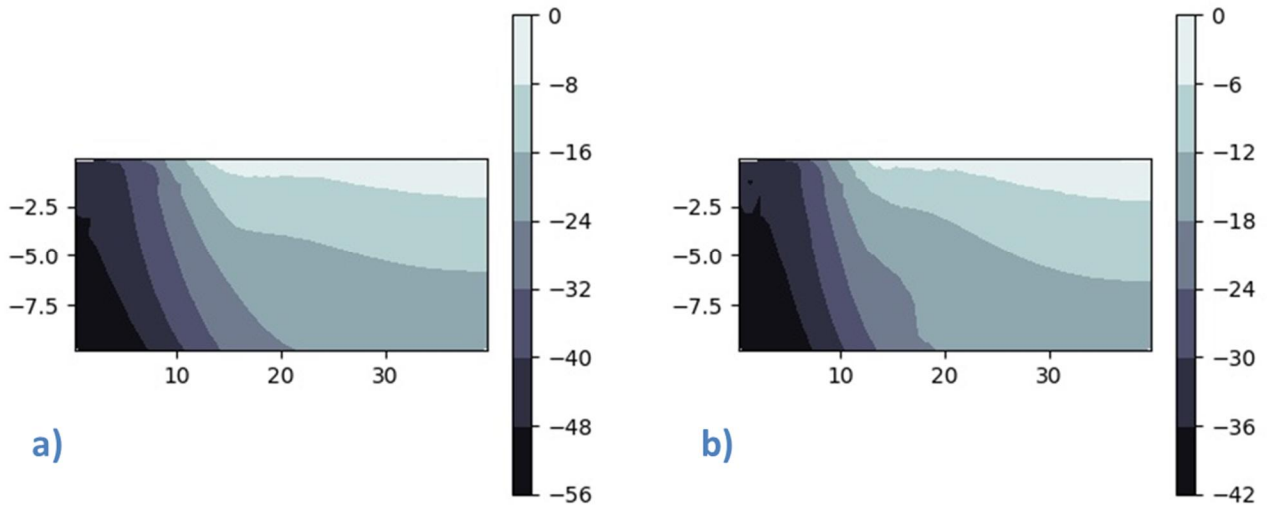Figure C.29 First principal stress (kPa): Case 2: a) alpha_0 = 0, b) alpha_0 = 0.5
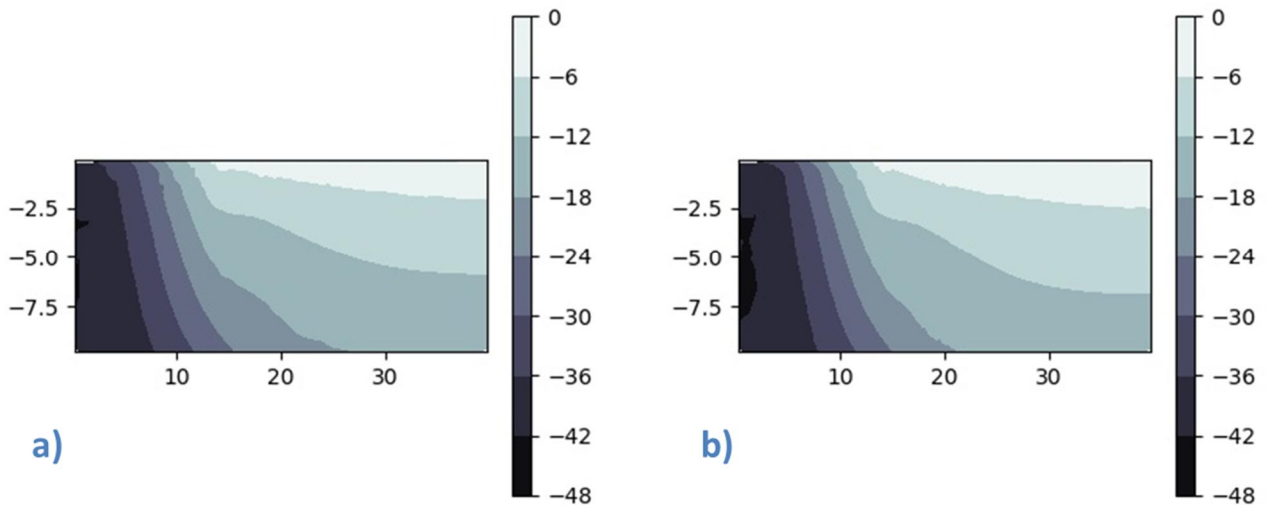
Figure C.30 Second principal stress (kPa): Case 2: a) alpha_0 = 0, b) alpha_0 = 0.5
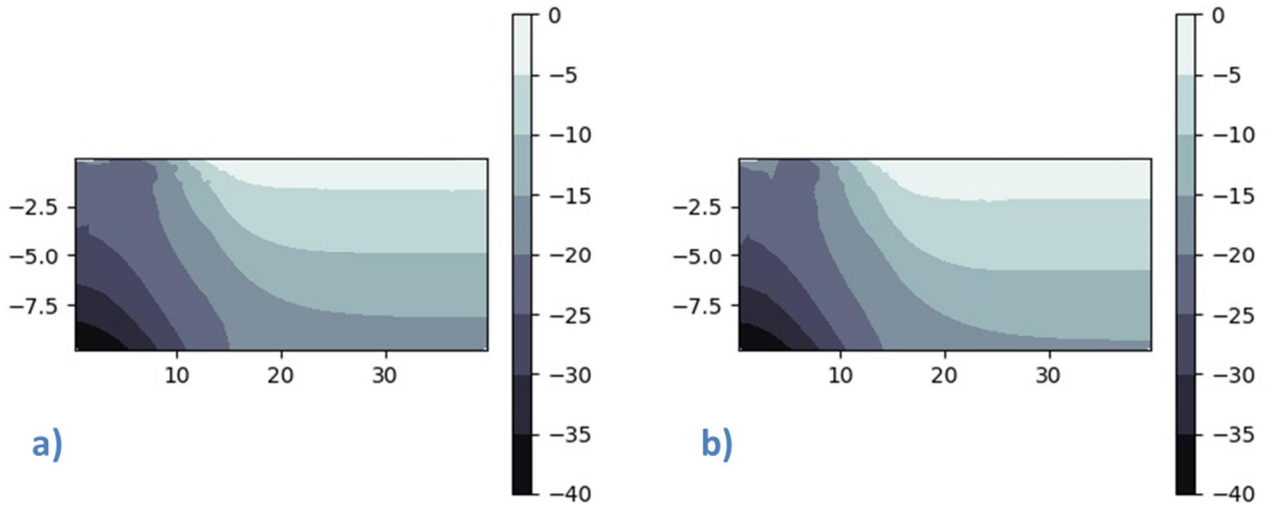
Figure C.31 Third principal stress (kPa): Case 2: a) alpha_0 = 0, b) alpha_0 = 0.5
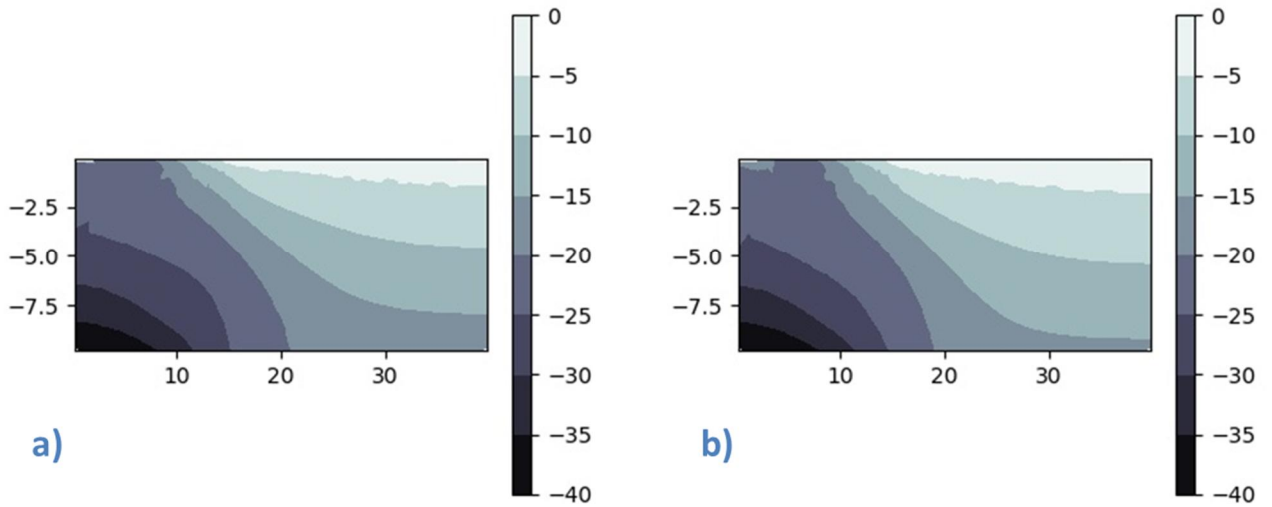
Figure C.32 Horizontal Effective Stress (kPa): Case 2: a) alpha_0 = 0, b) alpha_0 = 0.5
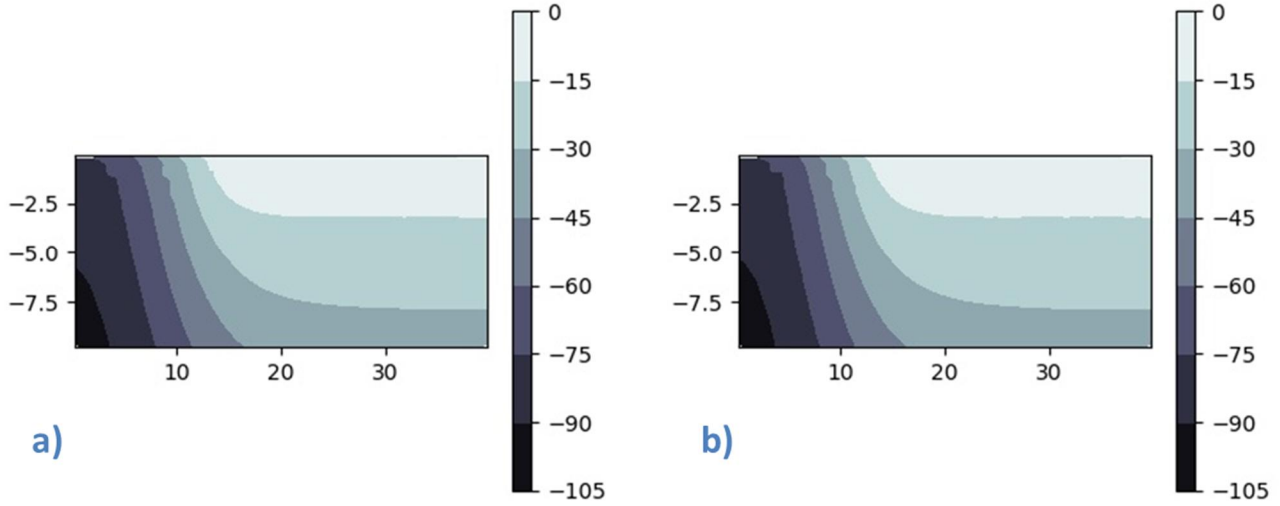
Figure C.33 Vertical Effective Stress (kPa): Case 2: a) alpha_0 = 0, b) alpha_0 = 0.5
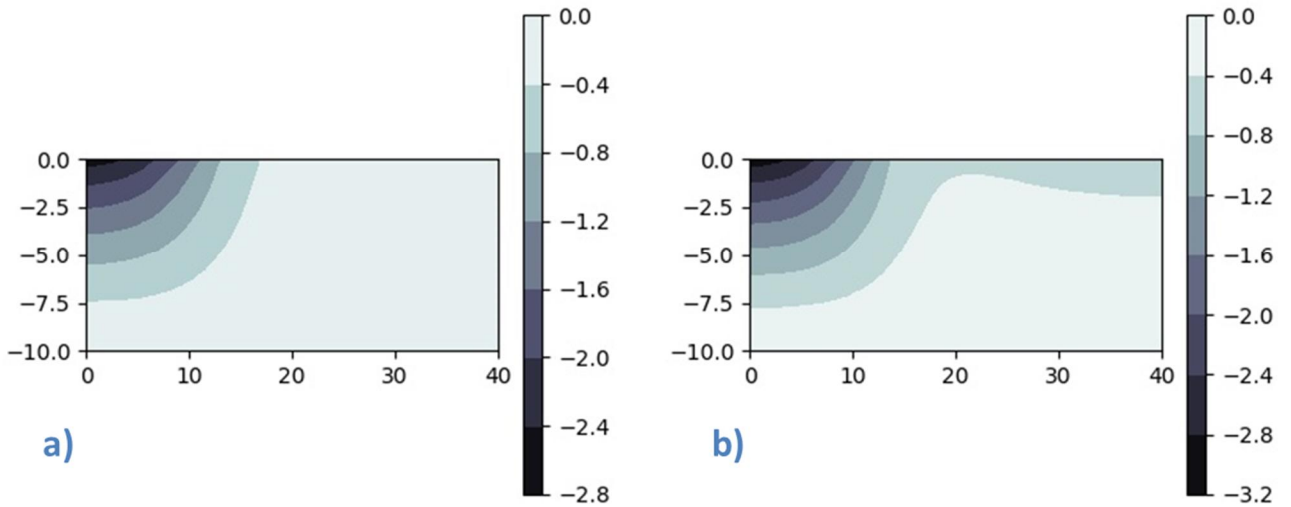
Figure C.34 Vertical Displacement (m) : Case 2: a) alpha_0 = 0, b) alpha_0 = 0.5

C.3.2.3   Case 3
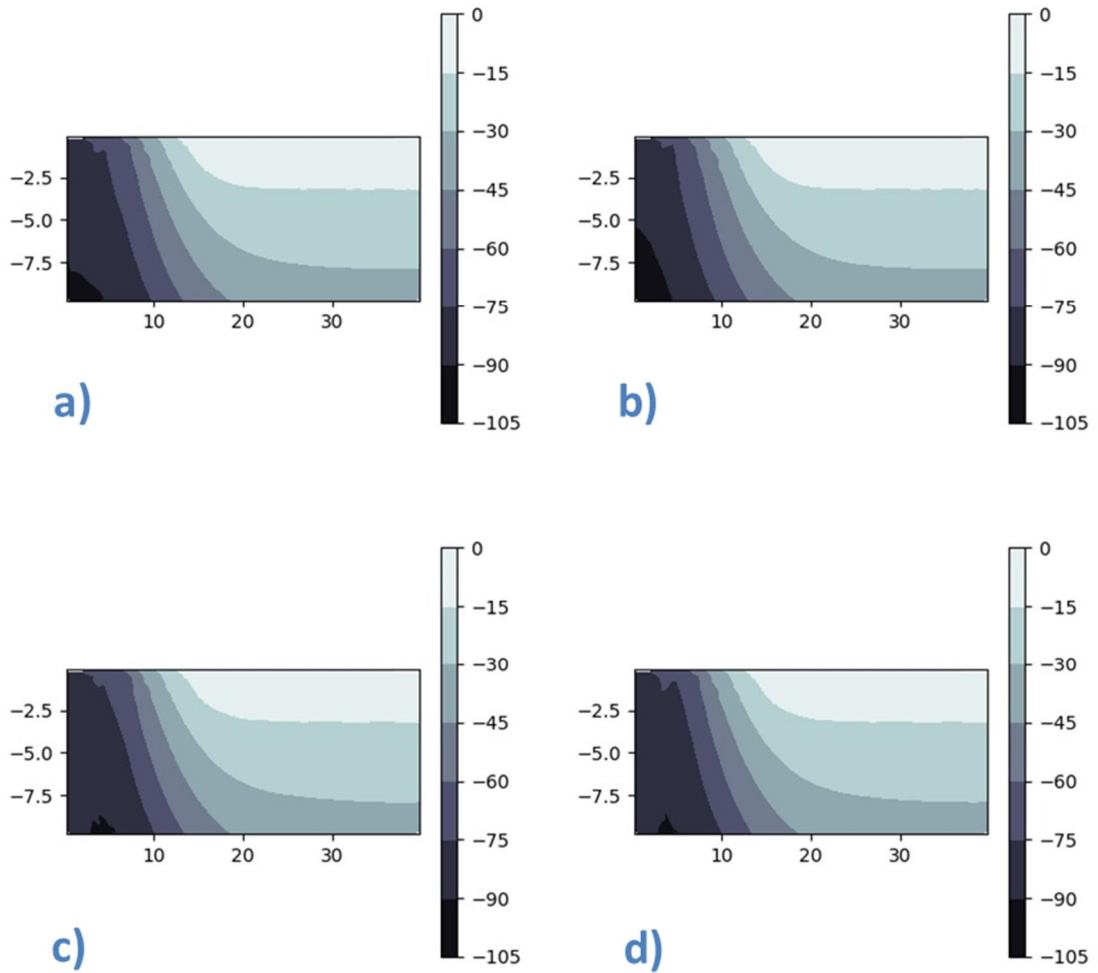
Figure C.35 First Principal Stress (kPa): Case 3: a) r = 0.9, b) r = 1.0, c) r = -1, d) r = 0.8
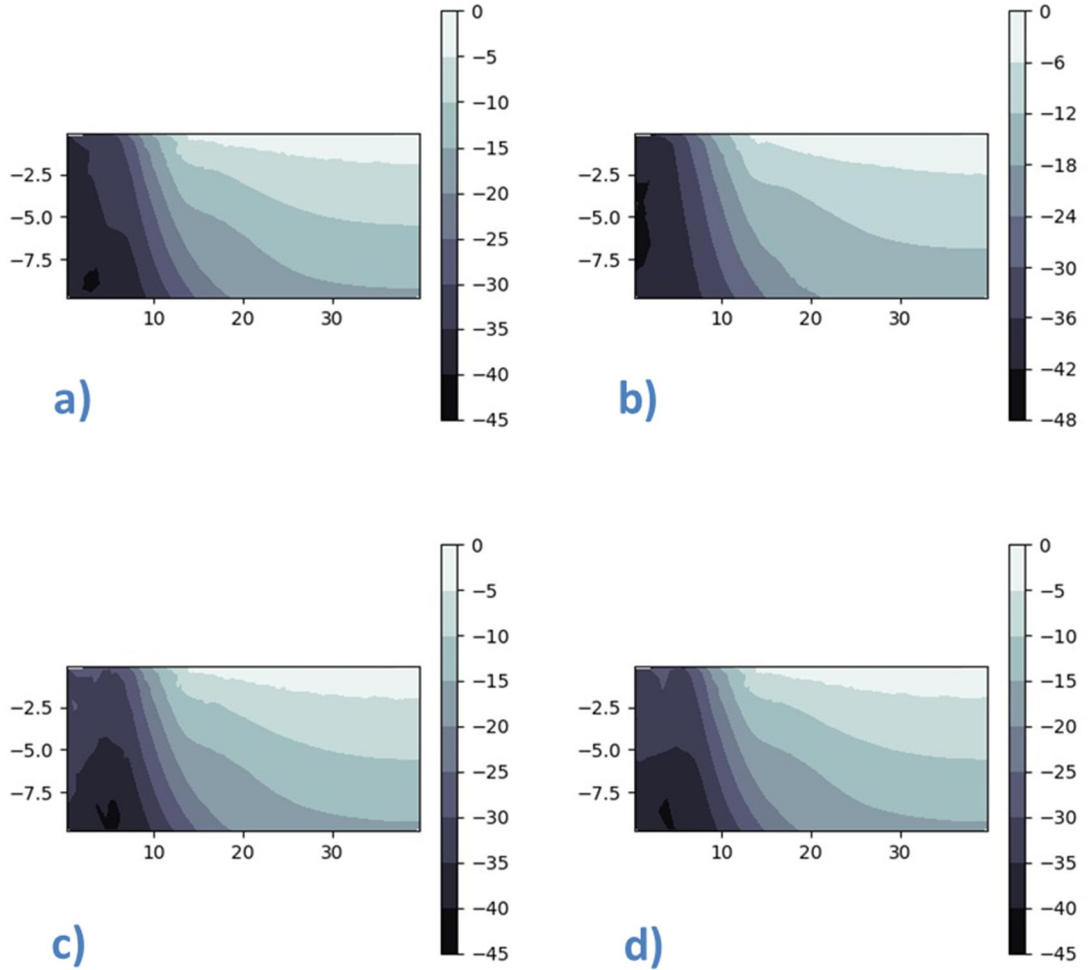
Figure C.36 Second Principal Stress (kPa): Case 3: a) r = 0.9, b) r = 1.0, c) r = -1, d) r = 0.8
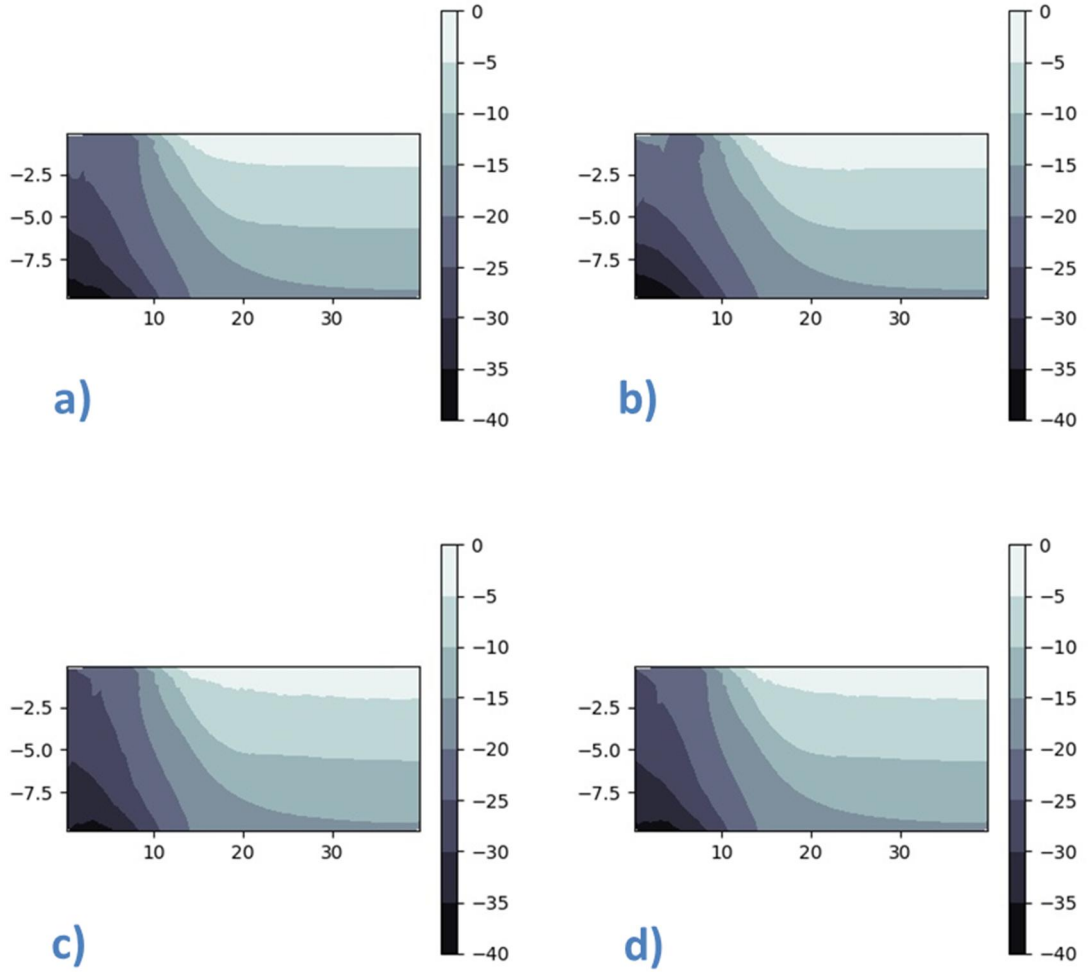
Figure C.37 Third principal stress (kPa): Case 3: a) r = 0.9, b) r = 1, c) r = -1, d) r = 0.8
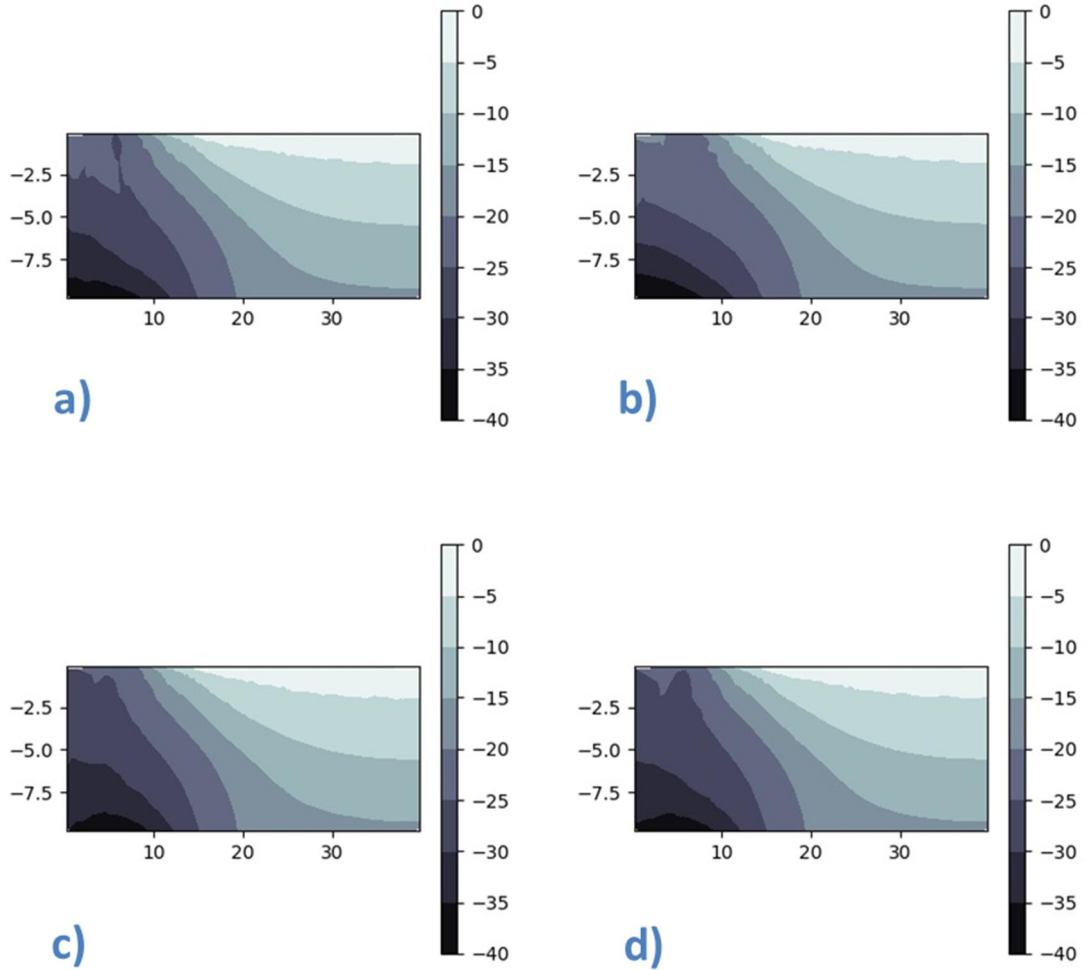
Figure C.38 Horizontal Effective Stress (kPa): Case 3: a) r = 0.9, b) r = 1, c) r = -1, d) r = 0.8
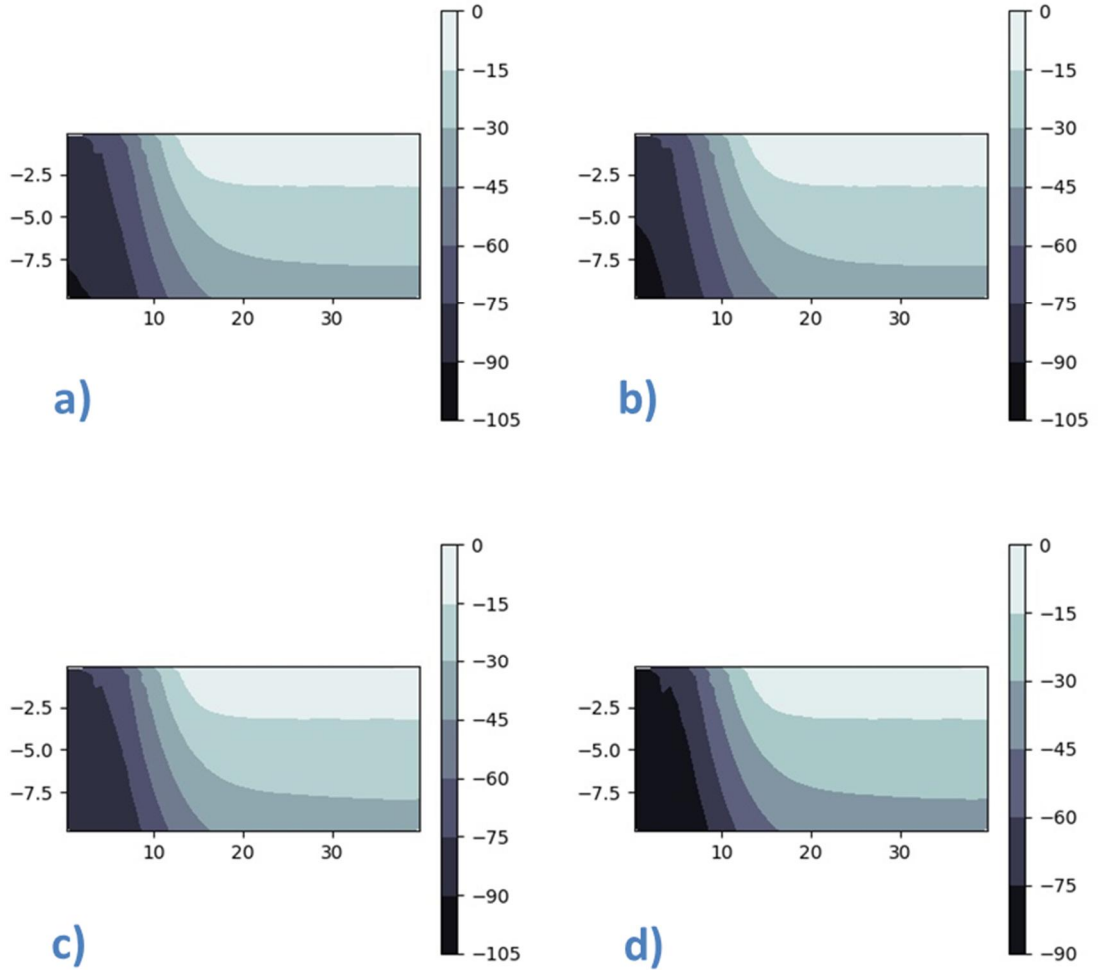
Figure C.39 Vertical Effective Stress (kPa): Case 3: a) r = 0.9, b) r = 1, c) r = -1, d) r = 0.8
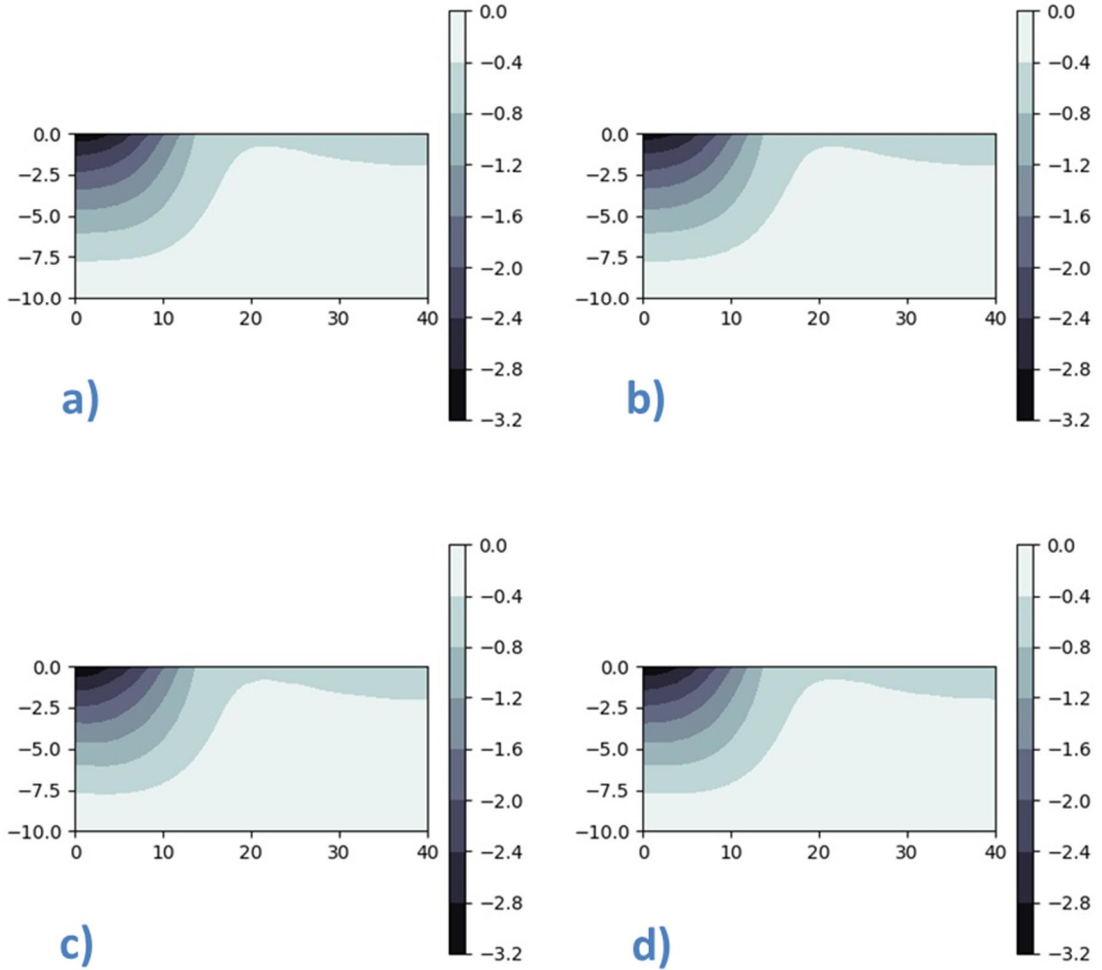
Figure C.40 Vertical displacement (m): Case 3: a) r = 0.9, b) r = 1, c) r = -1, d) r= 0.8

C.3.2.4   Case 4
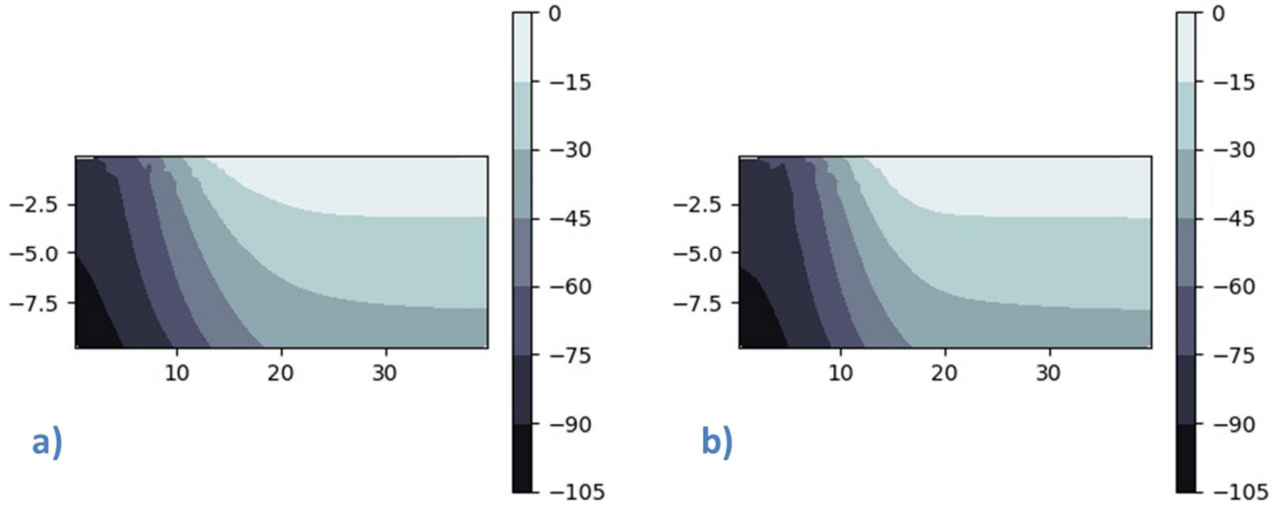
Figure C.41 First principal stress (kPa): Case 4: a) alpha_0 = 0, b) alpha_0 = 0.5

Figure C.42 : Second principal stress (kPa): Case 4: a) alpha_0 = 0, b) alpha_0 = 0.5
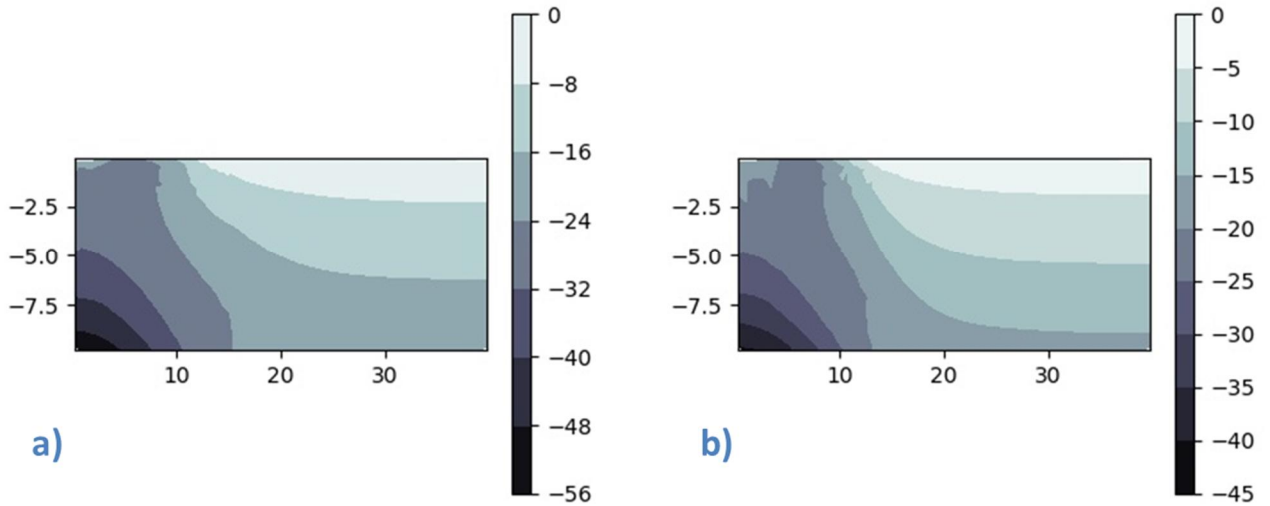
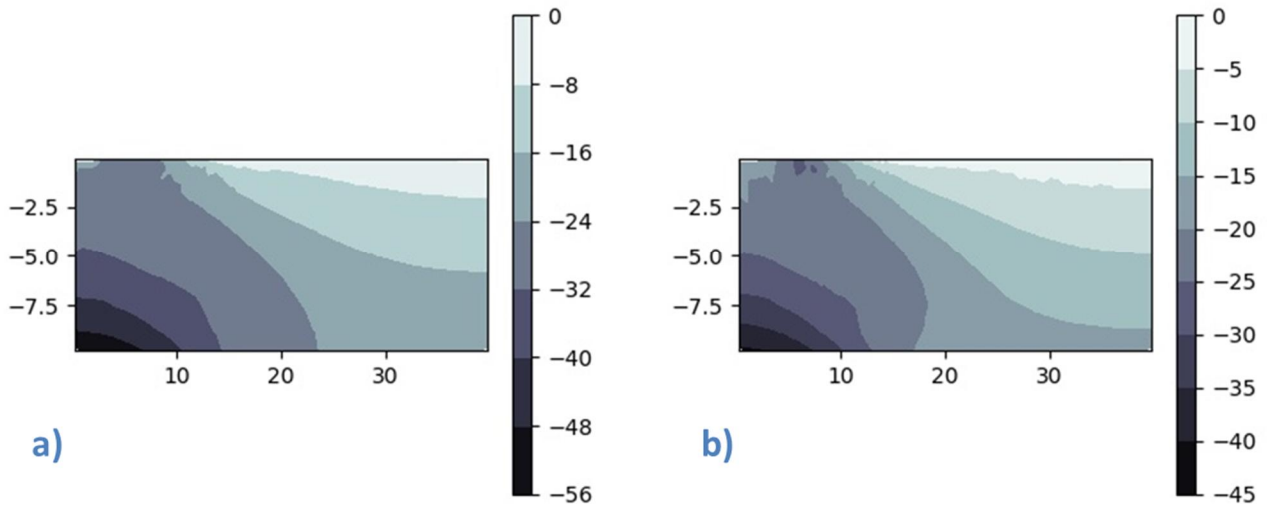*Figure C.43: Third principal stress (kPa): Case 4: a) alpha_0 = 0, b) alpha_0 = 0.5*

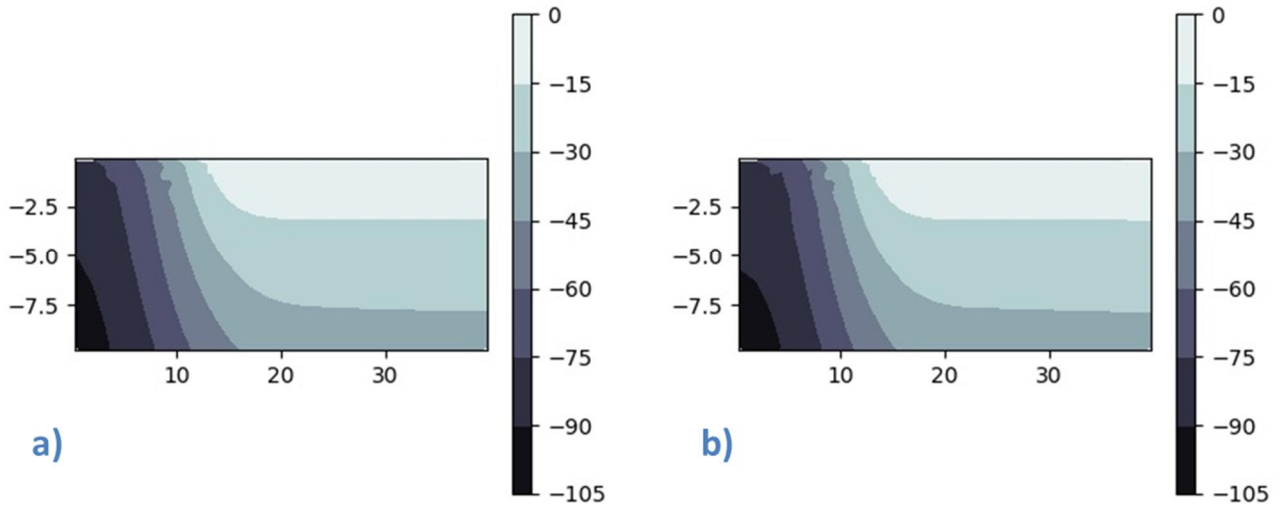*Figure C.44: Horizontal Effective Stress (kPa): Case 4: a) alpha_0 = 0, b) alpha_0 = 0.5*

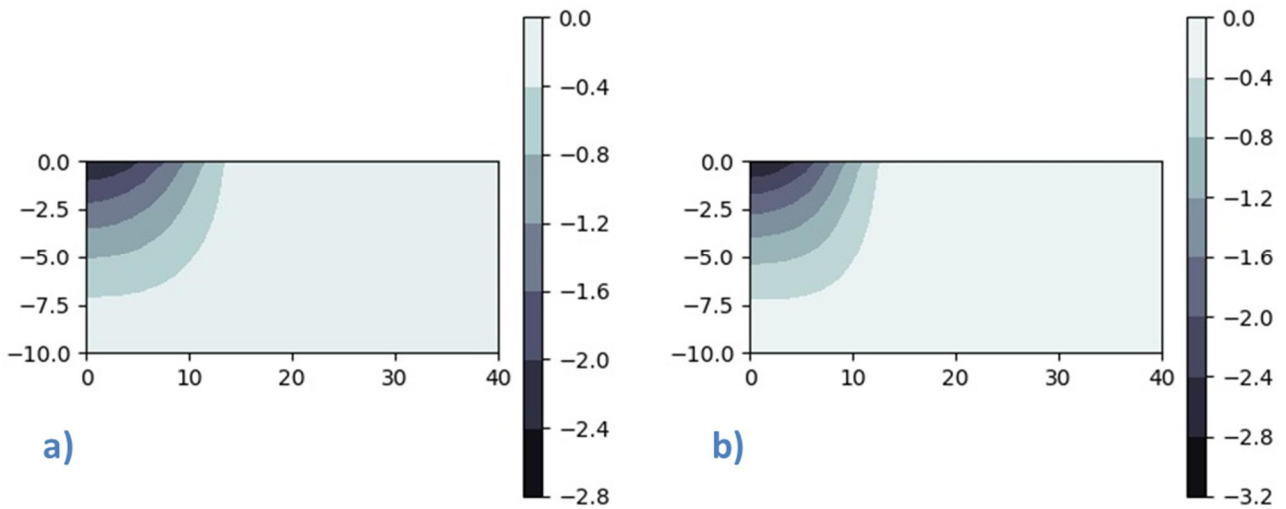*Figure C.45: Vertical effective stress (kPa): Case 4: a) alpha_0 = 0, b) alpha_0 = 0.5*

Figure C.46: Vertical displacement (m): Case 4: a) alpha_0 = 0, b) alpha_0 = 0.5